ON SOME ASPECTS OF THE AERODYNAMIC PERFORMANCE OF GROUND-EFFECT WINGS

by

P.R. Ashill

ACKNOWLEDGMENTS

To Dr. H.J. Davies, the author's supervisor, for many helpful suggestions, constructive criticisms and constant encouragement.

To Professor G.M. Lilley for suggesting the problem and for giving much useful advice.

To The Ministry of Technology for supporting this work financially.

To the aerodynamics staff at The College of Aeronautics for their willingness to help with any problem. In particular, mention should be made of the help in practical matters given by Mr. S.H. Lilley during the course of the experiments.

ABSTRACT

FACULTY OF ENGINEERING

AERONAUTICS AND ASTRONAUTICS

Doctor of Philosophy

ON SOME ASPECTS OF THE AERODYNAMIC PERFORMANCE OF GROUND-EFFECT WINGS

by Patrick Ralph Ashill

With the advent of the hovercraft and hydrofoil, high-speed, overwater travel has become a practical proposition. Nevertheless, there would appear to be an upper limit to the speed of these craft imposed by, on the one hand, the intake momentum drag of the hovercraft and, on the other, the drag of the submerged foils of the hydrofoil. One method proposed for reducing these drags employs aerodynamic lifting surfaces to off-load the cushion or hydrodynamic lifting systems. These surfaces, which are referred to as 'ground-effect wings', fall into two main categories, namely 'open' and 'closed'. The latter type is defined as that which may, in theory, be designed for zero induced drag; the former type is that which may not.

By employing the linearized lifting-surface theory the minimum induced drag of an open configuration, consisting of a planar wing with end plates, is determined. The results of this theory are in agreement with experiment in predicting that the effect of end plates is to reduce the induced drag. However, the indications of the experiments are that the reduction in induced drag is somewhat greater than the theoretical prediction. There is evidence that this is due to the tendency of the end plates to suppress harmful non-linear effects such as edge separations at the tips of the wing and the sidewash at the wing.

A theoretical and experimental study of the lift and induced drag of a closed configuration, comprised of a substantially planar wing with end plates and not designed ab initio for zero induced drag, is

described. The need to represent certain non-linear effects in the theory in order to obtain accurate values of lift is demonstrated. Further, it is shown that with the type of closed configuration examined, namely that with chordwise camber, thickness and incidence which vary slowly round the configuration, the induced drag is small. In some cases, however, it is evident that the end plates are expected to provide a large thrust to offset a large drag contributed by the wing component. Thus, in these circumstances, it is important to ensure that the end plates are designed to sustain the requisite thrust.

The image method was used in wind-tunnel experiments to simulate the effect of the presence of a water surface on the air flow about a wing. This technique has been criticized by various authors for a number of reasons. Nevertheless, experiments performed on representative configurations have indicated that the method is suitable for assessing the accuracy of many features of the theories.

CONTENTS

III. EXPERIMENTAL INVESTIGATION

REFERENCE SYSTEM

In this thesis, chapters are distinguished by roman numerals. Within each chapter, sections and equations are numbered consecutively in arabic numerals. References to sections or equations inside the same chapter are not prefixed by the chapter number; the remainder are.

References to original papers are listed near the end of the thesis with the names of the authors in alphabetical order.

LIST OF PRINCIPAL SYMBOLS

AR	Wing aspect ratio = b/c
$a^{(w)}$	Lift derivative $\partial\overline{C}_L/\partial\alpha^{(w)}$
$a^{(E)}$	Lift derivative $\partial\overline{C}_L/\partial\alpha^{(E)}$
$a_o^{(e)}$, $a_o^{(o)}$	Coefficients of even and odd vortex distributions (II.2.35)
$a_o, a_1, \ldots a_n$	Coefficients of vortex distribution (II.3.3)
b	Span of wing and vortex trace
B_m	Transformation constants (Section I.3.2)
B_m	Coefficients of superposition flows (Section II.5.22)
c	Chord of wing and cylindrical surface
$C, \overline{C}$	Transformation constants
C_p	Pressure coefficient
C_L	Sectional-lift coefficient
C_{DB}	Sectional boundary-layer-drag coefficient
C_T	Sectional edge-thrust coefficient
$\overline{C}_L$	Overall-lift coefficient
$\overline{C}_{L(C.T.)}$	Overall-lift coefficient associated with chordwise camber and thickness
$\overline{C}_D$	Overall-drag coefficient
$\overline{C}_{Di}$	Overall induced-drag coefficient
$\overline{C}_{DB}$	Overall boundary-layer-drag coefficient
$\overline{C}_D^{(w)}$	Overall-drag coefficient of wing
$\overline{C}_D^{(E)}$	Overall-drag coefficient of both end plates
$\overline{C}_{Di}^{(w)}$	Overall induced-drag coefficient of wing
$\overline{C}_{DB}^{(w)}$	Overall boundary-layer-drag coefficient of wing
$\overline{C}_{DB}^{(E)}$	Overall boundary-layer-drag coefficient of both end plates
$\overline{C}_S$	Overall side-force coefficient of one end plate plus its image beneath the 'ground'

based on the wing area bc

$D_f(y)$	Sectional drag in forward flight
$D_r(y)$	Sectional drag of a wing in reverse flight having a y' component of vorticity identical with the y component of vorticity of forward flight
$D_i(y)$	Induced drag gradient = $\frac{1}{2}\rho w_\infty(y)\Gamma(y)$
$\overline{D}_f$	Overall drag in forward flight
$\overline{D}_i$	Overall induced drag
$\overline{D}_i^{(w)}$	Overall induced drag of wing
$\overline{D}_i^{(E)}$	Overall induced drag of both end plates
$\partial/\partial n$	Differentiation normal to a contour
$f(2y/b)$	Function employed to define the class of vortex distribution $\gamma(x,y) \equiv \gamma(x)f(2y/b)$
h	Height of wing trace above ground
h_p	Height of wing pivot above ground
h_t	Height of wing trailing edge above ground
k	Transformation parameter and modulus of elliptic functions
ℓ	Dimension of each end-plate trace
ℓ_p	Distance between end-plate base and wing pivot (see Fig. 34)
$P_m^{(w)}, P_m^{(E)}$ $Q_{mn}^{(w)}, Q_{mn}^{(E)}$ $R_m^{(w)}, R_m^{(E)}$ $S_{mn}^{(w)}, S_{mn}^{(E)}$	Non-dimensional quantities defined in equations (II.5.21)
q	Parameter of theta functions = $\exp(-\pi K'/K)$
q	Strength of source distribution used to represent thickness
R, R_1, R_2	Residuals obtained by interchanging the order of double integrations

R_c		Chordal Reynolds number based on U_o
s		Complex variable of rectangular plane
s_1	=	$sn^{-1}(\lambda/k)/2K$
s_2	=	$dn^{-1}(1/\alpha,k')/2K$
(s,n)		Curvilinear, orthogonal coordinate system of vortex trace, n being normal to the trace
s		Distance along outside of closed configuration in a direction normal to wind
t		Complex variable of upper half-plane
$t^{(n)}$		Complex variable of approximations to an exact upper half-plane
T		Sectional edge thrust
U_o		Forward speed of wing
$v_\infty(z)$		y - wash at trace of starboard end plate in Trefftz plane
$v_{n\infty}(s)$		n - wash at vortex trace in Trefftz plane
$v_{nf}(x,s)$		n - wash at lifting system in forward flight
$v_{nf}^{(e)}, v_{nf}^{(o)}$		n - washes at lifting system in forward flight corresponding to the vortex distributions $\gamma^{(e)}(x,s)$ and $\gamma^{(o)}(x,s)$
$w_\infty(y)$		Upwash at wing trace in Trefftz plane
$w_f(x,y)$		Upwash at wing in forward flight
$w_f^{(e)}, w_f^{(o)}$		Upwashes at wing in forward flight corresponding to the vortex distributions $\gamma^{(o)}(x,y)$ and $\gamma^{(o)}(x,y)$
$w_f(x',y')$		Upwash at wing in reverse flight having a y' component of vorticity identical with y component of vorticity of forward flight
W		Complex potential of flow in Trefftz plane = $\phi + i\psi$
(x,y,z)		Right-handed, cartesian coordinate system fixed with respect to wing; z is upward

$\tilde{x}$	Chordwise distance measured from section leading edge
(x',y',z')	Coordinate system defined in equation (II.2.2)
y_c, z_c	y and z ordinates of the camber lines of the starboard end plate and wing, respectively
y_t, z_t	y and z ordinates of the outside surface of the thickness distributions of the starboard end plate and wing, respectively, when $\alpha^{(E)} = \alpha^{(w)} = 0$
α	Transformation parameter
α	Angle of incidence
$\alpha^{(w)}$	Incidence of wing
$\alpha_o^{(w)}$	Incidence of wing for zero overall lift
$\alpha^{(E)}$	Incidence of end plates
$\{\alpha^{(E)}/\alpha^{(w)}\}_{eq}$	Incidence ratio of uncambered configuration of zero thickness yielding the same induced-drag factors as a thick, cambered configuration
$\alpha_b^{(E)}$	End-plate wedge angle (see Fig. 34)
β	Transformation parameter
β	Vortex-distribution parameter defined in equation (II.2.44)
Γ	Circulation
$\gamma(x,s)$	s component of vorticity of lifting system = $\partial\Gamma(x,s)/\partial x$
$\gamma^{(e)}, \gamma^{(o)}$	Even and odd components of the chordwise distribution of s-wise vortices
γ_t	Chordwise distribution of s-wise vortices associated with thickness
γ_w, γ_E	Chordwise distributions of s-wise vortices corresponding to the camber distributions of wing and end plates
γ	Angle between base and top of end plate (see Fig. 34)
$\Delta\beta(\alpha^{(w)}, \infty)$	Non-linear increment in β deduced from de Haller's (1936) theory
$\varepsilon(\theta)$	Radial coordinate of indentation AB in t plane (see Fig. 6)

$\bar{\varepsilon}(\tilde{\theta})$		Radial coordinate of indentation AB in s plane (see Fig. 8)
ε		Small parameter
θ		Angular coordinate of indentation AB in t plane (see Fig. 6)
θ	=	$\cos^{-1}\xi$ (Chapter II)
κ	=	$(2C/bk)^2$
κ		Aerofoil-section curvature
λ		Transformation parameter
λ	=	$2\mathfrak{l}/c$
μ	=	$\pi/2\mathfrak{R}$
ξ	=	$2x/c$
ξ'	=	$2x'/c$
ρ		Density of medium surrounding wing
σ		Overall induced-drag factor defined in equation (I.2.33)
$\sigma^{(w)}$		Overall induced-drag factor of wing } defined in
$\sigma^{(E)}$		Overall induced-drag factor of end plates } equation (II.5.31)
Σ	=	$\bar{D}_i/\frac{1}{2}\rho w_\infty^2 b^2$
ϕ		Velocity potential of flow relative to wing
Φ	=	$\sin^{-1} k$
χ	=	$\mathrm{sn}^{-1}(\lambda/k)90/K$
ψ		Stream function of flow in Trefftz plane
Ω		Complex variable of Trefftz plane = y + iz

Subscripts

T	Quantity uncorrected for wind-tunnel interference
c	Combined-flow quantity
u	Upper part of vortex trace
l	Lower part of vortex trace

INTRODUCTION

1. General

Interest in the possibility of high-speed, economic, overwater travel has been encouraged in recent years by rapid advances in the technology of hovercraft and hydrofoils. Unfortunately, at present, both types of craft would seem to be economically inferior to conventional subsonic aircraft at speeds in excess of 100 knots. This is due, on the one hand, to the large momentum drag of the hovercraft and on the other to the hydrodynamic drag of the hydrofoil.

One method which has been proposed for reducing the inherent large drag of these craft relies on aerodynamic surfaces to off-load the cushion or hydrodynamic lifting systems. Provided the design of the aerodynamic surfaces is not greatly compromised by considerations other than aerodynamic the result could be a reduction in overall drag. However, there are indications from various authors, including Ando, Miyashita and Terai (1964) and Strand, Royce and Fujita (1962), that structural requirements will favour wings of low aspect ratio. In turn, this implies that the induced drag of the wing could be prohibitively large. On the other hand, this component of drag is reduced somewhat by the proximity of the water surface. When smooth this acts in a similar manner to a solid, impermeable ground plane and thus provides what is known as 'ground effect'. This phenomenon, in its various forms, has been discussed in numerous papers including those of Wieselsberger (1921) and de Haller (1936). Using the linearized lifting-surface theory they showed that the induced drag of a planar wing flying at a given lift decreases monotonically to zero as the ground is approached. In practice, however, the minimum operating height of the wing will be limited by the need to minimize wave impact. Consequently, there will exist an upper bound to the amount of favourable ground effect obtainable by a planar wing.

In the next section, two practical methods of overcoming this apparent limitation will be described.

2. The ground-effect wing as a maritime craft.

In recent years, a number of maritime craft, which are supported during the cruise almost wholely by aerodynamic lifting surfaces, have been built. Ando (1966) refers to these craft as 'ground-effect wings' (G.E.Ws.). This title would seem to be preferable to the popular name 'ram wings' and will be used hereafter not only to describe such craft but also lifting surfaces which are close to the ground.

The Kawasaki KAG-3 represents a Japanese approach to the design of a G.E.W. This is a small prototype craft consisting basically of separate wing and fuselage structures and with planing hulls situated at the wing tips. These hulls act as aerodynamic end plates during the cruise as well as providing the craft with hydrodynamic form and support at low airspeed. This is one solution to the problem of reducing the induced drag of a planar G.E.W., the hulls tending to reduce the effective height of the trailing vortices above the ground. However, in the case of the KAG-3, the gap between the water surface and the planing hulls is a considerable proportion of the height of the wing above the water.

Flight tests have revealed that the cruise lift/drag ratio of the KAG-3 is 11.4. This low figure is partly attributable to the low aspect ratio of the wing (0.75) and the apparent failure of the planing hulls to prevent the formation of a powerful trailing - vortex sheet.

Vehicle Research Corporation's prototype of the projected 'Columbia' G.E.W. is an example of a design which embodies the requirement of low induced drag during the cruise. The craft is supported at zero and low airspeed by a peripheral-jet sustained cushion of air. During the cruise, the front and rear jets are

shut down, allowing the integrated wing-body layout to generate aerodynamic lift. The side jets remain on, effectively sealing the gaps between the spanwise extremities of the craft and the water surface.

The 'Columbia' prototype and the KAG-3 fall respectively into classes of G.E.W. which will be called 'closed' and 'open'. The former class typifies those G.E.Ws. which may, in theory, be designed for zero induced drag whilst giving a non-zero lift. All G.E.Ws. which do not come under this definition are referred to as open.

That the KAG-3 is an open G.E.W. follows from the fact that the lower extremities of its end plates are above the water surface. According to the fundamental theorem of Helmholtz, vortices cannot end in space in a frictionless fluid. Thus, trailing vorticity and hence induced drag are necessary features of the flow around, and the drag forces on, the KAG-3. The 'Columbia' prototype, on the other hand, is ostensibly closed by virtue of the jet sheets at its spanwise extremities. In other words, the trailing vorticity of this craft is virtually eliminated by utilizing the jet sheets to continue the 'bound' vortices to the water surface.

3. The aerodynamic performance of ground-effect wings: possible area for study.

3.1 Open ground-effect wings.

Over a considerable period, theoretical and experimental research has been conducted into the aerodynamic properties of wings flying near the ground. Until recently, however, the emphasis of this work has been on the determination of the effect of the ground on the take-off and landing performance of conventional aircraft. Consequently, the ratios of wing height to chord considered have invariably been larger than those of current G.E.W. designs. Furthermore, in the past, the theoretical analyses and experimental studies have been largely concerned with planar wings of large aspect ratio.

Recently, investigations with more relevance to G.E.W. design have been described. In particular, mention should be made of the experiments of Fink and Lastinger (1961) and Carter (1961). The first-named authors used the image method to determine the forces and moments on planar wings of various aspect ratios and rectangular planform in ground proximity. Carter, on the other hand, confined his attention to the forces and moments on planar, rectangular wings of aspect ratio unity and employed a towing carriage to convey the models above a water surface.

Both investigations gave results for the induced drag of planar wings which seem to be in reasonable accord with Wieselsberger's (1921) theory. However, Carter found that the agreement between this theory and experiment was far from adequate when end plates were attached to the wing. As the indications are that G.E.Ws. will require non-planar tip extensions to limit the induced drag to reasonable values, there would seem to be a need for a more suitable theory. For this reason, therefore, a theoretical method for calculating the minimum induced drag of planar wings with end plates in ground effect will be described in Chapter I. Subsequently, the results of this theory will be compared with experiment in Chapter III.

Within the limitations of the linearized lifting-surface theory, Saunders (1963) has obtained computer solutions for the lift and pitching moment of planar and non-planar wings in ground effect. His calculations of the lift/incidence slope of planar wings at zero incidence compare reasonably well with the experimental results of Carter and Fink. Unfortunately, linear theories such as Saunders' are necessarily restricted, in their predictions of the lift, to small wing incidence and camber. This limitation rather restricts their usefulness and there is certainly scope for improvement. Regrettably, in the case of open configurations, a consistent non-

linear theory would seem, at present, beyond our resources. The main reason for this is that there is no *a priori* knowledge of the shape of the trailing-vortex sheet.

3.2 Closed ground-effect wings

The prospects for theoretical work are better for closed configurations which would seem, in the cases of interest, to possess either weak or zero trailing vorticity. Consequently the non-linear effects associated with the trailing vortices may probably be neglected. An approximate theory, based on this approach, is applied to the determination of the lift of a closed wing/end-plate configuration in Chapter II.

Most of the available information on the design and performance of closed G.E.Ws. has come from the Vehicle Research Corporation. Among the papers released by this firm are those of Strand (1960) and Strand, Royce and Fujita (1962). In these reports a simple method, which has been used in the design of the 'Columbia', is described. This technique employs the assumption that the flow underneath the craft is one-dimensional whilst over the outer surface it is considered to be like that over a mound. On the basis of these simple concepts, Strand concluded that the induced drag of the craft is essentially zero. It is possible, however, that this conclusion would be modified by a more detailed theoretical method. The non-linear approach mentioned above is an attempt to provide such a method. This will be employed in Chapter II to obtain the induced drag of a closed wing/end-plate configuration. In Chapter III the induced drag and lift predicted by this method will be compared with experiment.

CHAPTER I

ON THE MINIMUM INDUCED DRAG OF OPEN GROUND-EFFECT WINGS

1. Basic considerations

1.1 Assumptions of the theory

In the analysis of the induced drag of two types of open ground-effect wing to be described in this chapter the following assumptions will be made:

(i) The flow around the wing is inviscid and incompressible.

(ii) The linearized lifting-surface theory, as formulated for example by Thwaites (1960), is applicable.

(iii) The water surface over which the wing flies behaves like a solid, impermeable ground plane.

Assumption (i) should lead to a reasonable approximation for the flow far in the rear of the wing provided (a) the Reynolds number based on a typical wing chord is sufficiently large and (b) the Mach number is small compared with unity.

One of the assumptions of the linearized lifting-surface theory is that the wing and its trailing-vortex sheet lie on a cylindrical surface with generators parallel to the direction of the motion of the wing. As there is no force on the trailing vortices it follows that the trailing-vortex vector is everywhere in the direction of the flow relative to, and infinitely far forward of, the wing. Thus, if the wing consists of a single surface, the spanwise cross-section of the vortex sheet is the same as that at the maximum span of the wing.

1.2 Conditions for minimum induced drag

Within the limitations imposed by assumptions (i) and (ii) Munk (1921) has given an elaborate proof of the condition for the induced drag of a lifting system to be a minimum subject to the lift being given. This condition, which is necessary and sufficient,

may be stated as follows:

'The induced drag of an arbitrary lifting system is a minimum, for a given lift, provided that the normal component of velocity at the vortex sheet infinitely far in the rear of the lifting system, is everywhere proportional to the cosine of the local angle of lateral inclination of the sheet'.

In mathematical terms this may be written as

$$v_{n\infty} = w_{\infty} \cos \theta \ . \qquad (1.1)$$

Here $v_{n\infty}$ and θ are the local component of normal velocity and angle of lateral inclination at the vortex sheet infinitely far behind the lifting system and w_{∞} is a constant having the dimensions of velocity.

The direction of positive $v_{n\infty}$ is illustrated in the sketch below which shows a spanwise cross-section of a typical vortex sheet (the vortex trace) viewed in the direction of the motion of the lifting system.

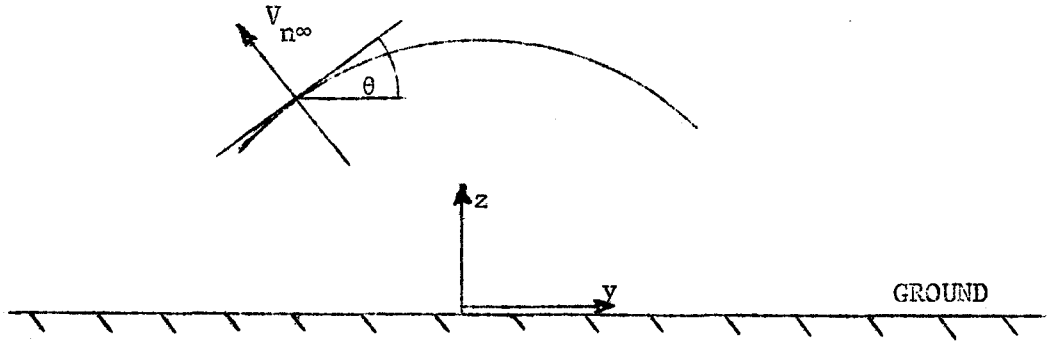

The plane infinitely far behind, and perpendicular to the direction of motion of the lifting system is known as the Trefftz plane. As a consequence of assumptions (i) and (ii) the flow in this plane is two-dimensional and characterized by a velocity potential, ϕ, which is a solution of the equation

$$\partial^2\phi/\partial y^2 + \partial^2\phi/\partial z^2 = 0. \qquad (1.2)$$

This is the well-known Laplace equation in two dimensions, y and z being the cartesian coordinates shown in the sketch above.

Thus, in order to determine the distribution of velocity potential in the Trefftz plane accompanying minimum induced drag, it is necessary to solve equation (1.2) subject to equation (1.1) being satisfied. Additional conditions, the nature of which depends on whether the vortex trace is adjacent to or isolated from boundaries, will also need to be satisfied.

1.3 Flow – superposition methods.

The linearity of Laplace's equation permits the superposition of its solutions to obtain other, perhaps more complex, solutions. This fact prompted Munk (1921) to suggest a simple method of obtaining the velocity potential in the Trefftz plane of isolated lifting systems having an induced drag which is a minimum for a given lift. This consists of superposing on the Trefftz-plane flow a flow which destroys the normal component of velocity at the vortex trace without disturbing the discontinuity in ϕ there. Munk found that a flow having the desired property is the uniform stream described by

$$\phi = -w_\infty z \qquad (1.3)$$

The addition of this flow to the Trefftz-plane flow reduces the problem to that of finding the velocity potential of a uniform flow past an obstacle shaped like the trace. This may be considered solved when the appropriate conformal transformation between the Trefftz plane and the upper half-plane has been discovered. The velocity potential of the Trefftz-plane flow is then determined by subtracting the superposition velocity potential (1.3) from the velocity potential of the combined flow.

For isolated lifting systems Munk's method represents a considerable improvement over methods relying on singularity distributions. Unfortunately, it is usually not as suitable when the vortex trace is in the vicinity of additional boundaries. The reason for this is that, in general, a uniform stream does not satisfy the additional boundary conditions. Consequently the velocity potential of the combined flow may be as difficult to determine as that of the Trefftz-plane flow. As an illustration, suppose that the same lifting system is near an infinite ground plane. As with the isolated lifting system the boundary condition for the normal velocity of the combined flow at the vortex trace is of the obstacle flow type. At the trace of the ground, on the other hand, the normal velocity is non-zero. Therefore a suitable source distribution will be required in the upper half-plane. In consequence, the determination of the velocity potential of the combined flow will entail an integration.

The advantages of Munk's method may be recovered for lifting-systems near additional solid boundaries by employing a potential flow which when added to the Trefftz-plane flow:

(i) destroys the normal component of velocity at the vortex trace;

(ii) does not alter the discontinuity in the velocity potential at the vortex trace;

(iii) satisfies the additional boundary conditions in the finite part of the Trefftz-plane.

The velocity potential of the resulting combined flow is essentially determined once the conformal transformation between the physical plane and the upper half-plane has been found.

This method may be considered a generalization of Munk's method to include the presence of solid boundaries.

2. The planar ground-effect wing of minimum induced drag.

In this section, the determination of the minimum induced drag of a planar wing in ground effect will be described. This problem was considered by de Haller (1936). However, the expression he derived for the velocity potential of the Trefftz-plane flow is somewhat cumbersome and his results for the induced drag would seem to have been obtained either by numerical or graphical integration.

The method to be presented here, which is based on the combined - flow method discussed previously, permits the derivation of the minimum induced drag in analytical form. In consequence, it is more suitable than de Haller's method for checking the accuracy of a perturbation technique which will be used to determine the influence of end plates in Section 3.

2.1 The flow problem.

Fig. 1 shows the Trefftz plane of a planar ground-effect wing. It will be seen that the vortex trace is of span b and height h above the ground. Also evident in the figure is the barrier AB, which renders the Trefftz plane singly connected, and the bounding contour IABCEGHI. This consists of 'the point at infinity' I, the trace of the ground, the vortex trace and the barrier.

Equation (1.1) indicates that the induced drag of a planar wing is a minimum for a given lift if $v_{n_\infty} = w_\infty$. Thus, by reference to the coordinate system of Fig. 1, the boundary conditions for the normal velocity at the bounding contour may be written as follows:

$$\left.\begin{array}{lll} \text{(i)} & \partial\phi/\partial n = -w_\infty; & |y| \leq b/2,\ z = +h^+; \\ \text{(ii)} & \partial\phi/\partial n = +w_\infty; & |y| < b/2,\ z = +h^-; \\ \text{(iii)} & \partial\phi/\partial n = 0; & |y| < \infty,\ z = 0; \\ \text{(iv)} & \partial\phi/\partial n = 0; & y = 0,\ 0 < z < +h; \\ \text{(v)} & |dW/d\Omega| \sim 0; & |\Omega| \to \infty. \end{array}\right\} \qquad (2.1)$$

In the above expressions $\partial/\partial n$ denotes normal differentiation outward from the domain D (shown in Fig. 1) and $+h^+$ and $+h^-$ are to be interpreted as $\lim_{\varepsilon\to 0}(+h+\varepsilon)$ and $\lim_{\varepsilon\to 0}(+h-\varepsilon)$. Also, $W = \phi + i\psi$ is the

complex potential, ψ being the stream function, and $\Omega = y + iz$ is the complex variable of the Trefftz plane.

It should be remarked that condition (2.1) (iii) follows from considerations of the symmetry of the Trefftz-plane flow.

The domain D is mapped onto the upper half-plane t (Fig. 2) by means of the Schwarz-Christoffel formula. This has been given in general terms by Thwaites (1960) and in the present case may be written in the form

$$d\Omega/dt = C(\beta^2-t^2)(1-t^2)^{-\frac{1}{2}}(1-k^2t^2)^{-\frac{1}{2}};\ \beta\leq 1\leq 1/k, \qquad (2.2)$$

where C is the (real) transformation constant whilst β and k are parameters of the transformation.

Equation (2.2) may be integrated with the aid of the transformation

$$t = sn\{2K(k)s,\ k\}. \qquad (2.3)$$

Here K(k) is the complete elliptic integral of the first kind and $sn\{2K(k)s,\ k\}$ is a Jacobian elliptic function, each of these quantities being defined by Byrd and Friedman (1954). Hereafter, unless otherwise stated, it is to be understood that the elliptic functions and integrals are functions of k.

By differentiating equation (2.3) with respect to 2Ks there is obtained, after reference to equations (121.00) and (713.01) of Byrd and Friedman,

$$dt/d2Ks = (1-sn^2 2Ks)^{\frac{1}{2}}(1-k^2sn^2 2Ks)^{\frac{1}{2}}. \qquad (2.4)$$

Therefore, if equations (2.2), (2.3) and (2.4) are combined, there results

$$d\Omega/d2Ks = C(\beta^2 - sn^2 2Ks). \qquad (2.5)$$

which may be integrated with the aid of equation (310.02) of Byrd and Friedman to yield the result

$$\Omega = C\left[2\beta^2 Ks - \{2Ks - E(2Ks)\}/k^2\right] + C_1 .$$

In this expression E(2Ks) is the incomplete elliptic integral of the second kind, as defined by Byrd and Friedman, and C_1 is the integration constant.

The s plane, which is illustrated in Fig. 3, will be seen to consist of the interior of a rectangle having corners A,B,G and H. The complex coordinates of these corners may be found by employing the properties of the transformation (2.3) given by Byrd and Friedman (p.17). Thus it is found that, at A,B,G and H, 2Ks is $-K + iK'$, $-K$, $+K$ and $+K + iK'$, where $K' = K(k')$ and $k' = (1 - k^2)^{\frac{1}{2}}$.

The requirement of correspondence between the Ω and s planes at point G demands that

$$ih = C\left[\beta^2 K - \{K - E(K)\}/k^2\right] + C_1 . \qquad (2.6)$$

Similarly, the requirement of correspondence at B leads to the result

$$ih = -C\left[\beta^2 K - \{K - E(K)\}/k^2\right] + C_1 . \qquad (2.7)^*$$

Therefore, by comparing equations (2.6) and (2.7), it is found that

$$C_1 = ih \qquad (2.8)$$

and

$$\beta^2 = \{K - E(K)\}/k^2 K. \qquad (2.9)$$

Correspondence of the Ω and s planes at point H is assured if

$$0 = C\left[\beta^2(K + iK') - \{K + iK' - E(K + iK')\}/k^2\right] + C_1 . \qquad (2.10)$$

This result may be reduced somewhat by employing equations (122.02), (140.01) and (141.01) of Byrd and Friedman to derive the relationship

$$E(K + iK') = E(K) + i(2E(K)K' - \pi)/2K . \qquad (2.11)$$

This may be combined with equations (2.8), (2.9) and (2.10) to give

*In obtaining this expression use is made of the fact that $E(-2Ks) = -E(2Ks)$.

$$0 = C\left[\frac{(K-E(K))(K+iK')}{k^2K} - \frac{\{K+iK'-E(K)-i(2E(K)K'-\pi)/2K\}}{k^2}\right] + ih$$

which after rearrangement gives the result

$$h = \pi C/2k^2K. \qquad (2.12)$$

The Ω and s planes correspond at point E if

$$b/2 + ih = C\left[\beta^2 sn^{-1}\beta - \{sn^{-1}\beta - E(sn^{-1}\beta)\}/k^2\right] + C_1.$$

Consequently, by combining this result with equations (2.8) and (2.9), one finds that

$$b = 2C\{E(sn^{-1}\beta)K - E(K)sn^{-1}\beta\}/k^2K. \qquad (2.13)$$

Equations (2.12) and (2.13) may be combined to yield the result

$$2h/b = \pi/2\{E(sn^{-1}\beta)K - E(K)sn^{-1}\beta\}. \qquad (2.14)$$

So far, the present method has differed little from that of de Haller. The difference between the methods is in their treatment of the flow problem. The present technique employs the flow-superposition method proposed in Section 1.3 whilst de Haller's approach involves the integration of singularity distributions. As will be seen, the present technique is relatively simple, leading to a closed-form solution for the induced drag.

A class of complex potentials which is regular in the finite part of the Ω plane and satisfies boundary conditions (2.1)(iii) and (iv) is given by

$$W_m = A_m\Omega^{2m} \quad ; \quad m = 1,2,3, \ldots\ldots,$$

where A_m are real constants.

The z velocity components at the vortex trace associated with W_m, namely w_m, are given by

$$w_m = 2m\, A_m\, y^{2m-1} \sum_{n=1}^{n=m} \frac{(-1)^n (2m-1)!\,(h/y)^{2n-1}}{(2(m-n)!\;(2n-1)!}\,.$$

For m=1 this becomes

$$w_1 = -\,2A_1 h.$$

which, it will be seen, is equal and opposite to the z component of velocity of the Trefftz-plane flow at the vortex trace if

$$A_1 = w_\infty/2h.$$

It follows, therefore, that, with this value of A_1, w_1 may be used as a superposition flow in view of the fact that it satisfies requirements (i), (ii) and (iii) given in Section 1.3.

An examination of the resulting combined flow indicates that $\partial\phi_c/\partial n = 0$ at all segments of the bounding contour in the finite part of the Ω plane, the subscript c denoting combined-flow conditions. Therefore in the t plane

$$\partial\phi_c/\partial n = 0; \quad |\mathrm{Re}(t)| < \infty\,, \quad \mathrm{Im}(t) = 0. \tag{2.15}$$

The only remaining boundary condition to be satisfied by the combined flow in the t plane is an asymptotic one near the point at infinity. This may be determined by noting that

$$dW_c/d\Omega \sim w_\infty \Omega/h; \quad |\Omega| \to \infty. \tag{2.16}$$

In order to determine the corresponding condition in the t plane it is necessary to consider the behaviour of $d\Omega/dt$ and Ω for large $|t|$. Thus, by expanding the right-hand side of equation (2.2) in powers of $1/t^2$, it is found that

$$d\Omega/dt = (-C/k) + O(1/t^2); \quad |t| \to \infty. \tag{2.17}$$

In turn, this expression may be integrated to yield

$$\Omega = (-Ct/k) + C_2 + O(1/t); \quad |t| \to \infty, \tag{2.18}$$

where C_2 is the integration constant. Therefore, by combining equations (2.16), (2.17) and (2.18), it is found that

$$dW_c/dt \sim w_\infty C^2 t/k^2 h \; ; \quad |t| \to \infty. \tag{2.19}$$

There is no unique complex potential satisfying equations (2.15) and (2.19). There are, however, two additional conditions to be imposed on the combined-flow solution. Firstly, only Trefftz-plane flows with regular complex potentials within the domain D are physically acceptable. Therefore, as W_1 is regular in the finite part of the Ω plane, it is necessary for W_c to be regular in the finite part of domain D. Secondly, the Trefftz-plane flow and the superposition flow are symmetrical with respect to the z axis. Hence the combined flow is required to be symmetrical about this axis and, in consequence, also about the imaginary axis of the t plane.

A complex potential which satisfies equations (2.15), (2.19) and the two additional conditions mentioned above is given by

$$W_c = (w_\infty C^2 t^2/2k^2 h) + C_3, \tag{2.20}$$

where C_3 is an arbitrary constant.

The complex potential of the Trefftz-plane flow, W, may be found by subtracting W_1 (with the appropriate value of A_1) from W_c. Thus, as W_1 is single-valued at the vortex trace, it follows from equation (2.20) that the jump in velocity potential there, $\Gamma(y)$, is given by

$$\Gamma(y) = \phi_u(y) - \phi_l(y) = w_\infty C^2 \{t_u^2(y) - t_l^2(y)\}/2k^2 h. \tag{2.21}$$

Here the subscripts u and l imply that the functions concerned are to be evaluated at adjacent points on the upper and lower segments of the vortex trace, respectively.

It will be observed that $\Gamma(y)$ does not depend on the arbitrary constant C_3.

Equation (2.3) may be employed to rewrite equation (2.21) as

$$\Gamma(y) = w_\infty C^2\{sn^2 2Ks_u\,(y) - sn^2 2Ks_l\,(y)\}/2k^2h.$$

This should be compared with the result obtained by de Haller which, in the present notation, is given by

$$\Gamma(y) = \frac{2\pi w_\infty C}{k^2 K} \sum_{m=1}^{\infty} \frac{q^m(1+q^{2m})}{(1-q^{2m})^2} \{\cos 2m\pi\, s_u\,(y) - \cos 2m\pi\, s_l\,(y)\},$$

where

$$q = \exp(-\pi K'/K).$$

2.2 Determination of the induced drag.

Robinson and Laurmann (1956) show that, to the order of approximation of the linearized theory, the overall induced drag of a wing, $\overline{D}_i$, may be written as

$$\overline{D}_i = \tfrac{1}{2}\rho \int_T \phi(\partial\phi/\partial n)\,d\overline{s}. \qquad (2.22)$$

In this expression, ρ is the density of the medium surrounding the wing and the subscript T denotes that the line integration is to be performed in a clockwise fashion about the vortex trace in the Ω plane. The term $d\overline{s}$ is an element of length around the vortex trace.

For a planar wing of minimum induced drag it is possible to rewrite equation (2.22) in the form

$$\overline{D}_i = -\tfrac{1}{2}\rho w_\infty \int_T \phi\, d\Omega. \qquad (2.23)$$

Thus, by noting that $\phi=\phi_c-\phi_1$ and employing equations (2.20), it is found that

$$\overline{D}_i = -\tfrac{1}{2}\rho w_\infty \int_T \{(w_\infty C^2 t^2/2k^2 h) + \mathrm{Re}(C_3) - \phi_1\} d\Omega. \qquad (2.24)$$

The last two terms under the integral sign of equation (2.24) do not contribute to $\overline{D}_i$ as they are single-valued at the vortex trace. Therefore, by employing equations (2.3) and (2.5), it is permissible to rewrite equation (2.24) in the form

$$\overline{D}_i = -\rho w_\infty^2 C^3 \int_{-K}^{+K} sn^2 2Ks\ (\beta^2 - sn^2 2Ks)\ d2Ks/4k^2 h, \qquad (2.25)$$

the subscript T being dropped in favour of the limits of the integration.

The integral of equation (2.25) may be evaluated explicitly with the aid of Byrd and Friedman's equations (310.02) and (310.04) to give the result

$$\overline{D}_i = -\rho w_\infty^2 C^3 \left[\{2\beta^2(K-E(K))/k^2\} - 2\{K(2+k^2) - 2E(K)(1+k^2)\}/3k^4\right] /4k^2 h. \qquad (2.26)$$

The term C may be eliminated from equation (2.26) with the aid of equation (2.12) to give the expression

$$\overline{D}_i = -2\rho w_\infty^2 k^4 K^3 h^2 \left[\{2\beta^2(K-E(K))/k^2\} - 2\{K(2+k^2) - 2E(K)(1+k^2)\}/3k^4\right] /\pi^3. \qquad (2.27)$$

It is convenient at this point to define a non-dimensional quantity Σ as

$$\Sigma = \overline{D}_i / \tfrac{1}{2}\rho w_\infty^2 b^2. \qquad (2.28)$$

Thus, by combining this equation with equations (2.14) and (2.27), it is found that

$$\Sigma = \frac{-k^4K^3\left[\{2\beta^2(K-E(K))/k^2\} - 2\{K(2+k^2) - 2E(K)(1+k^2)\}/3k^4\right]}{4\pi\{E(sn^{-1}\beta)K - E(K)sn^{-1}\beta\}^2}. \tag{2.29}$$

Robinson and Laurmann show that the linearized theory yields the following expression for the overall lift of a wing:

$$\bar{L} = \rho U_o \int_T \phi \, dy, \tag{2.30}$$

where $\bar{L}$ is the overall lift and U_o is the forward speed of the wing. Thus, for the present configuration, the overall lift may be written as

$$\bar{L} = \rho U_o \int_T \phi \, d\Omega. \tag{2.31}$$

Hence, by comparing equations (2.23), (2.28) and (2.31), it is evident that

$$\bar{L} = -\rho w_\infty U_o b^2 \Sigma. \tag{2.32}$$

De Haller defines the induced-drag factor σ according to the relationship

$$\sigma = \pi\rho U_o^2 b^2 \bar{D}_i / 2\bar{L}^2. \tag{2.33}$$

Therefore, upon combining equations (2.28), (2.32) and (2.33), it is found that

$$\sigma = \pi/4\Sigma. \tag{2.34}$$

Consequently, substituting equation (2.29) into equation (2.34), one has, after rearrangement,

$$\sigma = \frac{3\pi^2\{E(sn^{-1}\beta)K - E(K)sn^{-1}\beta\}^2}{2K^3\{K(2+k^2) - 2E(K)(1+k^2) - 3\beta^2k^2(K-E(K))\}}. \tag{2.35}$$

The induced-drag factor may be determined as a function of 2h/b by employing equations (2.9), (2.14), (2.35) and the tables of K and E(2Ks) given by Byrd and Friedman for various k. The graph of σ against 2h/b thus obtained is shown in Fig. 4 where it is compared

with curves given by Wieselsberger (1921) and de Haller. It will be seen that de Haller's results for σ are consistently lower than the present values in the range $0.5 \leqslant 2h/b \leqslant 1.2$. In particular, for $2h/b = 0.7$, de Haller's value of σ is approximately 95% of the value given by the present method.

Wieselsberger's theory, which is based on the assumption that $\Gamma(y)$ is elliptic, is seen to give results which lie close to the results of the present theory.

3. The influence of end plates.

This section deals, in the main, with the determination of the minimum induced drag of planar wings with end plates in ground effect.

The vortex trace of the particular end-plate configuration to be examined is illustrated in Fig. 5. It will be inferred from this that the end plates project vertically downwards from the wing tips.

As before, the domain D of the Trefftz plane Ω (Fig. 5) is rendered singly connected by the barrier AB and is transformed to the upper half-plane t by the Schwarz - Christoffel transformation

$$\frac{d\Omega}{dt} = \frac{\overline{C}(\alpha^2-t^2)(1-t^2)^{\frac{1}{2}}}{(1-\lambda^2t^2)^{\frac{1}{2}}(1-\delta^2t^2)^{\frac{1}{2}}(1-k^2t^2)^{\frac{1}{2}}}, 1 \leqslant \alpha \leqslant 1/k \leqslant 1/\lambda \leqslant 1/\delta. \tag{3.1}$$

In this expression $\overline{C}$ is the (real) transformation constant and α, k, λ and δ are parameters of the transformation. The k defined here should not be confused with the k employed previously. The reason for its retention as a quite different parameter arises from the need to comply with the convention of elliptic functions.

In principle, the transformation between the Ω and t planes may be established by direct integration of equation (3.1). Unfortunately, the integral which occurs is of the hyperelliptic type (Byrd and Friedman p. 252) and seems not to be amenable to explicit evaluation.

It is necessary, therefore, to devise an alternative method of solving equation (3.1) analytically.

3.1 Description of the proposed method.

The method to be employed may be summarized as follows:

(i) The right-hand side of equation (3.1) is expanded in powers of a parameter which is considered to be small for the Trefftz-plane configurations of interest.

(ii) The first term of the resulting expansion is integrated to give either an approximate transformation between the Ω plane and the upper half-plane or an exact transformation between the Ω plane and a perturbed upper half-plane. Interpreted in the former sense, the transformation fails to be uniformly valid in a restricted area of the Ω plane, usually in the region of interest. For this reason, therefore, the method to be employed here utilizes the second interpretation.

(iii) An additional conformal transformation is needed to map the perturbed upper half-plane onto an exact upper half-plane.

A suitable small parameter for the expansion may be found by examining the 'exact' solution for the planar wing given previously. This suggests that, as $\lambda \to \delta$, $h/b \to 0$. Therefore, as current G.E.W. designs are intended for operation at small h/b, an appropriate small parameter would seem to be $\delta' = (\lambda^2-\delta^2)^{\frac{1}{2}}$. Thus the right-hand side of equation (3.1) is expanded in powers of δ' and all but the first term are neglected to give the result

$$d\Omega/dt = \bar{C}(\alpha^2-t^2)(1-t^2)^{\frac{1}{2}}/(1-\lambda^2t^2)(1-k^2t^2)^{\frac{1}{2}}. \qquad (3.2)$$

Here, for convenience, t is also used to denote the perturbed upper half-plane which is illustrated in Fig. 6. This figure shows that the perturbations consist of the indentations AE and GH surrounding the points $t = \mp 1/\lambda$.

In general, the shape of either indentation is not simple.

Consequently it may be difficult to transform the perturbed plane into an exact upper half-plane. It is possible, however, that a simplification may be achieved by employing various approximations to the shape of the indentations which are known to be asymptotically correct as $h/b \to 0$. Therefore, in order to examine the accuracy of such an approach, it will be applied to the planar-wing problem in Section 3.2. The success of the method will be gauged by comparing the results obtained for σ with those given by the 'exact' solution.

3.2 Application to the planar-wing problem.

For the planar wing, $k=1$. Therefore, as $1 \leq \alpha \leq 1/k$, equation (3.2) reduces to the following form:

$$d\Omega/dt = \overline{C}(1-t^2)/(1-\lambda^2 t^2).$$

This expression may be integrated to yield the result

$$\Omega = \frac{\overline{C}}{\lambda^2}\{t + \frac{(1-\lambda^2)}{2\lambda}\ln(\frac{\lambda t-1}{\lambda t+1})\} + C_4, \qquad (3.3)$$

where C_4 is the integration constant.

The t plane corresponding to the planar wing is similar to that shown in Fig. 6 except that the points C and C' coincide with D at $t = -1$ and, at $t = +1$, E and E' coincide with F. Hereafter, these coincident points will be called C and E, respectively.

Point-to-point correspondence between the Ω and t planes at C and E demands that

$$-\frac{b}{2} + ih = \frac{\overline{C}}{\lambda^2}\{-1 + \frac{(1-\lambda^2)}{2\lambda}\ln(\frac{1+\lambda}{1-\lambda}) + \frac{i\pi(1-\lambda^2)}{2\lambda}\} + C_4 \qquad (3.4)^*$$

and

$$\frac{b}{2} + ih = \frac{\overline{C}}{\lambda^2}\{1 + \frac{(1-\lambda^2)}{2\lambda}\ln(\frac{1-\lambda}{1+\lambda}) + \frac{i\pi(1-\lambda^2)}{2\lambda}\} + C_4. \qquad (3.5)^*$$

By comparing equations (3.4) and (3.5) it is found that

$$\mathrm{Re}(C_4) = 0, \qquad (3.6)$$

$$\frac{b}{2} = \frac{\overline{C}}{\lambda^2}\{1 + \frac{(1-\lambda^2)}{2\lambda}\ln(\frac{1-\lambda}{1+\lambda})\} \qquad (3.7)$$

---

*That the principal values of the logarithms are taken in these equations follows from the fact that only the physical part of the Riemann sheet is being considered.

and $$h = \frac{\pi\bar{C}(1-\lambda^2)}{2\lambda^3} + \mathrm{Im}(C_4). \qquad (3.8)$$

On the segments of the real axis of the t plane where $|t|>1/\lambda$ the variable Ω is purely real, as is the bracketed term of equation (3.3). Thus it may be inferred from the same equation that $\mathrm{Im}(C_4)=0$. Therefore this result may be combined with equations (3.7) and (3.8) to give the expression

$$2h/b = \pi(1-\lambda^2)/[2\lambda + (1-\lambda^2)\ln\{(1-\lambda)/(1+\lambda)\}]. \qquad (3.9)$$

The curve of indentation AB may be defined by the equation

$$t = (-1+\varepsilon(\theta)e^{i\theta})/\lambda, \qquad (3.10)$$

where, with the origin at $t = -1/\lambda$, $\varepsilon(\theta)$ is the radial coordinate of the curve and θ is the angle between the radial generator and the real axis as shown in Fig. 6.

On the indentation AB, $\mathrm{Re}(\Omega) = 0$. Therefore, by substituting equations (3.6) and (3.10) into equation (3.3) and equating real parts, one finds that

$$\ln\{\varepsilon(\theta)\} = \tfrac{1}{2}\ln\{4-4\varepsilon(\theta)\cos\theta+\varepsilon^2(\theta)\}-2(1-\varepsilon(\theta)\cos\theta)/(1-\lambda^2). \qquad (3.11)$$

Thus, in order to find $\varepsilon(\theta)$, it is necessary to solve this equation. Unfortunately, it would seem to be rather difficult to obtain a solution in closed form.

Inspection of equation (3.9) shows that $h/b \sim 0$ as $\lambda\to1$. As B lies between $t = -1/\lambda$ and -1 this suggests the possibility that $\varepsilon(\theta) \sim 0$ as $h/b\to0$. Therefore equation (3.11) will be solved by an iteration scheme which employs the assumption that $\varepsilon(\theta)<<1$, namely

$$\ln\{\varepsilon^{(n)}(\theta)\} = \tfrac{1}{2}\ln[4-4\varepsilon^{(n-1)}(\theta)+\{\varepsilon^{(n-1)}(\theta)\}^2]-2(1-\varepsilon^{(n-1)}(\theta)\cos\theta)/(1-\lambda^2), \qquad (3.12)$$

with $\varepsilon^{(o)}(\theta) = 0$. Thus the first iterate for $\varepsilon(\theta)$ is given by

$$\varepsilon^{(1)}(\theta) = 2\exp\{2/(\lambda^2-1)\}. \qquad (3.13)$$

This iterate is evidently invariant with θ and, consistent with the previous postulation, approaches zero asymptotically as $h/b \to 0$.

The second iterate for $\varepsilon(\theta)$ is derived by placing n=2 in equation (3.12). Thus, by expanding the logarithmic term on the right-hand side of this equation in powers of $\varepsilon^{(1)}(\theta)$, it is possible to write

$$\varepsilon^{(2)}(\theta) = \varepsilon\exp\{\varepsilon\cos\theta(\frac{2}{1-\lambda^2} - \tfrac{1}{2})+O(\varepsilon^2)\}. \qquad (3.14)$$

Here, for convenience, $\varepsilon^{(1)}(\theta)$ has been replaced by ε.

The term λ may be eliminated from equation (3.14) by employing equation (3.13) to give the result

$$\varepsilon^{(2)}(0) = \varepsilon\exp\left[\varepsilon\cos\theta\{\ln(2/\varepsilon)- \tfrac{1}{2}\} + O(\varepsilon^2)\right]$$

which, after expanding the exponential for small ε, becomes

$$\varepsilon^{(2)}(\theta) = \varepsilon\{1-\varepsilon\ln\varepsilon\cos\theta+\varepsilon(\ln2-1/2)\cos\theta+O\left[(\varepsilon\ln\varepsilon)^2\right]\}.$$

On the assumption that $\varepsilon(\theta) = \lim_{N\to\infty}\{\varepsilon^{(N)}(\theta)\}$ it is possible to conclude that the iteration scheme yields an asymptotic expansion for $\varepsilon(\theta)$ in powers of ε, that is

$$\varepsilon(\theta) = \varepsilon\{1-\varepsilon\ln\varepsilon\cos\theta+\varepsilon(\ln2-1/2)\cos\theta+O\left[(\varepsilon\ln\varepsilon)^2\right]\}, \quad \varepsilon\to 0. \qquad (3.15)$$

Although no formal proof of convergence will be given, the following table of values of ε and $\left|(\varepsilon^{(2)}(0)-\varepsilon)/\varepsilon\right|$ is included to illustrate the apparent rapidity of convergence of the scheme for small h/b.

λ	2h/b	ε	$\lvert(\varepsilon^{(2)}(0)-\varepsilon)/\varepsilon\rvert$
0.995	0.016	2.78×10^{-87}	$0(10^{-85})$
0.960	0.153	1.67×10^{-11}	$0(10^{-10})$
0.900	0.481	5.36×10^{-5}	$0(10^{-4})$
0.800	1.398	0.77×10^{-2}	$0(10^{-2})$

The main indications of the above analysis are that for small h/b the indentation AB is extremely small and nearly semi-circular in shape. That this also applies to indentation GH follows from the fact that it is the mirror image of indentation AB in the imaginary axis. Therefore a suitable series of approximations to an exact upper half-plane would seem to be

$$t^{(n)} = \lambda t + \sum_{m=o}^{m=n} B_m \{\frac{1}{(\lambda t-1)^m} + \frac{1}{(\lambda t+1)^m}\}, \quad n=0,1,2,3, \ldots\ldots, \qquad (3.16)$$

where $t^{(n)}$ are approximations to an exact upper half-plane and B_m are real constants.

B_m are found by requiring that on the identation boundaries $\mathrm{Im}(t^{(n)})$ is of lower mathematical order than ε^n. This is intended to ensure that, with each successive approximation, $t^{(n)}$ becomes closer in form to an exact upper half-plane.

In order to determine B_o and B_1, it is necessary to write $\mathrm{Im}(t^{(1)})$, on the indentation AB, as a function of $\varepsilon(\theta)$ and θ. This is achieved by combining equations (3.10) and (3.16) to give the result

$$\mathrm{Im}\{t^{(1)}(\frac{-1+\varepsilon(\theta)e^{i\theta}}{\lambda})\} = \varepsilon(\theta)\sin\theta + B_1\{-\frac{\sin\theta}{\varepsilon(\theta)} + \mathrm{Im}(\frac{1}{-2+\varepsilon(\theta)e^{i\theta}})\}. \qquad (3.17)$$

Therefore, by replacing $\varepsilon(\theta)$ in equation (3.17) with its asymptotic form (equation 3.15) and expanding the resulting expression for small ε, it is found that

$$\mathrm{Im}\{t^{(1)}(\tfrac{-1+\varepsilon(\theta)e^{i\theta}}{\lambda})\} = \varepsilon\sin\theta\{1 + O(\varepsilon\ln\varepsilon)\} + B_1\left[-\frac{\sin\theta}{\varepsilon}\{1 + O(\varepsilon\ln\varepsilon)\}-\right.$$

$$\left.-\frac{\varepsilon\sin\theta}{4}\{1 + O(\varepsilon\ln\varepsilon)\}\right] \quad \varepsilon \to 0. \qquad (3.18)$$

Thus the above-mentioned requirement on the mathematical order of $\mathrm{Im}[t^{(1)}\{(-1+\varepsilon(\theta)e^{i\theta})/\lambda\}]$ is satisfied if $B_1 = \varepsilon^2$. The constant B_0, on the other hand, does not influence the mathematical order of this expression; therefore it is arbitrarily placed equal to zero. Consequently the zeroth and first approximations to an exact upper half-plane are given by

$$t^{(o)} = \lambda t; \qquad t^{(1)} = \lambda t + \varepsilon^2\{\frac{1}{(\lambda t-1)} + \frac{1}{(\lambda t+1)}\}. \qquad (3.19)$$

It is worth while to enquire into the status of these approximations. Thus it is apparent that the use of $t^{(o)}$ is equivalent to the assumption that the indentations may be ignored altogether whereas the approximation $t^{(1)}$ is evidently similar in status to the first, semi-circular, approximation for the indentation shape. This is demonstrated in Fig. 7 which illustrates the form of the $t^{(1)}$ plane. It will be seen that $\mathrm{Im}(t^{(1)})$ on the indentations is $O(\varepsilon^2\ln\varepsilon)$ which is the same order as the terms neglected in employing the first approximation for $\varepsilon(\theta)$.

It is necessary to determine the points at which the two approximate transformations given above cease to be conformal. Thus it is evident that the zeroth approximation is conformal everywhere whilst the first approximation ceases to be conformal at $t = \pm 1/\lambda$ and

$$t = \pm \{1 \pm \varepsilon + O(\varepsilon^3)\}/\lambda, \quad (\varepsilon \to 0).$$

The first two of these points are outside the domain D and are therefore of no consequence. The remaining four points, on the other hand, coincide with the right-angle corners of the indentations in the t plane to the order of accuracy of the $t^{(1)}$ approximation. By being there they effect the removal of the corners of the indentations in the $t^{(1)}$ plane and, as such, may be considered acceptable singular points. It is anticipated that higher approximations to an exact upper half-plane will also yield transformations with singular points at the indentations' corners.

In establishing the solution to the flow problem it is assumed that $t^{(n)}$ are exact upper half-planes. Therefore the boundary conditions for the normal velocity of the combined flow in the $t^{(n)}$ planes are as follows:

$$\left.\begin{aligned} &\partial\phi_c/\partial n = 0; \quad |\mathrm{Re}(t^{(n)})| < \infty, \quad \mathrm{Im}(t^{(n)}) = 0; \\ &dW_c/dt^{(n)} \sim w_\infty \bar{C}^2 t^{(n)}/\lambda^6 h; \quad |t^{(n)}| \to \infty. \end{aligned}\right\} \tag{3.20}$$

By following the argument leading to equations (2.20) it is found that regular complex potentials which satisfy equations (3.20) and the symmetry condition are given by

$$W_c^{(n)} = w_\infty \bar{C}^2 (t^{(n)})^2/2\lambda^6 h. \tag{3.21}$$

Here it should be noted that the arbitrary constant which should appear on the right-hand side of equation (3.21) has been ignored for the reason that it does not influence the value of σ.

Following the reasoning employed in deriving equation (2.29) one may write an n^{th} approximation for Σ corresponding to $W_c^{(n)}$ as

$$\Sigma^{(n)} = -(\overline{C}^3/2\lambda^6 hb^2) \int_{-(1-\varepsilon(0))/\lambda}^{+(1-\varepsilon(0))/\lambda} (t^{(n)})^2\{(1-t^2)/(1-\lambda^2t^2)\}dt.$$

For the particular case n=1 this becomes, after combination with equation (3.19) and rearrangement,

$$\Sigma^{(1)} = -\frac{\overline{C}^3}{2\lambda^2 hb^2} \int_{-(1-\varepsilon(0))/\lambda}^{+(1-\varepsilon(0))/\lambda} \{\lambda^2t^2 + \frac{4\lambda^2t^2\varepsilon^2}{\lambda^2t^2-1} + \frac{4\lambda^2t^2\varepsilon^4}{(\lambda^2t^2-1)^2}\}(\frac{1-t^2}{1-\lambda^2t^2})dt. \quad (3.22)$$

The errors implicit in the use of $\Sigma^{(1)}$ may be found by determining the order of magnitude of $\{(\Sigma^{(2)}-\Sigma^{(1)})/\Sigma^{(1)}\}$. In fact, it is found that this latter quantity is $O(\varepsilon^2 \ln\varepsilon)$. This implies that no extra accuracy can be expected from $\Sigma^{(1)}$ by retaining terms of this order. Consequently equation (3.22) is integrated and the resultant expression is expanded in powers of ε, terms of $O(\varepsilon^2\ln\varepsilon)$being neglected. Thus there is obtained

$$\Sigma^{(1)} = \frac{\overline{C}^3}{2\lambda^6 hb^2}\left[\frac{(1-\lambda^2)}{\lambda^3}\{\ln(\frac{2}{\varepsilon})+\varepsilon\ln(\frac{\varepsilon}{2})\} - \frac{2}{3\lambda^3}(1-3\varepsilon) - \frac{2(1-\lambda^2)(1-\varepsilon)}{\lambda^3} + \frac{2\varepsilon(\lambda^2-1)}{\lambda^3}\right]. \quad (3.23)$$

A similar analysis applied to $\Sigma^{(o)}$yields the result

$$\Sigma^{(o)} = \frac{\overline{C}^3}{2\lambda^6 hb^2}\left[\frac{(1-\lambda^2)}{\lambda^3}\ln(\frac{2}{\varepsilon}) - \frac{2}{3\lambda^3} - \frac{2(1-\lambda^2)}{\lambda^3}\right], \quad (3.24)$$

terms $O(\varepsilon)$ inside the square brackets having been neglected as by themselves they cannot improve the accuracy of $\Sigma^{(o)}$.

A cursory inspection of equations (3.23) and (3.24) would seem to suggest that $\Sigma^{(1)}$ gives a higher order of accuracy than $\Sigma^{(o)}$. However, if ε eliminated from both these equations by employing equation (3.13) (with $\varepsilon(\theta)^{(1)} = \varepsilon$), it is found that

$$\Sigma^{(o)} = \Sigma^{(1)} = (\bar{C}^3/3\lambda^9 hb^2)(3\lambda^2-1). \qquad (3.25)$$

This result was quite unexpected and must be due to the fortuitous cancellation of the first-order correction terms in $\Sigma^{(1)}$.

Equation (3.25) may be combined with equations (2.34), (3.7) and (3.9) to give the result

$$\sigma^{(o)} = \sigma^{(1)} = 3\pi^2(1-\lambda^2)\left[2\lambda + (1-\lambda^2)\ln\{(1-\lambda)/(1+\lambda)\}\right]^2/8(3\lambda^2-1), \qquad (3.26)$$

where $\sigma^{(o)}$ and $\sigma^{(1)}$ are zeroth and first approximations to the induced-drag factor. Fig. 4 shows them plotted against 2h/b and it will be seen that they compare well with the 'exact' result (equation 2.35) in the range $0.45 \lesssim 2h/b \lesssim 1.6$. Comparison has not been possible below the lower value owing to the limited amount of data on the elliptic integrals available from Byrd and Friedman's tables. Nevertheless, the asymptotic behaviour of σ for small h/b may be found by reference to asymptotic expansions of the elliptic integrals given by these authors. Thus, without giving details, it is found that equations (2.14) and (2.35) may be replaced by the following asymptotic forms:

$$\left.\begin{aligned} 2h/b &\sim \pi(1-\beta^2)/\left[2\beta+(1-\beta^2)\ln\{(1-\beta)/(1+\beta)\}\right], \quad \beta \to 1; \\ \sigma &\sim 3\pi^2(1-\beta^2)\left[2\beta+(1-\beta^2)\ln\{(1-\beta)/(1+\beta)\}\right]^2/8(3\beta^2-1), \quad \beta \to 1. \end{aligned}\right\} \qquad (3.27)$$

By comparing equations (3.27) with equations (3.9) and (3.26) it is evident that $\sigma^{(o)}$ and $\sigma^{(1)}$ as functions of 2h/b are identical with the asymptotic form of σ.

The relative error of $\sigma^{(o)}$ and $\sigma^{(1)}$ is $O(\varepsilon^2 \ln\varepsilon)$ which for $2h/b = 0.48$ is $O(10^{-8})$. It is not surprising, therefore, that the agreement between the approximate and 'exact' values of σ is good in the range of 2h/b considered.

3.3 Application of the technique to the end-plate problem.

The accuracy of the zeroth approximation for the case of the planar wing having been established it is intended to apply the same approach to the problem of the planar wing with end plates. Actually, a slightly different interpretation of the approximation is necessary but, essentially, the basic approach remains the same.

3.3.1 Relationship between the Ω plane and the transformed planes.

The integration of equation (3.2), which is the differential relationship between Ω and t, is facilitated by using transformation (2.3) and equation (2.4). Thus, after rearrangement, there is obtained instead of equation (3.2)

$$d\Omega/d2Ks = \bar{C}\{\alpha^2 - sn^2 2Ks/\lambda^2 + (\lambda^2-1)(\alpha^2-1/\lambda^2)sn^2 2Ks/(1-\lambda^2 sn^2 2Ks)\}. \tag{3.28}$$

In turn, this may be integrated with the aid of equation (310.02) of Byrd and Friedman (which is used to integrate the second term in the brackets) to yield the expression

$$\Omega = \bar{C}\left[\alpha^2 2Ks - \frac{\{2Ks-E(2Ks)\}}{k^2\lambda^2} - \frac{(\alpha^2-1/\lambda^2)(1-\lambda^2)^{\frac{1}{2}}}{\lambda(k^2-\lambda^2)^{\frac{1}{2}}}\,\Pi(2Ks,2Ks_1)\right] + C_5. \tag{3.29}$$

Here C_5 is the integration constant, $s_1 = sn^{-1}(\lambda/k)/2K$ and

$$\Pi(2Ks,2Ks_1) = \int_0^{2Ks} \frac{k^2 sn2Ks_1\ cn2Ks_1\ dn2Ks_1\ sn^2 2Ks'\ d2Ks'}{1 - k^2 sn^2 2Ks_1\ sn^2 2Ks'},$$

where $cn2Ks_1$ and $dn2Ks_1$ are Jacobian elliptic functions as defined by Byrd and Friedman.

Woods (1961) has shown that $\Pi(2Ks,2Ks_1)$ may be replaced by an expression containing Jacobian theta and zeta functions. Thus, by employing his equation (78)(p. 125), it is possible to write instead of equation (3.29)

$$\Omega = \overline{C}\left[\alpha^2 2Ks - \frac{\{2Ks-E(2Ks)\}}{k^2\lambda^2} - \frac{(\alpha^2-1/\lambda^2)(1-\lambda^2)^{\frac{1}{2}}}{\lambda(k^2-\lambda^2)^{\frac{1}{2}}}\{\tfrac{1}{2}\ln\left[\frac{\theta_o(\pi s-\pi s_1,q)}{\theta_o(\pi s+\pi s_1,q)}\right] + \right.$$

$$\left. + 2Ks\ Z(2Ks_1,k)\}\right] + C_5, \qquad (3.30)$$

where, with Byrd and Friedman's notation, $\theta_\nu(,q)$ ($\nu = 0,1,2$ and 3) are Jacobian theta functions and $Z(,k)$ is the Jacobian zeta function.* Hereafter, unless otherwise shown, it is to be understood that $\theta_\nu(\ )$ are functions of $q = \exp(-\pi K'/K)$ and $Z(\ )$ is a function of k.

The s plane, which is illustrated in Fig. 8, consists of a rectangular domain which is indented at AB and GH.

By referring to the coordinate systems and notation of Figs. 5 and 8 it may be concluded that, on C'E', $\Omega = b/2 + ih$ and the term in equation (3.30) multiplied by $\overline{C}$ is purely real. Therefore $C_5 = ih$, a result which will be used implicitly when point-to-point correspondence between the Ω and s planes is considered.

Correspondence between the two planes at point E is established provided that

$$\frac{b}{2} + ih = \overline{C}\left[\alpha^2(K+iK') - \frac{\{K+iK'-E(K+iK')\}}{k^2\lambda^2} - \frac{(\alpha^2-1/\lambda^2)(1-\lambda^2)^{\frac{1}{2}}}{\lambda(k^2-\lambda^2)^{\frac{1}{2}}}\{\right.$$

$$\left.\tfrac{1}{2}\ln\left[\frac{\theta_o(\pi/2+i\pi K'/2K-\pi s_1)}{\theta_o(\pi/2+i\pi K'/2K+\pi s_1)}\right] + (K+iK')Z(2Ks_1)\}\right] + ih. \qquad (3.31)$$

The logarithmic term in equation (3.31) may be reduced by using properties of the theta functions given by Woods (p. 117), namely

$$\theta_o(\pi s + \pi/2 + i\pi K'/2K) = q^{-\frac{1}{4}}e^{-i\pi s}\theta_2(\pi s)$$

and

$$\theta_2(-\pi s) = \theta_2(\pi s).$$

---

* It should be noted that $\theta_o(\ )$ and $Z(\ )$ are written as $\theta_4(\ )$ and $Z_4(\ )$ by Woods.

Thus, by employing these two results in conjunction with equation (2.11), which is used to expand the term $E(K + iK')$, it is possible to rewrite equation (3.31) in a form having the real and imaginary parts

$$b/2 = \overline{C}\{\alpha^2 K - (K-E(K))/k^2\lambda^2 - (\alpha^2-1/\lambda^2)(1-\lambda^2)^{\frac{1}{2}} KZ(2Ks_1)/\lambda(k^2-\lambda^2)^{\frac{1}{2}}\} \tag{3.32}$$

and $$0 = \overline{C}\left[\alpha^2 K' - \frac{K'(K-E(K))}{Kk^2\lambda^2} - \frac{\pi}{2Kk^2\lambda^2} - \frac{(\alpha^2-1/\lambda^2)(1-\lambda^2)^{\frac{1}{2}}}{\lambda(k^2-\lambda^2)^{\frac{1}{2}}}\{\pi s_1 + K'Z(2Ks_1)\}\right], \tag{3.33}$$

respectively.

Equation (3.33) may be rearranged to give the result

$$\alpha^2 = \frac{KK' - E(K)K' + \pi/2 - Kk^2(1-\lambda^2)^{\frac{1}{2}}\{\pi s_1 + K'Z(2Ks_1)\}/\lambda(k^2-\lambda^2)^{\frac{1}{2}}}{Kk^2\lambda^2\left[K'-(1-\lambda^2)^{\frac{1}{2}}\{\pi s_1 + K'Z(2Ks_1)\}/\lambda(k^2-\lambda^2)^{\frac{1}{2}}\right]}. \tag{3.34}$$

Fig. 9 shows α plotted against $\chi = sn^{-1}(\lambda/k)(90/K)$ for various $\Phi = \sin^{-1}k$ (the modular angle).

The curve of the indentation AB may be defined by the relationship

$$s = -s_1 + iK'/2K - \overline{\epsilon}(\tilde{\theta})e^{i\tilde{\theta}}, \tag{3.35}$$

where, with the origin at $s = -s_1 + iK'/2K$, $\overline{\epsilon}$ and $\tilde{\theta}$ are polar coordinates as shown in Fig. 8. Thus, by employing equations (3.30) and (3.35) and the properties of the theta functions given by Woods (p. 117), namely

$$\theta_o(\pi s + i\pi K'/2K) = iq^{-\frac{1}{4}}e^{-i\pi s}\theta_1(\pi s)$$

and $$\theta_1(-\pi s) = -\theta_1(\pi s), \tag{3.36}$$

it is apparent that correspondence between the Ω and s planes on AB demands that

$$iz = \overline{C}\left[\alpha^2(-2Ks_1 + iK' - 2K\overline{\epsilon}(\tilde{\theta})e^{i\tilde{\theta}}) - \frac{1}{k^2\lambda^2}\{-2Ks_1 + iK' - 2K\overline{\epsilon}(\tilde{\theta})e^{i\tilde{\theta}} - \right.$$

$$\left. -E(-2Ks_1 + iK' - 2K\overline{\epsilon}(\tilde{\theta})e^{i\tilde{\theta}})\} - \frac{(\alpha^2-1/\lambda^2)(1-\lambda^2)^{\frac{1}{2}}}{\lambda(k^2-\lambda^2)^{\frac{1}{2}}}\{ i\pi s_1 + \right.$$

$$+ \tfrac{1}{2} \ln\left[\frac{\theta_1(2\pi s_1 + \pi\bar{\varepsilon}(\tilde{\theta})e^{i\tilde{\theta}})}{\theta_1(\pi\bar{\varepsilon}(\tilde{\theta})e^{i\tilde{\theta}})}\right] - (2Ks_1 - iK' + 2K\bar{\varepsilon}(\tilde{\theta})e^{i\tilde{\theta}})Z(2Ks_1)\}\Big] + ih. \tag{3.37}$$

Therefore, if the values appropriate to point A, $z = 0$ and $\tilde{\theta} = \pi$, are substituted into equation (3.37) and use is made of equation (3.36), it is found that the imaginary part of the resulting expression yields the result

$$0 = \bar{C}\left[\alpha^2K' - \frac{1}{k^2\lambda^2}\{K' - \mathrm{Im}\left[E(-2Ks_1 + 2K\bar{\varepsilon}(\pi) + iK')\right]\} - \frac{(\alpha^2 - 1/\lambda^2)(1-\lambda^2)^{\frac{1}{2}}}{\lambda(k^2-\lambda^2)^{\frac{1}{2}}}\{\right.$$

$$\left.\pi(s_1 - \tfrac{1}{2}) + K'Z(2Ks_1)\}\right] + h. \tag{3.38}$$

In turn, this may be simplified with the aid of a result which may be deduced from equations (122.00), (140.01) and (141.01) of Byrd and Friedman, namely

$$E(-2Ks + iK') = -Z(2Ks) - \frac{\mathrm{cn}2Ks\ \mathrm{dn}2Ks}{\mathrm{sn}2ks} - \frac{i\pi}{2K} - \frac{E(K)(2Ks - iK')}{K}. \tag{3.39}$$

Thus, by eliminating $E(-2Ks_1 + 2K\bar{\varepsilon}(\pi) + iK')$ from equation (3.38) with the aid of equation (3.39) and comparing the modified expression with equation (3.33), it is found that

$$h = \pi\bar{C}(1/\lambda^2 - \alpha^2)(1 - \lambda^2)^{\frac{1}{2}}/2\lambda(k^2 - \lambda^2)^{\frac{1}{2}}. \tag{3.40}$$

Equations (3.32) and (3.40) may be combined to give a relationship between $2h/b$ and α, k and λ. The term α may be eliminated from this expression by means of equation (3.34). Thus it is possible to calculate $2h/b$ as a function of χ for various Φ and the results of such calculations are shown in Fig. 10.

In principle, the real part of equation (3.37) permits the determination of $\bar{\varepsilon}$ in the form $\bar{\varepsilon} = \bar{\varepsilon}(\theta,\lambda,k)$. Unfortunately, as with equation (3.11), it would seem difficult to obtain a closed-form solution. Therefore, by analogy with the planar-wing case, an iteration solution is sought as follows:

$$\mathrm{Re}\left[\ln\{\theta_1(\pi\bar{\varepsilon}^{(n)}(\tilde{\theta})e^{i\tilde{\theta}})\}\right]=\mathrm{Re}\left[\ln\{\theta_1(2\pi s_1+\pi\bar{\varepsilon}^{(n-1)}(\tilde{\theta})e^{i\tilde{\theta}})\}\right]-4K(s_1+$$

$$+\bar{\varepsilon}^{(n-1)}(\tilde{\theta})\cos\tilde{\theta})Z(2Ks_1)+\frac{4K\lambda(k^2-\lambda^2)^{\frac{1}{2}}}{(\alpha^2-1/\lambda^2)(1-\lambda^2)}\Bigg[\alpha^2(s_1+\bar{\varepsilon}^{(n-1)}(\tilde{\theta})\cos\tilde{\theta})-$$

$$-\frac{1}{k^2\lambda^2}\{s_1+\bar{\varepsilon}^{(n-1)}(\tilde{\theta})\cos\tilde{\theta}+\frac{\mathrm{Re}[E(-2Ks_1+iK'-2K\bar{\varepsilon}^{(n-1)}(\tilde{\theta})e^{i\tilde{\theta}})]}{2K}\}\Bigg]\ .$$

with $\varepsilon^{(o)}(\tilde{\theta})=0$. Thus, by employing equation (3.39) to eliminate the incomplete elliptic integral, there is obtained the result

$$\mathrm{Re}\left[\ln\{\theta_1(\pi\bar{\varepsilon}^{(1)}(\tilde{\theta})e^{i\tilde{\theta}})\}\right]=\ln\{\theta_1(2\pi s_1)\}-4Ks_1Z(2Ks_1)+$$

$$+\frac{4K\lambda(k^2-\lambda^2)^{\frac{1}{2}}}{(\alpha^2-1/\lambda^2)(1-\lambda^2)^{\frac{1}{2}}}\Bigg[\{\alpha^2-\frac{1}{Kk^2\lambda^2}(K-E(K))\}s_1+\frac{1}{2Kk^2\lambda^2}\{Z(2Ks_1)+$$

$$+\frac{\mathrm{cn}2Ks_1\ \mathrm{dn}2Ks_1}{\mathrm{sn}2Ks_1}\}\Bigg]\ . \qquad (3.41)$$

However, even with this simplification it would not appear possible to obtain an explicit solution. Nevertheless, a solution which possesses the apparent asymptotic form of the first iterate may be derived by noting that

$$\theta_1(\pi s)\ \sim\ (2k'kK/\pi)^{\frac{1}{2}}2Ks,\quad 2Ks\to 0, \qquad (3.42)$$

a result which may be deduced from Byrd and Friedman's equations (105.01), (105.02) and (907.01). Thus equation (3.42) may be used to replace the left-hand side of equation (3.41) by its asymptotic form for small $\bar{\varepsilon}^{(1)}(\tilde{\theta})$, that is $\ln\{(8k'k\,K^3/\pi)^{\frac{1}{2}}\bar{\varepsilon}^{(1)}(\tilde{\theta})\}$. Consequently, upon noting from equation (3.41) that $\bar{\varepsilon}^{(1)}(\tilde{\theta})\sim 0$ as $\lambda\to k$, it may be concluded that

$$\bar{\varepsilon}^{(1)}(\tilde{\theta})\sim\left(\frac{\pi}{8k'k\,K^3}\right)^{\frac{1}{2}}\theta_1(2\pi s_1)\exp\Bigg[-4Ks_1Z(2Ks_1)+\frac{4K\lambda(k^2-\lambda^2)^{\frac{1}{2}}}{(\alpha^2-1/\lambda^2)(1-\lambda^2)^{\frac{1}{2}}}\{$$

$$\left(\alpha^2-\frac{1}{Kk^2\lambda^2}(K-E(K))\right)s_1+\frac{1}{2Kk^2\lambda^2}\left(Z(2Ks_1)+\frac{\mathrm{cn}2Ks_1\ \mathrm{dn}2Ks_1}{\mathrm{sn}2Ks_1}\right)\}\Bigg],\quad \lambda\to k. \qquad (3.43)$$

The coordinates of the indentation AB in the t and s planes are related by the expression

$$(-1+\varepsilon(\theta)e^{i\theta})/\lambda = sn(-2Ks_1 + iK' - 2K\bar{\varepsilon}(\tilde{\theta})e^{i\tilde{\theta}}), \qquad (3.44)$$

where, as for the planar wing, $\varepsilon(\theta)$ and θ are the polar coordinates (with origin at $t = -1/\lambda$) of the indentation AB in the t plane.

Byrd and Friedman's equations (122.07) and (123.01) may be utilized to yield the asymptotic relationship

$$\varepsilon(\theta)e^{i\theta} \sim 2K\bar{\varepsilon}(\tilde{\theta})e^{i\tilde{\theta}}cn2Ks_1\ dn2Ks_1/sn2Ks_1,\ \ \bar{\varepsilon}(\tilde{\theta})\to 0,\ (\lambda\to k). \qquad (3.45)$$

Thus, by equating the moduli of equation (3.45), it is found that

$$\varepsilon(\theta) \sim 2K\bar{\varepsilon}(\tilde{\theta})cn2Ks_1\ dn2Ks_1/sn2Ks_1,\ \ \bar{\varepsilon}(\tilde{\theta})\to 0,\ (\lambda\to k). \qquad (3.46)$$

Therefore it is possible to infer from equations (3.43) and (3.46) that a first approximation to $\varepsilon(\theta)$, ε, may be written as

$$\varepsilon = \frac{cn2Ks_1\ dn2Ks_1}{sn2Ks_1}\left(\frac{\pi}{2k'kK}\right)^{\frac{1}{2}}\theta_1(2\pi s_1)\exp\left[-4Ks_1\ Z(2Ks_1) + \frac{4K\lambda(k^2-\lambda^2)^{\frac{1}{2}}}{(\alpha^2-1/\lambda^2)(1-\lambda^2)^{\frac{1}{2}}}\{\right.$$

$$\left.\left(\alpha^2 - \frac{1}{Kk^2\lambda^2}(K-E(K))\right)s_1 + \frac{1}{2Kk^2\lambda^2}\left(Z(2Ks_1) + \frac{cn2Ks_1\ dn2Ks_1}{sn2Ks_1}\right)\}\right], \qquad (3.47)$$

a result which would seem to represent the asymptotic form of $\varepsilon(\theta)$ as $\lambda\to k$.

Although details will not be given, it may be shown that with k=1, which corresponds to end plates of zero height, equation (3.47) is identical with equation (3.13) if $\varepsilon^{(1)}(\theta)$ is replaced by ε. Hence the present approximation for $\varepsilon(\theta)$ is equivalent to the first iterate of the planar wing. Therefore, in view of the apparent accuracy of of the latter approximation for small 2h/b, it is assumed that ε is sufficiently accurate for wings with end plates near the ground.

Curves of $\ln(\varepsilon/\lambda)$ against χ for various Φ are shown in Fig. 11. This indicates that, for the range of χ and Φ examined, ε is extremely

small, a fact which is consistent with the assumption that $\bar{\varepsilon}^{(o)}(\tilde{\theta}) = 0$ is a good approximation for $\bar{\varepsilon}(\tilde{\theta})$.

The vertical dimension of the end-plate traces, ℓ, may be written in terms of the transformation constant and parameters by insisting on correspondence between the Ω and s planes at point F. This requirement gives the result

$$\frac{b}{2} + i(h-\ell) = \bar{C}\left[\alpha^2(K + i2Ks_2) - \frac{1}{k^2\lambda^2}\{K + i2Ks_2 - E(K+ i2Ks_2)\} - \right.$$

$$\left. - \frac{(\alpha^2-1/\lambda^2)(1-\lambda^2)^{\frac{1}{2}}}{\lambda(k^2-\lambda^2)^{\frac{1}{2}}}\left\{\tfrac{1}{2}\ln\left[\frac{\theta_o(\pi/2 + i\pi s_2 - \pi s_1)}{\theta_o(\pi/2 + i\pi s_2 + \pi s_1)}\right] + (K+i2Ks_2)Z(2Ks_1)\right\}\right] + ih, \tag{3.48}$$

where $$s_2 = dn^{-1}(1/\alpha,k')/2K.$$

By employing the properties of the elliptic functions given by Byrd and Friedman (p.20) and their equations (140.01) and (143.01) it is possible to derive the result

$$E(K + i2Ks_2) = -i\{Z(2Ks_2,k') + \frac{\pi s_2}{K'} - \frac{k'^2 cn(2Ks_2,k')sn(2Ks_2,k')}{dn(2Ks_2,k')}\} +$$

$$+ \frac{E(K)(K + i2Ks_2)}{K}. \tag{3.49}$$

This result will be used in the simplification of equation (3.48) as will the property given by Woods (p.117)

$$\theta_3(\pi s) = \theta_o(\pi/2 + \pi s). \tag{3.50}$$

Therefore, by using equations (3.49) and (3.50) to rewrite $E(K + i2Ks_2)$ and the theta functions in equation (3.48), it is found, after rearrangement, that

$$\frac{b}{2} - i\ell = \bar{C}\left[\{\alpha^2 - \frac{1}{Kk^2\lambda^2}(K-E(K))\}(K + i2Ks_2) - \frac{i}{k^2\lambda^2}\{Z(2Ks_2,k') + \frac{\pi s_2}{K'} - \right.$$

$$\left. - \frac{k'^2 cn(2Ks_2,k')sn(2Ks_2,k')}{dn(2Ks_2,k')}\} - \frac{(\alpha^2-1/\lambda^2)(1-\lambda^2)^{\frac{1}{2}}}{\lambda(k^2-\lambda^2)^{\frac{1}{2}}}\left\{\tfrac{1}{2}\ln\left[\frac{\theta_3(i\pi s_2-\pi s_1)}{\theta_3(i\pi s_2+\pi s_1)}\right] + \right.$$

$$+ (K + i2Ks_2)Z(2Ks_1)\}\Big].$$

Hence, comparing this expression with equation (3.32), one is able to obtain the result

$$\eta = \bar{C}\Big[\{\frac{1}{Kk^2\lambda^2}(K-E(K))-\alpha^2\}2Ks_2 + \frac{1}{k^2\lambda^2}\{Z(2Ks_2,k') + \frac{\pi s_2}{K'} - \frac{k'^2 cn(2Ks_2,k')\,sn(2Ks_2,k')}{dn(2Ks_2,k')}\} + \frac{(\alpha^2-1/\lambda^2)(1-\lambda^2)^{\frac{1}{2}}}{\lambda(k^2-\lambda^2)^{\frac{1}{2}}}\{\frac{1}{2i}\ln\Big[\frac{\theta_3(i\pi s_2-\pi s_1)}{\theta_3(i\pi s_2+\pi s_1)}\Big] + 2Ks_2\,Z(2Ks_1)\}\Big]. \qquad (3.51)$$

This may be put into a form more suitable for computation by using Jacobi's imaginary transformation of the θ_3 function given by Woods (p.118), that is

$$\theta_3(\pi s,q) = (K/K')^{\frac{1}{2}}\exp(-\pi Ks^2/K')\,\theta_3(-iK\pi s/K',q'), \qquad (3.52)$$

where $q'=q(k')$. Therefore equation (3.52) makes it possible to rewrite equation (3.51) in the following form:

$$\eta = \bar{C}\Big[\{\frac{1}{Kk^2\lambda^2}(K - E(K)) - \alpha^2\}2Ks_2 + \frac{1}{k^2\lambda^2}\{Z(2Ks_2,k') + \frac{\pi s_2}{K'} - \frac{k'^2 cn(2Ks_2,k')sn(2Ks_2,k')}{dn(2Ks_2,k')}\} + \frac{(\alpha^2-1/\lambda^2)(1-\lambda^2)^{\frac{1}{2}}}{\lambda(k^2-\lambda^2)^{\frac{1}{2}}}\{\frac{2\pi s_1 s_2 K}{K'} + \frac{1}{2i}\ln\Big[\frac{\theta_3\{\pi K(s_2+is_1)/K',q'\}}{\theta_3\{\pi K(s_2-is_1)/K',q'\}}\Big] + 2Ks_2\,Z(2Ks_1)\}\Big]. \qquad (3.53)$$

Finally, equation (3.53) may be simplified by comparison with equation (3.33), and the θ_3 functions may be replaced by the series form

$$\theta_3(\pi s) = 1 + 2\sum_{m=1}^{\infty} q^{m^2}\cos(2m\pi s)$$

given by Byrd and Friedman (equation 1050.01). Thus, after performing some routine operations on the logarithmic term of the modified expression, there is obtained the expression

$$l = \bar{C}\left[\frac{1}{k^2\lambda^2}\{Z(2Ks_2,k') - \frac{k'^2 cn(2Ks_2,k')sn(2Ks_2,k')}{dn(2Ks_2,k')}\} - \right.$$

$$\left. - \frac{(\alpha^2-1/\lambda^2)(1-\lambda^2)^{\frac{1}{2}}}{\lambda(k^2-\lambda^2)^{\frac{1}{2}}}\tan^{-1}\left(\frac{2\sum_{m=1}^{\infty} q'^{m^2}\sin(2mK\pi s_2/K')\sinh(2mK\pi s_1/K')}{1+2\sum_{m=1}^{\infty} q'^{m^2}\cos(2mK\pi s_2/K')\cosh(2mK\pi s_1/K')}\right)\right]. \tag{3.54}$$

The ratio l/h may be written as a function of α, λ and k by combining equations (3.40) and (3.54). Thus it is possible, by eliminating α from the resulting expression, to calculate l/h as a function of χ for various Φ and the results obtained are illustrated in Fig. 12. It should be remarked, in passing, that the series expansions of equation (3.54) appear to converge very rapidly in the range of χ and Φ considered. Therefore, only 4 terms were retained in the calculations, the error involved being considered negligible.

3.3.2 The flow problem.

By referring to equation (1.1) it is found that the boundary conditions for normal velocity in the Ω plane are identical to those of equation (2.1) at the corresponding segments of the bounding contour. Furthermore, at the end-plate traces $\partial\phi/\partial n = 0$.

In accordance with the method proposed in Section 1.3, a suitable superposition flow is sought. Unfortunately, it has not been possible to find such a flow which has a complex potential in closed form. On the other hand, by combining a number of simple flows, it is conceivable that the conditions could be satisfied with reasonable accuracy. However, it is difficult to state with certainty how many of these flows would be required to ensure an adequate approximation (except in the degenerate case of the planar wing). This is an undesirable feature and would seem to outweigh the advantages of the superposition method. Nevertheless, it is

instructive to discover the extent to which the boundary conditions at the vortex trace are affected by the addition of a simple flow. An obvious choice is the superposition flow employed for the planar wing. Thus, if this is added to the Trefftz-plane flow, it is found that $\partial\phi_c/\partial n = 0$ everywhere at the finite part of the bounding contour except the traces of the end plates. Consequently the solution of the combined flow in the t plane entails the integration of the flow field of source distributions. The integrals involved are complicated and appear to be difficult to evaluate explicitly, Suppose, however, that a source distribution of strength $-w_\infty b/h$ is placed on the imaginary axis of the Ω plane in the interval $-\infty<z<+\infty$. Firstly, it is found that the normal velocity at the end plates is nullified whilst, other than at AB and GH, the remaining boundary conditions are undisturbed. Secondly, except at the imaginary axis, the complex potential of the source flow is regular everywhere and, in consequence, does not alter the jump in velocity potential at the vortex trace.

The adoption of the modified combined flow stems from the fact that as $h/b \to 0$ the flow induced near the end-plate traces by the sources of the imaginary axis becomes more like the flow of a uniform stream parallel to the y direction. Furthermore, for the purpose of calculating the influence of the end plates, the vortex trace may be considered semi-infinite in span. Thus, in this limiting case, which is of particular interest, it is possible to identify a combination of simple superposition flows which, together, satisfy the requirements.

If h/b is not very small, it is necessary to solve the full problem of the modified combined flow about an obstacle shaped like the vortex trace. Unfortunately, the solution for this flow field contains a complicated integral which is attributable to the imaginary-axis sources. However, it will be shown that this may

be simplified by expanding the integrand in such a form that the first term is recognizable as part of the semi-infinite-wing approximation.

The boundary conditions for the modified combined flow in the negative half of the t plane may be written as follows:

$$\left.\begin{aligned}
&\text{(i)}\quad \partial\phi_c/\partial n = 0;\ (-1+\varepsilon(0))/\lambda < \mathrm{Re}(t) < 0,\quad \mathrm{Im}(t) = 0;\\
&\text{(ii)}\quad \partial\phi_c/\partial n = 0;\ -\infty < \mathrm{Re}(t) < (-1-\varepsilon(\pi))/\lambda,\ \mathrm{Im}(t) = 0;\\
&\text{(iii)}\quad \frac{\partial\phi_c}{\partial n} = \frac{w_\infty b\,\overline{C}}{2h}\,\mathrm{Re}\left[\frac{\alpha^2-t^2}{1-\lambda^2t^2}\left(\frac{1-t^2}{1-k^2t^2}\right)^{\frac{1}{2}}\right];\ \mathrm{Re}(t) = 0,\ 0 < \mathrm{Im}(t) < \infty;\\
&\text{(iv)}\quad \frac{\partial\phi_c}{\partial n} = \frac{w_\infty b\,\overline{C}}{2h}\left|\frac{\alpha^2-t^2}{1-\lambda^2t^2}\left(\frac{1-t^2}{1-k^2t^2}\right)^{\frac{1}{2}}\right|;\ t = (-1+\varepsilon(\theta)e^{i\theta})/\lambda,\ 0 < \theta < \pi;\\
&\text{(v)}\quad dW_c/dt \sim w_\infty\overline{C}^2t/k^2\lambda^4h;\quad |t| \to \infty.
\end{aligned}\right\} \qquad (3.55)$$

Conditions (iii) and (iv) are determined by noting that the obstacle flow is symmetrical with respect to the z axis.

The fourth condition may be rewritten in terms of the polar coordinates $\varepsilon(\theta)$ and θ. Thus, if, in this expression, $\varepsilon(\theta)$ is replaced by ε and the resultant expression is expanded for small ε, it is found that

$$\left(\frac{\partial\phi_c}{\partial n}\right)_{AB} \simeq \frac{w_\infty b\overline{C}}{2h}\left|\frac{\alpha^2-1/\lambda^2}{2}\left(\frac{1-\lambda^2}{k^2-\lambda^2}\right)^{\frac{1}{2}}\frac{e^{-i\theta}}{\varepsilon} + \left(\frac{1-\lambda^2}{k^2-\lambda^2}\right)^{\frac{1}{2}}\left\{\frac{3+\lambda^2\alpha^2}{4\lambda^2} + \frac{(\lambda^2\alpha^2-1)k'^2}{2(1-\lambda^2)(k^2-\lambda^2)}\right\} + \text{etc.}\right|, \qquad (3.56)$$

where subscripts AB denote conditions at the boundary of indentation AB.

Before any approximations of equation (3.56) are made it is relevant to remark that $\varepsilon = \varepsilon(\lambda,k)$. Therefore, in general, the second term of the above expansion is not O(1). However, an examination of the relative magnitude of the first two terms of the

expansion indicates that the modulus of the second term is negligible compared with that of the first for $2h/b < 1$. On this basis, therefore, all terms but the first are neglected to give a result which, when combined with equation (3.40), yields the expression

$$(\partial\phi_c/\partial n)_{AB} \simeq w_\infty b\lambda/2\pi\varepsilon. \tag{3.57}$$

Thus, to the order of accuracy of the first, semi-circular, approximation for $\varepsilon(\theta)$, the normal velocity induced at the boundary of indentation AB is identical with that induced at the same place by a sink of strength $w_\infty b$ situated at $t = 1/\lambda$.

One interpretation of the zeroth approximation to an exact upper half-plane is that the boundary conditions of the indentations are ignored in determining the flow field. In the present case, however, such an interpretation will lead to large errors in σ owing to the fact that $(\partial\phi_c/\partial n)_{AB}$ increases monotonically as $\varepsilon \to 0$. A preferable interpretation is that the zeroth approximation satisfies the boundary conditions of the indentations in the mean around their boundaries.

Upon placing the above-mentioned sink at $t = -1/\lambda$ it is apparent that not only is the approximate boundary condition (3.57) satisfied but also the exact boundary condition (3.55) (iv) in the mean. This may be verified by examining the change in stream function from A to B, $\psi_A - \psi_B$, in each case. Therefore, in order to satisfy the second interpretation of the zeroth approximation, it is a condition that additional flows, which are needed to satisfy the remaining boundary conditions, must not alter $\psi_A - \psi_B$.

A flow which satisfies the asymptotic condition (3.55) (v) has a complex potential given by

$$W = w_\infty \overline{C}^2 t^2/2k^2\lambda^4 h \tag{3.58}$$

This also satisfies conditions (3.55) (i) and (ii) and induces zero normal velocity at Re(t) = 0. Further, as its complex potential is regular in the finite part of the t plane, this flow does not affect the value of $\psi_A - \psi_B$. Therefore, to the order of accuracy of the zeroth approximation, it does not disturb the boundary condition of indentation AB.

Condition (3.55)(iii) is satisfied by a distribution of sinks of strength $w_\infty b\ \overline{C}\ \mathrm{Re}\{(\alpha^2-t^2)(1-t^2)^{\frac{1}{2}}/(1-\lambda^2t^2)(1-k^2t^2)^{\frac{1}{2}}\}/h$ and situated on the imaginary axis in the interval $0 \leq \mathrm{Im}(t) \leq \infty$. In general, these sinks do not satisfy conditions (3.55)(i) and (ii). This may be remedied, however, by an image distribution of sinks beneath Im(t) = 0 which, it will be observed, does not disturb condition (3.55)(iii). Thus, by integrating the contributions of all the elementary sinks on the imaginary axis, it is found that their complex velocity is given by

$$\frac{dW(t)}{dt} = -\frac{w_\infty b\ \overline{C}}{2\pi h} \int_{-\infty}^{+\infty} \frac{t(\alpha^2+t_1^2)(1+t_1^2)^{\frac{1}{2}}dt_1}{(t_1^2+t^2)(1+\lambda^2t_1^2)(1+k^2t_1^2)^{\frac{1}{2}}}. \qquad (3.59)$$

This expression is seen to be regular for Re(t) < 0. Therefore, according to the zeroth approximation, the imaginary-axis sinks do not invalidate the boundary condition of the indentation AB.

Finally, it is observed that whilst the sink at $t = -1/\lambda$ satisfies conditions (3.5)(i) and (ii) it does not satisfy condition (3.5)(iii). However, this may be corrected by the introduction at $t = +1/\lambda$ of an image of the sink at $t = -1/\lambda$. This image has a regular complex potential except at $t = +1/\lambda$. Therefore, within the limitations of the zeroth approximation, it does not disturb the boundary condition of indentation AB.

Thus the zeroth approximation for the modified combined flow, $W_c^{(o)}$, may be written as follows:

$$Wc^{(o)}(t) = -\frac{w_\infty b\,\bar{C}}{2\pi h}\int_0^t dt_2 \int_{-\infty}^{+\infty} \frac{t_2(\alpha^2+t_1^2)(1+t_1^2)^{\frac{1}{2}}dt_1}{(t_1^2+t_2^2)(1+\lambda^2 t_1^2)(1+k^2t_1^2)^{\frac{1}{2}}} - \frac{w_\infty b}{2\pi}\ln(1-\lambda^2t^2) +$$

$$+ \frac{w_\infty \bar{C}^2 t^2}{2k^2\lambda^4 h}. \qquad (3.60)$$

Here the first term on the right-hand side is the complex potential of the sink distribution on the imaginary axis. This term is obtained by replacing t by t_2 in equation (3.59) and integrating with respect to t_2. The second term is due to the sink at $t= -1/\lambda$ and its image whilst the last term is the complex potential of equation (3.58).

Strictly, equation (3.60) should contain an arbitrary constant but, as was evident in the planar-wing case, such constants do not influence σ and thus the constant is neglected.

The integral of equation (3.60) may be evaluated by employing the expansion

$$\left(\frac{1+t_1^2}{1+k^2t_1^2}\right)^{\frac{1}{2}} = \frac{1}{k}\left\{1 - \frac{k'^2}{2(1+k^2t_1^2)} - \frac{k'^4}{8(1+k^2t_1^2)} + O(k'^6)\right\}.$$

This expansion is uniformly valid if $|1+k^2t_1^2| > k'^2$, a condition which is satisfied within the limits of the inner integration if $k' < 1$. Furthermore, it should converge rapidly for small h/b as, in this case, k' is small.

Thus the term $\{(1+t_1^2)/(1+k^2t_1^2)\}^{\frac{1}{2}}$ may be replaced in equation (3.60) by the expanded form and the inner integration performed term-by-term. This is achieved most conveniently by contour integration of the inner integrand in the complex t_1 plane. Here the contour consists of a semi-circle situated in the upper half of the plane with its centre at the origin and that part of the real axis directly underneath the semi-circle.

For $Re(t_2) < 0$ the contour surrounds simple poles at $t_1= -it_2$ and $t_1= i/\lambda$ and poles of various order at $t_1= i/k$. There are, however, no branch points within the contour; therefore it

is possible to use Cauchy's residue theorem.

The integral to be evaluated consists of the contribution of the real axis part of the contour to the contour integral in the limit as the radius of the semi-circle tends to infinity. Upon performing this limit it is found that the contribution of the semi-circle vanishes. Consequently the inner integral of equation (3.60) is simply $2\pi i$ times the residues within the contour. Therefore, after determining these residues, it is found that

$$\int_{-\infty}^{+\infty} \frac{t_2(\alpha^2+t_1^2)(1+t_1^2)^{\frac{1}{2}}dt_1}{(t_1^2+t_2^2)(1+\lambda^2t_1^2)(1+k^2t_1^2)^{\frac{1}{2}}} = \frac{\pi}{k}\left[-\frac{1}{\lambda^2}-\frac{(\alpha^2-1/\lambda^2)}{(1-\lambda t)}+\frac{k'^2}{2}\left\{\frac{(\lambda^2\alpha^2-1)}{(\lambda^2-k^2)(1-\lambda t)}-\right.\right.$$

$$-\frac{(k^2\alpha^2-1)}{(\lambda^2-k^2)(1-kt)}\Big\}+\frac{k'^4}{16}\left\{\frac{2\lambda^2(\lambda^2\alpha^2-1)}{(\lambda^2-k^2)^2(1-\lambda t)}-\frac{(3k^2\alpha^2\lambda^2-k^4\alpha^2-\lambda^2-k^2)}{(\lambda^2-k^2)^2(1-kt)}-\right.$$

$$\left.\left.-\frac{(k^2\alpha^2-1)}{(\lambda^2-k^2)(1-kt)^2}\right\}+O(k'^6)\right], \quad \mathrm{Re}(t_2) < 0. \tag{3.61}$$

Upon combining equations (3.60) and (3.61) and performing the t_2 integration one is able to obtain the following result :

$$W_c^{(o)}(t)=\frac{w_\infty b\,\bar{C}}{2hk}\left[\frac{t}{\lambda^2}-\frac{(\alpha^2-1/\lambda^2)}{\lambda}\ln(1-\lambda t)-\frac{k'^2}{2}\left\{\frac{(k^2\alpha^2-1)}{k(\lambda^2-k^2)}\ln(1-kt)-\right.\right.$$

$$-\frac{(\lambda^2\alpha^2-1)}{\lambda(\lambda^2-k^2)}\ln(1-\lambda t)\Big\}+\frac{k'^4}{16}\left\{\frac{2\lambda(\lambda^2\alpha^2-1)}{(\lambda^2-k^2)^2}\ln(1-\lambda t)-\right.$$

$$\left.\left.-\frac{(3k^2\alpha^2\lambda^2-k^4\alpha^2-\lambda^2-k^2)}{k(\lambda^2-k^2)^2}\ln(1-kt)+\frac{(k^2\alpha^2-1)t}{(\lambda^2-k^2)(1-kt)}\right\}+O(k'^6)\right]-$$

$$-\frac{w_\infty b}{2\pi}\ln(1-\lambda^2t^2)+\frac{w_\infty\bar{C}^2t^2}{2k^2\lambda^4h}, \qquad \mathrm{Re}(t) < 0\,. \tag{3.62}$$

The terms

$$\frac{w_\infty b\,\bar{C}}{2hk\lambda^2}\,t-\frac{w_\infty b}{2\pi}\ln(1+\lambda t)$$

of equation (3.62), together, represent the flow of a uniform stream with complex potential $w_\infty b\Omega/2h$ in the Riemann sheet containing the physical region $\mathrm{Re}|\Omega| < 0$. As Fig. 13 shows, this is identical

with the flow of the same uniform stream around the vortex trace of a planar wing of semi-infinite span and with an end plate. This confirms the remark made previously that the expanded form of integral (3.59) yields a first term which is part of the semi-infinite-wing approximation. Thus it seems likely that for small h/b a truncated form of the above expansion should yield reasonably accurate values of σ within the limits of accuracy imposed by the zeroth approximation.

3.3.3 Determination of the induced drag

The velocity potentials of the superposition flows are single-valued at the vortex trace. Therefore by employing equations (2.22) and (2.28) it is possible to write the zeroth approximation for Σ in the form

$$\Sigma^{(o)} = -2 \left\{ \int_{(-1+\varepsilon(0))/\lambda}^{-1/k} + \int_{-1}^{0} \right\} \phi_c^{(o)} (d\Omega/dt)\, dt \,/ w_\infty b^2 .$$

Therefore this equation may be combined with equations (3.2) and (3.62) to give the result

$$\Sigma^{(o)} = \Sigma_1^{(o)} + \Sigma_2^{(o)} + \Sigma_3^{(o)} .$$

Here

$$\Sigma_1^{(o)} = -\frac{\bar{C}^2}{kbh} \left\{ \int_{(-1+\varepsilon(0))/\lambda}^{1/k} + \int_{-1}^{0} \right\} \frac{f(t,k,\lambda)(\alpha^2-t^2)(1-t^2)^{\frac{1}{2}} dt}{(1-\lambda^2t^2)(1-k^2t^2)^{\frac{1}{2}}},$$

(where $f(t,k,\lambda)$ is the expression inside the square brackets of equation 3.62)

$$\Sigma_2^{(o)} = \frac{\bar{C}}{\pi b} \left\{ \int_{(-1+\varepsilon(0))/\lambda}^{-1/k} + \int_{-1}^{0} \right\} \frac{\ln(1-\lambda^2t^2)(\alpha^2-t^2)(1-t^2)^{\frac{1}{2}} dt}{(1-\lambda^2t^2)(1-k^2t^2)^{\frac{1}{2}}}$$

and

$$\Sigma_3^{(o)} = -\frac{\bar{C}^3}{k^2\lambda^4 b^2 h} \left\{ \int_{(-1+\varepsilon(0))/\lambda}^{-1/k} + \int_{-1}^{0} \right\} \frac{t^2(\alpha^2-t^2)(1-t^2)^{\frac{1}{2}} dt}{(1-\lambda^2t^2)(1-k^2t^2)^{\frac{1}{2}}} .$$

Of the three integral expressions given above it would seem that only $\Sigma_3^{(o)}$ may be evaluated explicitly. This is made possible by transformation (2.3) and equation (2.4) which enables one to

rewrite $\Sigma_3^{(o)}$ in the form

$$\Sigma_3^{(o)} = -\frac{\bar{C}^3}{k^2\lambda^4 b^2 h}\Big\{\int_{-2K(s_1+\bar{\varepsilon}(0))+iK'}^{-K+iK'} + \int_{-K}^{0}\Big\}\frac{sn^2 2Ks(\alpha^2-sn^2 2Ks)(1-sn^2 2Ks)\,d2Ks}{1-\lambda^2 sn^2 2Ks}\,. \tag{3.63}$$

After rearrangement, equation (3.63) may be replaced by

$$\Sigma_3^{(o)} = -\frac{\bar{C}^3}{k^2\lambda^4 b^2 h}\Big\{\int_{-2K(s_1+\bar{\varepsilon}(0))+iK'}^{-K+iK'} + \int_{-K}^{0}\Big\}\Big\{\frac{(1+\alpha^2-1/\lambda^2)sn^2 2Ks}{\lambda^2} - \frac{sn^4 2Ks}{\lambda^2} +$$

$$+\frac{(\lambda^2-1)(\alpha^2-1/\lambda^2)sn^2 2Ks}{\lambda^2(1-\lambda^2 sn^2 2Ks)}\Big\}d2Ks.$$

Thus, by comparing this expression with equation (3.28), it is evident that

$$\Sigma_3^{(o)} = -\frac{\bar{C}^3}{k^2\lambda^4 b^2 h}\Big\{\int_{-2K(s_1+\bar{\varepsilon}(0))+iK'}^{-K+iK'} + \int_{-K}^{0}\Big\}\Big\{\frac{(1+\alpha^2)sn^2 2Ks}{\lambda^2} - \frac{sn^4 2Ks}{\lambda^2} +$$

$$+\frac{1}{\lambda^2\bar{C}}\frac{d\Omega}{d2Ks} - \frac{\alpha^2}{\lambda^2}\Big\}\,d2Ks. \tag{3.64}$$

The first two terms of the integrand of equation (3.64) may be integrated by means of equations (310.02) and (310.04) of Byrd and Friedman. The third term, on the other hand, does not contribute to $\Sigma_3^{(o)}$ owing to the requirement of point-to-point correspondence between the Ω and s planes which demands that

$$\Omega(-K + iK') = \Omega(-K);$$
$$\Omega\{-2K(s_1 + \bar{\varepsilon}(0)) + iK'\} = \Omega(0).$$

Therefore, after performing the integration, equation (3.64) becomes

$$\Sigma_3^{(o)} = -\frac{\bar{C}^3}{k^2\lambda^4 b^2 h}\Big[\frac{(1+\alpha^2)}{k^2\lambda^2}\Big(2K(s_1+\bar{\varepsilon}(0)) - E(-K+iK') + E\{-2K(s_1+\bar{\varepsilon}(0)) + iK'\} -$$

$$- E(0) + E(-K)\Big) - \frac{1}{3k^4\lambda^2}\Big((2+k^2)2K(s_1+\bar{\varepsilon}(0)) - 2(1+k^2)\Big[E(-K+iK') -$$

$$-E\{-2K(s_1+\bar{\varepsilon}(0)) + iK'\} + E(0) - E(-K)\Big] +$$

$$+k^2\Big[\mathrm{sn}(-K+iK')\,\mathrm{cn}(-K+iK')\,\mathrm{dn}(-K+iK')-$$

$$-\,\mathrm{sn}\{-2K(s_1+\bar{\varepsilon}(0))+iK'\}\,\mathrm{cn}\{-2K(s_1+\bar{\varepsilon}(0))+iK'\}\,\mathrm{dn}\{-2K(s_1+\bar{\varepsilon}(0))+iK'\}+$$

$$+\,\mathrm{sn}(0)\,\mathrm{cn}(0)\,\mathrm{dn}(0)-\mathrm{sn}(-K)\,\mathrm{cn}(-K)\,\mathrm{dn}(-K)\Big]\Big)-\frac{\alpha^2}{\lambda^2}\,2K(s_1+\bar{\varepsilon}(0))\Big]\,. \tag{3.65}$$

An examination of the magnitude of $\bar{\varepsilon}^{(1)}(0)$ would seem to suggest that, for $2h/b < 1$, $\bar{\varepsilon}(0)$ is negligible compared with s_1 and hence it is ignored in equation (3.65). The resulting expression is then simplified by employing equation (3.39) to expand the elliptic integrals. In turn, this equation may be further simplified by employing properties of the elliptic functions and integrals given by Byrd and Friedman in equations (111.00), (113.01), (122.00), (122.01), (122.02), (122.07) and (141.01) to yield finally

$$\Sigma_3^{(o)} = -\frac{\bar{C}^3}{k^2\lambda^4b^2h}\Big[\frac{(1+\alpha^2)}{k^2\lambda^2}\{2Ks_1(1+\frac{E(K)}{K})-Z(2Ks_1)-\frac{\mathrm{cn}2Ks_1\,\mathrm{dn}2Ks_1}{\mathrm{sn}2Ks_1}\}-$$

$$-\frac{1}{3k^4\lambda^2}\{(2+k^2)2Ks_1-2(1+k^2)\Big[Z(2ks_1)-\frac{E(K)2Ks_1}{K}+\frac{\mathrm{cn}2Ks_1\,\mathrm{dn}2Ks_1}{\mathrm{sn}2Ks_1}\Big]$$

$$-\frac{\mathrm{cn}2Ks_1\,\mathrm{dn}2Ks_1}{\mathrm{sn}^3 2Ks_1}\}-\frac{\alpha^2}{\lambda^2}\,2Ks_1\Big]\,.$$

Before $\Sigma_1^{(o)}$ and $\Sigma_2^{(o)}$ may be evaluated it is necessary to replace $\varepsilon(0)$ by ε in the limits of the integrals which appear in these expressions. Although the error implicit in this approximation has not been determined for arbitrary k it seems likely that it is extremely small for $h/b < \frac{1}{2}$. This view is supported by a study performed for $k = 1$ ($\gamma/b = 0$) which indicates that the error involved with this approximation is $O(\varepsilon^2)$ compared with $\Sigma^{(o)}$.

The only other approximation to be employed is in the expansion appearing in $f(t,k,\lambda)$, terms of $O(k'^6)$ being neglected. Examination of the neglected terms indicates that the error so caused in $\Sigma^{(o)}$ is negligible for the cases considered.

As a check on the status of the present interpretation of $\Sigma^{(o)}$ it is worth while to consider its asymptotic behaviour as $\ell/b \to o$ ($k' \to o$). Thus, without giving details, one finds that

$$\Sigma^{(o)} \sim \frac{\overline{C}^3}{2\lambda^6 h b^2}\left[\frac{(1-\lambda^2)}{\lambda^3}\ln\left(\frac{2}{\epsilon}\right) - \frac{2}{3\lambda^3} - \frac{2(1-\lambda^2)}{\lambda^5} + O(\epsilon^2)\right], \quad k'\to o, (\ell/b\to o).$$

It will be seen that this expression is identical with that of $\Sigma^{(o)}$ for the planar wing (equation 3.24) to the order of accuracy of that approximation.

The integrals of $\Sigma_1^{(o)}$ and $\Sigma_2^{(o)}$ have been evaluated numerically by employing the Gaussian method of mechanical quadrature This technique was applied directly between the limits of integration -1 to 0, a fifteen-point interpolation scheme having been used. However, between $(-1 + \epsilon)/\lambda$ and $-1/k$ an alternative approach was necessary owing to the singularities in the integrands within or very close to these limits. This consisted of replacing each integrand by the sum of a function which is bounded for $(-1 + \epsilon)/\lambda \leq t \leq -1/k$ and a function which may be integrated explicitly. Thus, for example, the integrand of $\Sigma_2^{(o)}$ was rewritten in the form

$$\frac{\ln(1-\lambda^2t^2)(\alpha^2-t^2)(1-t^2)^{\frac{1}{2}}}{(1-\lambda^2t^2)(1-k^2t^2)^{\frac{1}{2}}} = \frac{A(\lambda,k)}{(k^2t^2-1)^{\frac{1}{2}}} + \frac{B(\lambda,k)\{\ln(1+\lambda t)+\ln(1+\lambda/k)\}}{(1+\lambda t)} +$$

$$+ C(t,\lambda,k). \qquad (3.66)$$

Here $A(\lambda,k)$ and $B(\lambda,k)$ are terms obtained by expanding the integrand about the singularities at $t = -1/k$ and $t = -1/\lambda$ whilst $C(t,\lambda,k)$ is a function which is bounded in the interval of integration.

A similar process was applied to the integrand of $\Sigma_1^{(o)}$ to give an expression of the form

$$\frac{f(t,k,\lambda)(\alpha^2-t^2)(1-t^2)^{\frac{1}{2}}}{(1-\lambda^2t^2)(1-k^2t^2)^{\frac{1}{2}}} = \frac{A'(\lambda,k)}{(k^2t^2-1)^{\frac{1}{2}}} + \frac{B'(\lambda,k)}{(1-\lambda^2t^2)} + C'(t,\lambda,k), \qquad (3.67)$$

where $A'(\lambda,k)$, $B'(\lambda,k)$ and $C'(t,\lambda,k)$ are analogous with $A(\lambda,k)$, $B(\lambda,k)$ and $C(t,\lambda,k)$.

The first two terms on the right-hand side of equations (3.66) and (3.67) may be integrated analytically. Thus, in order to determine $\Sigma_1^{(o)}$ and $\Sigma_2^{(o)}$, it is only necessary to integrate $C(t,\lambda,k)$ and $C'(t,\lambda,k)$ between the limits $(-1 + \varepsilon)/\lambda$ and $-1/k$. This was achieved by using the Gaussian method with a seven-point interpolation.

All the numerical integration described has been programmed for computation on a Ferranti Pegasus computer.

The accuracy of the final result obtained for $\Sigma^{(o)}$ was checked for the case $l/b = 0$ by comparing this result with the planar-wing value (equation 3.24). There was found to be excellent agreement between the two results.

By noting that the end plates do not contribute to the overall lift of the configuration it is possible to conclude that $\sigma^{(o)}$ is related to $\Sigma^{(o)}$ in the manner of equation (2.34). Thus $\sigma^{(o)}$ has been determined and the results obtained are plotted against 2h/b for various $2l/b$ and against l/h for various 2h/b in Figs. 14 and 15.

4. Discussion

The results confirm what might be expected on an intuitive basis, namely that for a given 2h/b an increase in $2l/b$ reduces the induced-drag factor. What is more important, perhaps, is that they show that the reduction is greatest in the vicinity of $2l/b \approx 2h/b$, yielding $\sigma^{(o)} = 0$ for $2l/b = 2h/b$. The reason for this is that for $2l/b = 2h/b$ the only physically acceptable value for w_∞ is zero. On the other hand, for quite small $2(h-l)/b$, $|w_\infty|$ and $\sigma^{(o)}_\infty$ can be appreciable owing to the large mass flow between the ground and the tips of the end-plate traces caused by the singular velocities there. However, this is an unrealistic feature which will not occur in practice owing to the action of viscosity.

Other features of the theory which may be criticized are, firstly, that it does not represent the deformation of the trailing-

vortex sheet. Secondly, it does not allow for the non-linear influence of the ground on the relationship between lift and circulation. To represent these effects completely in a theory is extremely difficult. A more promising approach would seem to be to compare the linearized theory with experiment in the hope of achieving the following aims:

(i) To decide on the limits to be placed on the accuracy of the linearized theory.

(ii) To identify important effects not included in the theory. Such a comparison is effected in Chapter III which also deals with a discussion of the experiments on various open configurations.

CHAPTER II

THE LIFT AND INDUCED DRAG OF A CLOSED GROUND-EFFECT WING

1. Introduction

Closed G.E.Ws. may, in theory, be designed for zero induced drag whilst giving non-zero lift. However, in practice, there are many factors which may prevent this ideal from being achieved. For example, in the case of a G.E.W. with end plates, structural requirements will, to a large extent, influence the design of the end plates. The reason for this is that the end plates will be exposed to wave impact and, in consequence, will transmit large, transient loads to the main structure. It is conceivable, therefore, that the end plates will be required to have minimum hydrodynamic drag, a requirement which may conflict with the requirement of minimum induced drag.

Thus the main aim of this chapter is to describe a method of determining the lift and induced drag of a closed configuration which is not designed ab initio for zero induced drag. This method is based on a study of sectional-drag relationships which will be described in Part I of this chapter. Subsequently, in Part II, the technique developed in Part I will be applied to the problem stated above.

There is evidence from the two-dimensional theory of de Haller (1936) that unless the non-linear features of the problem are included in the theory it will be inaccurate. Therefore, although initially the theory will be developed on the basis of the linearized theory, it will be modified in Section 7 to allow for the most significant non-linearities.

PART I

FOUNDATIONS

2. The relationship between sectional drag and induced drag.

This section is concerned with an analysis of the sectional drag of various lifting systems including those representative of the G.E.W. configurations to be considered in Part II. Throughout the analysis, the discussion will be confined to wings having chordwise sections of zero thickness and the following assumptions will be employed:

(i) The flow relative to the lifting system is inviscid and incompressible.

(ii) The approximations of the linearized lifting-surface theory are applicable.

2.1 Wings with arbitrary planforms and vorticity distributions

Consider an isolated planar wing of arbitrary planform in forward flight. Suppose that the wing, which is shown in Fig. 16 with the right-hand coordinate system (x,y,z), is designed to sustain a y component of vorticity $\gamma(x,y)$. The linearized form of the sectional drag of the wing may be found by reference to the analysis of Jones and Cohen (1957, p.p.23-24). This enables one to derive the result

$$D_f(y) = -\rho \int_0^{c(y)} w_f(x,y)\gamma(x,y)dx - T(y). \qquad (2.1)$$

Here $D_f(y)$ and $w_f(x,y)$ are the sectional drag and upwash at the wing in forward flight, $T(y)$ is the sectional edge thrust (negative drag) and $c(y)$ is the local chord.

The motion of the wing is reversed and a new right-handed coordinate system (x',y',z'), which is defined by

$$x' = -x, \quad y' = -y, \quad z' = z, \qquad (2.2)$$

is introduced. At the same time, the camber distribution of the wing is modified such that at all stations (x,y) of the wing the y' component of vorticity is identical with $\gamma(x,y)$.

Robinson and Laurmann (1956, p.p. 172-174) have shown that, within the limitations of the linearized theory, the sectional edge thrust of a given planform depends only on $\gamma(x,y)$. Therefore the sectional drag in reverse flight is given by

$$D_r(y) = -\rho \int_{-c(y)}^{o} w_r(x',y')\gamma(x,y)dx' + T(y), \qquad (2.3)$$

where the subscript r denotes reverse-flight quantities.

Equation (2.2) may be used to rewrite equation (2.3) in the form

$$D_r(y) = -\rho \int_{o}^{c(y)} w_r(x',y')\gamma(x,y)dx + T(y).$$

In turn, this result may be combined with equation (2.1) to yield the result

$$D_f(y) + D_r(y) = -\rho \int_{o}^{c(y)} \{w_f(x,y) + w_r(x',y')\}\gamma(x,y)dx. \qquad (2.4)$$

As noted in Section I. 1.1, the linearized theory employs the assumption that the wing and its trailing-vortex sheet lie on a cylindrical surface with generators parallel to the direction of motion. It is also observed in the same section that the trailing-vortex vector is everywhere parallel to the flow relative to, and infinitely far forward of, the wing. Therefore, if the flow fields of the two motions are superposed, there results an infinite vortex strip which is in the plane $z = 0$ and parallel to x. Further, the span of the strip is the same as that of the wing.

By recalling the fundamental laws of vortex motion, (Thwaites, 1960, p.32) it may be concluded that at all x-wise stations the circulation distribution of the vortex strip is the same as that at the vortex trace in the Trefftz plane of either motion. Hence, if $w_\infty(y)$ is the upwash at the vortex trace in the Trefftz plane of

the forward motion, it follows that

$$w_f(x,y) + w_r(x',y') = w_\infty(y), \tag{2.5}$$

a result originally due to Jones (1951). Therefore equations (2.4) and (2.5) may be combined to give the result

$$D_f(y) + D_r(y) = -\rho\, w_\infty(y)\, \Gamma(y), \tag{2.6}$$

where

$$\Gamma(y) = \int_0^{c(y)} \gamma(x,y)\,dx$$

is the circulation around the section, defined positive in the lifting sense. That this is the same as the jump in velocity potential, $\phi_u(y) - \phi_l(y)$, at the vortex trace in the Trefftz plane of either motion follows from the laws of vortex motion.

Equation (2.6) may be written in the alternative form

$$D_f(y) + D_r(y) = 2\, D_i(y), \tag{2.7}$$

where $D_i(y) = -\rho\, w_\infty(y)\, \Gamma(y)/2$ is referred to as the induced-drag gradient. This title is suggested from considerations of the form of the expression for the overall induced drag of the wing which, by employing equation (I. 2.22), may be written in the form

$$\overline{D}_i = -\rho \int_b w_\infty(y)\, \Gamma(y)\,dy/2.$$

Here the subscript b denotes integration across the span of the wing.

Equations (2.4) and (2.7) may be generalized without difficulty to include non-planar lifting systems as follows:

$$\left.\begin{aligned} D_f(s) + D_r(s) &= -\rho v_{n\infty}(s)\, \Gamma(s), \\ &= 2\, D_i(s), \end{aligned}\right\} \tag{2.8}$$

where (s, n) are curvilinear, orthogonal coordinates in planes normal to the direction of motion such that n is constant on the trace of the cylindrical surface. Also, $v_{n\infty}(s)$ is the velocity in the direction of n at the vortex trace in the Trefftz plane.

The circulation $\Gamma(s)$ is defined positive if the sectional force in the direction of n is positive.

2.2 Wings with a spanwise plane of symmetry

Equations (2.7) and (2.8) provide no information about the separate values of the sectional drags for the two motions. However, some progress in this direction is possible in the case of wings with a spanwise plane of symmetry.

2.2.1 Symmetrical chordwise distributions of $\gamma(x,y)$

Consider an isolated planar wing with a spanwise plane of symmetry and a vortex distribution $\gamma(x,y)$ which is symmetrical with respect to the mid-chord axis. Thus, if the origin of the axes is placed on the mid-chord axis of the wing, it may be concluded from symmetry considerations that

$$w_f(x,y) = w_r(x,y') \tag{2.9}$$

This relationship is illustrated diagramatically in the sketch below

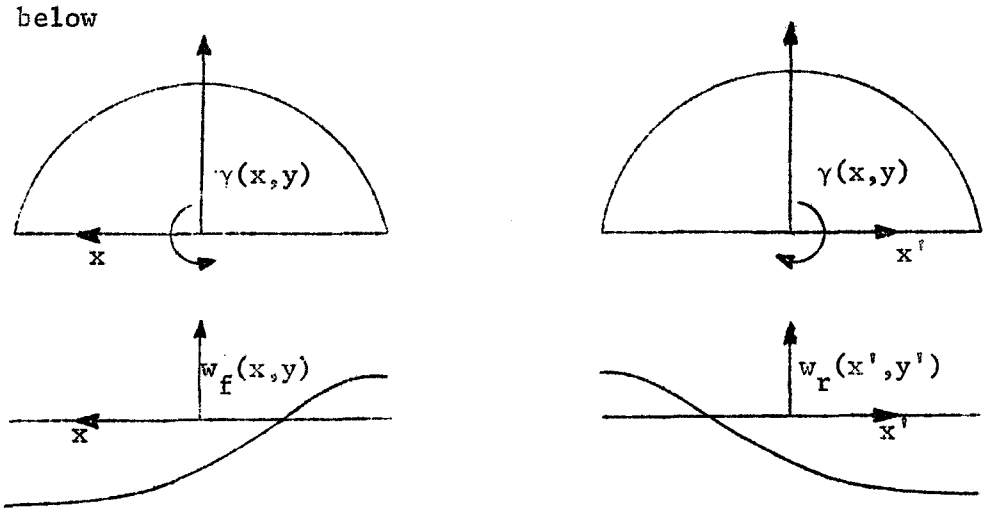

FORWARD REVERSE

For convenience, $w_f(x,y)$ and $w_r(x,y)$ are written in the following forms:

$$\left.\begin{aligned} w_f(x,y) &= w_f^{(a)}(x,y) + w_f^{(s)}(x,y), \\ w_r(x',y') &= w_r^{(a)}(x',y') + w_r^{(s)}(x',y'), \end{aligned}\right\} \quad (2.10)$$

where the superscripts (a) and (s) imply that the respective functions are antisymmetric and symmetric with respect to the mid-chord axis.

The antisymmetric part of $w_f(x,y)$ is given by

$$\begin{aligned} w_f^{(a)}(x,y) &= \tfrac{1}{2}\{w_f(x,y) - w_f(-x,y)\}, \\ &= \tfrac{1}{2}\{w_r(x,y') - w_r(-x,y')\} \end{aligned} \quad (2.11)$$

from equation (2.9). But

$$w_r^{(a)}(x',y') = \tfrac{1}{2}\{w_r(x',y') - w_r(-x',y')\}. \quad (2.12)$$

Hence, by comparing equations (2.2), (2.11) and (2.12), it is evident that

$$w_f^{(a)}(x,y) = -w_r^{(a)}(x',y'). \quad (2.13)$$

A similar analysis applied to the symmetric parts of $w_f(x,y)$ and $w_r(x',y')$ reveals that

$$w_f^{(s)}(x,y) = w_r^{(s)}(x',y'). \quad (2.14)$$

By combining equations (2.5) and (2.10) it is possible to obtain the result

$$w_f^{(a)}(x,y) + w_r^{(a)}(x',y') + w_f^{(s)}(x,y) + w_r^{(s)}(x',y') = w_\infty(y).$$

In turn, this expression may be combined with equations (2.13) and (2.14) to give the result

$$w_f^{(s)}(x,y) = w_\infty(y)/2. \quad (2.15)$$

Thus it is apparent from equations (2.10) and (2.15) that

$$w_f(x,y) = w_f^{(a)}(x,y) + w_\infty(y)/2. \tag{2.16}$$

As a consequence of the chordwise symmetry of the planform and the vortex distribution the sectional edge thrust is zero. Therefore

$$D_f(y) = -\rho \int_{-c(y)/2}^{+c(y)/2} w_f(x,y)\gamma(x,y)dx,$$

$$= -\rho \int_{-c(y)/2}^{+c(y)/2} \{w_f^{(a)}(x,y) + w_\infty(y)/2\}\gamma(x,y)dx \tag{2.17}$$

from equation (2.16). Hence, by recalling that $\gamma(x,y)$ is symmetric about the mid-chord axis and examining the form of the integrand of equation (2.17), one may conclude that

$$D_f(y) = -\rho\, w_\infty(y)\, \Gamma(y)/2,$$

$$= D_i(y). \tag{2.18}$$

It is not difficult to generalize equation (2.18) to include wings of non-planar span having the following properties:

(a) a chordwise distribution of the s component of vorticity which is symmetrical about the mid-chord point at each s-wise station;

(b) elements with mid-chord points occupying a single plane which is normal to the direction of motion.

For non-planar wings with these properties

$$D_f(s) = D_i(s).$$

2.2.2 Arbitrary chordwise distributions of $\gamma(x,y)$

The preceding analysis may be generalized somewhat by considering arbitrary chordwise distributions of $\gamma(x,y)$ which, for convenience, will be written in the form

$$\gamma(x,y) = \gamma^{(e)}(x,y) + \gamma^{(o)}(x,y).$$

Here $\gamma^{(e)}(x,y)$ and $\gamma^{(o)}(x,y)$ are even and odd functions of x with respect to $x = 0$, respectively. Thus, hereafter, any function which is superscripted with (e) or (o) corresponds to the even or odd components of $\gamma(x,y)$. However, it need not necessarily be an even or odd function of x.

The sectional drag in forward motion may be written in the form

$$\begin{aligned} D_f(y) &= -\rho \int_{-c(y)/2}^{+c(y)/2} \{w_f^{(e)}(x,y) + w_f^{(o)}(x,y)\}\{\gamma^{(e)}(x,y) + \gamma^{(o)}(x,y)\}dx - T(y), \\ &= -\rho \int_{-c(y)/2}^{+c(y)/2} w_f^{(e)}(x,y)\gamma^{(e)}(x,y)dx - \rho \int_{-c(y)/2}^{+c(y)/2} w_f^{(o)}(x,y)\gamma^{(o)}(x,y)dx - \\ &\quad -\rho \int_{-c(y)/2}^{+c(y)/2} w_f^{(o)}(x,y)\gamma^{(e)}(x,y)dx - \rho \int_{-c(y)/2}^{+c(y)/2} w_f^{(e)}(x,y)\gamma^{(o)}(x,y)dx - T(y), \end{aligned} \tag{2.19}$$

The first term on the right-hand side of equation (2.19) is the sectional drag of the distribution $\gamma^{(e)}(x,y)$. Only this distribution contributes to $\Gamma(y)$ and hence to $D_i(y)$ owing to the fact that $\Gamma^{(o)}(y) = 0$. Therefore

$$D_i(y) = D_i^{(e)}(y) .$$

It has been shown in Section 2.2.1, however, that $D_i^{(e)}(y) = D_f^{(e)}(y)$. Hence

$$D_f^{(e)}(y) \equiv -\rho \int_{-c(y)/2}^{+c(y)/2} w_f^{(e)}(x,y)\gamma^{(e)}(x,y)dx = D_i(y). \tag{2.20}$$

As $\Gamma^{(o)}(y) = 0$, it follows that $w_\infty{}^{(o)}(y) = 0$. Thus, by employing equation (2.5), which applies for arbitrary $\gamma(x,y)$, it may be concluded that

$$w_f{}^{(o)}(x,y) + w_r{}^{(o)}(x',y') = 0. \qquad (2.21)$$

It is apparent from an examination of the symmetry of the induced velocity field of the distribution $\gamma^{(o)}(x,y)$ that

$$w_f{}^{(o)}(x',y) = -w_r{}^{(o)}(x',y'), \qquad (2.22)$$

a relationship which is illustrated in the accompanying sketch

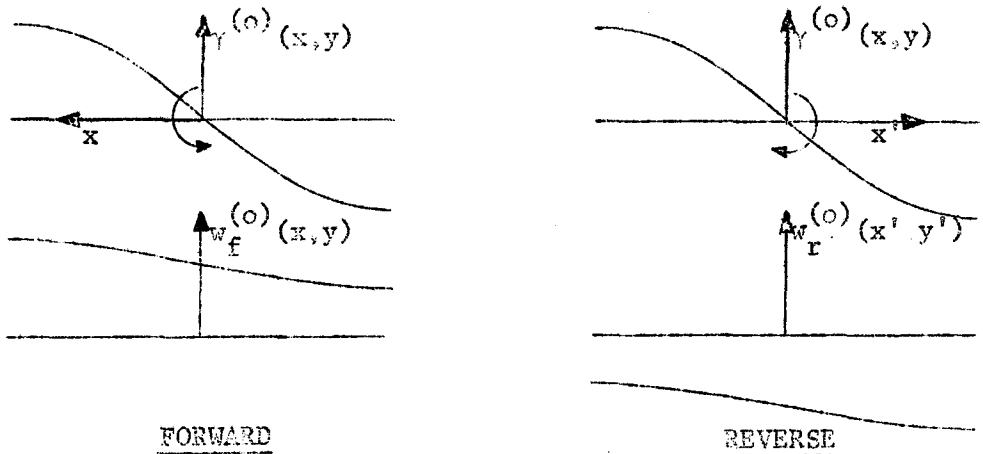

FORWARD REVERSE

Therefore $w_r{}^{(o)}(x',y')$ may be eliminated from equations (2.21) and (2.22) to provide the result

$$w_f{}^{(o)}(x,y) - w_f{}^{(o)}(x',y) = 0.$$

Hence it follows that, as $x' = -x$, $w_f{}^{(o)}(x,y)$ is an even function of x and consequently

$$\int_{-c(y)/2}^{+c(y)/2} w_f{}^{(o)}(x,y)\gamma^{(o)}(x,y)dx = 0. \qquad (2.23)$$

Thus, upon combining equations (2.19), (2.20) and (2.23), it is found that

$$D_f(y) = D_i(y) - \rho \int_{-c(y)/2}^{+c(y)/2} w_f^{(o)}(x,y)\gamma^{(e)}(x,y)dx - \rho \int_{-c(y)/2}^{+c(y)/2} w_f^{(e)}(x,y)\gamma^{(o)}(x,y)dx - T(y). \tag{2.24}$$

It appears not to be possible to reduce equation (2.24) without explicit knowledge of the form of $\gamma^{(e)}(x,y)$ and $\gamma^{(o)}(x,y)$. However, it may be inferred from this equation that, provided that

$$\rho \int_{-c(y)/2}^{+c(y)/2} w_f^{(o)}(x,y)\gamma^{(e)}(x,y)dx + \rho \int_{-c(y)/2}^{+c(y)/2} w_f^{(e)}(x,y)\gamma^{(o)}(x,y)dx + T(y) = 0, \tag{2.25}$$

$D_f(y) = D_i(y)$.

It is difficult, in general, to determine classes of vorticity distributions which satisfy equation (2.25). On the other hand, as the overall drag is identical with the overall induced drag, it follows from equation (2.24) that equation (2.25) is satisfied in the mean across the span of the wing. Thus equation (2.25) is approximately correct if the quantities in this equation which vary with y do so slowly. On this basis, therefore, it is anticipated that this equation applies approximately for planar wings of large aspect ratio and with a spanwise plane of symmetry. Thwaites (1960) has shown that, for uncambered wings of this class, $\gamma(x,y)$ is of the form

$$\gamma(x,y) \equiv \gamma\{2x/c(y)\}f(2y/b), \tag{2.26}$$

where, it will be recalled, b is the span of the wing. This type of distribution has been employed in the approximate lifting-surface theories of Weighardt(1940) and Küchemann (1952) to determine the lift of uncambered planar wings. The latter author justified its

use on the basis that in the region of the wing tips, where it is unrepresentative, the lift is comparatively small. Therefore he argued that the error thereby introduced into the lift is likely to be unimportant.

The distribution (2.26) is of particular interest here as it seems that it approximates well to the vortex distributions of certain closed G.E.Ws. (see Section 5). It is instructive, therefore, to examine in more detail the sectional drag equation associated with this class of distribution.

2.2.3 Sectional drag of the distribution $\gamma\{(2x/c(y)\}\bar{f}(2y/b)$

In order to obtain a more explicit form for equation (2.24) it is necessary to know the relationship between $\gamma(x,y)$ and $w_f(x,y)$. This has been derived by Lawrence (1951) for isolated planar wings as follows:

$$w_f(x_1,y_1) = -\frac{1}{4\pi}\frac{\partial}{\partial y_1}\int_S\int\frac{\gamma(x,y)}{y_1-y}\left[1+\frac{\{(x_1-x)^2+(y_1-y)^2\}^{\frac{1}{2}}}{x_1-x}\right]dx\,dy, \tag{2.27}$$

where the subscript S denotes integration over the planform. Therefore, if the wing has a spanwise plane of symmetry and $\gamma(x,y)$ is as given by equation (2.26), equation (2.27) becomes

$$w_f(\xi_1,y_1) = -\frac{1}{8\pi}\frac{\partial}{\partial y_1}\int_{-1}^{+1}\gamma(\xi)d\xi\int_{-b/2}^{+b/2}\frac{c(y)\bar{f}(2y/b)}{y_1-y}\left[1+\right.$$

$$\left.+\frac{\{(c(y_1)\xi_1-c(y)\xi)^2+4(y_1-y)^2\}^{\frac{1}{2}}}{c(y_1)\xi_1-c(y)\xi}\right]dy, \tag{2.28}$$

where $\xi = 2x/c(y)$, $\xi_1 = 2x_1/c(y_1)$.

The right-hand side of equation (2.28) is evaluated subject to Cauchy principal values (as defined by Thwaites, 1960, p. 118) being taken where required.

Thus, by employing equation (2.28), it is possible to replace the first integral of equation (2.24) by the expression

$$\int_{-c(y_1)/2}^{+c(y_1)/2} \gamma^{(e)}(\xi_1) f(2y_1/b)\, w_f^{(o)}(x_1, y_1)\, dx_1 =$$

$$= -\frac{c(y_1) f(2y_1/b)}{16\pi}\left[\int_{-1}^{+1} \gamma^{(e)}(\xi_1) d\xi_1 \frac{\partial}{\partial y_1} \int_{-1}^{+1} \gamma^{(o)}(\xi) d\xi \int_{-b/2}^{+b/2} \frac{c(y) f(2y/b) dy}{y_1 - y} + \right.$$

$$\left. + \int_{-1}^{+1} \gamma^{(e)}(\xi_1) d\xi_1 \frac{\partial}{\partial y_1} \int_{-1}^{+1} \gamma^{(o)}(\xi) d\xi \int_{-b/2}^{+b/2} A(y, y_1, \xi, \xi_1) dy\right], \quad (2.29)$$

where

$$A(y, y_1, \xi, \xi_1) = \frac{c(y) f(2y/b)\{(c(y_1)\xi_1 - c(y)\xi)^2 + 4(y_1 - y)^2\}^{\frac{1}{2}}}{(y_1 - y)(c(y_1)\xi_1 - c(y)\xi)}. \quad (2.30)$$

The ξ integrand of the first multiple integral of equation (2.29) is antisymmetric. Therefore this term vanishes identically to yield the expression

$$\int_{-c(y_1)/2}^{+c(y_1)/2} \gamma^{(e)}(\xi_1) f(2y_1/b) w_f^{(o)}(x_1, y_1) dx_1 =$$

$$= -\frac{c(y_1) f(2y_1/b)}{16\pi} \int_{-1}^{+1} \gamma^{(e)}(\xi_1) d\xi_1 \int_{-1}^{+1} \gamma^{(o)}(\xi) d\xi \frac{\partial}{\partial y_1} \int_{-b/2}^{+b/2} A(y, y_1, \xi, \xi_1) dy, \quad (2.31)$$

where it has been assumed permissible to perform the y_1 differentiation under the ξ integral sign.

In a similar fashion the second integral of equation (2.24) becomes

$$\int_{-c(y_1)/2}^{+c(y_1)/2} \gamma^{(o)}(\xi_1) f(2y_1/b) w_f^{(e)}(x_1, y_1) dx_1 =$$

$$= -\frac{c(y_1) f(2y_1/b)}{16\pi}\left[\int_{-1}^{+1} \gamma^{(o)}(\xi_1) d\xi_1 \frac{\partial}{\partial y_1} \int_{-1}^{+1} \gamma^{(e)}(\xi) d\xi \int_{-b/2}^{+b/2} \frac{c(y) f(2y/b)}{y_1 - y} dy + \right.$$

$$\left. + \int_{-1}^{+1} \gamma^{(o)}(\xi_1) d\xi_1 \frac{\partial}{\partial y_1} \int_{-1}^{+1} \gamma^{(e)}(\xi) d\xi \int_{-b/2}^{+b/2} A(y, y_1, \xi, \xi_1) dy\right].$$

The first multiple integral of this expression is identically zero, a fact which may be proved by noting the anti-symmetric form of the ξ_1 integrand of this integral. Hence

$$\int_{-c(y_1)/2}^{+c(y_1)/2} \gamma^{(o)}(\xi_1) f(2y_1/b)\, w_f^{(e)}(x_1,y_1)dx_1 =$$

$$= -\frac{c(y_1)f(2y_1/b)}{16\pi} \int_{-1}^{+1} \gamma^{(o)}(\xi_1)d\xi_1 \int_{-1}^{+1} \gamma^{(e)}(\xi)d\xi \frac{\partial}{\partial y_1} \int_{-b/2}^{+b/2} A(y,y_1,\xi,\xi_1)dy \ , \qquad (2.32)$$

the differentiation with respect to y_1 being taken under the ξ integral sign as before.

An examination of equations (2.31) and (2.32) suggests that the two multiple integrals become basically similar if the order of the ξ and ξ_1 integration is reversed in one of them. Therefore, before these equations are used to rewrite equation (2.42), the order of the ξ and ξ_1 integration of equation (2.32) will be interchanged. This may be performed according to the following rule given by Measlet and Lomax (1955):

$$\int_S d\xi_1 \int \psi(\xi,\xi_1)d\xi = \int_S d\xi \int \psi(\xi,\xi_1)d\xi_1 + R \ ,$$

where R is the 'residual'. According to these authors, if the singularity causing the residual is located at the upper limits of the integration, say $\xi_1 = +1$, $\xi = +1$, then

$$R = \lim_{\varepsilon \to o} \left[\int_{1-\varepsilon}^{1} d\xi_1 \int_{1-\varepsilon}^{1} \psi(\xi,\xi_1)d\xi - \int_{1-\varepsilon}^{1} d\xi \int_{1-\varepsilon}^{1} \psi(\xi,\xi_1)d\xi_1 \right] . \qquad (2.33)$$

In general, however, the singularity or singularities producing residuals may occur anywhere within the area of integration. Their location can be determined by means of a simple test given by Measlet and Lomax. This states that a residual results if, at the point $\xi=a$, $\xi_1=b$ in the area of integration,

$$\lim_{\varepsilon \to o} \varepsilon^2 \psi(a-\varepsilon\eta,\ b-\varepsilon\eta_1) \neq 0,$$

where $\varepsilon\eta = a-\xi$; $\varepsilon\eta_1 = b-\xi_1$. (2.34)

Heaslet and Lomax have remarked that if this test reveals the presence of more than one residual then the total residual is the sum of the separate residuals.

The residual corresponding to equation (2.32) may be found by replacing $\gamma^{(e)}(\xi)$ and $\gamma^{(o)}(\xi)$ in this equation by the representative forms

$$\left.\begin{aligned} \gamma^{(e)}(\xi) &= a_o^{(e)} U_o/(1-\xi^2)^{\frac{1}{2}} + \text{even bounded terms;} \\ \gamma^{(o)}(\xi) &= -a_o^{(o)} U_o \xi/(1-\xi^2)^{\frac{1}{2}} + \text{odd bounded terms,} \end{aligned}\right\} \quad (2.35)$$

where $a_o^{(e)}$ and $a_o^{(o)}$ are non-dimensional coefficients. These distributions are representative insofar as they conform to the requirement (noted by Robinson and Laurmann, 1956) that if $\gamma^{(e)}(\xi)$ and $\gamma^{(o)}(\xi)$ become singular at the edges they do so as $(1-\xi^2)^{-\frac{1}{2}}$.

Thus the above-mentioned test reveals that there are two residuals associated with the multiple integral of equation (2.32), both being caused by the cross-product of the singular terms of $\gamma^{(e)}(\xi)$ and $\gamma^{(o)}(\xi_1)$. Therefore, if the order of the ξ and ξ_1 integration in equation (2.32) is interchanged, there is obtained the result

$$\int_{-c(y_1)/2}^{+c(y_1)/2} \gamma^{(o)}(\xi_1) f(2y_1/b) w_f^{(e)}(x_1,y_1)\,dx_1 =$$

$$= -\frac{c(y_1) f(2y_1/b)}{16\pi} \int_{-1}^{+1} \gamma^{(e)}(\xi)\,d\xi \int_{-1}^{+1} \gamma^{(o)}(\xi_1)\,d\xi_1 \frac{\partial}{\partial y_1} \int_{-b/2}^{+b/2} A(y,y_1,\xi,\xi_1)\,dy +$$

$$+ R_1 + R_2 , \quad (2.36)$$

where R_1 and R_2 are the two residuals. The first of these, which results from the singularity at $\xi = +1$, $\xi_1 = +1$, may be found with the aid of equation (2.33) as follows:

$$R_1(y_1) = \frac{a_o^{(e)} a_o^{(o)} U_o^2 \, c(y_1) f(2y_1/b)}{16\pi} \lim_{\varepsilon \to o} \Bigg[\int_{+1-\varepsilon}^{+1} \frac{\xi_1 d\xi_1}{(1-\xi_1^2)^{\frac{1}{2}}} \int_{+1-\varepsilon}^{+1} \frac{d\xi}{(1-\xi^2)^{\frac{1}{2}}} \frac{\partial}{\partial y_1} \int_{-b/2}^{+b/2} A(y,y_1,\xi,\xi_1)dy -$$

$$- \int_{+1-\varepsilon}^{+1} \frac{d\xi}{(1-\xi^2)^{\frac{1}{2}}} \int_{+1-\varepsilon}^{+1} \frac{\xi_1 \, d\xi_1}{(1-\xi_1^2)^{\frac{1}{2}}} \frac{\partial}{\partial y_1} \int_{-b/2}^{+b/2} A(y,y_1,\xi,\xi_1)dy \Bigg] .$$

By employing transformation (2.34) with a=b=1 it is possible to rewrite the above equation in the form

$$R_1(y_1) = \frac{a_o^{(e)} a_o^{(o)} U_o^2 \, c(y_1) f(2y_1/b)}{16\pi} \lim_{\varepsilon \to o} \Bigg[\varepsilon \int_o^1 \frac{(1-\xi\eta_1)d\eta_1}{(2\eta_1-\varepsilon\eta_1^2)^{\frac{1}{2}}} \int_o^1 \frac{d\eta}{(2\eta-\varepsilon\eta^2)^{\frac{1}{2}}} \frac{\partial}{\partial y_1} \int_{-b/2}^{+b/2} A(y,y_1,1-\varepsilon\eta,1-\varepsilon\eta_1)dy -$$

$$- \varepsilon \int_o^1 \frac{d\eta}{(2\eta-\varepsilon\eta^2)^{\frac{1}{2}}} \int_o^1 \frac{(1-\varepsilon\eta_1)d\eta_1}{(2\eta_1-\varepsilon\eta_1^2)^{\frac{1}{2}}} \frac{\partial}{\partial y_1} \int_{-b/2}^{+b/2} A(y,y_1,1-\varepsilon\eta,1-\varepsilon\eta_1)dy \Bigg] . \qquad (2.37)$$

The limit of equation (2.37) is taken in Appendix I which yields the result

$$R_1(y_1) = \frac{a_o^{(e)} a_o^{(o)} U_o^2 \, c(y_1) f^2(2y_1/b)}{4\pi} \Big\{ 1 + \frac{1}{4} \Big(\frac{dc(y_1)}{dy_1}\Big)^2 \Big\}^{\frac{1}{2}} \int_o^1 \frac{d\eta_1}{\eta_1^{\frac{1}{2}}} \int_o^1 \frac{d\eta}{\eta^{\frac{1}{2}}(\eta-\eta_1)} .$$

Therefore the η integration of this equation may be performed, subject to a Cauchy principal value being defined at $\eta = \eta_1$, to give the expression

$$R_1(y_1) = - \frac{a_o^{(e)} a_o^{(o)} U_o^2 \, c(y_1) f^2(2y_1/b)}{4\pi} \Big\{ 1 + \frac{1}{4} \Big(\frac{dc(y_1)}{dy_1}\Big)^2 \Big\}^{\frac{1}{2}} \int_o^1 \ln\Big(\frac{1+\eta_1^{\frac{1}{2}}}{1-\eta_1^{\frac{1}{2}}}\Big) \frac{d\eta_1}{\eta_1} .$$

In turn, this equation may be integrated by employing the transformation

$$\eta_1 = u^2$$

and equation (864.12) of Dwight (1961), thus providing the result

$$R_1(y_1) = -\frac{\pi a_o^{(e)} a_o^{(o)} U_\infty^2 c(y_1) f^2(2y_1/b)}{8}\left\{1 + \frac{1}{4}\left(\frac{dc(y_1)}{dy_1}\right)^2\right\}^{\frac{1}{2}}. \tag{2.38}$$

The residual R_2, which is caused by the singularity at $\xi=-1$, $\xi_1=-1$, may be found by using an analysis which is identical with that used to obtain R_1 if the transformations

$$\xi' = -\xi \qquad \xi_1' = -\xi_1$$

are used. In fact, it may be concluded from this analysis that

$$R_2 = R_1 \tag{2.39}$$

Hence equations (2.38) and (2.39) may be employed to rewrite equation (2.36) as follows:

$$\int_{-c(y_1)/2}^{+c(y_1)/2} \gamma^{(o)}(\xi_1) f(2y_1/b) w_f^{(e)}(x_1,y_1)\,dx_1 =$$

$$= -\frac{c(y_1) f(2y_1/b)}{16\pi}\int_{-1}^{+1}\gamma^{(e)}(\xi)\,d\xi \int_{-1}^{+1}\gamma^{(o)}(\xi_1)\,d\xi_1 \frac{\partial}{\partial y_1}\int_{-b/2}^{+b/2} A(y,y_1,\xi,\xi_1)\,dy -$$

$$- \frac{\pi a_o^{(e)} a_o^{(o)} U_\infty^2 c(y_1) f^2(2y_1/b)}{4}\left\{1 + \frac{1}{4}\left(\frac{dc(y_1)}{dy_1}\right)^2\right\}^{\frac{1}{2}}.$$

This expression may be rewritten by interchanging the roles of ξ and ξ_1. Thus, upon combining the modified expression with equations (2.24), (2.30) and (2.31), one finds that

$$D_f(y_1) = D_i(y_1) + \frac{\rho c(y_1) f(2y_1/b)}{16\pi}\int_{-1}^{+1}\gamma^{(e)}(\xi_1)\,d\xi_1 \int_{-1}^{+1}\gamma^{(o)}(\xi)\,d\xi \frac{\partial}{\partial y_1}\int_{-b/2}^{+b/2}\frac{c(y) f(2y/b)}{y_1 - y}\left[\right.$$

$$\left.\frac{\{(c(y_1)\xi_1 - c(y)\xi)^2 + 4(y_1-y)^2\}^{\frac{1}{2}}}{c(y_1)\xi_1 - c(y)\xi} + \frac{\{(c(y_1)\xi - c(y)\xi_1)^2 + 4(y_1-y)^2\}^{\frac{1}{2}}}{c(y_1)\xi - c(y)\xi_1}\right] dy +$$

$$+ \frac{\pi a_o^{(e)} a_o^{(o)} \rho U_\infty^2 c(y_1) f^2(2y_1/b)}{4}\left\{1 + \frac{1}{4}\left(\frac{dc(y_1)}{dy_1}\right)^2\right\}^{\frac{1}{2}} - T(y_1). \tag{2.40}$$

Finally, it is necessary to give an explicit form to $T(y_1)$. This is achieved by employing a result given by Robinson and Laurmann

(equation 3.2, 10) for the contribution of one edge to the sectional edge thrust. Thus, after allowing for the contributions of both edges, one may use this result to obtain the expression

$$T(y_1) = \frac{\pi a_o^{(e)} a_o^{(o)} \rho U_o^2 c(y_1) f^2(2y_1/b)}{4}\{1 + \frac{1}{4}(\frac{dc(y_1)}{dy_1})^2\}^{\frac{1}{2}}. \quad (2.41)$$

Therefore equations (2.40) and (2.41) may be combined to give the result

$$D_f(y_1) = D_i(y_1) + \frac{\rho c(y_1) f(2y_1/b)}{16\pi} \int_{-1}^{+1} \gamma^{(e)}(\xi_1) d\xi_1 \int_{-1}^{+1} \gamma^{(o)}(\xi) d\xi \frac{\partial}{\partial y_1} \int_{-b/2}^{+b/2} \frac{c(y) f(2y/b)}{y_1 - y} \Bigg[$$

$$\frac{\{(c(y_1)\xi_1 - c(y)\xi)^2 + 4(y_1-y)^2\}^{\frac{1}{2}}}{c(y_1)\xi_1 - c(y)\xi} + \frac{\{(c(y_1)\xi - c(y)\xi_1)^2 + 4(y_1-y)^2\}^{\frac{1}{2}}}{c(y_1)\xi - c(y)\xi_1}\Bigg] dy. \quad (2.42)$$

It has not been possible to simplify equation (2.42), without making approximations, except in the case $c(y) = c(y_1) = c$ corresponding to the rectangular planform. It may be inferred that for this planform the integral term is identically zero leaving

$$D_f(y) = D_i(y),$$

where y_1 has been replaced by y. This result, which would seem to be approximately correct for wings of quasi-rectangular planform, may be written in the alternative forms

$$\left.\begin{aligned} \rho \int_{-c/2}^{+c/2} \gamma(\xi) f(2y/b) w_f(x,y) dx + T(y) &= \rho w_\infty(y) \Gamma(y)/2, \\ &= \rho w_\infty(y) \int_{-c/2}^{+c/2} \gamma(\xi) f(2y/b) dx/2, \end{aligned}\right\} \quad (2.43)$$

Therefore, by employing equation (2.41) with $c(y_1)$ replaced by c and writing

$$\beta = \{\int_{-1}^{+1} \gamma(\xi) d\xi / \pi U_o\}^2 / a_o^{(e)} a_o^{(o)}, \quad (2.44)$$

it is possible to replace equations (2.43) by the expression

$$\Gamma(y) = -\pi\beta c\{\int_{-1}^{+1}\gamma(\xi)w_f(\xi,y)d\xi/\int_{-1}^{+1}\gamma(\xi)d\xi - w_\infty(y)/2\}. \qquad (2.45)$$

Equation (2.45) will be generalized in Section 2.2.4 to include non-planar lifting systems of the type considered in Section 2.2.1 but with the added restriction that the chord is constant on all surfaces. This type of lifting system is representative of the closed G.E.W. to be considered in Part II of this chapter.

2.2.4 Non-planar, constant-chord distribution of the type $\gamma(x)f(s)$.

Consider a non-planar lifting system having elements with (a) mid-chord points occupying a single plane normal to the direction of motion and (b) the same, constant chord, c. The sectional drag of this type of system may be written in the same form as equation (2.24) by using arguments identical with those used to obtain this equation. Thus it is found that

$$D_f(s) = D_i(s) - \rho\int_{-c/2}^{+c/2} v_{nf}^{(o)}(x,\varepsilon)\gamma^{(e)}(x,s)dx - \rho\int_{-c/2}^{+c/2} v_{nf}^{(e)}(x,s)\gamma^{(o)}(x,s)dx - T(s). \qquad (2.46)$$

Here $\gamma(x,s)$ is to be interpreted as the s component of vorticity and v_n is the 'n - wash' at the system.

An examination of the velocity field of elementary horseshoe vortices indicates that

$$v_{nf}(x_1,s_1) = -\iint_D \gamma(x,s)K(x_1-x,s_1,s)dx\,ds, \qquad (2.47)$$

where subscript D denotes integration over the developed area of the lifting system and $K(x_1-x,s_1,s)$ is an operator which may be written as follows:

$$K(x_1-x,s_1,s) = K_\infty(s_1,s)/2 + K_1(x_1-x,s_1,s). \qquad (2.48)$$

Here $K_\infty(s_1,s)$ is an operator which appears in the expression

$$v_{n_\infty}(s_1) = -\iint_D \gamma(x,s)K_\infty(s_1,s)dx\,ds \qquad (2.49)$$

and $K_1(x_1-x,\ s_1,\ s)$ has the property

$$K_1(x_1-x,\ s_1,\ s) = -K_1(x-x_1,\ s_1,\ s). \tag{2.50}$$

That $K(x_1-x,\ s_1,\ s)$ is of the form given by equation (2.48) may also be verified fairly easily by employing equation (2.8).

If the vortex distribution is of the type $\gamma(x)f(s)$ it is possible, by using equation (2.48), to rewrite equation (2.47) in the form

$$v_{nf}(x_1,s_1) = -\int_{-c/2}^{+c/2} \gamma(x)dx \int_B f(s)\{K_\infty(s_1,s)/2 + K_1(x_1-x,s_1,s)\}ds,$$

where B denotes integration over all s of the vortex trace. Thus, by employing this result and equation (2.50), it is found that

$$\int_{-c/2}^{+c/2} \gamma^{(o)}(x_1)f(s_1)v_{nf}^{(e)}(x_1,s_1)dx_1 = -\int_{-c/2}^{+c/2} \gamma^{(e)}(x_1)f(s_1)v_{nf}^{(o)}(x_1,s_1)dx_1 + R(s_1), \tag{2.51}$$

where $R(s_1)$ is the residual resulting from the reversal of the x and x_1 integration in the integral

$$-\int_{-c/2}^{+c/2} \gamma^{(o)}(x_1)dx_1 \int_{-c/2}^{+c/2} \gamma^{(e)}(x)dx \int_B f(s)K_1(x_1-x,s_1,s)ds$$

The residual, $R = R_1 + R_2$, of the planar wing of rectangular planform is independent of wing span if $\gamma(x,y)$ is specified. This is because in the regions contributing to the residual (the edges) the induced flows of $\gamma^{(e)}$ and $\gamma^{(o)}$ are two-dimensional. This may be attributed to the fact that near the edges these flows depend only on the local geometry. Evidently, non-planar systems also possess this property. Therefore the residual may be determined in the present case by assuming that each section is part of a planar wing. Consequently it may be inferred from equations (2.38) and (2.39) that

$$R(s_1) = -\pi a_o^{(e)}\ a_o^{(o)}\ U_o^2\ c\ f^2(s_1)/4\ . \qquad (2.52)$$

The previously-mentioned analysis of Robinson and Laurmann may be employed to determine the following result for the sectional edge thrust

$$T(s_1) = \pi a_o^{(e)}\ a_o^{(o)}\ \rho U_o^2\ c\ f^2(s_1)/4. \qquad (2.53)$$

Hence it may be concluded from equations (2.46), (2.51), (2.52) and (2.53) that

$$D_f(s) = D_i(s).$$

Consequently, by analogy with equation (2.45),

$$\Gamma(s) = -\pi\beta c\{ \int_{-1}^{+1}\gamma(\xi)v_{nf}(\xi,s)d\xi / \int_{-1}^{+1}\gamma(\xi)d\xi - v_{n\infty}(s)/2\}. \qquad (2.54)$$

3. Sectional-drag relationships applied to wing theory.

The aim of this section is to employ sectional-drag relationships derived previously to formulate an approximate method for determining the overall lift and induced drag of certain types of wings. It will be shown that this method resembles that given by Küchemann (1952) except in one important detail.

In Section 3.1 the analysis will be concerned with wings of zero chordwise camber whilst in Section 3.2 the influence of chordwise camber will be considered. The whole of this analysis will be restricted to wings having chordwise sections of zero thickness and will be based on the assumptions of Section 2.

3.1 Wings of zero chordwise camber

Consider an isolated planar wing of rectangular planform and zero chordwise camber in forward flight. According to Thwaites (1960, p. 304) the linearized boundary condition at the surface of this wing is given by

$$w_f(x,y) = -U_o\alpha(y), \qquad (3.1)$$

where $\alpha(y)$, the sectional incidence, is defined as the angle between the vectors of the forward chordwise direction and the direction of motion. Therefore, if it is assumed that $\gamma(x,y)$ is of the form $\gamma(\xi)f(2y/b)$, equations (2.45) and (3.1) may be combined to give the result

$$\Gamma(y) = \pi\beta c\{U_o\alpha(y) + w_\infty(y)/2\} . \qquad (3.2)$$

For a given y/b, the quantity $w_\infty(y)/U_o$ depends exclusively on $\Gamma(y)/U_o b$. Therefore, in principle, equation (3.2) may be solved for $\Gamma(y)/U_o b$ provided $\mathcal{R}(=b/c)$, $\alpha(y)$ and β are known. As may be inferred from equation (2.44), the last of these quantities depends only on $\gamma(\xi)$. Therefore, in order to solve equation (3.2), it is necessary to know the form of $\gamma(\xi)$. This is dictated, to some extent, by the conventional assumption of wing theory, namely that the flow relative to the wing separates smoothly from the trailing edge. This leads to the requirement that $\gamma(+1) < \infty$, a condition which is satisfied by the distribution

$$\gamma(\theta)/U_o = a_o \tan\theta/2 + \sum_{n=1} a_n \sin n\theta, \qquad (3.3)$$

where $a_o, a_1, a_2, \ldots\ldots$ are non-dimensional coefficients and

$$\theta = \cos^{-1}\xi. \qquad (3.4)$$

Glauert (1926) employed essentially the same distribution in his two-dimensional theory of thin aerofoils. Thus it may be argued that, strictly, its use is only justified for wings of large $\mathcal{R}$. Nevertheless, it has been applied, with apparent success, by Wieghardt (1940) to the determination of the overall lift of low-aspect-ratio wings.

By comparing equations (2.35), (3.3) and (3.4) it may be concluded that

$$a_o^{(e)} = a_o^{(o)} = a_o \qquad (3.5)$$

Therefore, after eliminating $\gamma(\xi)$, ξ, $a_o^{(e)}$ and $a_o^{(o)}$ from equation (2.44) by using equations (3.3), (3.4) and (3.5), it is possible to integrate equation (2.44) to obtain the result

$$\beta = \{(a_o + a_1/2)/a_o\}^2 \tag{3.6}$$

Glauert's theory indicates that, for a flat plate at incidence in a two-dimensional uniform flow, $a_1 = o$. Therefore it may be concluded from equation (3.6) that the corresponding value of β is unity. Hence it would seem reasonable to suppose that, for the type of wing presently being considered, $\beta \sim 1$ as $AR \to \infty$. Consequently, for sufficiently large AR, equation (3.2) may be replaced by the result

$$\Gamma(y) = \pi c\{U_o \alpha(y) + w_\infty(y)/2\}$$

This expression, which is known as the Prandtl 'lifting-line' equation, has been examined in detail by Küchemann (1952) who also derived the equivalent form

$$\Gamma(y) = \{C_L^2(y)/C_T(y)\}U_o \; c \; \alpha_e(y)/2. \tag{3.7}$$

Here $C_L(y)$ and $C_T(y)$ are the sectional lift and edge-thrust coefficients based on the quantity $\frac{1}{2}\rho U_o^2 c$ whilst

$$\alpha_e(y) = \alpha(y) - \alpha_{io}(y), \tag{3.8}$$

where

$$\alpha_{io}(y) = -w_\infty(y)/2\,U_o$$

is the incidence induced at the wing by the chordwise and trailing vortices.

On the eivdence of experimental data, Küchemann concluded that equation (3.7) also applies if AR is not large. However, he assumed that, in general, $\alpha_{io}(y)$ is replaced in equation (3.8) by $\omega\alpha_{io}(y)$, where ω is a factor depending on AR such that $\omega \sim 1$ as $AR \to \infty$. Consequently, by assuming that $\gamma(x,y) \equiv \gamma(\xi)f(2y/b)$, he obtained the result

$$\Gamma(y) = \pi\beta c\{U_o\alpha(y) + \omega\, w_\infty(y)/2\}. \qquad (3.9)$$

This expression may be compared with equation (3.2) and from this it is apparent that there is an inconsistency in Küchemann's method. In fact, it is possible to deduce from equation (3.9) that his method yields the result

$$\bar{D}_f = \omega\,\bar{D}_i,$$

where $\bar{D}_f$ is the overall drag in forward flight. Clearly, unless $\omega = 1$ (which is not the case for $AR < \infty$), this is inadmissible. Further, it is indicative that the predictions of Küchemann's method for the overall forces might be in error. Therefore the comparison between the methods will be taken a stage further by using both methods to calculate the overall lift and induced drag of a flat, rectangular wing of small AR. This will be performed, initially, by using a value of β deduced from the low-aspect-ratio approximation of Jones (1946). Unfortunately, owing to the fact that this approximation fails near the leading edge of a rectangular wing it seems not to permit a direct evaluation of a_o and hence β. However, there is an alternative, though indirect, method of deducing β from Jones' theory which is based on the requirement that $\bar{D}_f = \bar{D}_i$. Provided $\gamma(x,y) \equiv \gamma(\xi)f(2y/b)$ this leads to the result

$$\int_{-c/2}^{+c/2} \Gamma^2(y)dy = \pi\beta c\{U_o\alpha \int_{-c/2}^{+c/2} \Gamma(y)dy + \int_{-c/2}^{+c/2} w_\infty(y)\Gamma(y)dy/2\} \qquad (3.10)$$

for a flat, rectangular wing at incidence α. Therefore, if the results of the low-aspect-ratio approximation for the same wing, namely

$$w_\infty(y) = -U_o\alpha; \qquad \Gamma(y) = U_o\alpha b\{1-(2y/b)^2\}^{\frac{1}{2}},$$

are used to eliminate $w_\infty(y)$ and $\Gamma(y)$ from equation (3.10) and the integration is performed, it is found that

$$\beta = 16\mathcal{R}/3\pi^2. \tag{3.11}$$

Consequently, for a flat, rectangular wing of small aspect ratio, equation (3.11) may be employed to replace equation (3.2) by the expression

$$\Gamma(y) = (16b/3\pi)\{U_o\alpha + w_\infty(y)/2\}. \tag{3.12}$$

The overall forces corresponding to the solution of equation (3.12) may be determined by interpolating results given by Glauert (1926, p. 147) for the same type of equation. Thus it is found that

$$\bar{C}_{Di} = 1.01\,\bar{C}_L^2/\pi\mathcal{R}; \quad \bar{C}_L = 1.57\,\mathcal{R}\,\alpha,$$

where $\bar{C}_{Di}$ and $\bar{C}_L$ are the overall induced-drag and lift coefficients based on the product of $\frac{1}{2}\rho U_o^2$ and the planform area bc. These results should be compared with the corresponding results of the low-aspect-ratio approximation, that is

$$\bar{C}_{Di} = \bar{C}_L^2/\pi\mathcal{R}; \qquad \bar{C}_L = \pi\mathcal{R}\alpha/2.$$

Evidently, the agreement is good.

On the basis of the assumption that $\Gamma(y)/\pi\beta c \sim o$ as $\mathcal{R} \to o$ Küchemann concluded from the low-aspect-ratio approximation that, for sufficiently small $\mathcal{R}$, $\omega = 2$. Therefore, by utilizing equation (3.11) and this value of ω, Küchemann's result, equation (3.9), may, for a flat, rectangular wing of small $\mathcal{R}$, be replaced by the expression

$$\Gamma(y) = (16b/3\pi)\{U_o\alpha + w_\infty(y)\}.$$

This equation, it is found, yields an overall-lift coefficient which is approximately 30% lower than that of the low-aspect-ratio approximation. On the other hand, its prediction of the quantity $\pi\mathcal{R}\bar{C}_{Di}/\bar{C}_L^2$ is not as greatly in error.

That Küchemann's method, in practice, gives an overall-lift coefficient which asymptotes to the low-aspect-ratio approximation is due to his use of a different asymptotic form for β. After making a number of assumptions, which will not be discussed here, he obtained the result

$$\beta \sim (AR/2)^{\frac{1}{2}}, \quad AR \to 0. \tag{3.13}$$

This relationship is plotted in Fig. 17, together with the curve of equation (3.11) and some results deduced from the lifting-surface theory of Wieghardt (1940). These results are calculated by two methods. The first method relies on a direct evaluation of β from an examination of $\gamma(\xi)$ whilst the second is identical with the method used to derive equation (3.11). Also included in Fig. 17 is a curve representing a semi-empirical relationship suggested by Küchemann. This has the same asymptotic behaviour as equation (3.13) and correctly ensures that $\beta \sim 1$ as $AR \to \infty$. However, the evidence provided by the results obtained from Wieghardt's theory is that this relationship overestimates β for $AR < 2$.

The conclusion to be drawn from this comparison is that, of the two methods examined, the present approach would seem to be the more fundamental. On the other hand, the degree of success achieved with this method must depend largely on the accuracy of the estimate of β. In general, this varies across the span of the wing. Hence the problem of interpreting a mean value arises. In this respect, a particularly suitable interpretation is the one based on the requirement that $\overline{D}_f = \overline{D}_i$. By employing equations (2.43) it may be shown that this is satisfied for the type of wing under consideration if

$$\int_{-b/2}^{+b/2}\int_{-1}^{+1}\gamma(\xi)f(2y/b)w_f(\xi,y)\,d\xi dy = -\int_{-b/2}^{+b/2}\int_{-1}^{+1}\gamma(\xi)f(2y/b)U_o\alpha(y)\,d\xi dy$$

or

$$\int_{-b/2}^{+b/2} f(2y/b)w_f(\xi,y)\,dy = -\int_{-b/2}^{+b/2} f(2y/b)U_o\alpha(y)\,dy. \tag{3.14}$$

Therefore, provided $f(2y/b)$ is known, equation (3.14) may be solved for $\gamma(\xi)$ and hence β. Unfortunately, $f(2y/b)$ is not known until the solution of equation (3.2) has been obtained and this depends on β. Therefore it is necessary to solve equations (3.2) and (3.14) simultaneously. In practice, this is probably best performed by a successive-approximation scheme by which an assumed $f(2y/b)$ is substituted into equation (3.14). Consequently a value of β is found which is substituted into equation (3.2) to give a new $f(2y/b)$, and so on.

This method may be extended to non-planar vortex distributions of the type considered in Section 2.2.4. In this case, the linearized form of the surface boundary condition is given by

$$v_{nf}(x,s) = -U_o\alpha(s). \tag{3.15}$$

Therefore equations (2.54) and (3.15) may be combined to give the result

$$\Gamma(s) = \pi\beta c\{U_o\alpha(s) + v_{n_\infty}(s)/2\} \tag{3.16}$$

whilst by analogy with equation (3.14) the requirement that $\overline{D}_f = \overline{D}_i$ leads to the result

$$\int_B f(s)v_{nf}(\xi,s)ds = -\int_B f(s)U_o\alpha(s)ds. \tag{3.17}$$

3.2 Wings with chordwise camber

In this section, a relationship, which allows the determination of the effect of chordwise camber on the overall lift and induced drag of wings with smooth flow at their trailing edges, will be derived.

Consider an isolated planar wing of rectangular planform in forward flight with the y component of vorticity $\gamma_1(\xi)f(2y/b)$ and $\gamma_1(+1) < \infty$ (the condition of smooth flow at the trailing edge). In the manner of equations (2.43), the sectional-drag relationship of this combination of wing and vortex distribution is written as

$$\rho \int_{-c/2}^{+c/2} \gamma_1(\xi) f(2y/b) w_{f1}(x,y)\,dx + T_1(y) = \rho w_{\infty 1}(y)\Gamma_1(y)/2. \qquad (3.18)$$

Here the subscript 1 refers to those quantities corresponding to $\gamma_1(\xi)f(2y/b)$.

Suppose that the same wing in forward flight has, instead, the y component of vorticity $\gamma_2(\xi)f(2y/b)$ with $\gamma_2(+1) < \infty$. The corresponding upwash distribution at the wing is $w_{f2}(x,y)$. Thus if the motion of the wing is reversed and the y' component of vorticity is $\gamma_2(\xi)f(2y/b)$ the upwash at the wing becomes $w_{r2}(x',y')$. Consequently, it follows from symmetry considerations, that if then the wing is rotated about the z axis through π radians the y component of vorticity becomes $\gamma_2(\xi')f(2y/b)$ and the upwash $w_{r2}(x,y')$. Furthermore, the motion becomes forward again and the corresponding sectional-drag relationship may be written in the form

$$\rho \int_{-c/2}^{+c/2} \gamma_2(\xi') f(2y/b) w_{r2}(x,y')\,dx - T_2(y) = \rho w_{\infty 2}(y)\Gamma_2(y)/2. \qquad (3.19)$$

If $\gamma_2(\xi')f(2y/b)$ and $\gamma_1(\xi)f(2y/b)$ are superposed, the sectional-drag relationship for forward flight becomes

$$\rho \int_{-c/2}^{+c/2} \{\gamma_1(\xi) + \gamma_2(\xi')\}\{w_{f1}(x,y) + w_{r2}(x,y')\}f(2y/b)\,dx + T_1(y) - T_2(y) =$$

$$= \rho\{w_{\infty 1}(y) + w_{\infty 2}(y)\}\{\Gamma_1(y) + \Gamma_2(y)\}/2. \qquad (3.20)$$

Here, it will be noted, the edge thrusts are additive owing to the requirement of smooth flow at $\xi = +1$ for $\gamma_1(\xi)$ and $\xi = -1$ for $\gamma_2(\xi')$. This ensures that the singularities of the two vortex distributions do not combine.

Thus, by combining equations (3.18), (3.19) and (3.20), it is found that

$$\int_{-c/2}^{+c/2} \gamma_1(\xi) f(2y/b) w_{r2}(x,y')\,dx + \int_{-c/2}^{+c/2} \gamma_2(\xi') f(2y/b) w_{f1}(x,y)\,dx =$$

$$= w_{\infty 1}(y)\Gamma_2(y)/2 + w_{\infty 2}(y)\Gamma_1(y)/2\,. \qquad (3.21)$$

It is possible to infer from equation (2.5) that

$$w_{r2}(x,y') = w_{\infty 2}(y) - w_{f2}(x'y). \tag{3.22}$$

Therefore equations (3.21) and (3.22) may be combined to yield the result

$$-\int_{-c/2}^{+c/2} \gamma_1(\xi) f(2y/b) w_{f2}(x',y)dx + \int_{-c/2}^{+c/2} \gamma_2(\xi') f(2y/b) w_{f1}(x,y)dx =$$

$$= w_{\infty 1}(y)\Gamma_2(y)/2 - w_{\infty 2}(y)\Gamma_1(y)/2. \tag{3.23}$$

From considerations of the similarity of the flow variables of the Trefftz plane it may be concluded that

$$w_{\infty 1}(y)\Gamma_2(y) = w_{\infty 2}(y)\Gamma_1(y) \quad . \tag{3.24}$$

Therefore, by comparing equations (3.23) and (3.24), one is able to obtain the expression

$$\int_{-c/2}^{+c/2} \gamma_1(\xi) w_{f2}(x',y)dx = \int_{-c/2}^{+c/2} \gamma_2(\xi') w_{f1}(x,y)dx \tag{3.25}$$

Hence, by employing the linearized form of the camber-surface boundary condition for a wing of arbitrary chordwise shape given by Thwaites (1960, p. 304), namely

$$w_f(x,y) = U_o \, \partial z_c(x,y)/\partial x,$$

equation (3.25) may be rewritten in the form

$$\int_{-c/2}^{+c/2} \gamma_1(\xi) \left[\partial z_c(x',y)/\partial x\right]_2 dx = \int_{-c/2}^{+c/2} \gamma_2(\xi') \left[\partial z_c(x,y)/\partial x\right]_1 dx. \tag{3.26}$$

Here z_c is the z ordinate of the camber lines. Therefore, if

$$\left[\partial z_c(x',y)/\partial x\right]_2 = -\alpha(y),$$

equation (3.26) becomes

$$\alpha(y)\int_{-c/2}^{+c/2}\gamma_1(\xi)d\xi = -\int_{-c/2}^{+c/2}\gamma_2(\xi')\left[\partial z_c(x,y)/\partial x\right]_1 dx. \qquad (3.27)$$

Consequently, if $\gamma_2(\xi')$ has been determined by using the method presented in Section 3.1 and $\left[\partial z_c(x,y)/\partial x\right]_1$ is specified, the right-hand side of equation (3.27) may be evaluated. It will be seen that this side of the equation is required to have a y dependence similar to that of $\alpha(y)$. Therefore, provided this requirement is satisfied, equation (3.27) may be used to determine $\Gamma_1(y)$, the information on $f(2y/b)$ coming from the solution $\gamma_2(\xi)f(2y/b)$ for the uncambered wing. In consequence, the overall lift and induced drag appropriate to the slope distribution $\left[\partial z_c(x,y)/\partial x\right]_1$ may be found.

Equation (3.25) may be generalized without difficulty to include non-planar vortex distributions of the type considered in Section 2.2.4. Thus there is obtained the result

$$\int_{-c/2}^{+c/2}\gamma_1(\xi)v_{nf2}(x',s)dx = \int_{-c/2}^{+c/2}\gamma_2(\xi')v_{nf1}(x,s)dx \qquad (3.28)$$

provided γ_1 and γ_2 are bounded at $\xi = +1$. This relationship may be used in a similar way to that shown previously to determine the effect of chordwise camber on the overall lift and induced drag of non-planar wings of the type described.

PART II

THE DETERMINATION OF THE LIFT AND INDUCED DRAG OF A CLOSED GROUND-EFFECT WING.

4. Scope of the investigation

This part of the chapter consists of a description of a method for calculating the lift and induced drag of a closed G.E.W. consisting of an essentially planar wing fitted with end plates.

The chordal surface of the configuration is shown in Fig. 18 which illustrates the following features:

(i) The lower extremities of the end plates, which are vertical and project from the wing tips, touch the ground, thus ensuring that the configuration is closed.

(ii) The leading and trailing edges each lie in a plane which is normal to the direction of motion.

(iii) The wing and end plates are untwisted.

A considerable simplification of the analysis may be effected by employing the linearized theory and neglecting the chordwise camber and thickness. This, therefore, will be the approach adopted in Section 5. Subsequently, in Section 6, a method for calculating the effect of chordwise camber and thickness on the lift and induced drag, to a linear approximation, will be described. Finally, the basic method will be modified to include the most important non-linearities in Section 7.

5. Zero chordwise camber and thickness : a linearized approach.

5.1 Statement of problem and method of solution.

As previously, the flow relative to the configuration, which is in forward motion, is assumed inviscid and incompressible. Also, in keeping with classical wing theory, the flow is assumed to be smooth at the trailing edge. This ensures a unique solution for the velocity potential of the flow relative to the configuration, ϕ.

In accordance with the assumptions of the linearized theory, the boundary conditions of the wing and end plates are satisfied at a cylindrical surface adjacent to the configuration. This surface, which is shown in Fig. 18, may be generated by moving a typical spanwise cross section of the chordal surface normal to itself between

the leading and trailing edges. This cross-section is of span b and height from the ground ℓ. Thus, in the absence of chordwise camber and thickness, the linearized form of the surface boundary conditions of the configuration is as follows:

$$\left.\begin{aligned} v_{nf}(x,y,+\ell) &= -U_o\alpha(s) = -U_o\alpha^{(w)}; \quad |x| \leq c/2, \ |y| \leq b/2; \\ v_{nf}(x,\pm b/2,z) &= -U_o\alpha(s) = -U_o\alpha^{(E)}; \quad |x| \leq c/2, \ 0 \leq z \leq +\ell. \end{aligned}\right\} \quad (5.1)$$

Here $\alpha^{(w)}$ is the wing incidence and $\alpha^{(E)}$ is the incidence of the end plates whilst the coordinate systems (s,n) and (x,y,z), which are fixed relative to the configuration, are as shown in Fig. 18.

There remain two other boundary conditions to be satisfied. The first is the zero normal-velocity condition at the ground plane which, throughout the remainder of the analysis, will be assumed solid and impermeable. The second demands that

$$\partial\phi/\partial x \sim U_o, \quad \begin{matrix} |x| \to \infty \\ |y| \to \infty; \\ z \to +\infty \end{matrix} \quad \partial\phi/\partial y \sim 0, \ \partial\phi/\partial z \sim 0, \quad \begin{matrix} x \to -\infty \\ |y| \to \infty \\ z \to +\infty \end{matrix}$$

which constitutes a requirement on the flow infinitely far from the configuration.

Thus the problem is to determine the lift and induced drag subject to the above conditions. This requires a knowledge of the jump in ϕ across the cylindrical surface which information is obtained by solving the boundary-value problem. In fact, this reduces to the problem of solving an integral equation relating the vortex distribution $\gamma(x,y,z)$ placed on the cylindrical surface to the boundary conditions (5.1). Unfortunately, this equation is extremely complicated and, in general, seems not to be amenable to analytical methods of solution. It might be possible, however, to solve it numerically. In this respect, there is available the method of Multhopp (1950) which has been developed for isolated

planar wings. It would seem, however, that his method has not been applied in the same detail to non-planar wings or wings in ground proximity. On this basis, therefore, it was considered desirable to develop an alternative technique based on the assumption that $\gamma(x,s)$ is of the form $\gamma(x)f(s)$.

The no-flow condition of the ground plane may be satisfied by an image distribution of vortices obtained by rotating the cylindrical surface about the x axis through π radians. Therefore, if it is assumed that $\gamma(x,s) \equiv \gamma(x)f(s)$, the resulting combined vortex distribution is of the type considered in Section 2.2.4. Consequently it is permissible to combine equations (3.16) and (5.1) to yield the expressions

$$\left.\begin{aligned} &\text{(i)}\quad \Gamma(y) = \pi\beta c\{U_o\alpha^{(w)} + w_\infty(y)/2\}; \quad |y| \leq b/2, \quad z = +1; \\ &\text{(ii)}\quad \Gamma(z) = \pi\beta c\{U_o\alpha^{(E)} + v_\infty(z)/2\}; \quad y = \pm b/2, \quad 0 \leq z \leq +1. \end{aligned}\right\} \quad (5.2)$$

Here $v_\infty(z)$ is the y component of velocity at the trace of the starboard end plate in the Trefftz plane. That this velocity is equal in magnitude but opposite in sign to the y component of velocity at the trace of the port end plate follows from symmetry considerations.

No attempt will be made to justify the assumption that $\gamma(x,s) \equiv \gamma(x)f(s)$ rigorously. Nevertheless, it is relevant to note the following remarks:

(i) For $\alpha^{(w)} \simeq \alpha^{(E)}$, the trailing vorticity is likely to be comparatively weak, as $\Gamma(s)$ should not vary noticeably with s. Consequently the effect of the trailing vorticity on the chordwise form of $\gamma(x,s)$ should not depend greatly on s.

(ii) In the case of a closed G.E.W. with a cylindrical surface of semi-circular spanwise cross-section, the vortex distribution is of the type $\gamma(x)f(s)$ provided $\alpha(s)$ = constant.

5.2 Distribution of circulation around the vortex trace

In this section the aim is to discuss a method for solving equations (5.2)(i) and (ii) simultaneously. In general, this has to be performed approximately but in Section 5.2.1 a formally exact solution is discussed.

5.2.1 An exact solution

It is apparent that in the case $\Gamma(s) = \Gamma$ (a constant) the trailing vorticity is zero everywhere. Hence $w_\infty(y) = v_\infty(z) = 0$. Therefore it may be inferred from equations (5.2) that for $\alpha^{(w)} = \alpha^{(E)} = \alpha$

$$\Gamma = \pi\beta c\, U_o \alpha. \tag{5.3}$$

In other words, the present theory predicts that the circulation is invariant around the trailing edge of the configuration if $\alpha^{(w)} = \alpha^{(E)} = \alpha$. Furthermore, it predicts that the corresponding overall induced drag is zero.

5.2.2 The flow in the Trefftz plane

Apart from the exact solution discussed previously, it has not been possible to derive closed-form solutions of equations (5.2). Instead, an approximate method, which is based on the use of particular solutions for ϕ in the Trefftz plane, is employed. Thus equations (5.2) are rewritten as follows:

$$\left.\begin{aligned} \sum_{m=o} \Gamma_m(y) &= \pi\beta c\{U_o \alpha^{(w)} + \sum_{m=o} w_{\infty m}(y)/2\};\ |y| \le b/2,\ z = +\zeta; \\ \sum_{m=o} \Gamma_m(z) &= \pi\beta c\{U_o \alpha^{(E)} + \sum_{m=o} v_{\infty m}(z)/2\};\ y = \pm b/2,\ 0 \le z \le +\zeta. \end{aligned}\right\} \tag{5.4}$$

Here Γ_m, $w_{\infty m}$ and $v_{\infty m}$ are, respectively, particular circulation distributions and the corresponding velocities at the vortex trace

in the Trefftz plane. These distributions are not entirely arbitrary, being derived from Trefftz-plane flows which satisfy the following conditions:

(i) The velocity potential is regular everywhere except at the vortex trace.

(ii) $\partial\phi/\partial z = 0$ at $z = 0$.

(iii) $\partial\phi/\partial y = 0$ at $y = 0$, a condition which follows from symmetry considerations.

(iv) $\partial\phi/\partial y \sim 0$, $\partial\phi/\partial z \sim 0$; $(y^2+z^2)^{\frac{1}{2}} \to 0$.

A convenient method for determining a suitable family of circulation distributions is the combined-flow method described in Section I.1.3. This, therefore, is the method which will be employed here.

A suitable class of superposition complex potentials corresponding to Γ_m would seem to be

$$W_m = -U_o b\, B_m (2\Omega/b)^{2m},$$

where B_m are real, dimensionless constants and, as before, $\Omega = y + iz$ is the complex variable of the Trefftz plane (Fig. 19). This class is regular in the finite part of the Ω plane and satisfies conditions (ii) and (iii) given previously. Therefore the required combined flows also have these properties and possess zero normal velocity at the vortex trace provided that

$$\left.\begin{aligned} w_{\infty m}(y) &= U_o\, 4m\, B_m \left(\frac{2y}{b}\right)^{2m-1} \sum_{n=1}^{n=m} \frac{(-1)^n (2m-1)!\,(l/y)^{2n-1}}{\{2(m-n)\}!\,(2n-1)!}, \quad (m \neq 0), \\ v_{\infty m}(z) &= U_o\, 4m\, B_m \sum_{n=o}^{n=m-1} \frac{(-1)^n (2m-1)!\,(2z/b)^{2n}}{\{2(m-n)-1\}!\,(2n)!}, \quad (m \neq 0) \end{aligned}\right\} \quad (5.5)$$

and $$w_{\infty o}(y) = v_{\infty o}(z) = 0.$$

Thus, provided equations (5.5) are satisfied, the boundary conditions for the combined flows in the domain D_2 (Fig. 19) are as follows:

(i) $\partial\phi_c/\partial n = 0$; $b/2 \leq |y| < \infty$, $z = 0$;

(ii) $\partial\phi_c/\partial n = 0$; $y = \pm b/2$, $0 < z \leq +l$;

(iii) $\partial\phi_c/\partial n = 0$; $|y| < b/2$, $z = +l$;

(iv) $dW_c/d\Omega \sim -U_o\, 4m\, B_m\, (2\Omega/b)^{2m-1}$; $|\Omega| \to \infty$.

This boundary - value problem may be simplified by transforming the domain D_2 into the upper half-plane t (Fig. 20). This is made possible by means of the Schwarz-Christoffel transformation

$$d\Omega/dt = C\{(1-t^2)/(1-k^2t^2)\}^{\frac{1}{2}}; \quad 1/k \geq 1. \tag{5.6}$$

Here, as in Section I.2.1, C is the (real) transformation constant and k is a transformation parameter which is also to be interpreted as the modulus of the elliptic functions appearing hereafter.

By employing transformation (I.2.3), equation (I.2.4) and equation (310.02) of Byrd and Friedman (1954), equation (5.6) may be integrated to yield the expression

$$\Omega = C\left[2Ks^* - \{2Ks^* - E(2Ks^*)\}/k^2\right] + C_1.$$

Here the s in equations (I.2.3) and (I.2.4) has been replaced by s* to prevent confusion with the curvilinear coordinate s whilst C_1 is the constant of integration.

Point-to-point correspondence between the Ω plane and the s* plane (Fig. 21) at B and C is obtained provided that

$$b/2 + i\eta = C\left[K - \{K - E(K)\}/k^2\right] + C_1$$

and

$$-b/2 + i\eta = -C\left[K - \{K - E(K)\}/k^2\right] + C_1.$$

Therefore, by comparing these two equations, it may be concluded that

$$C_1 = i\eta \tag{5.7}$$

and

$$b/2 = C\left[K - \{K - E(K)\}/k^2\right],$$

$$= C\{E(K) - k'^2K\}/k^2. \tag{5.8}$$

The Ω and s* planes correspond at point D provided that

$$b/2 = C\left[K + iK' - \{K + iK' - E(K + iK')\}/k^2\right] + C_1.$$

Thus, by combining this expression with equations (I.2.11), (5.7) and (5.8), there is obtained

$$\eta = -C\left[K' - \{2KK' + 2E(K)K' - \pi\}/2Kk^2\right].$$

This may be simplified by means of equation (110.01) of Byrd and Friedman to give the result

$$\ell = C\{E'(K) - k^2K'\}/k^2, \tag{5.9}$$

where $E'(K) = E(K')$. Therefore, upon combining equations (5.8) and (5.9), one finds that

$$2\ell/b = \{E'(K) - k^2K'\}/\{E(K) - k'^2K\}.$$

The boundary conditions for the combined flows in the t plane are as follows:

$$\left.\begin{array}{ll} \text{(i)} & \partial\phi_c/\partial n = 0; \quad |\mathrm{Re}(t)| < \infty, \quad \mathrm{Im}(t) = 0; \\ \text{(ii)} & dW_c/dt \sim -U_o\ 4m\ B_m(2\Omega/b)^{2m-1} d\Omega/dt; \quad |t| \to \infty. \end{array}\right\} \tag{5.10}$$

Equation (5.10)(ii) may be rewritten in terms of t by employing the asymptotic forms of $\Omega(t)$ and $d\Omega(t)/dt$ for large $|t|$. These may be found by expanding the right-hand side of equation (5.6) in powers of $1/t$. Thus there is obtained the result

$$\frac{d\Omega}{dt} = \frac{C}{k}\left\{1 + \frac{k'^2}{2k^2t^2} + \frac{(3-2k^2-k^4)}{8k^4t^4} + O\left(\frac{1}{t^6}\right)\right\}; \quad |t| \to \infty \tag{5.11}$$

which, for sufficiently large $|t|$, may be integrated term-by-term to yield the expression

$$\Omega = \frac{C}{k}\left\{t - \frac{k'^2}{2k^2t} - \frac{(3-2k^2-k^4)}{24k^4t^3} + O\left(\frac{1}{t^5}\right)\right\} + C_2; \quad |t| \to \infty. \tag{5.12}$$

Here C_2 is the integration constant which may be shown to be zero by examining the symmetry of the transformation between Ω and t planes. Therefore this fact may be used in conjunction with equations (5.11) and (5.12) to rewrite equation (5.10)(ii) in the form

$$\frac{dW}{dt}c \sim -U_o b\ 2m\ B_m\left(\frac{2C}{bk}\right)^{2m}\left\{t - \frac{k'^2}{2k^2t} - \frac{(3-2k^2-k^4)}{24k^4t^3} + O\left(\frac{1}{t^5}\right)\right\}^{2m-1}$$
$$\cdot\left\{1 + \frac{k'^2}{2k^2t^2} + \frac{(3-2k^2-k^4)}{8k^4t^4} + O\left(\frac{1}{t^6}\right)\right\}; \quad |t| \to \infty \tag{5.13}$$

The corresponding family of complex potentials, W_{cm}, which (a) satisfies equations (5.10)(i) and (5.13), (b) is regular in the finite part of D_2 and (c) obeys the symmetry condition $\partial\phi/\partial y = 0$ at $y = 0$ is as follows for $m < 4$:

$$\left.\begin{aligned} W_{co} &= -U_o b\, B_o; \\ W_{c1} &= -U_o b\, B_1 \kappa\, t^2; \\ W_{c2} &= -U_o b\, B_2 \kappa^2 (t^4 - 2k'^2 t^2/k^2); \\ W_{c3} &= -U_o b\, B_3 \kappa^3 \{t^6 - 3k'^2 t^4/k^2 + t^2(3-7k^2+4k^4)/k^4\}, \end{aligned}\right\} \quad (5.14)$$

where $\kappa = (2C/bk)^2$.

Provided equations (5.5) are satisfied, the boundary conditions for the combined flows in the domain D_1 (see Fig. 19) are given by

(i) $\partial\phi_c/\partial n = 0; \quad |y| \leq b/2, \ z = 0;$

(ii) $\partial\phi_c/\partial n = 0; \quad y = \pm b/2, \ 0 < z \leq +\infty;$

(iii) $\partial\phi_c/\partial n = 0; \quad |y| < b/2, \ z = +\infty.$

A solution to this boundary-value problem which is regular and gives symmetrical flows about the z axis is, regardless of m,

$$W_c = 0.$$

Hence, as the superposition complex potentials are regular in the finite part of the Ω plane, it follows that circulation distributions with the correct normal velocities at the vortex trace are given by

$$\Gamma_m(t) = W_{cm}(t); \quad |\mathrm{Re}(t)| \leq 1/k, \quad \mathrm{Im}(t) = 0. \qquad (5.15)$$

These solutions for the circulation are not unique insofar as an arbitrary constant may be added to them without altering the corresponding normal velocities at the vortex trace. However, these constants may be considered accounted for by the constant circulation Γ_o.

5.2.3 A variational solution

A number of methods for solving equations similar to equations (5.4) have been reviewed by Robinson and Laurmann (1956, p.p. 188-196).

They conclude that the preference for one or other of these methods depends on the nature of the data required. It also appears that the choice could be influenced by the type of lifting system under examination. For example, methods based on variational principles are often suitable for obtaining the overall forces of non-planar lifting systems. As the configuration under examination is of this type, a critical examination will be made of three existing variational methods. As applied to the determination of the solution of equation (3.16) these may be written as follows:

(i) Gates (1928)

$$\delta\left[\int_B \{\Gamma(s) - \pi\beta c(U_o\alpha(s) + v_{n\infty}(s)/2)\}^2 ds\right] = 0.$$

(ii) Ziller (1940)

$$\delta\left[\int_B \{-\Gamma(s)v_{n\infty}(s)/2 + \pi\beta c\, v_{n\infty}^2(s)/4 + \pi\beta c\, U_o\alpha(s)v_{n\infty}(s)\}ds\right] = 0.$$

(iii) Flax (1950)

$$\delta\left[\int_B \{\Gamma^2(s)/\pi\beta c - 2\Gamma(s)U_o\alpha(s) - \Gamma(s)v_{n\infty}(s)/2\}ds\right] = 0.$$

Here δ implies a variation of the integrands with respect to $\Gamma(s)$. Therefore, if β is assumed insensitive to changes in $\Gamma(s)$ and the indicated variations are performed, it is found that the solution of each of these equations is the solution of equation (3.16).

Evidently, all three variational equations require the evaluation of the integral $\int_B \Gamma(s)v_{n\infty}(s)\,ds$. Unfortunately, in the present case, this integral seems not to be amenable to explicit evaluation. In view of this, consideration is given to an alternative variational equation not containing this integral. Such an equation is derived by subtracting the equation of Flax from Ziller's equation, thus giving the result

$$\delta\left[\int_B \{\pi\beta c\ v_{n\infty}^2(s)/4 + \pi\beta c\ U_o\alpha(s)v_{n\infty}(s) - \Gamma^2(s)/\pi\beta c + 2\Gamma(s)U_o\alpha(s)\}ds\right] = 0 \tag{5.16}$$

That this equation also has the same solution as equation (3.16) may be proved by performing the variational operation and noting that

$$\int_B v_{n\infty}(s)\delta\Gamma(s)ds = \int_B \Gamma(s)\ \delta v_{n\infty}(s)ds,$$

a result which may be inferred from equation (3.5, 11) of Robinson and Laurmann.

It should be remarked that the derivation of equation (5.16) was suggested by the fact, not previously noticed it seems, that Gates' equation may be obtained by adding together the equations of Flax and Ziller.

For the present configuration, equation (5.16) may be rewritten in the form

$$\delta\left[\int_{-b/2}^{+b/2} \{\pi\beta c\ w_\infty^2(y)/4 + \pi\beta c\ U_o\alpha^{(w)}w_\infty(y) - \Gamma^2(y)/\pi\beta c + 2\Gamma(y)U_o\alpha^{(w)}\}dy + \right.$$
$$\left. + 2\int_o^{\infty} \{\pi\beta c\ v_\infty^2(z)/4 + \pi\beta c\ U_o\alpha^{(E)}v_\infty(z) - \Gamma^2(z)/\pi\beta c + 2\Gamma(z)U_o\alpha^{(E)}\}dz\right] = 0 \tag{5.17}$$

This equation, which has the same solution as equations (5.2), may be solved approximately with the aid of the particular solutions described previously and the Rayleigh-Ritz method (see Robinson and Laurmann p. 224). For the application of this technique it is convenient to write

$$w_{\infty m}(y) = U_o\ B_m\ \tilde{w}_{\infty m}(y);\quad v_{\infty m}(z) = U_o\ B_m\ \tilde{v}_{\infty m}(z) \tag{5.18}$$

and

$$\Gamma_m(t) = -U_o b\ B_m\ \kappa^m\ G_m(t), \tag{5.19}$$

where $\tilde{w}_{\infty m}$ and $\tilde{v}_{\infty m}$ may be found by comparing equations (5.5) and (5.18) whilst, for $m < 4$, G_m may be deduced from equations (5.14), (5.15) and (5.19). Thus, by utilizing equations (5.18) and (5.19), equation (5.17) may be replaced, in the manner of the Rayleigh-Ritz

technique, by the expression

$$\frac{\partial}{\partial B_m}\left[\int_{-b/2}^{+b/2}\{(\sum_{m=o} B_m \tilde{w}_{\infty m}(y))^2 + 4\alpha^{(w)}\sum_{m=o} B_m \tilde{w}_{\infty m}(y) - \frac{1}{\beta^2\mu^2}(\sum_{m=o} B_m \kappa^m G_m(t))^2 - \right.$$

$$\left. - \frac{4\alpha^{(w)}}{\beta\mu}\sum_{m=o} B_m \kappa^m G_m(t)\}dy + 2\int_o^{\lambda}\{(\sum_{m=o} B_m \tilde{v}_{\infty m}(z))^2 + 4\alpha^{(E)}\sum_{m=o} B_m \tilde{v}_{\infty m}(z) - \right.$$

$$\left. - \frac{1}{\beta^2\mu^2}(\sum_{m=o} B_m \kappa^m G_m(t))^2 - \frac{4\alpha^{(E)}}{\beta\mu}\sum_{m=o} B_m \kappa^m G_m(t)\}dz\right] = 0;\ m = 0,1,2,\ldots\ldots, \tag{5.20}$$

where $\mu = \pi/2AR$

and AR is the aspect ratio of the wing component of the cylindrical surface.

Equation (5.20) yields an infinite set of linear, simultaneous equations for the unknown coefficients B_m. These equations are rather unwieldy but may be written in a more concise form by employing the following definitions:

$$\left.\begin{aligned}
P_m^{(w)} &= \int_{-b/2}^{+b/2} \tilde{w}_{\infty m}(y)dy/b; \quad P_m^{(E)} = 2\int_o^{\lambda} \tilde{v}_{\infty m}(z)dz/b; \\
Q_{mn}^{(w)} &= \int_{-b/2}^{+b/2} \tilde{w}_{\infty m}(y)\tilde{w}_{\infty n}(y)dy/b; \quad Q_{mn}^{(E)} = 2\int_o^{\lambda} \tilde{v}_{\infty m}(z)\tilde{v}_{\infty n}(z)dz/b; \\
R_m^{(w)} &= \int_{-b/2}^{+b/2} G_m(t)dy(t)/b; \quad R_m^{(E)} = 2\int_o^{\lambda} G_m(t)dz(t)/b; \\
S_{mn}^{(w)} &= \int_{-b/2}^{+b/2} G_m(t)G_n(t)dy(t)/b; \quad S_{mn}^{(E)} = 2\int_o^{\lambda} G_m(t)G_n(t)dz(t)/b.
\end{aligned}\right\} \tag{5.21}$$

The evaluation of the quantities of equation (5.21) for various m and n is dealt with in Appendix II.

On performing the differentiation shown in equation (5.20) and interchanging the order of the integration and summation one obtains, after employing equations (5.21),

$$\sum_{m=o} B_m \{\beta^2\mu^2(Q_{mn}^{(w)} + Q_{mn}^{(E)}) - \kappa^m\kappa^n(S_{mn}^{(w)} + S_{mn}^{(E)})\} + 2\beta^2\mu^2(\alpha^{(w)}P_n^{(w)} + \alpha^{(E)}P_n^{(E)}) -$$

$$- 2\beta\mu\kappa^n(\alpha^{(w)}R_n^{(w)} + \alpha^{(E)}R_n^{(E)}) = 0; \quad n = 0,1,2,3, \ldots\ldots . \qquad (5.22)$$

This equation represents an infinite number of simultaneous equations. In practice, only a finite number of these equations are retained on the assumption that a finite number of coefficients will give adequate accuracy. Thus, in the present case, it is assumed that the first four coefficients are sufficient. This yields, in place of equation (5.22), four simultaneous equations in the unknowns B_o, B_1, B_2 and B_3. These equations have been programmed for solution on a Ferranti Pegasus computer.

By employing Robinson and Laurmann's equation (3.2, 28) it is found that the expression for the overall lift may be written in the form

$$\overline{L} = \rho U_o \int_{-b/2}^{+b/2} \Gamma(y)\, dy. \qquad (5.23)$$

Therefore, when rewritten in terms of the solution of equation (5.22), this expression becomes

$$\overline{L} = \rho U_o \int_{-b/2}^{+b/2} \sum_{m=o} \Gamma_m(t) dy(t).$$

Hence, by interchanging the order of integration and summation in this equation and employing equations (5.19) and (5.21), one finds that

$$\overline{L} = -\rho U_o^2 b^2 \sum_{m=o} B_m \kappa^m R_m^{(w)}. \qquad (5.24)$$

Thus the overall lift coefficient based on the plan area of the wing component of the cylindrical surface is given by

$$\overline{C}_L = -2 AR \sum_{m=o} B_m \kappa^m R_m^{(w)}. \qquad (5.25)$$

It will be shown in Section 5.3 that β is independent of $\alpha^{(w)}$ and $\alpha^{(E)}$. Therefore it may be concluded from equations (5.22)

and (5.25) that $\overline{C}_L$ may be written in the form

$$\overline{C}_L = a^{(w)}\alpha^{(w)} + a^{(E)}\alpha^{(E)}, \tag{5.26}$$

where $a^{(w)}$ and $a^{(E)}$ are 'lift derivatives' which are independent of $\alpha^{(w)}$ and $\alpha^{(E)}$. Results for these derivatives, calculated according to the present method, are shown in Figs. 22 and 23 which are graphs of $AR/a^{(w)}$ and $AR/a^{(E)}$ against $AR/2\pi\beta$ for various $2\lambda/b$.

In solving equations (5.2) it is assumed implicitly that $D_f = D_i$. For this reason, therefore, reference will be made hereafter in Section 5 to 'the induced drag' rather than the drag of the wing or end plates. Thus, by integrating the induced drag gradient across the wing part of the vortex trace, it is found that the total induced drag of the wing, $\overline{D}_i^{(w)}$, is given by

$$\overline{D}_i^{(w)} = -\rho \int_{-b/2}^{+b/2} w_\infty(y)\Gamma(y)dy/2. \tag{5.27}$$

Similarly, the total induced drag of <u>both</u> end plates, $\overline{D}_i^{(E)}$, is found from the result

$$\overline{D}_i^{(E)} = -\rho \int_0^{\lambda} v_\infty(z)\Gamma(z)dz. \tag{5.28}$$

It has not been possible, with the particular solutions employed, to evaluate the integrals of equations (5.27) and (5.28). However, Γ may be eliminated from these expressions by means of equations (5.2) to give instead

$$\left.\begin{aligned} \overline{D}_i^{(w)} &= -\rho\pi\beta c \int_{-b/2}^{+b/2} \{U_o\alpha^{(w)} w_\infty(y) + w_\infty^2(y)/2\}dy/2; \\ \overline{D}_i^{(E)} &= -\rho\pi\beta c \int_0^{\lambda} \{U_o\alpha^{(E)} v_\infty(z) + v_\infty^2(z)/2\}dz. \end{aligned}\right\} \tag{5.29}$$

Therefore, if w_∞ and v_∞ are replaced in equations (5.29) by linear combinations of particular velocities and the order of the integration and summation is changed, it is found, after employing equations (5.18) and (5.21), that

$$\left.\begin{aligned} \overline{D}_i^{(w)} &= -\tfrac{1}{2}\rho U_o^2 \pi\beta bc\{\alpha^{(w)} \sum_{m=o} B_m P_m^{(w)} + \tfrac{1}{2} \sum_{m=o} \sum_{n=o} B_m B_n Q_{mn}^{(w)}\}; \\ \overline{D}_i^{(E)} &= -\tfrac{1}{2}\rho U_o^2 \pi\beta bc\{\alpha^{(E)} \sum_{m=o} B_m P_m^{(E)} + \tfrac{1}{2} \sum_{m=o} \sum_{n=o} B_m B_n Q_{mn}^{(E)}\}. \end{aligned}\right\} \quad (5.30)$$

The induced-drag factors of the wing and end plates, $\sigma^{(w)}$ and $\sigma^{(E)}$, are defined as follows:

$$\sigma^{(w)} = \pi\rho U_o^2 b^2 \overline{D}_i^{(w)}/2\overline{L}^2; \quad \sigma^{(E)} = \pi\rho U_o^2 b^2 \overline{D}_i^{(E)}/2\overline{L}^2. \quad (5.31)$$

Therefore equations (5.31) may be combined with equations (5.24) and (5.30) to give the results

$$\sigma^{(w)} = -\frac{\pi^2\beta\{\alpha^{(w)} \sum_{m=o} B_m P_m^{(w)} + \tfrac{1}{2} \sum_{m=o} \sum_{n=o} B_m B_n Q_{mn}^{(w)}\}}{4\,AR\{\sum_{m=o} B_m \kappa^m R_m^{(w)}\}^2};$$

$$\sigma^{(E)} = -\frac{\pi^2\beta\{\alpha^{(E)} \sum_{m=o} B_m P_m^{(E)} + \tfrac{1}{2} \sum_{m=o} \sum_{n=o} B_m B_n Q_{mn}^{(E)}\}}{4\,AR\{\sum_{m=o} B_m \kappa^m R_m^{(w)}\}^2}.$$

The overall induced-drag factor of the configuration, σ, is found simply by adding $\sigma^{(w)}$ and $\sigma^{(E)}$.

Representative results for σ, $\sigma^{(w)}$ and $\sigma^{(E)}$ are given in Figs. 24, 25 and 26. These show graphs of σ against $AR/2\pi\beta$ for $\alpha^{(E)}/\alpha^{(w)} = 0$ and σ, $\sigma^{(w)}$ and $\sigma^{(E)}$ against $\alpha^{(w)}/\alpha^{(E)}$ for $AR/2\pi\beta = 0.25$. In particular, Fig. 25 indicates that $\sigma = o$ when $\alpha^{(w)} = \alpha^{(E)}$, in agreement with the exact solution of equations (5.2). That the variational method yields this result regardless of where the series of coefficients B_o, B_1, B_2 ..... B_m is truncated for $m > o$ may be proved by examining equation (5.22). This study also

reveals that the circulation, $\Gamma(t)$, predicted by the variational method for the case $\alpha^{(w)} = \alpha^{(E)}$ is in agreement with the exact solution (5.3) for all $m \geq 0$.

Fig. 26 illustrates the essential feature of the distribution of induced-drag gradient if the circulation varies slowly around the vortex trace. It shows that if there is an induced drag acting on the wing the end plates yield an induced thrust and vice versa. This may be attributed to the fact, which may be proved by continuity considerations, that a mean downwash at the wing trace is accompanied by a sidewash in the outward direction at the end-plate traces. It follows, therefore, from equations (5.27) and (5.28) that, for slowly-varying, positive $\Gamma(s)$, $\bar{D}_i^{(w)} \geq 0$ and $\bar{D}_i^{(E)} \leq 0$.

5.3 The determination of β

In this section, the method for determining β, which was introduced in Section 3.1, will be applied to the present configuration.

5.3.1 The integral equation

In the present case, equation (3.17) may be replaced by the expression

$$\int_{-b/2}^{+b/2} f(y) w_f(\xi,y)\,dy + 2\int_0^1 f(z) v_f(\xi,z)\,dz = -\int_{-b/2}^{+b/2} f(y) U_o \alpha^{(w)}\,dy - 2\int_0^1 f(z) U_o \alpha^{(E)}\,dz, \qquad (5.32)$$

where $w_f(\xi,y)$ and $v_f(\xi,z)$ are, respectively, the z-wash at the wing component and the y-wash at the starboard end-plate component of the cylindrical surface.

By adopting the procedure introduced in Section 3.1 a suitable first approximation is sought for $f\left(\frac{y}{z}\right)$. Thus, for example, it is evident from Section 5.2.1 that a good approximation corresponding

to $\alpha^{(w)} \simeq \alpha^{(E)}$ is $f(\frac{y}{z}) = 1$. Therefore this is used as a first approximation and, in consequence, the vortex distribution is assumed to be $\gamma(\xi)$.

The velocity field associated with this vortex distribution and its image system is derived in Appendix III where it is shown that

$$\left.\begin{aligned} 4\pi w_f(\xi,\eta) &= P\int_{-1}^{+1}\gamma(\xi_1)F(\xi_1,\xi,\eta,AR,\lambda)d\xi_1 \\ \text{and}\qquad 4\pi v_f(\xi,\zeta) &= P\int_{-1}^{+1}\gamma(\xi_1)F(\xi_1,\xi,\zeta,\lambda,AR)d\xi_1 . \end{aligned}\right\} \qquad (5.33)$$

Here

$$F(\xi_1,\xi,\eta,AR,\lambda) = \frac{1}{\xi_1-\xi}\left[\frac{AR(1-\eta)}{\{AR^2(1-\eta)^2+(\xi_1-\xi)^2\}^{\frac{1}{2}}} + \frac{AR(1+\eta)}{\{AR^2(1+\eta)^2+(\xi_1-\xi)^2\}^{\frac{1}{2}}}\right] +$$

$$+ \frac{\xi-\xi_1}{(\xi_1-\xi)^2+4\lambda^2}\left[\frac{AR(1-\eta)}{\{AR^2(1-\eta)^2+(\xi_1-\xi)^2+4\lambda^2\}^{\frac{1}{2}}} + \frac{AR(1+\eta)}{\{AR^2(1+\eta)^2+(\xi_1-\xi)^2+4\lambda^2\}^{\frac{1}{2}}}\right],$$

$$\lambda = 2\ell/c, \quad \eta = 2y/b, \quad \zeta = z/\ell$$

and P denotes that the Cauchy principal value is taken where required. Therefore, by recalling that $f(\frac{y}{z}) = 1$, it is possible to combine equations (5.32) and (5.33) to give the result

$$\int_{-1}^{+1}d\eta\, P\int_{-1}^{+1}\gamma(\xi_1)F(\xi_1,\xi,\eta,AR,\lambda)d\xi_1 + (4\ell/b)\int_{-1}^{+1}d\zeta\, P\int_{-1}^{+1}\gamma(\xi_1)F(\xi_1,\xi,\zeta,\lambda,AR)d\xi_1 =$$

$$= -8\pi U_o(\alpha^{(w)} + \alpha^{(E)}2\ell/b).$$

Consequently, by interchanging the order of integration of the integrals of this expression (an operation which is permissible in this case) and performing the η and ζ integration, one obtains the expression

$$P\int_{-1}^{+1}\frac{\gamma(\xi_1)}{\xi_1-\xi}\left[\{4AR^2+(\xi_1-\xi)^2\}^{\frac{1}{2}} - |\xi_1-\xi|\right]d\xi_1 + \int_{-1}^{+1}\frac{\gamma(\xi_1)(\xi-\xi_1)}{(\xi_1-\xi)^2+4\lambda^2}\cdot$$

$$\cdot\left[\{4AR^2+4\lambda^2+(\xi_1-\xi)^2\}^{\frac{1}{2}} - \{4\lambda^2+(\xi_1-\xi)^2\}^{\frac{1}{2}}\right]d\xi_1 + P\int_{-1}^{+1}\frac{\gamma(\xi_1)}{\xi_1-\xi}\cdot$$

$$\cdot\left[\{4\lambda^2+(\xi_1-\xi)^2\}^{\frac{1}{2}} - |\xi_1-\xi|\right]d\xi_1 + \int_{-1}^{+1}\frac{\gamma(\xi_1)(\xi-\xi_1)}{(\xi_1-\xi)^2+4AR^2}\left[\{4\lambda^2+4AR^2+(\xi_1-\xi)^2\}^{\frac{1}{2}} -\right.$$

$$- \{4\,\mathbb{R}^2 + (\xi_1-\xi)^2\}^{\frac{1}{2}}\Big]d\xi_1 = -4\pi U_o(\mathbb{R}\alpha^{(w)} + \lambda\alpha^{(E)}). \qquad (5.34)$$

This represents an integral equation in the unknown $\gamma(\xi_1)$ which is solved as follows: $\gamma(\xi)/U_o$ is approximated by the first four terms of the series (3.3) which satisfies the condition $\gamma(+1) < \infty$. Consequently, equation (5.34) is satisfied at four isolated points in the interval $-1 \leq \xi \leq +1$, thus yielding four linear, simultaneous equations for a_o, a_1, a_2 and a_3. These are then solved and a first approximation for β is found by using equation (3.6). A second approximation for β may then be determined by means of the method outlined in Section 3.1. However, as will be shown, this is unnecessary because the first approximation is 'exact'.

In the case $\alpha^{(E)} = \alpha^{(w)}$, $f(\frac{Y}{2}) = 1$ regardless of the value of β. Hence the first approximation for $\beta\{\alpha^{(w)}, \alpha^{(E)} = \alpha^{(w)}\}$ is 'exact'. That this also applies to $\beta\{\alpha^{(w)}, \alpha^{(E)}\}$ may be proved as follows: by employing equation (30.8) of Heaslet and Lomax (1955) it is possible to write

$$\int_B \int_{-c/2}^{+c/2} \gamma_1(\xi) f_1(s) v_{nf2}(x',s)\,dx\,ds = \int_B \int_{-c/2}^{+c/2} \gamma_2(\xi') f_2(s) v_{nf1}(x,s)\,dx\,ds \qquad (5.35)$$

provided γ_1 and γ_2 are bounded at $\xi = +1$.

Suppose that

$$\left.\begin{aligned} v_{nf1}(x,y,+\zeta) &= -U_o\alpha^{(w)}; \quad v_{nf1}(x,\pm b/2,z) = -U_o\alpha^{(w)}; \\ v_{nf2}(x',y,+\zeta) &= -U_o\alpha^{(w)}; \quad v_{nf2}(x',\pm b/2,z) = -U_o\alpha^{(E)}. \end{aligned}\right\} \qquad (5.36)$$

According to the present theory the corresponding circulation distributions are given by

$$\left.\begin{aligned} \Gamma_1 &= \pi\beta\{\alpha^{(w)}, \alpha^{(w)}\}c\,U_o\alpha^{(w)}; \\ \Gamma_2(y) &= \pi\beta\{\alpha^{(w)}, \alpha^{(E)}\}c\{U_o\alpha^{(w)} + w_{\infty 2}(y)/2\}; \quad |y| \leq b/2,\ z = +\zeta; \\ \Gamma_2(z) &= \pi\beta\{\alpha^{(w)}, \alpha^{(E)}\}c\{U_o\alpha^{(E)} + v_{\infty 2}(z)/2\}; \quad |y| = b/2,\ 0 \leq z \leq +\zeta. \end{aligned}\right\} \qquad (5.37)$$

Therefore, by substituting equations (5.36) into equation (5.35), one obtains, after performing the integration and comparing the result with equations (5.37), the expression

$$\beta\{\alpha^{(w)},\alpha^{(w)}\}\left[b\alpha^{(w)} + 2\ell\alpha^{(E)}\right] = \beta\{\alpha^{(w)},\alpha^{(E)}\}\left[b\alpha^{(w)} + 2\ell\alpha^{(E)} + \int_{-b/2}^{+b/2}(w_{\infty 2}(y)/2U_o)dy + \int_{o}^{\ell}(v_{\infty 2}(z)/U_o)dz\right] . \tag{5.38}$$

Considerations of flow continuity in the Trefftz plane indicate that the integrals of equation (5.38) cancel. Therefore

$$\beta\{\alpha^{(w)},\alpha^{(E)}\} = \beta\{\alpha^{(w)},\alpha^{(w)}\}$$

for all $\alpha^{(w)}$ and $\alpha^{(E)}$ except possibly those values corresponding to $\alpha^{(w)} = -(2\ell/b)\alpha^{(E)}$. However, for a given $(2\ell/b)$ and $\alpha^{(E)}$, this is an isolated case which will be disregarded. It follows, therefore, that the first approximation for $\beta\{\alpha^{(w)},\alpha^{(E)}\}$ is 'exact' and is independent of $\alpha^{(E)}$. Therefore, in view of the similarity of the roles of the half-span of the wing plane and the corresponding end plate, it follows that β is also independent of $\alpha^{(w)}$.

5.3.2 Evaluation of the integrals

With the exception of integrals of the type

$$I_1(\xi) = P\int_{-1}^{+1}\gamma(\xi_1)\,|\xi - \xi_1|\,(\xi-\xi_1)^{-1}d\xi_1 \tag{5.39}$$

the integrals of equation (5.34) are, for the vortex distribution of equation (3.3), of the form

$$I_2(\xi) = P\int_{-1}^{+1} g(\xi_1,\xi)(\xi-\xi_1)^{-1}\,d\xi_1 , \tag{5.40}$$

where $g(\xi_1,\xi)$ is continuous for $-1 < \xi_1 < +1$. Weber (1954) has shown that, subject to certain restrictions being placed on $g(\xi_1,\xi)$,

this type of integral may be replaced by an expression containing Gaussian quadratures, namely

$$I_2(\xi_\nu) = \pi g_o(\xi_\nu)\left[1 - \tfrac{1}{2}\sum_{\mu=1}^{N-1} R_{\mu\nu}\{(1-\xi_\mu)/(1+\xi_\mu)\}^{\frac{1}{2}}\right] + \frac{\pi}{2}\sum_{\mu=1}^{N-1} R_{\mu\nu} g(\xi_\mu,\xi_\nu). \tag{5.41}$$

Here $\xi_\mu = \cos(\mu\pi/N)$, $\xi_\nu = \cos(\nu\pi/N)$, $(\mu,\nu = 1,2, \ldots N-1.)$,

$$g_o(\xi_\nu) = \lim_{\xi\to-1}\left[g(\xi,\xi_\nu)\{(1+\xi)/(1-\xi)\}^{\frac{1}{2}}\right],$$

$$R_{\mu\nu} = \begin{cases} \dfrac{2\{(-1)^{\mu-\nu} - 1\}(1-\xi_\mu^2)^{\frac{1}{2}}}{N(\xi_\mu-\xi_\nu)}, & (\mu \neq \nu), \\ 0 & (\mu = \nu) \end{cases}$$

and N is an integer.

The previously-mentioned restrictions on $g(\xi_1,\xi)$ are as follows:

(i) It is bounded, continuous and differentiable in the interval $-1 < \xi_1 < +1$.

(ii) $\lim_{\xi_1\to-1}\left[g(\xi_1,\xi) - g_o(\xi)\{(1-\xi_1)/(1+\xi_1)\}^{\frac{1}{2}}\right] = 0.$

(iii) $g(1,\xi) = 0.$

These conditions are satisfied by the integrals of the type I_2 in equation (5.34) with $\gamma(\xi)$ replaced by the vortex distribution of equation (3.3). Hence these integrals are evaluated by using equation (5.41) with N = 16. The integral I_1, on the other hand, may be evaluated explicitly to give the result

$$I_1(\theta) = U_o\left[2a_o\{\pi/2 - \theta + \sin\theta\} + a_1\{\pi/2 - \theta + \sin 2\theta/2\} - \right.$$
$$\left. - \sum_{n=2} a_n\{\sin(n-1)\theta/(n-1) - \sin(n+1)\theta/(n+1)\}\right] \tag{5.42}$$

for the vortex distribution (3.3). Thus, by using equations (5.41) and (5.42), it is possible to evaluate the left-hand side of equation (5.34), with $\gamma(\xi)/U_o$ replaced by the first four terms of the series (3.3), at four isolated points. These were arbitrarily chosen as $\theta = n\pi/8$, with n = 1,3,5 and 7. This procedure and the inversion of the resultant 4 x 4 matrix has been programmed for calculation on a Ferranti Pegasus computer.

5.3.3 Discussion of results

In the case $\alpha^{(w)} = \alpha^{(E)} = \alpha$ the values of β and Γ, which are determined from the exact solution of equation (5.34), are required to be consistent with the condition $\overline{D}_f = 0$. In this case, however, $D_i = 0$ everywhere at the vortex trace; hence this requirement may be replaced by $D_f = 0$. This is implicit in equation (5.3) which, in effect, relates the sectional edge thrust to the drag component of the sectional normal force. Consequently the above-mentioned values of β and Γ satisfy this equation. In other words, the value of β derived from the expression

$$\beta = \Gamma/\pi\, c\, U_o \alpha \,, \quad (\alpha^{(w)} = \alpha^{(E)} = \alpha), \tag{5.43}$$

is identical with that obtained from the exact solution of equation (5.34) by using the original definition of β, equation (3.6). Thus the accuracy of the present approximate method of solving equation (5.34) may be checked by comparing the two values of β obtained.

Shown in Table 1 are typical results for β calculated by means of equations (3.6) and (5.43). It will be seen that the two sets of results are in reasonable agreement, the differences being in the region of 1%. Therefore, it is assumed that the arithmetic mean of the two values is a good approximation for β. The results thus obtained are shown in Fig. 27 plotted against λ for various $\mathfrak{R}$. It will be seen that β increases monotonically with either decreasing λ or decreasing $\mathfrak{R}$. Each of these tendencies may be explained by examining the case $\alpha^{(w)} = \alpha^{(E)}$ which according to the present theory yields chordwise and trailing vorticity of zero strength.

Thus it is apparent that, for a given $\mathcal{R}$ and $\alpha^{(w)}$, a reduction in λ produces an increase in the upwash induced at the wing plane by the images of the wing-plane vortices. In consequence, there results an increase in Γ which, according to equation (5.43), implies an increase in β. There is also an increase in β due to the consequent reduction in the 'aspect ratio' of the end plates. This is similar to the effect of $\mathcal{R}$ on β. This effect may be identified with the influence of the span of the wing vortices and their images as follows: as $\mathcal{R}$ decreases, the effectiveness of the wing vortices in producing a downwash at the wing plane is reduced. Also, the upwash of the image-wing vortices is there diminished. However, the overall effect is a reduction in downwash. Therefore an increased circulation is required to produce the same downwash, thus resulting in an increase in β.

Another effect associated with a reduction in $\mathcal{R}$ is the increase in the mutual influence of the end plates. This is analogous with the effect of the image wing on the wing and vice versa. Therefore, this also produces an increase in β.

5.4 Lift and induced drag

The values for β given previously may be combined with the results of the variational solution to obtain the lift derivatives $a^{(w)}$ and $a^{(E)}$ and the induced-drag factors. In Section 5.4.1 consideration is given to the results for the lift derivatives and in Section 5.4.2 the results for the induced-drag factors are described.

5.4.1 Lift

The results derived for $a^{(w)}$ and $a^{(E)}$ are plotted against λ for various $\mathcal{R}$ in Figs. 28 and 29. These figures show that, for constant λ, $a^{(w)}$ and $a^{(E)}$ increase slowly and decrease with $\mathcal{R}$, respectively. Also, they indicate that, with $\mathcal{R}$ constant, $a^{(w)}$ and

$a^{(E)}$ increase and decrease with λ, respectively.

It is difficult to give simple explanations for these trends. Nevertheless, some progress towards an understanding of the mechanisms involved may be made with the aid of the expression

$$\bar{C}_L = 2\pi\beta\{\alpha^{(w)} + \bar{w}_\infty/2U_o\} , \qquad (5.44)$$

where $\bar{w}_\infty$ is the mean upwash at the trace of the wing plane in the Trefftz plane. This equation is obtained simply by integrating equations (5.2) across the wing vortex trace and using equation (5.23) to obtain the lift.

By differentiating equation (5.44) with respect to $\alpha^{(w)}$ it is found that

$$\partial\bar{C}_L/\partial\alpha^{(w)} \equiv a^{(w)} = 2\pi\beta\{1 + \partial(\bar{w}_\infty/2U_o)/\partial\alpha^{(w)}\} .$$

This expression for $a^{(w)}$ has a right-hand side comprised of two parts which may be identified with two different properties of the vortex distribution. The first part, $2\pi\beta$, which depends on the chordwise distribution of vortices normal to the direction of motion, decreases with increasing $\mathcal{AR}$ in the range of $\mathcal{AR}$ and λ considered. This is opposite to the trend exhibited by the remaining part which depends on the strength and distribution of trailing vortices round the vortex trace. The behaviour of this part may be explained by noting that the term $\partial(\bar{w}_\infty/2U_o)/\partial\alpha^{(w)}$ increases towards zero as $\mathcal{AR}\to\infty$ owing to the reduction in the strength of the trailing vortices. Unfortunately, it is not possible to infer from this the likely trend of $a^{(w)}$ with $\mathcal{AR}$.

For reasons which have been mentioned before, β increases monotonically as λ decreases. Further, the term $\partial(\bar{w}_\infty/2U_o)/\partial\alpha^{(w)}$ increases with reducing λ owing to the influence of the image trailing vortices. Therefore $a^{(w)}$ increases as λ decreases, in accord with the calculations.

By differentiating equation (5.44) partially with respect to $\alpha^{(E)}$, one obtains the result

$$\partial \bar{C}_L / \partial \alpha^{(E)} \equiv a^{(E)} = 2\pi\beta\partial(\bar{w}_\infty/2U_o)/\partial\alpha^{(E)}. \qquad (5.45)$$

An increase in $\alpha^{(E)}$ produces additional trailing vortices, the sign of which is such as to increase the upwash at the wing trace. This implies that $\partial(\bar{w}_\infty/2U_o)/\partial\alpha^{(E)}$ is positive. Therefore, as β is positive, it follows from equation (5.45) that $a^{(E)}$ is positive, a fact which also emerges from the calculations.

As noted before, the effect of increasing AR is to reduce the strength of the trailing vorticity. Consequently $\partial(\bar{w}_\infty/2U_o)/\partial\alpha^{(E)}$ decreases monotonically with increasing AR. Therefore, in view of the fact that β decreases monotonically with increasing AR, it may be inferred from equation (5.45) that $a^{(E)}$ decreases as AR increases.

It has not been possible to draw any firm conclusions from equation (5.45) regarding the influence of λ on $a^{(E)}$.

5.4.2 Induced drag

An illustration of the influence of λ and AR on the induced-drag factor σ is provided by Fig. 30 for the case $\alpha^{(E)}/\alpha^{(w)} = 0$. This shows that σ is small within the range of AR and λ considered but that it increases with AR and λ. The corresponding results for $\sigma^{(w)}$ are shown in Fig. 31 which indicates that, for the range of λ and AR considered, this factor is considerably larger than σ. This emphasizes the need to ensure that, in practice, the end plates can sustain the required thrust.

6. Chordwise camber and thickness

In this section, consideration will be given to the influence of distributions of chordwise camber and thickness on the lift and induced drag. The class of distributions to be examined, which is considered representative of current trends in G.E.W. design, may

be described as follows;

(i) For $\alpha^{(E)} = 0$ the wing section is constant across the span.

(ii) The end plates' sections are different from that of the wing, in general, and for $\alpha^{(w)}=0$ they are independent of z.

(iii) At any z-wise station the sections of the end plates are the mirror image of each other in the plane y = 0.

Throughout the analysis of Section 6 the assumptions of Section 5 will be employed. Included among these, it will be recalled, are the assumptions of the linearized theory. Thus the vorticity distributions associated with incidence, chordwise camber and thickness may be superposed to yield the vortex distribution of a configuration with a combination of these section properties. The linearizations do, however, restrict the analysis to configurations of 'small' incidence, chordwise camber and thickness.

6.1 Chordwise camber

According to the linearized theory the boundary conditions at the cylindrical surface are, for the type of camber distribution under consideration,

$$v_{nf}(x,y,+1) = U_o \, dz_c(x)/dx; \quad v_{nf}(x,\pm b/2,z) = U_o \, dy_c(x)/dx. \tag{6.1}$$

Here y_c and z_c are the (y and z) ordinates of the camber lines of the starboard end plate and the wing.

As a consequence of the assumptions that the vortex distribution is of the form $\gamma(\xi)f(\frac{y}{z})$ and the flow is smooth at the trailing edge in forward flight, equations (3.28) and (6.1) may be combined to yield

$$\left.\begin{aligned} \int_{-c/2}^{+c/2} \gamma_1(\xi)\left[dz_c(x')/dx\right]_2 dx &= \int_{-c/2}^{+c/2} \gamma_2(\xi')\left[dz_c(x)/dx\right]_1 dx, \\ \int_{-c/2}^{+c/2} \gamma_1(\xi)\left[dy_c(x')/dx\right]_2 dx &= \int_{-c/2}^{+c/2} \gamma_2(\xi')\left[dy_c(x)/dx\right]_1 dx \end{aligned}\right\} \quad (6.2)$$

provided that $f_1(\frac{y}{z}) = f_2(\frac{y}{z})$. Consequently, if $\left[dz_c(x')/dx\right]_2 = \left[dy_c(x')/dx\right]_2 = -\alpha$, equations (6.2) become

$$-\int_{-c/2}^{+c/2} \gamma_1(\xi)\alpha\, dx = \int_{-c/2}^{+c/2} \gamma_2(\xi',\alpha)\left[dz_c(x)/dx\right]_1 dx = \int_{-c/2}^{+c/2} \gamma_2(\xi',\alpha)\left[dy_c(x)/dx\right]_1 dx. \quad (6.3)$$

Therefore, as $f_2(\frac{y}{z}) = 1$, it follows that $f_1(\frac{y}{z}) = 1$. Hence it may deduced from equation (6.3) that the circulation distribution (round the vortex trace) corresponding to γ_1 is given by

$$\Gamma_1(\tfrac{y}{z}) \equiv \int_{-c/2}^{+c/2} \gamma_1(\xi)\, dx = -\int_{-c/2}^{+c/2} \gamma_2(\xi',\alpha)\left[dz_c(x)/dx\right]_1 dx/\alpha. \quad (6.4)$$

Thus, by combining equations (5.23) and (6.4), it is found that the overall-lift coefficient associated with this circulation distribution may be written as

$$\bar{C}_{L1} \equiv 2\int_{-c/2}^{+c/2} \gamma_1(\xi)dx/U_o c = -2\int_{-c/2}^{+c/2} \gamma_2(\xi',\alpha)\left[dz_c(x)/dx\right]_1 dx/U_o c\alpha\,. \quad (6.5)$$

Consider the slope distribution

$$dz_c(x)/dx = \left[dz_c(x)/dx\right]_1; \quad dy_c(x)/dx = \left[dy_c(x)/dx\right]_1 - \Delta\alpha^{(E)}, \quad (6.6)$$

where $\Delta\alpha^{(E)}$ represents an increment in end-plate incidence. These expressions may be used in conjunction with equation (6.3) to obtain the result

$$\int_{-c/2}^{+c/2} \gamma_2(\xi',\alpha)(dz_c(x)/dx)dx = \int_{-c/2}^{+c/2} \gamma_2(\xi',\alpha)(dy_c(x)/dx + \Delta\alpha^{(E)})dx\,. \quad (6.7)$$

It will be seen that, for arbitrary $\Delta\alpha^{(E)}$, equation (6.7) is satisfied by arbitrary $dz_c(x)/dx$ and $dy_c(x)/dx$ provided these slopes are such that the integrals of this equation exist.

It may be inferred from equations (5.26) and (6.6) that, within the limitations of the linearized theory, the overall-lift coefficient appropriate to the slope distribution (6.6) is given by

$$\bar{C}_L = \bar{C}_{L1} + a^{(E)}\,\Delta\alpha^{(E)}.$$

Therefore, by employing equations (6.5), (6.6) and (6.7), this may be rewritter in the form

$$\bar{C}_L = -\frac{2\int_{-c/2}^{+c/2}\gamma_2(\xi',\alpha)(dz_c(x)/dx)dx}{U_o\, c\,\alpha} + \frac{a^{(E)}\int_{-c/2}^{+c/2}\gamma_2(\xi',\alpha)(dz_c(x)/dx - dy_c(x)/dx)dx}{\int_{-c/2}^{+c/2}\gamma_2(\xi',\alpha)dx}. \tag{6.8}$$

Equation (6.8) may be written in a more suitable form by noting from equation (5.26) that

$$\bar{C}_{L2} \equiv 2\int_{-c/2}^{+c/2}\gamma_2(\xi',\alpha)dx/U_o c = (a^{(w)} + a^{(E)})\alpha, \tag{6.9}$$

where $\bar{C}_{L2}$ is the overall-lift coefficient corresponding to γ_2. Therefore equations (6.8) and (6.9) may be combined to give the result

$$\bar{C}_L = \frac{-2\{a^{(w)}\int_{-c/2}^{+c/2}\gamma_2(\xi',\alpha)(dz_c(x)/dx)dx + a^{(E)}\int_{-c/2}^{+c/2}\gamma_2(\xi',\alpha)(dy_c(x)/dx)dx\}}{\bar{C}_{L2}\,U_o c}. \tag{6.10}$$

This expression allows the determination of the overall-lift coefficient corresponding to the arbitrary slope distribution $\{dz_c(x)/dx,\ dy_c(x)/dx\}$. Unfortunately, it would seem that, in general, the integrals of this equation will have to be evaluated numerically. This may be avoided, however, by writing

$$\left.\begin{aligned} \alpha \int_{-c/2}^{+c/2} \gamma_w(\xi)dx &= -\int_{-c/2}^{+c/2} \gamma_2(\xi',\alpha)(dz_c(x)/dx)dx \\ \text{and}\quad \alpha \int_{-c/2}^{+c/2} \gamma_E(\xi)dx &= -\int_{-c/2}^{+c/2} \gamma_2(\xi',\alpha)(dy_c(x)/dx)dx. \end{aligned}\right\} \qquad (6.11)$$

Here $\gamma_w(\xi)$ is identifiable with the slope distribution $\{dz_c(x)/dx, dz_c(x)/dx\}$ and $\gamma_E(\xi)$ with $\{dy_c(x)/dx, dy_c(x)/dx\}$, facts which may be proved by comparing equations (6.3) and (6.11). These vortex distributions are, in fact, solutions of integral equations which are similar in most respects to equation (5.34). The only differences occur in the right-hand sides which instead of that of equation (5.34) are, respectively, $4\pi U_o(\mathcal{R} + \lambda)dz_c(x)/dx$ and $4\pi U_o(\mathcal{R}+\lambda)dy_c(x)/dx$.* Therefore, by solving these equations in the manner indicated in Section 5.3.1, it is possible to determine $\gamma_w(\xi)$ and $\gamma_E(\xi)$ in simple analytical terms. Thus it is apparent that the expression found by combining equations (6.10) and (6.11), namely

$$\overline{C}_L = 2\alpha\left\{a^{(w)}\int_{-c/2}^{+c/2} \gamma_w(\xi)dx + a^{(E)}\int_{-c/2}^{+c/2} \gamma_E(\xi)dx\right\}\Big/\overline{C}_{L2}\, U_o c, \qquad (6.12)$$

may be evaluated without difficulty, $\overline{C}_{L2}$ being found by the method of Section 5.

In order to obtain the induced-drag factors of the slope distribution (6.6) it is necessary to know the circulation distribution of the vortex trace. This may be found as follows: it may be inferred from equation (6.3) that, if $\Gamma_o(\frac{y}{z})$ is the circulation distribution of a configuration with the slope distribution $\{-\alpha^{(w)}, -\alpha^{(E)}\}$, $\Gamma_o(\frac{y}{z}) = \Gamma_1(\frac{y}{z})$ = constant, provided that

---

*That these terms are correct may be proved by writing $\alpha^{(w)} = \alpha^{(E)} = \alpha$ and, correspondingly, $\gamma(\xi_1) = \gamma_2(\xi_1,\alpha)$ in equation (5.34). This equation is then multiplied in turn by $\gamma_w(\xi')$ and $\gamma_E(\xi')$ and integrated with respect to ξ' between -1 and +1. The order of integration of the left-hand side of each equation is then interchanged and the resultant expressions are compared with equations (6.11).

$$\alpha^{(w)} = \alpha^{(E)} = \alpha \int_{-c/2}^{+c/2} \gamma_1(\xi)dx \Big/ \int_{-c/2}^{+c/2} \gamma_2(\xi',\alpha)dx . \qquad (6.13)$$

Thus it may be deduced from equations (6.6) that if, instead, $\Gamma_o(\frac{y}{z})$ is required to be identical with the circulation distribution corresponding to the slope distribution (6.6) then

$$\left.\begin{aligned} \alpha^{(w)} &= \alpha \int_{-c/2}^{+c/2} \gamma_1(\xi)dx \Big/ \int_{-c/2}^{+c/2} \gamma_2(\xi',\alpha)dx; \\ \alpha^{(E)} &= \alpha^{(w)} + \Delta\alpha^{(E)}. \end{aligned}\right\} \qquad (6.14)$$

Therefore the circulation distribution and hence the induced-drag factors of the slope distribution (6.6) may be determined by the method of Section 5. It is unnecessary, however, to perform these calculations as the required results for σ, $\sigma^{(w)}$ and $\sigma^{(E)}$ may be found directly from the results of Section 5 if AR, λ and $\alpha^{(E)}/\alpha^{(w)}$ are given. Therefore, in order to facilitate this, equations (6.14) are used to derive the result

$$\{\alpha^{(E)}/\alpha^{(w)}\}_{eq} = \{\alpha \int_{-c/2}^{+c/2} \gamma_1(\xi)dx + \Delta\alpha^{(E)} \int_{-c/2}^{+c/2} \gamma_2(\xi',\alpha)dx\} \Big/ \alpha \int_{-c/2}^{+c/2} \gamma_1(\xi)dx .$$

Here the subscripts eq have been added to show that the term concerned applies to an uncambered configuration with equivalent induced-drag factors. Thus, by employing equations (6.4) and (6.7) to eliminate $\gamma_1(\xi)$ and $\Delta\alpha^{(E)}$ from this expression, there is obtained the result

$$\begin{aligned} \{\alpha^{(E)}/\alpha^{(w)}\}_{eq} &= \{ \int_{-c/2}^{+c/2} \gamma_2(\xi',\alpha)\left[dz_c(x)/dx\right]_1 dx - \int_{-c/2}^{+c/2} \gamma_2(\xi',\alpha) \cdot \\ &\quad \cdot (dz_c(x)/dx - dy_c(x)/dx)dx\} \Big/ \int_{-c/2}^{+c/2} \gamma_2(\xi',\alpha)\left[dz_c(x)/dx\right]_1 dx , \\ &= \int_{-c/2}^{+c/2} \gamma_2(\xi',\alpha)(dy_c(x)/dx)dx \Big/ \int_{-c/2}^{+c/2} \gamma_2(\xi',\alpha)(dz_c(x)/dx)dx \end{aligned}$$

(6.15)

from equations (6.6). Alternatively, by employing equations (6.11), equation (6.15) may be written in the form

$$\{\alpha^{(E)}/\alpha^{(w)}\}_{eq} = \int_{-c/2}^{+c/2} \gamma_E(\xi)dx \Big/ \int_{-c/2}^{+c/2} \gamma_w(\xi)\,dx. \qquad (6.16)$$

6.2 Thickness distributions

Time has not permitted a complete discussion of the effects of thickness even within the limitations of the linearized theory. Instead, what will be described here is an approximate linearized method of determining the lift and induced drag associated with thickness. This method is considered to be valid for 'thin' configurations of moderate or large $\mathcal{R}$.

The linearized form of the boundary conditions at the cylindrical surface of a thickness distribution, which satisfies the conditions stated at the beginning of Section 6, is as follows:

$$\left.\begin{aligned} v_{nf}(x,y,+\mathfrak{l}^{\pm}) &= \pm U_o dz_t(x)/dx; \quad v_{nf}(x,+b^{\pm}/2,z) = \pm U_o dy_t(x)/dx; \\ v_{nf}(x,-b^{\pm}/2,z) &= \mp U_o\, dy_t(x)/dx. \end{aligned}\right\} \qquad (6.17)$$

Here z_t and y_t are the (z and y) ordinates of the outside surfaces of the thickness distributions of the wing and starboard end plate when $\alpha^{(E)} = \alpha^{(w)} = 0$. Also the superscripts $\pm$ may be defined by reference to the following example: $+\mathfrak{l}^{\pm} = \underset{\varepsilon\to o}{\mathrm{Lim}}(+\mathfrak{l} \pm \varepsilon)$.

Robinson and Laurmann (1956) have investigated flows which satisfy boundary conditions such as equations (6.17). Their results indicate that both these equations and the condition of zero flow across the ground plane are satisfied by a source distribution of strength q given by

$$\left.\begin{aligned} q(x,y,\pm\mathfrak{l}) &= 2U_o\, dz_t(x)/dx; \quad |x| \le c/2, \quad |y| \le b/2; \\ q(x,\pm b/2,z) &= 2U_o\, dy_t(x)/dx; \quad |x| \le c/2, \quad |z| \le \mathfrak{l}. \end{aligned}\right\} \qquad (6.18)$$

The upper half of this distribution may be regarded as the 'physical' source distribution required to satisfy equations (6.17). The lower half, on the other hand, is the image distribution which ensures that there is no flow across the ground plane.

The normal velocity induced at the cylindrical surface by the source distribution may be written in explicit form. However, instead of employing this expression, which is rather complicated, the normal velocity at the wing plane will be calculated on the basis of the following assumptions:

(i) The flow induced by the sources of the image wing is two-dimensional in planes parallel to the plane y = 0.

(ii) The flow associated with the end-plate sources and their images is disregarded.

Therefore the normal velocity induced at the wing plane may be found by using a result given by Bagley (1960) for a distribution of two-dimensional sources along a line parallel to, and height ζ from, the ground. In the present notation this may be written in the form

$$v_{nf}(\xi, y, +\zeta) = \int_{-1}^{+1} \frac{q(\xi_1, y, \pm\zeta)}{2\pi} \frac{2\lambda \, d\xi_1}{(\xi-\xi_1)^2 + 4\lambda^2}. \qquad (6.19)$$

Thus, by comparing equations (6.18) and (6.19), it is found that

$$\frac{v_{nf}(\xi, y, +\zeta)}{U_o} = \frac{1}{\pi} \int_{-1}^{+1} \frac{dz_t(\xi_1)}{dx_1} \frac{2\lambda \, d\xi_1}{(\xi-\xi_1)^2 + 4\lambda^2}. \qquad (6.20)$$

This equation should yield a satisfactory approximation for $v_{nf}(\xi, y, +\zeta)$, if $\mathcal{R}$ is sufficiently large, except possibly in the vicinity of $|y| = b/2$.

Equation (6.20) implies that the source distribution introduces an effective incidence and camber into the flow at the wing plane. Therefore, to prevent the boundary conditions of the camber surface from being disturbed, the normal velocity induced at the wing plane by the source distribution must be nullified. This is accomplished

by a suitable vortex distribution placed on the cylindrical surface and the image vortex distribution required to satisfy the boundary condition of the ground plane. As before, the former distribution is assumed to be of the type $\gamma_t(\xi)f_t(\frac{y}{z})$, where subscript t denotes that the distribution is associated with thickness. Therefore, in view of the assumption that $\gamma_t(1) < \infty$, it is permissible to use equations (3.28) and (6.20) to obtain the result

$$-\int_{-c/2}^{+c/2} \gamma_t(\xi)\alpha dx = -\frac{1}{\pi}\int_{-c/2}^{+c/2} \gamma_2(\xi',\alpha)dx \int_{-1}^{+1} \frac{dz_t(\xi_1)}{dx_1} \frac{2\lambda\, d\xi_1}{(\xi-\xi_1)^2 + 4\lambda^2}. \qquad (6.21)$$

Equation (6.21) may be used in conjunction with a knowledge of $f_t(\frac{y}{z})$ to determine the overall lift associated with thickness. However, $f_t(\frac{y}{z})$ cannot be found without more detailed information being available on the normal velocity induced by the source distribution at the cylindrical surface. Thus it will be assumed that this normal velocity does not vary with s. Consequently it may be inferred from equations (3.28) and (5.1) that a configuration of zero thickness and zero chordwise camber with $f(\frac{y}{z}) = f_t(\frac{y}{z})$ will have $\alpha(s)$ = constant. This implies, therefore, that $f_t(\frac{y}{z}) = 1$.

It seems likely that for arbitrary $z_t(x)$ the right-hand side of equation (6.21) will be difficult to evaluate explicitly and will involve a double numerical integration. However, a simpler method for obtaining $\gamma_t(\xi)$ may be devised by noting that associated with this vortex distribution there is a camber surface yielding $\overline{D}_f = 0$. Therefore, in the manner used to obtain equation (5.34), it is possible to formulate an integral equation which ensures that this condition is satisfied. In fact, this equation differs from equation (5.34) only in the right-hand side which is, instead,

$$-4U_o(AR + \lambda)\int_{-1}^{+1} \frac{dz_t(\xi_1)}{dx_1} \frac{2\lambda\, d\xi_1}{(\xi-\xi_1)^2 + 4\lambda^2}$$

This will have to be evaluated numerically, in general. There is available, however, a convenient method for achieving this which has been given by Bagley. This enables one to replace the above term by the Gaussian sum

$$- 32\pi U_o(AR + \lambda) \sum_{\mu=1}^{N-1} \frac{\{(-1)^{\mu-\nu}-1\}(1-\xi_\mu^2)^{\frac{1}{2}}(\xi_\nu - \xi_\mu)\lambda}{N\{(\xi_\nu - \xi_\mu)^2 + 4\lambda^2\}^2} \left(\frac{z_t(\xi_\mu) - z_t(1)}{c}\right)$$

Bagley has suggested that a seven-point interpolation (N = 8) will probably be adequate, as the thickness-induced lift is usually a small part of the overall lift. Therefore this suggestion will be adopted here. Hence values of the right-hand side of the integral equation will be obtained for $\theta = n\pi/8$, with n = 1,2,3 ... . 7. In the manner of Section 5.3.1, this permits one to satisfy the integral equation at the points $\theta = n\pi/4$ (n = 1,3,5 and 7).

The implicit assumption that $f_t(\frac{y}{z}) = 1$ is equivalent to the assumption that the thickness does not affect the overall induced drag. However, it may not be concluded from this that the sectional drag associated with thickness is zero. Nevertheless, for configurations of sufficiently small thickness/chord ratio, this drag is likely to be small and probably may be ignored. Therefore the sectional drag of a configuration with thickness, incidence and camber is assumed identical with D_i.

Finally, it should be remarked that the effects of thickness and camber may be combined by replacing γ_w and γ_E in equations (6.12) and (6.16) by $\gamma_w + \gamma_t$ and $\gamma_E + \gamma_t$. Thus there is obtained

$$\bar{C}_{L(C.T.)} = 2\alpha\left[a^{(w)}\int_{-c/2}^{+c/2}\{\gamma_w(\xi) + \gamma_t(\xi)\}dx + a^{(E)}\int_{-c/2}^{+c/2}\{\gamma_E(\xi) + \gamma_t(\xi)\}dx\right] \Big/ \bar{C}_{L2}U_o c \tag{6.22}$$

and $$\{\alpha^{(E)}/\alpha^{(w)}\}_{eq} = \int_{-c/2}^{+c/2}\{\gamma_E(\xi) + \gamma_t(\xi)\}dx \Big/ \int_{-c/2}^{+c/2}\{\gamma_w(\xi) + \gamma_t(\xi)\}dx, \tag{6.23}$$

where $\bar{C}_{L(C.T.)}$ is the overall-lift coefficient associated with camber and thickness.

As the vortex distributions due to thickness, camber and incidence may be superposed, it follows that the same property applies to the overall-lift coefficients. Therefore, in allowing for the effects of thickness and camber on the overall-lift coefficient of a configuration with non-zero $\alpha^{(w)}$ and $\alpha^{(E)}$, it is permissible to replace equation (5.26) by the expression

$$\bar{C}_L = a^{(w)}(\alpha^{(w)} - \alpha_o^{(w)}) , \qquad (6.24)$$

where $$\alpha_o^{(w)} = -\{\bar{C}_{L(C.T.)} + a^{(E)}\alpha^{(E)}\}/a^{(w)} \qquad (6.25)$$

is the incidence of the wing corresponding to zero overall lift.

7. The influence of non-linearities

The exact potential-flow theory of de Haller (1936) for the lift coefficient of a two-dimensional flat plate in ground effect shows that, for 'small' plate heights, β varies rapidly with incidence. It is anticipated, therefore, that the present theory will not be accurate for small λ unless non-linear effects, such as that described, are included. This section describes an approximate method for accomplishing this aim.

Initially, in Section 7.1, consideration is given to configurations of zero chordwise camber and thickness. The theory developed for this case is then extended in Section 7.2 to configurations of 'small' chordwise camber and thickness.

7.1. Uncambered configurations of zero thickness

Consider the wing plane of a configuration having zero chordwise camber and thickness. By noting that according to the

linearized theory $C_L(y) = 2\Gamma(y)/U_o c$ and examining equations (2.44) and (2.53) one finds that the linearized theory of Section 5 yields the result

$$C_L^2(y)/C_T(y) = 2\pi\beta, \tag{7.1}$$

where β is invariant with y, $\alpha^{(w)}$ and $\alpha^{(E)}$. However, although, in practice, β may not vary with y, it will depend on $\alpha^{(w)}$ and possibly $\alpha^{(E)}$. Therefore equation (7.1) is replaced by

$$C_L^2(y)/C_T(y) = 2\pi\beta(\alpha^{(w)}, \alpha^{(E)}). \tag{7.2}$$

The indications of the linearized theory are that for the cases of interest the trailing vorticity is comparatively weak. It seems reasonable to suppose, therefore, that the effect on the overall lift of the departure of the trailing-vortex sheet from the assumed cylindrical shape is negligible. Thus the Trefftz-plane concept is retained and the implicit assumption of the theory of Section 5 that $D_f(y) = D_i(y)$ is employed. Hence, by resolving the sectional forces in the drag direction, it is found that

$$C_T(y) = C_N(y) \sin \alpha^{(w)} - C_{Di}(y), \tag{7.3}$$

where $C_N(y)$ is the coefficient of sectional force normal to the chord and $C_{Di}(y) = D_i(y)/\frac{1}{2}\rho U_o^2 c$.

An examination of the sectional forces in the lift direction gives the result

$$C_L(y) = C_N(y)\cos\alpha^{(w)} + C_T(y)\tan\alpha^{(w)}.$$

Therefore, by using this equation to eliminate $C_N(y)$ from equation (7.3), one obtains the expression

$$C_T(y)\sec^2\alpha^{(w)} = C_L(y)\tan\alpha^{(w)} - C_{Di}(y)$$

which for small $\alpha^{(w)}$ may be replaced by the approximate form

$$C_T(y) = C_L(v)\,\alpha^{(w)} - C_{Di}(y). \tag{7.4}$$

This is, in fact, the result employed in the linearized theory but, evidently, for $-10^{o} < \alpha^{(w)} < +10^{o}$ it produces unimportant errors in $C_T(y)$. This range of incidences is considered sufficiently large to justify the use of equation (7.4). Therefore this equation is combined with equation (7.2) to give the result

$$C_L(y) = 2\pi\beta(\alpha^{(w)},\alpha^{(E)})\{\alpha^{(w)} - C_{Di}(y)/C_L(y)\} . \qquad (7.5)$$

This should be compared with the corresponding result predicted by the linearized method of Section 5, namely

$$C_L(y) \equiv 2\Gamma(y)/U_o c = 2\pi\beta\{\alpha^{(w)} + w_\infty(y)/2U_o\} .$$

As noted before, the trailing vorticity of configurations of practical interest is weak. Consequently, in these cases, $C_{Di}(y) << C_L(y)\alpha^{(w)}$. Therefore it seems reasonable to assume that the error produced in $C_L(y)$ by replacing the term $C_{Di}(y)/C_L(y)$ in equation (7.5) with its linearized form, $-w_\infty(y)/2U_o$, is insignificant. Therefore equation (7.5) is rewritten in the form

$$C_L(y) = 2\pi\beta(\alpha^{(w)},\alpha^{(E)})\{\alpha^{(w)} + w_\infty(y)/2U_o\}. \qquad (7.6)$$

As the non-linear effects associated with changes in $\alpha^{(E)}$ are largely confined to a limited region adjacent to the end plates it seems reasonable to suppose that β is not very sensitive to $\alpha^{(E)}$. Therefore β is assumed invariant with $\alpha^{(E)}$.

That β varies with $\alpha^{(w)}$ would seem to be due in the main to the non-linear influences of the image spanwise vortices which in a non-linear theory are located at the mirror image of the wing chordal plane. These effects are twofold. Firstly, as $\alpha^{(w)}$ changes, the disposition of the image spanwise vortices relative to the wing is altered. In consequence, $\gamma(\xi)$ is modified, thus altering C_L and C_T. Secondly, if $\gamma(\xi)$ is positive, the image spanwise vortices contribute to a reduction in the x component of velocity at the wing. This produces, directly, a reduction in C_L and, indirectly, a change in $\gamma(\xi)$ necessary to satisfy the boundary conditions of the wing.

It is convenient to write $\beta = \beta(\alpha^{(w)})$ in the form

$$\beta(\alpha^{(w)}) = \beta(0) + \Delta\beta(\alpha^{(w)}),$$

where $\Delta\beta(\alpha^{(w)})$ is the increment in β due to the non-linear effects and $\beta(0) \equiv \beta(\alpha^{(w)} = 0)$ is the linearized-theory prediction of β.

The linearized theory is indicative that, for $AR > 1$, $\beta(0)$ varies slowly with AR. This may be attributed largely to the small effect that changes in AR have on the velocities induced at the wing by the spanwise vortices and their images. It is anticipated, therefore, that $\Delta\beta(\alpha^{(w)})$ also varies slowly with AR for $AR > 1$. Thus it is assumed that $\Delta\beta(\alpha^{(w)}, AR) = \Delta\beta(\alpha^{(w)},\infty)$. Consequently

$$\beta(\alpha^{(w)},AR) = \beta(0,AR) + \Delta\beta(\alpha^{(w)},\infty). \qquad (7.7)$$

This is equivalent to the assumption that $\Delta\beta(\alpha^{(w)})$ may be deduced from the exact two-dimensional theory of de Haller mentioned previously.

It seems likely that, if either $\Delta\beta(\alpha^{(w)})$ is small compared with $\beta(0)$ or AR is large, the errors in β resulting from the use of equation (7.7) should not be important. Therefore, if $\beta(\alpha^{(w)},\alpha^{(E)})$ is replaced in equation (7.6) by the right-hand side of equation (7.7), it is found that

$$C_L(y) = 2\pi\{\beta(0,AR) + \Delta\beta(\alpha^{(w)},\infty)\}\{\alpha^{(w)} + w_\infty(y)/2U_o\}. \qquad (7.8)$$

If, however, $\Delta\beta(\alpha^{(w)},\infty)$ is small compared with $\beta(0,AR)$ the term $2\pi\Delta\beta(\alpha^{(w)},\infty)w_\infty(y)/2U_o$, which is obtained by expanding equation (7.8), is very small compared with $C_L(y)$. Therefore, on the assumption that $\Delta\beta(\alpha^{(w)},\infty) \ll \beta(0,AR)$, this term is neglected so that

$$C_L(y) = 2\pi\beta(0,AR)\{\alpha^{(w)} + w_\infty(y)/2U_o\} + 2\pi\Delta\beta(\alpha^{(w)},\infty)\alpha^{(w)}. \qquad (7.9)$$

If $w_\infty(y)$ is assumed to be linearly dependent on $\alpha^{(w)}$ it is found that the term in equation (7.9) multiplied by $\beta(0,AR)$

represents the contribution of the linearized theory to $C_L(y)$. Therefore, by employing this assumption, it is evident from equations (5.26) and (7.9) that the overall-lift coefficient may be written as follows:

$$\bar{C}_L = \{a^{(w)} + 2\pi\Delta\beta(\alpha^{(w)},\infty)\}\alpha^{(w)} + a^{(E)}\alpha^{(E)}. \qquad (7.10)$$

It would seem that the error in $\bar{C}_L$ resulting from the use of the previously-mentioned assumption is not likely to be important.

7.2 Chordwise camber and thickness

The extension of the preceding analysis to include the non-linear effects of thickness and camber is extremely complicated. Consequently, instead, a result will be introduced for $\bar{C}_L$ which, although tentative, would seem to be a reasonable approximation for configurations of 'small' thickness and camber.

According to the linearized theory, for a given $\mathbb{R}$ and λ, an uncambered configuration of zero thickness yielding the same $\bar{C}_L$ as a configuration with incidence, thickness and camber (equation 6.24) has the wing incidence $\alpha^{(w)} - \alpha_o^{(w)}(\alpha^{(E)} = 0)$ and end-plate incidence $\alpha^{(E)}$. Also, as may be inferred from equation (5.2)(i), it has a C_L distribution given by

$$C_L(y) = 2\pi\beta\{\overset{\sim}{\alpha}^{(w)} + w_\infty(y)/2U_o\}, \qquad (7.11)$$

where

$$\overset{\sim}{\alpha}^{(w)} = \alpha^{(w)} - \alpha_o^{(w)}(\alpha^{(E)} = 0).$$

Therefore, on the basis of a comparison between equations (7.6), (7.10) and (7.11), it is suggested that a reasonable approximation for the $\bar{C}_L$ of a configuration of 'small' thickness and camber is

$$\bar{C}_L = \{a^{(w)} + 2\pi\Delta\beta(\overset{\sim}{\alpha}^{(w)},\infty)\}\overset{\sim}{\alpha}^{(w)} + a^{(E)}\alpha^{(E)}. \qquad (7.12)$$

In effect, equation (7.12) extends the notion of the equivalent configuration of zero thickness and camber to include non-linear

effects. That it is a fair approximation for 'small' thickness and camber follows from the fact that it agrees with equation (7.10) when $\alpha_o^{(w)}(\alpha^{(E)}=0)=0$. It should also be observed that it is asymptotically in agreement with equation (6.24) as $\alpha^{(w)}$ and $\alpha_o^{(w)}(\alpha^{(E)}=0)$ simultaneously tend to zero.

Although equation (7.12) makes allowance for the lift induced by the image thickness distribution it does not include the effect of the change in chordwise velocity induced at the wing by thickness. Thwaites (1960, p. 298) has shown that for isolated aerofoils in an inviscid flow this produces an increase in $a^{(w)}$. However, in reality, these aerofoils rarely have a value of $a^{(w)}$ in excess of that calculated on the assumption that the aerofoil is of zero thickness. The reason for this is that the thickness effect is counteracted by the displacement effect of the boundary layer. Indeed, a typical calculation quoted by Küchemann (1952) for an isolated R.A.E. 101 (10% thick) aerofoil with a chordal Reynolds number of approximately 10^6 indicates that the two effects cancel. Therefore, in the absence of calculations of these effects for two-dimensional wings near the ground, this will be assumed to be the case with the present configuration. In other words, for the purpose of comparison with experiment, equation (7.12) will be employed without modification.

The influence of the various non-linearities on the overall induced drag is difficult to predict. Nevertheless, it seems probable that for configurations of practical interest this component of the drag will be small compared with the overall boundary-layer drag. It is suggested, therefore, that the linearized value of σ should be employed for performance prediction.

The results obtained by the present theory will be compared with experiment in Chapter III. In the same chapter the validity of a number of the assumptions of this theory will be examined in the light of experimental evidence.

CHAPTER III

EXPERIMENTAL INVESTIGATION

1. Introduction

This chapter is concerned with a discussion of some experiments which have been performed on various G.E.W. configurations. These experiments were conducted in a wind tunnel and the image technique was used to simulate the presence of a water surface. This method, which replaces the water surface by a plane of symmetry ostensibly introduced into the flow by an image of the wing, may be criticized as follows:

(i) In practice, the water surface is not planar, even in absolutely calm conditions, owing to the pressure field of the wing which distorts the surface.

(ii) The combined influences of the velocity field of the wing, the dynamic condition at the water surface and the viscosities of the two fluids produce a vorticity layer in the vicinity of the water surface. This vorticity layer, which is not present with the image method, affects the flow round the wing.

Both these criticisms apply to the theories introduced previously. Therefore the image technique may be regarded as a method of checking the accuracy of the theories within the limitations of the assumptions leading to the criticisms. Consequently, if the theoretical results agree reasonably with the results of the image method, it might be worth while to extend the theories to include the effects described in (i) and (ii). On the other hand, if the results are not in agreement the reasons for the discrepancies may possibly be isolated more easily.

The image method has also been criticized periodically on the basis that the vorticity layers comprising the wakes of the models

interact and, in consequence, disturb the plane of symmetry. On the evidence of Werlé's(1963) flow-visualization studies, de Sievers (1965) remarked that this wake interaction does not destroy the symmetry of the flow. Nevertheless, during the course of the present experiments, this criticism was considered and the results of the investigation will be described in Section 2.3.2.

When consideration was first given to devising the experiments there were few examples of G.E.Ws. in existence. There had, however, been some experiments performed by Fink and Lastinger (1961) and Carter (1961). Unfortunately, these experiments were confined to open configurations and the end plates used were made of thin metal sheet. Therefore it is likely that the flow was not attached at the end-plate leading edges. This is an undesirable feature, for a large overall drag may be obtained if the end plates do not yield a leading-edge thrust. Moreover, agreement between the (inviscid) theory and experiment can only be expected if the flow is attached at the end plates. Therefore it was decided that, for the majority of the experiments, end plates of aerofoil section would be fitted to the basic planar wing.

Both open and closed configurations were examined in the present series of experiments, the main aim behind them being to test the accuracy of the theories introduced previously. However, particular emphasis was placed on the study of the closed configurations. There are two reasons for this. Firstly, the closed G.E.W. appears to offer the best prospects for future development by virtue of its low induced drag. Secondly, the theory in Part II of Chapter II is based on a number of assumptions which it was felt desirable to check by detailed experiments.

2. Experimental Technique

2.1 Models and rigging

The wing component of the various models tested was rectangular in planform, with a span, b, of 4 ft. and a chord, c, of 2 ft. It was untwisted and possessed an 11½% Clark Y section. Also, it was made from laminated mahogany which was finished on the exterior with 'Phenoglaze' and constructed round a 6 in. x 4 in. x 2 ft. duralumin bar. Bolted to the top of this bar at each of the mid semi-span stations and approximately 4½ in. and 7½ in. from the wing leading-edge were two lugs to which the support struts were attached. These struts passed from the lugs vertically upwards to the wind-tunnel balance.

Continuous incidence adjustment was provided by means of slots in the support struts through which the bolts securing the struts to the lugs passed. These slots were arranged so that the wing pivoted about an axis on the wing lower surface at a chordwise distance of 6 in. from the wing leading edge.

The support struts each comprised two parts which were bolted together. This permitted variations in the height of the wing relative to the 'ground plane' which was horizontal and coincident with the axis of the tunnel. The height was changed simply by undoing the nuts and bolts fastening the two parts of the struts and moving the lower parts of the struts to new positions. A sufficient number of holes was provided in the struts to ensure a total vertical movement of 6 in. at 1/4 in. intervals.

Strut drag was sensibly excluded from the drag measurements by means of fairings surrounding the struts. These fairings were constructed from mild-steel plate and had an approximately 20% R.A.E. 101 aerofoil section. Their geometry is illustrated in Fig. 32.

Pressure tappings were located at two spanwise stations of the wing, namely centre span and 0.3 in. from the port wing tip. At

each station there were 45 tappings, one of which was located at the leading edge and the remainder were divided equally between the upper and lower surfaces. The chordwise distances of these tappings from the leading edge as fractions of the chord ($\tilde{x}/c$) are shown in Fig. 33.

The static pressures were relayed from the tappings by copper tubes, which were inlaid in the wing, to the bases of the struts. There the copper tubes were joined to plastic tubes which passed up recesses in the sides of the struts to manometers outside the tunnel.

The image wing (or image) and its rigging were similar to that described except in the following respects: firstly, the strut-attachment lugs were situated 3 in. from each wing tip. Secondly, the tappings were located at 12 in. from the port wing tip (45 holes) and centre span (11 holes), the latter tappings providing a check on the symmetry of the flow about the wings. The chordwise positions of the former tappings were the same as those of the wing whilst the latter may be found in Fig. 33. There it will be seen that 6 of these were at the image position of the wing upper surface, which is called 'image upper surface', and 5 were situated at the 'image lower surface'.

Fig. 34 illustrates the geometry of the end plates and the method of attaching them to the wings. It shows that when each end plate was attached to the wing tip its base was in a plane perpendicular to the end-plate leading and trailing edges. In turn, these edges were, respectively, in the same planes as the leading and trailing edges of the wing. Furthermore, it indicates that each end plate was faired into the wing with a fairing of semi-elliptic cross section. This had a major to minor axis ratio of 2.

Also shown in Fig. 34 is the method by which the incidence of the end plates was increased, namely by additions to the wing which

in plan view were wedge shaped.

At the stations of the end plates corresponding to maximum chord (taken in a direction parallel to the end-plate base) the aerofoil section was constant and untwisted with ordinates

$$z_1 = 0.010c + (z_1 - z_2)_{c.y.}/2 \; ; \quad z_2 = 0.3\,(z_2)_{c.y.}.$$

Here z_1 and z_2 are the upper and lower boundary ordinates, the 'upper boundary' being on the outside of the configuration or image, and the subscripts c.y. refer to the ordinates of the 11½% Clark Y section at the corresponding chordwise position. At the other stations the ordinates of the sections, which were also untwisted, were the same as those at the corresponding chordwise positions of the full-chord sections.

A general view of the model and image when fitted with end plates is provided by Fig. 35. In the particular case illustrated, the end plates virtually closed the spanwise gaps between the wing and the 'ground' plane.

Finally, it should be remarked that, when the end plates were not fitted, half-body fairings were attached to the wing tips.

2.2 Methods of measurement

The experiments were performed in The College of Aeronautics 8 ft. x 6 ft. wind tunnel. This has a closed working section of octagonal cross section and is equipped with a Warden six-component balance.

The surface static-pressures of the two wings were measured by alcohol-filled manometers connected to the tubes from the tappings. Before beginning the experiments, this system was checked for blockage and leaks. During the course of this investigation it was found that the copper tube leading from the hole on the lower surface of the wing at centre span and $\tilde{x}/c = 0.5$ was blocked. Attempts to remove the blockage failed; therefore no readings of static pressure were taken from this hole.

The incidence of the wing and image was measured with a bubble inclinometer. In the case of the wing, this was mounted on a platform which was specially made to fit on the upper surface of the wing. The incidence of the image, on the other hand, was measured by placing the inclinometer on the substantially flat 'image lower surface'.

In certain experiments, to be described later, the sectional boundary-layer drag at the centre span of the wing was measured. This was achieved with a five-tube yaw/pitch meter which gave the total head directly and was calibrated in order to give static pressure. This device, which has been described by Alexander (1961), can normally be traversed vertically and horizontally. However, to reduce blockage and transverse interference at the model, the horizontal traverse was not employed.

2.3 Preliminary Experiments

2.3.1 Initial flow studies

The initial flow studies were designed to ascertain whether the flow over the wing was acceptable and were conducted without the image in position or with end plates. Throughout these studies, and indeed all the experiments to be described in this chapter, the wind-tunnel speed was a nominal 100 ft/sec. corresponding to $R_c = 1.3 \times 10^6$.

For the purpose of investigating the flow, a surface-flow indicator and wool/nylon tufts, attached to the wing surface, were used. The indicator consisted of a mixture of 'Polyfilla', water and 'Teepol'.

During these tests the strut fairings terminated 1 in. above the upper surface of the wing and the unfaired portions of the struts were streamlined with 'Plastiscine'. Flow-visualization tests showed that in this case there were large turbulent wakes

being shed from the struts. These wakes were considered unacceptable. Thus it was decided to extend the fairings as near as possible to the wing surface. This was achieved by means of additional fairings made from copper sheet which reduced the gap between the base of the fairings and the wing to 0.02 in. The extra fairings were constructed in a manner so as to permit ready access to the incidence adjustment of the wing.

Subsequently, it was found that the width of the wakes behind the fairings was greatly reduced by the presence of the fairing extensions.

Another fact to emerge from this study is that there was no obvious boundary-layer separation near the leading edge of the wing in the incidence range 0° to 14°. To some extent this is confirmed by the pressure distributions measured at centre span and shown in Fig. 36*. On the other hand, in the case $\alpha^{(w)} = 11^{\circ}$, there is apparently a curious bulge in the pressure distribution of the upper surface. At first, it was thought that this might be due to a laminar-separation bubble. However, a similar bulge is evident in the inviscid distribution of a two-dimensional Clark Y aerofoil calculated by Karman and Burgers (1935) for the case $\alpha^{(w)} \simeq 9^{\circ}$. It seems likely, therefore, that this bulge is directly associated with the shape of the Clark Y section.

Balance measurements of the overall forces on the wing were made with the purpose of checking the conclusions of the flow studies. It became apparent from these results that there were

---

* In this figure the results are plotted in the form $C_{PT} = p - p_o/\frac{1}{2}\rho U_{oT}^2$ against $\tilde{x}/c$, where p and p_o are, respectively, the surface and tunnel static pressure whilst the subscript T denotes quantities uncorrected for tunnel interference.

day-to-day variations in the overall forces on the wing. It was thought that this might be due to alterations in the position of the transition region of the boundary layer on the upper surface of the wing. Therefore it was decided to fix the transition there by placing a trip wire along the span at a chordwise distance of $\frac{1}{4}$ in. from the leading edge. The diameter of this wire was decided by a criterion given by Pankhurst and Holder (1948, p. 463), namely

$$U_o d/\nu > 60,$$

where d is the diameter of the wire and ν is the kinematic viscosity. This criterion dictates the minimum diameter of wire needed to 'trip' the boundary layer. Thus with the values U_o = 100 ft./sec. and $\nu = 1.56 \times 10^{-4}$ ft.^{2}/sec., which are typical of the present experiments, this yields d > 0.011 in. Therefore the diameter 0.012 in. was chosen for the wire.

Wires of the same diameter and chordwise location were also placed on the 'image upper surface' and on the outside surfaces of the end plates.

2.3.2 Investigation into the validity of the image method

The aim of the experiments to be described here was to examine the validity of the image technique as a means of representing a steady plane of symmetry. In the first part of these experiments the symmetry of the flow over the wing and the image was investigated by comparing the pressure distributions of the two wings at centre span. Throughout this study the height of the pivotal axis of the wing above the 'ground' plane, h_p, was kept constant at 3 in. and end plates were not fitted.

The pressure distributions obtained for $\alpha^{(w)} = 2^o$, 5^o and 8^o are illustrated in Figs. 37, 38 and 39 which show plots of C_{PT} against $\tilde{x}/c$. It will be seen that in each case the two sets of results are almost indistinguishable except at $\tilde{x} = 0.042$ c on the

suction surfaces. Here the image consistently yielded a slightly larger negative C_{PT}. A possible explanation for this is that the interference of the wing strut fairings at the wing centre span was greater than that of the image strut fairings at the centre span of the image. This is plausible because the wing strut fairings were nearer centre span than the image strut fairings. Furthermore, it was found that the difference in pressure between the image and wing at $\tilde{x}$ = 0.042c could be altered by modifying the bases of the wing strut fairings. However, even if this conjecture is not correct, the effect of the discrepancy on the overall forces seems not to be important.

The second part of this investigation comprised an examination of the importance of the wake-interaction effect mentioned in Section 1. This phenomenon appears to consist of two effects. Firstly, the vorticity in the wakes of the wing and the image interacts to produce unsteadiness in the flow behind the wings. Secondly, the wakes mix owing to the action of turbulent mixing. Neither of these effects would occur with a wing in motion over a water surface. However, they may be removed in the present case by splitting the wakes with a thin plate placed along the horizontal plane of symmetry. Thus, on the assumption that the plate does not cause any flow interference, it may be argued that, if there is no difference in the overall forces on the wing with and without the splitter plate, the wake-interaction effect may be ignored. This, therefore, was the approach adopted.

The splitter plate employed was of 10 gauge aluminium alloy of 4 ft. chord and 4½ ft. span mounted on angles which were supported by struts from the tunnel floor. Additional stiffness was given to the plate by means of wire braces between the angles and the sides of the tunnel.

The incidence of the plate was adjusted to a nominal zero by using an inclinometer, an incidence tolerance of $\pm$ 3 minutes being applied to the readings.

During the tests, the splitter plate was placed with its leading edge in the plane of the trailing edges of the wing and the image. Furthermore, to avoid some form of interaction between the trailing vortices of the image and the support struts of the plate, the configurations chosen possessed comparatively weak trailing vorticity. One such configuration had h_p = 2 in., $\alpha^{(w)} = 8^o$ and end plates giving a constant gap of 0.025 in. between the bases of the end plates and the 'ground'. The results obtained in this case for $\overline{C}_{LT}$ and $\overline{C}_{DT}$ (which are based on the planform area of the wing, 8 ft^2) are as follows:

	WITH SPLITTER	WITHOUT SPLITTER
$\overline{C}_{LT}$	1.58	1.58
$\overline{C}_{DT}$	0.0274	0.0276

Evidently, there is no significant change in the overall forces resulting from placing the splitter plate in the tunnel. It is possible, however, that the wake-interaction effect was masked by the interference caused by the splitter and its supports. Nevertheless, calculations of this interference have indicated that its effect on the overall forces is negligible.

Another case examined was the configuration with h_p = 5 in., $\alpha^{(w)} = 12.5^o$ and end plates with l_p = 4" and $\gamma = 6^o$, where l_p and γ are defined in Fig. 34. The results obtained are as follows:

	WITH SPLITTER	WITHOUT SPLITTER
$\overline{C}_{LT}$	1.50	1.50
$\overline{C}_{DT}$	0.0972	0.0984

Again no significant differences between the overall forces with and without the splitter plate are apparent.

Both the cases cited are extreme insofar as the spanwise component of vorticity in the wake of either configuration is considered comparatively large and no smaller than that of any configuration tested. It is anticipated, therefore, that the wake-interaction effect may be ignored for the present configurations, at least. On this basis, the splitter plate, which made model rigging difficult, was not employed in the remainder of the experiments.

In the course of the investigation into the validity of the image method the rigidity of the model and its supports was examined. This was done with a Taylor-Hobson microalignment telescope which was sighted onto a point on the trailing edge of the wing before and after a run. For this test, which was performed with h_p = 5 in. and no end plates, the wing and the image were set at their maximum incidence (approximately 14°).

No change in the position of the point could be detected as the tunnel speed was increased from 0 to 100 ft/sec. The same was found to be true of a similar point on the image.

2.3.3 Determination of strut-fairing interference

Calculations performed with the aid of information given by Hoerner (1951, p 113) indicate that the strut-fairing interference on the overall forces of the wing may be significant in some cases. Unfortunately, Hoerner's results, which are taken from various experiments, are not sufficiently comprehensive. Therefore it was considered desirable to determine the strut-fairing interference experimentally.

It was considered impracticable to establish the fairing-interference corrections for all combinations of h_p, $\alpha^{(w)}$ and tip configurations. Consequently h_p was kept constant at 4 in. and end plates were fitted so that for the three incidences examined, $\alpha^{(w)} = 2^\circ$, 5° and 8°, there was a constant chordwise

gap of 0.01 in. between the bases of the end plates and the ground. At each of these incidences two end-plate wedge angles were tested, namely 0° and 9°.

The method of determining the strut-fairing interference was to measure the influence of a dummy fairing on the overall forces of the wing. This fairing was situated above the wing at centre span at the same chordwise position as the other fairings which it resembled in all respects. The gap at its base could be varied and the results for the overall forces were extrapolated to zero gap. The corresponding increments in the overall lift and drag coefficients due to the dummy fairing, $-(\Delta\overline{C}_L)_F = -\Delta\overline{L}_F/\frac{1}{2}\rho U_{oT}^2 bc$ and $-(\overline{C}_D)_F = \Delta\overline{D}_F/\frac{1}{2}\rho U_{oT}^2 bc$, are plotted against the sectional-lift coefficient at centre span (without the dummy fairing) in Figs. 40 and 41. This coefficient was obtained by integrating the pressure distributions in a manner to be described in Section 2.4.4.

The results for the increments appear to correlate reasonably with C_L. Therefore it is assumed that the curve through these results may be used to correct $\overline{C}_{LT}$ and $\overline{C}_{DT}$ for other configurations provided that (a) R_c is the same and (b) the sectional-lift coefficients at the spanwise stations of the real strut fairings are used in reading off Figs. 40 and 41. Further, it is assumed that the total fairing-interference correction may be found by doubling the correction of one fairing. This appears to be a reasonable assumption as the horizontal distance between the strut fairings is large compared with their chord.

Finally, mention should be made of the correction applied to the overall-drag coefficient to allow for the gaps between the bases of the strut fairings and the wing. Although these gaps were small compared with c, it was thought that the extra drag involved might be significant owing to the rather bluff shape of the struts. Tests on the above-mentioned configurations supported

this view by indicating that as the gaps were reduced the overall drag of the wing dropped noticeably. The results of these tests were used to obtain the correction for the gap on the overall forces. It was found that the lift correction was insignificant but as is shown in Fig. 42 the correction to the overall-drag coefficient $(\Delta\bar{C}_D)_G = \Delta\bar{D}_G/\frac{1}{2}\rho U_{oT}^2 bc$ cannot be ignored. In this figure $(\Delta\bar{C}_D)_G$ is plotted against $\bar{C}_{LT}$ and the correlation is seen to be reasonable. This graph has been employed to correct the overall-drag coefficients of all the cases examined.

2.4 Reduction of Observations

2.4.1 Blockage corrections

Consider, firstly, the blockage associated with the wing and the image. This will include contributions arising from the two wings, their boundary layers and wakes. However, it would appear from the discussion of Pankhurst and Holder (1952, p.p. 330-348) that the boundary-layer blockage is usually neglected. Therefore this leaves the solid blockage of the wings and their wake blockage.

In general, the distance between the wing and the image is small compared with the height of the tunnel working section. Therefore, for the purpose of calculating the solid blockage, it seems reasonable to replace the two wings by a single wing of twice the thickness and volume of the wing and mounted at the tunnel axis. Thus it is possible to use a result given by Pankhurst and Holder (p. 343) for the increment in axial speed due to the solid blockage (Δu_s) of an axially-mounted wing, namely

$$\Delta u_s = (\pi/4)\ \tau\ U_{oT}(1 + 1.2\ t/c)V/C^{3/2}. \qquad (2.1)$$

Here τ is a dimensionless constant depending on the cross-sectional shape of the working section and C is the cross-sectional area of the working section.

The quantities t/c and V are the thickness/chord ratio and the volume of the equivalent single wing.

An inspection of a table given by Pankhurst and Holder (p. 341) suggests that a reasonable value of τ for the 8 ft. x 6 ft. tunnel is 0.8. By employing this value together with t/c = 0.24, V = 2.28 ft.^{3} and C = 46.4 ft.^{2} in equation (2.1) it is found that

$$\Delta u_s = 0.0066\ U_{oT}$$

Pankhurst and Holder give a result for the increment in axial speed due to the wake blockage (Δu_w) of an axially-mounted wing in a closed rectangular tunnel. This may be written in the form

$$\Delta u_w = \overline{D}_{BT}/2\rho U_{oT} C, \qquad (2.2)$$

where $\overline{D}_B$ is the boundary-layer drag of the wing.

As before, it is assumed that the two wings may be treated as a single axially-mounted wing. Furthermore, it is assumed that equation (2.2) also applies to the cross section of the present working section which is nearly rectangular. Therefore, with the typical value for the equivalent wing $\overline{D}_{BT}/\frac{1}{2}\rho U_{oT}^2 = 0.192$ ft.^{2}, equation (2.2) may be employed to give for the velocity increment

$$\Delta u_w = 0.0010\ U_{oT}$$

The blockage caused by the end plates or the half-body fairings is ignored on the basis that the extra volume and boundary-layer drag thereby introduced is comparatively small. On the other hand, consideration will be given to the blockage caused by the strut fairings. With regard to the blockage of the wing strut-fairings this is accounted for by the interference correction discussed in Section 2.3.3. Therefore it is only necessary to correct for the blockage of the image strut-fairings. In determining this correction, use is made of the fact that the flow round the image strut-fairings has a vertical plane of symmetry at the centre span of the wings. Consequently only the flow in either the port or starboard halves of the tunnel need be considered. Furthermore, use may be made of the fact that the tunnel floor represents part of a plane of symmetry

of the flow about the image strut-fairings.

As with the wings it is permissible to employ equation (2.1) to determine the correction for the image strut-fairings. It should be noted, however, that this correction applies strictly to the longitudinal velocity at these fairings. Nevertheless, the errors obtained by assuming that this is the same as the correction required at the wing are likely to be insignificant.

It is possible to deduce from results given by Pankhurst and Holder that for this case $\tau \simeq 1.2$. Thus, by employing equation (2.1) with the appropriate values $\tau = 1.2$, $t/c = 0.20$, $V = 0.376$ ft.^{3} and $C = 46.4$ ft.^{2}, it is found that the solid-blockage correction due to the image strut fairings is

$$\Delta u_s = 0.0016\ U_{oT}$$

Finally, it should be remarked that the wake blockage of the image strut fairings is negligible and is therefore ignored. Thus the total increase in axial velocity at the wing due to blockage is found by adding together the separate contributions given previously. The corrected tunnel speed is then obtained and the overall-force coefficients are corrected accordingly.

2.4.2 Lift-effect corrections

In determining the lift-effect corrections it is assumed that it is permissible to employ the linearized theory. As these corrections are generally small it is supposed that the errors thus caused in the overall forces on the wing will not be important.

Suppose that the wing under consideration has zero chordwise camber and thickness. By making the assumption that $\gamma(x,y) \equiv \gamma(x)\ f(2y/b)$, it is found from Section II.3.1 that

$$\Gamma(y) = \pi(\beta_F + \Delta\beta)c\left[U_o \alpha^{(w)}(y) + \{[w_\infty(y)]_F + \Delta w_\infty(y)\}/2\right] \qquad (2.3)$$

Here the subscript F refers to unconstrained quantities whilst $\Delta\beta$ and $\Delta w_\infty(y)$ are increments in β and $w_\infty(y)$ due to the lift effect.

A qualitative study of the induced-velocity field of the image system required to satisfy the boundary condition of zero flow across the tunnel walls indicates that, for the various values of h_p/c examined, $\Delta\beta << \beta_F$. Therefore $\Delta\beta$ is ignored in equation (2.3). Consequently the lift effect may be regarded as an increase in the 'effective incidence' of the wing at any station y by an amount

$$\Delta\alpha^{(w)}(y) = \Delta w_\infty(y)/2U_o$$

As this is small compared with $\alpha^{(w)}(y)$ it is assumed that $\Delta\alpha^{(w)}(y)$ may be replaced by its mean value across the wing span, $\Delta\bar{\alpha}^{(w)}$. According to Pankhurst and Holder this may be written in the form

$$\Delta\bar{\alpha}^{(w)} = \bar{\delta}bc\bar{C}_L/C, \qquad (2.4)$$

where $\bar{\delta}$ is a factor depending on the cross-sectional shape of the working section, the ratio of the wing span to tunnel breadth and the spanwise lift distribution. Also it should be noted that $\bar{C}_L$ is corrected for blockage. Thus, for the case of a wing of zero twist, the $\bar{C}_L/\alpha^{(w)}$ curve is corrected simply by displacing it an amount $\Delta\bar{\alpha}^{(w)}$ in the direction of $\alpha^{(w)}$.

Owing to the increase in the effective incidence of the wing due to the lift effect the induced drag is reduced for a given lift. Thus provided that $\Gamma(y)$ and $\Delta\alpha^{(w)}(y)$ are slowly varying functions the unconstrained induced-drag coefficient may be written as

$$\bar{C}_{DiF} = \bar{C}_{DiT} + \Delta\bar{\alpha}^{(w)}\bar{C}_L,$$
$$= \bar{C}_{DiT} + \bar{\delta}bc\bar{C}_L^2/C$$

from equation (2.4).

The factor $\bar{\delta}$ has been determined for planar wings near a ground plane in a working section of rectangular cross section by Brown (1938). In his calculations he assumed a uniform

spanwise distribution of lift but this assumption should not cause any significant errors.

On the assumption that the effect of the corner fillets of the 8 ft. x 6 ft. tunnel may be ignored the following values have been deduced from Brown's results:

$2h_p/b$	$\bar{\delta}$	$\Delta\bar{\alpha}^{(w)^\circ}/\bar{C}_L$	$(\bar{C}_{DiF} - \bar{C}_{DiT}) / \bar{C}_L^2$
0.083	0.0022	0.022	0.00038
0.125	0.0050	0.050	0.00086
0.167	0.0086	0.085	0.00148
0.208	0.0124	0.123	0.00214
0.250	0.0194	0.192	0.00334

Within the limitations of the linearized theory the above results also apply to configurations with chordwise camber and thickness. Thus they have been used to correct the overall-force results for the planar configurations.

The corrections for the non-planar configurations have been obtained by employing the above tabulation with h_p replaced by $h_p - l_p$.

2.4.3 Circulation and sectional-lift measurements

In the course of the experiments on the closed configurations, measurements were made of the static pressures at various stations. These results were used to calculate the circulation and sectional-lift distributions. The method employed in these calculations and the theory on which the circulation calculations are based are described in this section.

Consider a chordwise section of the configuration. By reference to the sketch below and a result given by Goldstein (1938, p. 119) it is possible to write the component of vorticity normal to the plane of the section as

$$\eta = \frac{\kappa}{1 + \kappa\bar{z}}\bar{u} + \frac{\partial\bar{u}}{\partial\bar{z}} - \frac{1}{1 + \kappa\bar{z}}\frac{\partial\bar{w}}{\partial\bar{x}} . \qquad (2.5)$$

Here η, the vorticity component, is taken positive in the clockwise sense whilst $\bar{x}$ and $\bar{z}$ are distances along and normal to the aerofoil boundary which is of curvature κ. Parallel to $\bar{x}$ and $\bar{z}$ are the flow velocity components $\bar{u}$ and $\bar{w}$.

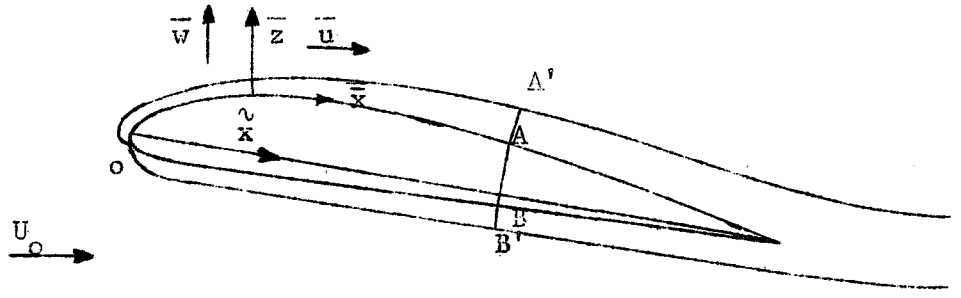

The sketch shows a line which is normal to the chord line at a chordwise distance $\tilde{x}$ from the leading edge and intersects the section contour at A and B. From these points are extended lines normal to the section contour which cross the edge of the boundary layer at A' and B'. Thus the circulation $\Gamma(\tilde{x})$ is defined as the sum of the circulations of all the elementary vortices upstream of A'ABB', being taken positive in the clockwise (lifting) sense. Hence, by employing equation (2.5), it is found that

$$\Gamma(\tilde{x}) = \int_B^A \int_o^\delta \left\{\frac{\kappa}{1 + \kappa\bar{z}}\bar{u} + \frac{\partial\bar{u}}{\partial\bar{z}} - \frac{1}{1 + \kappa\bar{z}}\frac{\partial\bar{w}}{\partial\bar{x}}\right\}(1 + \kappa\bar{z})d\bar{x}\, d\bar{z}, \qquad (2.6)$$

where δ is the thickness of the boundary layer along the direction of $\bar{z}$. Therefore, by noting the condition of no slip at the section boundary, equation (2.6) may be rewritten as follows:

$$\Gamma(\tilde{x}) = \int_B^A (1 + \kappa\delta)\bar{U}d\bar{x} - \int_B^A \int_o^\delta (\partial\bar{w}/\partial\bar{x})d\bar{x}\, d\bar{z}, \qquad (2.7)$$

where

$$\bar{U} = \bar{u}(\bar{z} = \delta).$$

An examination of the order of magnitude of the last term of equation (2.7) indicates that it is $O\{(\delta/c)^2\}$ compared with $\Gamma(\tilde{x})$. This may be considered insignificant for $R_c \simeq 10^6$ provided that the boundary layer is attached. Therefore this term is ignored to give the result

$$\Gamma(\tilde{x}) = \int_B^A (1 + \kappa\delta)\bar{U}\, d\bar{x} \tag{2.8}$$

At the stations of the configuration where static-pressure measurements were made, the curvature at the section boundary was confined to the chordwise direction. Therefore, according to the boundary-layer approximation, the pressure gradient across the layer at these stations is given by

$$\partial p/\partial \bar{z} = \kappa\rho\bar{u}^2 \tag{2.9}$$

(Rosenhead, 1963, p. 203). Thus the rise in static pressure across the layer, Δp, may be obtained by integrating equation (2.9) as follows:

$$\Delta p = \kappa\rho \int_0^\delta \bar{u}^2\, d\bar{z},$$

$$= \kappa\rho\bar{U}^2\{\delta - \delta_1 - \delta_2\}, \tag{2.10}$$

where δ_1 and δ_2 are the displacement and momentum thicknesses of the boundary layer.

By application of Bernoulli's theorem to the inviscid flow external to the boundary layer it is found that

$$\bar{U}/U_o = \pm(1 - C_p - 2\Delta p/\rho U_o^2 - \bar{v}^2/U_o^2)^{\frac{1}{2}}, \tag{2.11}$$

where $\bar{v}$ is the velocity of the flow, normal to the plane of the section, at the edge of the boundary layer whilst C_p is the surface static-pressure coefficient. The choice of root taken in this expression depends on the position of station $\bar{x}$ in relation to O, at which point $\bar{U} = 0$. Thus if $\bar{x}_o$ is the $\bar{x}$-wise station of O the positive root is taken if $\bar{x} - \bar{x}_o > 0$ whilst if $\bar{x} - \bar{x}_o < 0$ the negative root is employed.

If $|2\Delta p/\rho U_o^2 + \overline{v}^2/U_o^2| < |1 - C_p|$ the right-hand side of equation (2.11) may be expanded and the resultant expression combined with equations (2.8) and (2.10) to yield the result

$$\Gamma(\tilde{x}) = \int_B^A \{1 + \kappa(\delta_1+\delta_2) - \overline{v}^2/2\overline{U}^2 + O(\kappa^2\delta^2) + O(\overline{v}^4/\overline{U}^4)\}(\pm)U_o(1-C_p)^{\frac{1}{2}}dx \tag{2.12}$$

Calculations have indicated that for $R_c \simeq 10^6$ and for the closed configurations examined $\kappa(\delta_1+\delta_2)$ is negligible. Furthermore, yaw surveys with the five-tube meter have shown that $\overline{v}^2/2\overline{U}^2$ is extremely small. Therefore equation (2.12) is replaced by

$$\Gamma(\tilde{x}) = \int_B^A (\pm)U_o(1 - C_p)^{\frac{1}{2}}d\overline{x}$$

This was evaluated numerically according to Simpson's one-third rule, the number of interpolation points depending on $\tilde{x}$. Thus for example, 59 points were used in the determination of $\Gamma(c)$.

At each station, there was a point where C_p was between 0.99 and 1. It is evident from equation (2.11) that at these points $\overline{U}$ must have been very close to zero. Therefore these were regarded as being coincident with the point O at each station.

The sectional lift was found by integrating the liftwise component of the pressure forces round each section. As before, Simpson's rule was employed with a 59 - point interpolation.

In all cases the static pressures were corrected for blockage by using the results of Section 2.4.1.

2.4.4 Measurements of boundary-layer drag

For the purpose of an analysis of the drag of closed configurations to be described in Section 4.3, boundary-layer-drag surveys were made in the rear of the wing centre span. This was done on the assumption that the flow in the streamwise plane of this station was two-dimensional.

Total head and static-pressure readings were taken at intervals of 1/8 in. through the wake by means of the five-tube yaw/pitch meter situated 0.7c downstream of the wing. These results were used in conjunction with the method of Young (1948) to determine the sectional boundary-layer drag at the wing centre span. This technique is based on the method proposed by Jones (1936).

The required integration of the total-head deficit across the wake was performed by using Simpson's rule, the interpolating points corresponding to the points where the readings were taken.

2.4.5. Accuracy of the results

Throughout this chapter all overall-force coefficients will be based on the planform area of the basic wing, $bc = 8\ ft^2$. Thus, with $U_{oT} = 100$ ft./sec., it is found that the r.m.s. scatter of the coefficients of overall lift, drag and side force $\overline{C}_L$, $\overline{C}_D$ and $\overline{C}_S$ is as follows:

$$\overline{C}_L = \pm 0.002; \qquad \overline{C}_D = \pm 0.0003; \qquad \overline{C}_S = \pm 0.002.$$

The estimated scatter of the circulation, sectional-lift coefficient and sectional coefficient of boundary-layer drag (C_{DB}) is:

$$\Gamma(\tilde{x})/U_o c = \pm 0.005; \quad C_L = \pm 0.003; \quad C_{DB} = \pm 0.0002.$$

Incidence was measured with an accuracy of ± 3 minutes.

3. Lift and drag of open configurations : comparison with theory

In this section the results obtained for the overall forces on various open configurations are discussed. In Section 3.1 the configurations considered are substantially planar, that is wings without end plates, whilst in Section 3.2 the effect of non-planar additions in the form of end plates is discussed.

3.1 Planar configurations

3.1.1 Overall lift

Curves of $\bar{C}_L$ against $\alpha^{(w)}$ for various h_p/c are shown in Fig. 43 for the planar configuration. It will be seen that for the two lowest values of h_p/c the gradient $\partial\bar{C}_L/\partial\alpha^{(w)}$ increases with increasing $\alpha^{(w)}$. This is opposite to the trend exhibited by a number of two-dimensional theories including that of de Haller (1936). It seems likely, therefore, that the present behaviour of the lift curve is associated with the three-dimensional nature of the flow about the wing. Support for this belief comes from the fact that similar trends have been found with the lift curves of isolated planar wings of small aspect ratio. Küchemann (1952) has shown that this is due to non-planar vortex sheets leaving the side edges of the wings. Such vortex sheets were also observed in the present case by means of a tuft grid placed behind the two wings. However, this is not the only significant non-linearity, for with the three largest values of h_p/c the trend of $\partial\bar{C}_L/\partial\alpha^{(w)}$ with $\alpha^{(w)}$ is opposite to that mentioned.

The slope $\left[\partial\bar{C}_L/\partial\alpha^{(w)}\right]_{\alpha^{(w)}=0}$ is plotted against $h_t(\alpha^{(w)} = 0)/c$ (where $h_t(\alpha^{(w)})$ is the height of the wing trailing edge above the 'ground') in Fig. 44. Also plotted in this figure for comparison is the theoretical curve given by Saunders (1963) who computed his results on the basis of the linearized, inviscid theory. Evidently, the agreement between theory and experiment is good. Saunders' results for $\left[\partial\bar{C}_L/\partial\alpha^{(w)}\right]_{\alpha^{(w)}=0}$ have also exhibited good agreement with the experimental results of Fink and Lastinger (1961) and Carter (1961). This may seem surprising considering that Saunders did not correct his results for aerofoil thickness and boundary-layer displacement. On the other hand, it is known that for a number of conventional aerofoils out of ground effect these

effects almost cancel. Whether this is the case for wings near the ground has yet to be demonstrated but it seems to be the most plausible reason for the good agreement between Saunders' theory and experiment.

Unfortunately, a simple theoretical method for calculating the zero-lift incidence of open configurations seemsnot to be available. However,the present experimental results suggest that this incidence increases positively as h_p/c decreases.

3.1.2 Overall drag

Experimental results for the overall-drag coefficient, $\bar{C}_D$, of the planar configuration are plotted against $\bar{C}_L$ in Figs. 45, 46, 47 and 48 for h_p/c = 0.250, 0.167, 0.125 and 0.083. Also shown in each of these figures are two curves representing two interpretations of the linearized theory for minimum induced drag introduced in Section I.2. The first interpretation, which will be referred to as theory A, employs the assumption that the bound and trailing vortices occupy a plane which is everywhere at the same height, $h_t(\alpha^{(w)} = 0)$, above the ground. The second interpretation or theory B, on the other hand, is based on the supposition that the trailing vortices are in a plane parallel to, and height $h_t(\alpha^{(w)})$ above, the ground. Both interpretations use the assumption that the span of the vortex trace is everywhere the same as the span of the wing.

Theory A may be regarded as a consistent linearized theory whilst theory B represents an attempt to include the non-linearity associated with the reduction in the height of the trailing vortices with increasing $\alpha^{(w)}$. The latter interpretation is plotted on the same basis as the experimental results by using the experimental $\bar{C}_L/\alpha^{(w)}$ curves to determine $h_t(\alpha^{(w)})$ for a given $\bar{C}_L$ and h_p. It may be thought that this introduces an empirical

element into the theory. However, the results could equally be compared with h_t fixed. In this case it would be necessary only to correct the experimental results.

Comparison between the theory and experiment is facilitated by the assumption that

$$\overline{C}_{DB}(\overline{C}_L) = \overline{C}_{DB}(0) + \Lambda\overline{C}_L^2, \tag{3.1}$$

where $\overline{C}_{DB}$ is the coefficient of the overall boundary-layer drag and Λ is independent of $\overline{C}_L$. That this is a reasonable assumption is supported by the results of wake surveys which were made at the centre span of the wing when end plates were fitted. These surveys, which will be described in Section 4.3, indicate that for $h_p/c = 0.167$ a reasonable value of Λ is 0.0027. This value, it will be assumed, applies for all the values of h_p/c considered.

The overall-drag coefficient is given by

$$\overline{C}_D = \overline{C}_{DB} + \overline{C}_{Di}$$

This expression may be rewritten, by reference to equations (I.2.33) and (3.1), as follows:

$$\overline{C}_D(\overline{C}_L) = \overline{C}_{DB}(0) + (\Lambda + \sigma/\pi AR)\overline{C}_L^2 \tag{3.2}$$

The quantity $\overline{C}_{DB}(0)$ is obtained by noting from equation (3.2) that $\overline{C}_{DB}(0) = \overline{C}_D(0)$. Therefore, by plotting the experimental results for $\overline{C}_D$ against $\overline{C}_L^2$ and extrapolating the curves to $\overline{C}_L = 0$, it is found that $\overline{C}_{DB}(0) = 0.01$ regardless of h_p/c. Hence equation (3.2) is rewritten as

$$\overline{C}_D(\overline{C}_L) = 0.01 + (0.0027 + \sigma/\pi AR)\,\overline{C}_L^{\,2} \tag{3.3}$$

Thus, by substituting the theoretical values of σ into this equation and comparing the results with the experimental results, it is possible to assess the accuracy of the induced drag predicted by theories A and B.

Inspection of Figs. 45, 46, 47 and 48 shows that theory A is in better agreement with experiment than theory B, the latter theory generally underestimating $\bar{C}_{Di}$. This is somewhat surprising as it is not unreasonable to suppose that B gives a better approximation for the height of the wing trailing vortices above the ground than A. However, tuft-grid surveys revealed that this is not the case owing to non-planar vortex sheets which were being shed from the side edges of the wing. These evidently increase the mean height of the trailing vortices above the ground and, in consequence, increase the overall induced drag. In particular, for the case $h_t = 0$, theory B agrees with the exact potential - flow solution, based on the assumption that the flow at the side edges is attached, in predicting that $\bar{C}_{Di} = 0$. However, as a direct result of the vortex sheets shed from the side edges, $\bar{C}_{Di}$ is quite large in practice, a fact which is in evidence in Fig. 47.

As may be inferred from Figs. 45, 46, 47 and 48 the slopes $\left[\partial \bar{C}_{Di}/\partial \bar{C}_L^2\right]_{\bar{C}_L = 0}$ predicted by theories A and B are in good agreement with experiment. In fact, to an accuracy of two significant figures they are identical. This would seem to support the assertion that the induced drag of the wing is near the minimum, at least for sufficiently small $\bar{C}_L$. This was expected, however, because (a) the low-aspect-ratio approximation of the linearized lifting-surface theory predicts that σ is a minimum and (b) the aspect ratio of the wing is fairly small. Nevertheless, the relatively good agreement between theory A and experiment for large $\bar{C}_L$ must be regarded as fortuitous. On the other hand, it is worth while to record that the height of the trailing-vortex sheet employed in this theory, $h_t(0)$, is in good agreement with the height of the rolled-up trailing vortices observed in the experiments. Of course, this cannot be offered as a complete explanation as there are non-linear effects, not accounted for in theory A, which must surely be important for large $\bar{C}_L$. For example, the sidewash

induced at the wing by the image chordwise and trailing vortices affects the overall forces.

Finally, it is evident that with h_p/c constant the experimental results do not obey the proportionality $\bar{C}_D \propto \bar{C}_L^2$. This may be verified by noting that the experimental results do not lie exactly on the curves of theory A which predicts that $\bar{C}_D \propto \bar{C}_L^2$. It seems, however, that in the cases for which $\partial \bar{C}_L/\partial \alpha^{(w)}$ decreases with $\alpha^{(w)}$ the experimental results lie above these curves whilst if $\partial \bar{C}_L/\partial \alpha^{(w)}$ increases with $\alpha^{(w)}$ they lie below. It is conceivable, therefore, that this non-linearity in the experimental $\bar{C}_D/\bar{C}_L^2$ curve is associated with the non-linearity in the $\bar{C}_L/\alpha^{(w)}$ curve. Thus, in order to check this, the experimental results have been replotted on the basis of $\bar{C}_D$ against $\alpha^{(w)}$. The graph obtained for the case $h_p/c = 0.083$ is shown in Fig. 49 which also contains a curve deduced from theory A. This is obtained by replacing $\bar{C}_L$ in equation (3.3) with the consistent linearized form

$$\bar{C}_L = \left[\partial \bar{C}_L/\partial \alpha^{(w)}\right]_{\alpha^{(w)}=0} (\alpha^{(w)} - \alpha_o^{(w)}) \qquad (3.4)$$

Here, as before, $\alpha_o^{(w)}$ is the incidence of the wing for zero lift.

The terms $\left[\partial \bar{C}_L/\partial \alpha^{(w)}\right]_{\alpha^{(w)}=0}$ and $\alpha_o^{(w)}$ may be obtained theoretically. However, in order to include the effects of viscosity and aerofoil thickness the experimental values have been employed. The result of calculating $\bar{C}_D$ by using these values in conjunction with theory A is shown in Fig. 49 for $h_p/c = 0.083$. In this figure it will be seen that the agreement between the 'theory' and experiment is good - even better, in fact, than on the basis of $\bar{C}_D$ against $\bar{C}_L^2$. This is also found to be the case with the other values of h_p/c. Thus it would seem that the non-linearity in the experimental $\bar{C}_D/\bar{C}_L^2$ curve may be attributed to the non-linearity in the $\bar{C}_L/\alpha^{(w)}$ curve.

3.2 The effect of end plates

In all the experiments concerned with open configurations the end plates were fitted to the wing without the wedges. Consequently the inside surfaces of the end plates were parallel to the axis of the tunnel.

3.2.1 Overall lift

The influence of end plates on the overall lift is illustrated in Figs. 50, 51 and 52 which show experimental results for $\overline{C}_L$ plotted against $\alpha^{(w)}$ for various combinations of $h_p/c = 0.250$, 0.208 and 0.167, $l_p/c = 0$, 0.083 and 0.167 and $\gamma = 0$. It will be seen that with h_p/c and $\alpha^{(w)}$ constant an increase in l_p/c produces an increase in $\overline{C}_L$. That this must be so may be justified on qualitative grounds by noting that the end plates tend to reduce the height of the trailing vortices above the ground. Thus the downwash induced at the wing by these vortices and their images is reduced and, in consequence, the lift is increased.

An interesting feature of the $\overline{C}_L/\alpha^{(w)}$ curves for the case $l_p/c = 0.167$ is that their slopes increase noticeably with $\alpha^{(w)}$. Initially, it was thought that this might be due to separated-vortex sheets at the junctions of the wing and the end plates. However, the indication of tuft-grid surveys is that the vorticity in these sheets is relatively weak, the majority of the trailing vorticity being concentrated near the bases of the end plates.

Another possible explanation is that an increase in $\alpha^{(w)}$ causes the trailing vortices to be depressed nearer the 'ground', thus achieving a similar effect to an increase in end-plate length.

Figs. 53 and 54 shows plots of experimental results for $\overline{C}_L$ against $\alpha^{(w)}$ for $l_p/c = 0.083$ and 0.167 and $h_p/c = 0.250$ obtained with $\gamma = 3^o$ and 6^o. As with $\gamma = 0$ a marked non-linearity is evident in the curves for $l_p/c = 0.167$.

3.2.2 Overall drag

As before, two interpretations of the linearized theory for minimum induced drag are compared with experiment. The first of these, theory A, employs the assumption that the vortex trace is the projection of the trailing edge of the configuration onto a plane normal to the direction of motion when $\alpha^{(w)} = 0$ and has $h = h_t(\alpha^{(w)} = 0)$. The second interpretation, theory B, differs from this only insofar as no stipulation is placed on $\alpha^{(w)}$. Consequently, this theory represents, in some measure, the effect of the depression of the trailing-vortex sheet as $\alpha^{(w)}$ increases.

In common with the planar configuration the comparison between theory and experiment is effected on the basis of overall drag and equation (3.2) is used to calculate $\bar{C}_D$ for each interpretation of the theory. Also the same value of A is employed, namely 0.0027, and $\bar{C}_{DB}(0)$ is established in the way indicated for the planar case.

Theoretical and experimental results for $\bar{C}_D$ plotted against $\bar{C}_L$ are shown in Figs. 55, 56 and 57 for $l_p/c = 0.083$, $h_p/c = 0.250$; $l_p/c = 0.083$, $h_p/c = 0.167$ and $l_p/c = 0.167$, $h_p/c = 0.250$ with $\gamma = 0$ in all cases. In the first of these figures the experimental results will be seen to lie between theories A and B, being nearer A than B. However, the agreement between theory A and experiment is not as good as for the planar configuration. This is even more noticeable for $h_p/c = 0.167$, theory A agreeing quite well with experiment for the planar configuration but not for $l_p/c = 0.083$. Indeed, as is apparent in Fig. 56, in the latter case, theory B is in better agreement with experiment than theory A. This is also evident for the case $l_p/c = 0.167$, $h_p/c = 0.250$ (Fig. 57).

Possible reasons for the improvement in agreement between theory B and experiment as l_p increases in comparison with h_p in the interval $0 \leq l_p \leq h_p$ may be given as follows:

(i) Tuft-grid surveys have indicated that as $l_p \to h_p$ the non-planar vortex sheets shed from the junctions of the wing and end plates become weaker. Consequently the assumption of theory B that the trailing vortices of the wing are at the same height as the trailing edge of the wing becomes increasingly accurate as $l_p \to h_p$.

(ii) The linearized theory suggests that the effect of adding the end plates to the wing is to reduce the sidewash induced there by the image chordwise and trailing vortices. This sidewash causes a reduction in the overall lift without influencing the strength of the trailing vortices and hence the overall induced drag. Thus one possible cause for the poor agreement between theory B and experiment in the planar case is partially removed by the addition of end plates.

An examination of Figs. 55, 56 and 57 shows that both theories are in good agreement with experiment in their prediction of $\left[\partial \bar{C}_{Di}/\partial \bar{C}_L^2\right]_{\bar{C}_L} = 0$ for the various cases. This is to be expected because calculations on closed configurations of similar geometries have yielded values of σ very close to the minimum.

Thus it may be concluded that for a given h_p/c the end plates not only reduce the constant term in the expression $\bar{C}_{Di}(\bar{C}_L)/\bar{C}_L^2$ but also decrease the variable terms arising from the above-mentioned non-linear effects.

It is evident from Figs. 56 and 57 that for the cases $l_p/c = 0.083$, $h_p/c = 0.167$ and $l_p/c = 0.167$, $h_p/c = 0.250$ theory B and experiment are not in such good agreement for $\bar{C}_L > 0.8$. This would seem to be due, in part at least, to two contributory factors. Firstly, the linear theory does not include the influence of the image bound vortices on the streamwise flow at the wing. This causes a reduction in the overall lift without altering the overall induced drag (a fact which may be proved by momentum considerations). Secondly, there is reason to doubt whether the

overall induced drag is a minimum when the trailing edges at the bases of the end plates touch the ground. This may be expressed more clearly with the aid of the sketch below

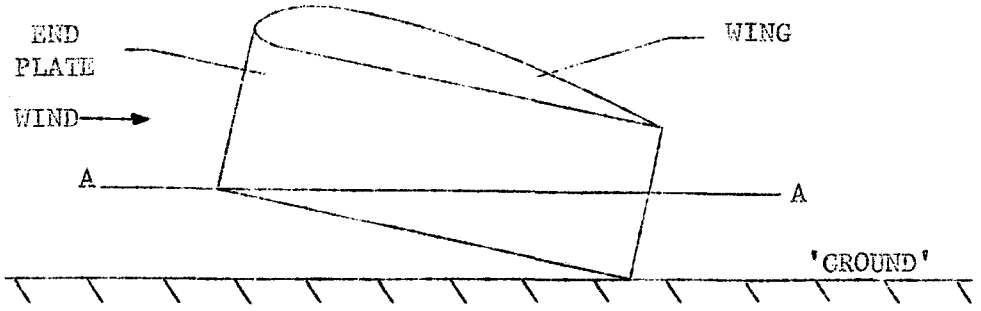

In this case, theory B predicts that the overall induced drag is zero. However, it is clear that in order to achieve the constant circulation required at all points of the trailing edge, the streamwise sections between AA and the 'ground' would require a large amount of twist. In the absence of twist, trailing vorticity would be generated, a fact which has been established for the present end plates by tuft-grid surveys.

For the largest experimental values of $\overline{C}_L$ recorded in Figs. 56 and 57 the gaps between the 'ground' and the rearward extremities of the end-plate bases are small compared with h_p. Thus it is concluded, on the basis of the above reasoning, that the overall induced drag is underestimated by theory B in these cases. This is supported by the experimental data shown in Figs. 56 and 57.

As will become evident in Section 4.3, when AA corresponds with the 'ground' the overall induced drag is very close to the minimum for this case, that is zero. It is worth while, therefore, to enquire into the agreement between theory B and experiment for configurations with the bases of their end plates parallel to the 'ground'. Results for the overall-drag coefficients of such configurations are illustrated in Fig. 58

which shows $\bar{C}_D$ plotted against $\bar{C}_L$ for $\ell_p/c = 0.083$ and 0.167 and $h_p/c = 0.250$. These configurations are obtained by altering γ and $\alpha^{(w)}$ in such a way that $\gamma^o = \alpha^{(w)o} - 2^o$. This ensures that the end-plate bases remain parallel with the ground as $\alpha^{(w)}$ and hence $\bar{C}_L$ are altered.

Evidently, the agreement between theory B and experiment is good for $\ell_p/c = 0.167$ whilst for $\ell_p/c = 0.083$ the theory underestimates $\bar{C}_{Di}$. The reason for this would seem to be that in the latter case the end plates are not completely effective in reducing the strength of the non-planar vortex sheets shed from the junctions of the wing and end plates. Consequently the mean height of the trailing vortices is rather higher than that predicted by theory B. In the case $\ell_p/c = 0.167$, on the other hand, these non-planar vortex sheets are largely eliminated.

According to theory A, $\bar{C}_{Di} \propto \bar{C}_L^2$ for γ, ℓ_p/c and h_p/c given. Thus it may be inferred from Figs. 55, 56 and 57 that the experimental results do not obey this proportionality. As with the planar configuration it is possible that this non-linearity in the experimental curves might be associated with the non-linearity in the $\bar{C}_L/\alpha^{(w)}$ curve. Therefore, to check this hypothesis, the results for $\bar{C}_D$ obtained with $\ell_p/c = 0.083$ and 0.167, $\gamma = 0$ and $h_p/c = 0.250$ have been plotted against $\alpha^{(w)}$. The graph obtained is shown in Fig. 59 where it will be seen that these results are compared with the $\bar{C}_D$ deduced from theory A. In common with the planar case, this coefficient is rewritten as a function of $\alpha^{(w)}$ by employing equation (3.4), $\left[\partial \bar{C}_L/\partial \alpha^{(w)}\right]_{\alpha^{(w)}} = 0$ and $\alpha_o^{(w)}$ being inferred from the experimental results.

Apparently, the agreement between 'theory' and experiment is good and considerably better than that found with the corresponding $\bar{C}_D/\bar{C}_L$ curves. It would seem reasonable to conclude, therefore, that the non-linearity in either of the

experimental curves is largely identifiable with the non-linearity in the associated $\overline{C}_L/\alpha^{(w)}$ curves.

Fig. 60 shows $\overline{C}_D$ plotted against $\overline{C}_L$ for the configuration $\gamma = 3^o$, $\ell_p/c = 0.167$ and $h_p/c = 0.250$. It indicates that theory B is in reasonable agreement with experiment in the interval $0 \leq \overline{C}_L \leq 1$.

The effect of a gap between the bases of the end plates and the 'ground' on $\overline{C}_D$ is shown in Fig. 61 for three configurations with $\gamma^o = \alpha^{(w)^o} - 2^o$ and $h_p/c = 0.250$. Also included for comparison is theory B and it will be observed that the agreement between the theory and experiment is particularly poor in the vicinity of $(h_p - \ell_p)/c = 0$. This would seem to be due, in the main, to the influence of viscosity on the flow between the end-plate bases and the 'ground'. It should be remarked, however, that neither the theory nor the experiment properly accounts for this effect for small $(h_p - \ell_p)/c$. In practice, the flow of air in the spanwise direction will be influenced by the presence of the water surface.

4. Closed configurations : an examination of the sectional and overall forces

In this section, a study of the overall and sectional-force characteristics of closed configurations will be described. These configurations were obtained by arranging the end plates to close completely the gaps between the wing tips and the 'ground'. In so doing, it was assumed that these configurations could, in theory, be designed for zero induced drag, thus making them, according to the definition, 'closed'.

In Section 4.1 the experimental results for the overall forces will be discussed and those for the overall lift will be compared with theory. Comparison between the overall induced

drag of the wing and end plates predicted by theory and experiment will not, however, be made in this section. This will be considered in Section 4.3 where a detailed drag analysis will be described.

Section 4.2 will be concerned with an investigation into the sectional-lift and circulation characteristics. Part of the aim of this study has been to check the validity of a number of the assumptions of the theory formulated in Part II of Chapter II.

4.1 Overall forces

Owing to the problem of balance constraint it was not possible to measure the overall forces of the closed configurations with the balance directly. This difficulty was overcome by permitting a small gap, g, in each end plate, g being invariant along the length of the gap. Thus it was assumed that by extrapolating the curve of overall force against gap to zero gap the overall force of the closed configuration would be obtained. If this assumption is correct, the limiting value of the overall force should not depend on gap position. In order to check this (and for another reason which will become clear later) various gap positions have been tested. These are illustrated in Fig. 62 and are labelled A, B and C. It will be observed that in cases A and C each end plate of the wing is attached to the corresponding end plate of the image, the joint between them being sealed with 'Sellotape'.

Figs. 63 and 64 show the effect of gap on the overall-lift and drag coefficients for the case $h_p/c = 0.167$ with $\alpha_b^{(E)} = 0$, where $\alpha_b^{(E)}$ is the angle of the wedges, between the wing and the end plates, in the plane of the wing chordal surface. In the first of these figures, the results for $\overline{C}_L$ are plotted for all three gap positions. The second figure, on the other hand, only includes results for gap positions B and C as only these positions ensure that the end-plate drag is properly included in the overall-drag measurements. In both figures, results are shown for $\alpha^{(w)} = 2^o$, 5^o and 8^o. Evidently, for all cases, the limiting values of

$\overline{C}_L$ and $\overline{C}_D$ as $g \to 0$ are independent of gap position. On the evidence of these results, therefore, the limiting method has been employed to determine the overall forces of the closed configurations.

4.1.1 Overall lift : comparison between theory and experiment

Results obtained for $\overline{C}_L$ by the limiting process are illustrated in Figs. 65, 66 and 67. These show graphs of $\overline{C}_L$ against $\alpha^{(w)}$ for $\ell_p/c = h_p/c = 0.083$, 0.167 and 0.250 with $\alpha_b^{(E)} = 0$. Also included for comparison are curves representing the linear and 'non-linear' versions of the theory described in Part II of Chapter II. The linear version employs the assumption that the cylindrical surface, on which the vortices and sources are placed, is best represented by the chordal surface of the test configuration corresponding to $\alpha^{(w)} = \alpha_b^{(E)} = 0$. Thus, to a very good approximation, $AR = 2$ and consequently the following values of $a^{(w)}$ and $a^{(E)}$ are obtained:

ℓ_p/c	0.083	0.167	0.250
λ	0.219	0.386	0.552
$a^{(w)}$	14.57	10.10	8.35
$a^{(E)}$	1.43	1.63	1.80

The thickness-induced upwash at the wing plane and $\gamma_t(\xi)$ are determined in the manner described in Section II.6.2, the integral-equation method being used to obtain $\gamma_t(\xi)$. In the next stage of the calculation the vortex distributions corresponding to the camber distributions of the wing and end plates, $\gamma_W(\xi)$ and $\gamma_E(\xi)$, are calculated. This is achieved by using the integral-equation method outlined in Section II.6.1. Actually, there is some difficulty in defining the camber of the end plates owing to the fact that their trailing edges are of non-zero thickness (0.25 in.). The definition adopted, however, is that their camber slope is the

mean of the streamwise slopes of their inside and outside surfaces when $\alpha_b^{(E)} = \gamma = 0$. This avoids the difficulty of not being able to define the chord line of each section of the end plates. In the case of the wing the definition of camber slope is more conventional, being the streamwise slope of the camber surface corresponding to $\alpha^{(w)} = \alpha_b^{(E)} = 0$.

Thus the results obtained for $\gamma_t(\xi)$, $\gamma_w(\xi)$ and $\gamma_E(\xi)$ may be combined according to equation (II.6.22) to yield the value of $\overline{C}_{L\ (C.T.)}$.

As a consequence of the above definition of end-plate camber equation (II.6.25) is rewritten as follows:

$$\alpha_o^{(w)} = -\{\overline{C}_{L(C.T.)} + a^{(E)}\alpha_b^{(E)}\}/a^{(w)}. \qquad (4.1)$$

Thus, by employing the results calculated for $\overline{C}_{L(C.T.)}$, $a^{(w)}$ and $a^{(E)}$ in conjunction with equation (4.1), there are obtained the following results for $-\alpha_o^{(w)}(\alpha_b^{(E)} = 0)$:

ℓ_p/c	0.083	0.167	0.250
$-\alpha_o^{(w)}(\alpha_b^{(E)}=0)^o$	0.868	2.26	2.92

Another implication of the definition of end-plate camber employed above is that the non-linear form of the overall-lift coefficient, equation (II.7.12), is rewritten in the form

$$\overline{C}_L = \{a^{(w)} + 2\pi\Delta\beta(\tilde{\alpha}^{(w)},\infty)\}\tilde{\alpha}^{(w)} + a^{(E)}\alpha_b^{(E)}, \qquad (4.2)$$

where

$$\tilde{\alpha}^{(w)} = \alpha^{(w)} - \alpha_o^{(w)}\ (\alpha_b^{(E)} = 0).$$

Thus, in order to determine $\overline{C}_L$ by means of equation (4.2), it is necessary to have a knowledge of $\Delta\beta(\tilde{\alpha}^{(w)},\infty)$. This is provided by de Haller's (1936) exact potential-flow theory and the results obtained from this theory for $2\pi\Delta\beta(\tilde{\alpha}^{(w)},\infty)$ are summarized below.

$\tilde{\alpha}^{(w)^\circ}$ / ℓ_p/c	1.8	3.6	7.2	10.8
0.083	-0.04	-0.18	-0.64	
0.167	-0.02	-0.09	-0.31	-0.67
-0.250	-0.02	-0.05	-0.19	-0.44

The conclusions to be drawn from the comparison between the two theories and experiment shown in Figs. 65, 66 and 67 are as follows:

(i) The incidence of the wing for zero overall lift, $\alpha_o^{(w)}$ ($\alpha_b^{(E)} = 0$), would seem to be overestimated negatively by the theories, the discrepancy becoming more apparent as ℓ_p/c increases. It seems possible that this is due to the assumptions made regarding the thickness-induced normal velocity at the configuration. For example, as ℓ_p/c increases, the upwash induced at the wing by the sources simulating end-plate thickness increases. Thus the assumption that this upwash may be disregarded becomes increasingly suspect as ℓ_p/c increases.

(ii) The linearized theory grossly overestimates the overall lift even for quite small $\alpha^{(w)}$ whilst the 'non-linear' theory is in comparative good agreement with experiment for $\bar{C}_L \lesssim 1$.

(iii) In the case $\ell_p/c = 0.083$ the 'non-linear' theory yields values of $\bar{C}_L$ only up to $\alpha^{(w)} \simeq 7.6^\circ$. This corresponds to the trailing edge touching the ground in the case of the two-dimensional flat plate. In other words, it is not possible to obtain values of $\Delta\beta(\tilde{\alpha}^{(w)}, \infty)$ beyond this incidence. However, it should be noted that, in the case cited, the experimental results are limited, by the wing trailing edge touching the ground, to a maximum incidence of approximately 8.5°.

Fig. 68 shows experimental results for the overall-lift coefficient plotted against $\alpha_b^{(E)}$ for $\alpha^{(w)} = 2^\circ$, 5° and 8° with

$\ell_p/c = 0.167$. Also included are curves representing the 'non-linear' theory. Evidently, although this theory is not in absolute agreement with experiment, the trends exhibited are both linear with approximately the same slope as shown below.

$\alpha^{(w)\circ}$	$\partial\bar{C}_L/\partial\alpha_b^{(E)}/^\circ$	
	THEORY	EXPERIMENT
2	0.028	0.026
5	0.028	0.026
8	0.028	0.025

This would also seem to support the assumption, implicit in equation (4.2), that $\bar{C}_L$ is linearly dependent on $\alpha_b^{(E)}$ with a slope, $\partial\bar{C}_L/\partial\alpha_b^{(E)}$, which is independent of $\alpha^{(w)}$.

4.1.2 Overall drag

Experimental results for the overall-drag coefficient of various closed configuration are shown in Figs. 69 and 70. In the former figure, $\bar{C}_D$ is plotted against $\bar{C}_L$ for $\alpha_b^{(E)} = 0^\circ$, 3°, 6° and 9° with $\ell_p/c = 0.167$. It will be seen that, as $\alpha_b^{(E)}$ increases, the $\bar{C}_D/\bar{C}_L$ curve is depressed. The reason for this is sought in the drag analysis to be described in Section 4.3.

Fig. 70 shows $\bar{C}_D$ plotted against $\bar{C}_L$ for $\ell_p/c = 0.083$, 0.167 and 0.250 with $\alpha_b^{(E)} = 0$. It shows that, as might be expected, $\bar{C}_D$ decreases with decreasing ℓ_p/c if $\bar{C}_L$ is constant. Nevertheless, the reduction in $\bar{C}_D$ resulting from a decrease in ℓ_p/c from 0.167 to 0.083 is greater than was anticipated.

4.2 Sectional characteristics

This section is concerned with a discussion of the results of an investigation into the sectional characteristics of closed configurations with $\ell_p/c = 0.167$. Firstly, in Section 4.2.1, the results for circulation will be described. Secondly, in Section 4.2.2, results obtained for the sectional-lift coefficient of the wing

will be discussed.

4.2.1 Circulation

The method employed for deducing the circulation from results for the surface static-pressures has been described in Section 2.4.3. Normally, the static-pressure information required was obtainable from two spanwise stations of the wing and one spanwise station of the image (see Fig. 33). However, in view of the apparent symmetry of the flow, this is equivalent to static-pressure distributions at three wing stations. Furthermore, in some cases, these were supplemented by static-pressure measurements at the 'ground' station of the port end plate. These were obtained with a static-pressure probe attached to the surface of the end plate. The whole of this information permitted, in certain cases, chordwise distributions of circulation at four stations.

Results obtained for $\Gamma(c)/U_o c$ are plotted against $2s/b$ in Figs. 71 and 72 for $\alpha^{(w)} = 2^o$ and 5^o, s being defined as the distance along the outside surface of the configuration, normal to the wind direction, from the wing centre span to the measuring station. In each case, results are presented for $\alpha_b^{(E)} = 0^o$, 3^o 6^o and 9^o and it will be seen that $\Gamma(c)$ increases with $\alpha_b^{(E)}$ particularly in the vicinity of the end plates. This results in the sign of the trailing vorticity, $d\Gamma(c)/ds$, being altered from negative for $\alpha_b^{(E)} = 0$ to positive for $\alpha_b^{(E)} = 9^o$. Further, for each value of $\alpha^{(w)}$ there corresponds a value of $\alpha_b^{(E)}$ which seems to give substantially zero $d\Gamma(c)/ds$ for all s. The respective values of $\alpha_b^{(E)}$ are approximately 3^o and 5^o. Clearly, the overall induced drags corresponding to these two combinations of $\alpha^{(w)}$ and $\alpha_b^{(E)}$ are either extremely small or zero. It is interesting, therefore, to compare the above values of $\alpha_b^{(E)}$ with those calculated to give zero overall induced drag by the linearized theory discussed in

Sections II.5 and II.6. These are 2.6^{o} and 5.7^{o}, respectively, which are seen to be in moderate agreement with the experimental values.

Figures 73 and 74 show experimentally-deduced lines of constant circulation on developments of the outside surfaces of configurations with $\alpha^{(w)} = 5^{o}$ and $\alpha_b^{(E)} = 0^{o}$ and 9^{o}. These figures demonstrate the unique feature of closed configurations, namely that some lines of constant circulation end at the spanwise extremities. It should be remarked, however, that in practice this property will not be realized owing to the dynamic condition at the water surface combining with the effect of viscosity to prevent the vortices ending there. On the other hand, there is reason to suppose that for sufficiently large R_c (say $> 10^6$) the essential conclusions of this investigation will not be altered.

In Figs. 75, 76 and 77 are shown experimentally-derived plots of $\Gamma(\tilde{x})/\Gamma(c)$ against $\tilde{x}/c$ for $\alpha^{(w)} = 2^{o}$, $\alpha_b^{(E)} = 0^{o}$, 9^{o} and $\alpha^{(w)} = 5^{o}$, $\alpha_b^{(E)} = 0^{o}$. In all cases, results are shown for the four s - wise stations. The object of presenting the chordwise circulation distributions in this form is to compare the type of distribution assumed in the theory of Sections II.5 and II.6 with experiment. If this assumed form is correct, $\Gamma(\tilde{x})/\Gamma(c)$ will be invariant with s. This is evidently the case over the majority of the wing for all three combinations of $\alpha^{(w)}$ and $\alpha_b^{(E)}$. On the other hand, for $\alpha^{(w)} = 2^{o}$, $\alpha_b^{(E)} = 9^{o}$ the assumed distribution seems not to be representative at the end plates. It appears that for this case the comparative strength of the s-wise vortices near the leading edge is greater at the end plates than at the wing. This suggests the possibility that for $\alpha^{(w)} = 2^{o}$, $\alpha_b^{(E)} = 9^{o}$ the theory of Section II.5 and II.6 overestimates the inviscid drag (that is the drag minus the boundary-layer drag) of the end plates. Consequently, if as seems likely, the corresponding overall induced

drag is small, the theory could conceivably underestimate the inviscid drag of the wing. This matter will be considered again in Section 4.3.

4.2.2 Sectional Lift

Fig. 78 is a graph of the experimentally-derived values of C_L against $\alpha_b^{(E)}$ for $\alpha^{(w)} = 2^o$, 5^o and 8^o and the three spanwise stations of the wing. It shows that these curves are linear with slopes which decrease towards the wing centre span. This would seem to give further support for the use of equation (4.2) to calculate the effect of $\alpha_b^{(E)}$ on $\bar{C}_L$.

In Fig. 79 are shown plots of experimental values of C_L against $\alpha^{(w)}$ for three spanwise stations of the wing and with $\alpha_b^{(E)} = 0^o$. This indicates that the non-linear part of the $C_L/\alpha^{(w)}$ curve does not vary greatly across the span. As the flow in the vertical plane of symmetry of the wing is almost two-dimensional in the cases examined this would, to some extent, seem to justify the use of non-linear correction to $\bar{C}_L$ obtained from two-dimensional theory.

4.3 Drag Analysis

This section deals with a description of a drag analysis performed on closed configurations with $\ell_p/c = 0.167$. The objectives of this analysis were, firstly, to provide information on the overall induced drag of the configurations and the separate inviscid drag of the wing and end plates. By so doing, it was intended that the accuracy of the theoretical predictions of these drag components should be checked. Secondly, it was considered desirable to have an independent check on the information provided by the circulation distributions.

The method employed in this analysis consisted of deducing from experiment the boundary-layer drags of the wing and the end

plates. This information was then combined with balance measurements of the separate drag of the wing and end-plate components to provide the inviscid drag of each component.

The results of the boundary-layer-drag measurements will be described in Section 4.3.1 whilst a discussion of the results for the drag of the wing and end plates and the subsequent determination of their inviscid drag will appear in Section 4.3.2.

4.3.1 Boundary-layer drag

In general, the wake-survey method, as described by Jones (1936), may not be used to determine the sectional boundary-layer drag at all spanwise stations of a finite wing. This is because Jones' method is based on the assumption that the flow round each section is two-dimensional which is certainly not the case near the tips of a finite wing. However, the indications of the theory of Section II.5 are that for closed configurations of nearly zero induced drag the flow at centre span is almost two-dimensional. Therefore it is assumed that Jones' technique may be employed to obtain the sectional boundary-layer drag at this station.

Fig. 80 shows the results for the coefficient of the sectional boundary-layer drag (C_{DB}) of the wing centre span plotted against C_L for various $\alpha_b^{(E)}$. It will be seen that the points appear to fall nearly on the same curve regardless of the value of $\alpha_b^{(E)}$. The relationship governing this curve may be approximated reasonably well in the interval $0 \leq C_L \leq 1$ by the expression

$$C_{DB} = 0.0081 + 0.0027\, C_L^2. \qquad (4.3)$$

In determining the total boundary-layer drag of the wing, consisting of the basic wing plus wedges and fairings, it will be assumed that, at all spanwise stations, C_{DB} is given by equation (4.3). Therefore the coefficient of the overall boundary-layer drag of the wing, $\overline{C}_{DB}^{(w)}$, may be written as

$$\bar{C}_{DB}^{(w)} = \{0.0081 + 0.0027(\bar{C}_L\ bc/S^{(w)})^2\}S^{(w)}/bc. \qquad (4.4)$$

Here $S^{(w)}$ is the planform area of the wing plus wedges and fairings. Similarly, the coefficient of the overall boundary-layer drag of one end plate and its image beneath the ground is assumed to be given by

$$\bar{C}_{DB}^{(E)} = \{0.0081 + 0.0027(\bar{C}_S\ bc/S^{(E)})^2\}S^{(E)}/bc. \qquad (4.5)$$

In this expression $\bar{C}_S$ is the coefficient of overall side force of one end plate plus its image beneath the 'ground', being defined positive in the outward direction, whilst $S^{(E)}$ is the combined planform area of the end plate and image.

No attempt will be made to justify the use of equations (4.4) and (4.5) rigorously. Nevertheless, as a consequence of the near two-dimensional nature of the flow over the wing, equation (4.4) should yield reasonably accurate values of $\bar{C}_{DB}^{(w)}$. The use of equation (4.5), on the other hand, is more questionable. It seems likely, however, that in the cases of interest the errors caused in the inviscid drag of the end plates should be small compared with the overall drag of the configuration. The justification for this is that in these cases $\bar{C}_{DB}^{(E)} << \bar{C}_D$.

4.3.2 Inviscid Drag

The overall drag of the wing was obtained by utilizing the balance and testing the configuration with gap position A (Fig. 62). As previously, the limiting method was employed and the results thus found are summarized in Fig. 81. This shows $\bar{C}_D^{(w)}$, the coefficient of the overall drag of the wing, plotted against $\alpha^{(w)}$ for $\alpha_b^{(E)} = 0^o$, 3^o, 6^o and 9^o.

Evidently, the result of increasing $\alpha_b^{(E)}$ with $\alpha^{(w)}$ fixed is to reduce $\bar{C}_D^{(w)}$ whilst, if $\alpha_b^{(E)}$ is kept constant and $\alpha^{(w)}$ is increased, $\bar{C}_D^{(w)}$ increases.

Upon subtracting $\overline{C}_D^{(w)}$ from $\overline{C}_D$ one obtains $\overline{C}_D^{(E)}$, the coefficient of the overall drag of one end plate and its image, or, alternatively, both end plates of the wing. The last coefficient is plotted against $\alpha^{(w)}$ for $\alpha_b^{(E)} = 0^o$, 3^o, 6^o and 9^o in Fig. 82. This shows that, for certain combinations of $\alpha^{(w)}$ and $\alpha_b^{(E)}$, $\overline{C}_D^{(E)}$ is actually negative and indicates that the trends of $\overline{C}_D^{(E)}$ with $\alpha^{(w)}$ and $\alpha_b^{(E)}$ are opposite to those described for $\overline{C}_D^{(w)}$.

The overall inviscid-drag coefficient of the wing is found by subtracting $\overline{C}_{DB}^{(w)}$, as deduced from equation (4.4), from $\overline{C}_D^{(w)}$. The results obtained by this process are shown in Fig. 83 where they are plotted against $\alpha_b^{(E)}$ for $\alpha^{(w)} = 2^o$, 5^o and 8^o. Also shown in this figure are curves calculated according to the following theoretical method:

(i) The vortex and source distributions are placed on the cylindrical surface used in the determination of the overall lift in Section 4.1.1.

(ii) The incidence ratio of the equivalent uncambered configuration of zero thickness, $\{\alpha^{(E)}/\alpha^{(w)}\}_{eq}$, is calculated by using equation (II.6.23). Actually, if the definitions of camber given in Section 4.1.1. are employed, it is found that this equation applies to configurations with $\alpha^{(w)} = \alpha_b^{(E)} = 0$ but it is easily modified for configurations of non-zero $\alpha_b^{(E)}$ and $\alpha^{(w)}$ to give the result

$$\left(\frac{\alpha^{(E)}}{\alpha^{(w)}}\right)_{eq} = \frac{\int_{-c/2}^{+c/2} \{\gamma_E(\xi) + \gamma_t(\xi)\}dx + \pi\beta U_o \alpha_b^{(E)} c}{\int_{-c/2}^{+c/2} \{\gamma_w(\xi) + \gamma_t(\xi)\}dx + \pi\beta U_o \alpha_b^{(E)} c}.$$

(iii) $\sigma^{(w)}$ is then determined from the results of Section II.5. Hence, if, as was suggested in Section II.6.2, it is assumed that the sectional inviscid drag associated with thickness is zero, the overall inviscid drag of the wing is identical with $\overline{D}_i^{(w)}$. The coefficient of this component of drag is determined from the result

$$\bar{C}_{Di}^{(w)} \equiv \bar{C}_D^{(w)} - \bar{C}_{DB}^{(w)} = \sigma^{(w)} \bar{C}_L^2/\pi \mathcal{R}. \qquad (4.6)$$

(iv) In order to plot $\bar{C}_{Di}^{(w)}$ as a function of $\alpha^{(w)}$ and $\alpha_b^{(E)}$, $\bar{C}_L$ is eliminated from equation (4.6) by employing equation (4.2).

Fig. 83 shows that the agreement between theory and experiment is not good although the slopes $\partial(\bar{C}_D^{(w)} - \bar{C}_{DB}^{(w)})/\partial\alpha_b^{(E)}$ and $\partial(\bar{C}_D^{(w)} - \bar{C}_{DB}^{(w)})/\partial\alpha^{(w)}$ predicted by theory in the vicinity of $\alpha^{(w)} = 2^o$ and $\alpha_b^{(E)} = 0^o$ are similar to the corresponding experimental slopes. One possible reason for the poor agreement is the neglect in the theory of the inviscid drag due to thickness. This could be checked in future experiments by varying the thickness of the end plates. Another possible cause is that the assumed form of the vortex distribution is incorrect. It will be recalled that the indications of the circulation distributions were that for $\alpha^{(w)} = 2^o$, $\alpha_b^{(E)} = 9^o$ a circulation distribution of the type $\Gamma(\tilde{x})f(s)$ would possibly underestimate the inviscid drag of the wing. This is evidently in agreement with the drag analysis, the theory underestimating the inviscid drag of the wing in this case. Generally, however, theory overestimates the inviscid drag, the discrepancy becoming more apparent as $\alpha^{(w)}$ increases.

Finally, there are the non-linear effects not included in the theory, the two most obvious examples being:

(a) the departure of the trailing-vortex sheet from the assumed cylindrical shape;

(b) the lift is not related to the circulation by the linearized theory form $L = \rho U_o \Gamma$.

Effect (b) may be allowed for by replacing equation (4.6) by

$$\bar{C}_{Di}^{(w)} = \sigma^{(w)}(2\bar{\Gamma}/U_o c)^2/\pi \mathcal{R}, \qquad (4.7)$$

where $\bar{\Gamma}$ is the mean circulation across the span of the wing. This result enables one to employ the values of $\sigma^{(w)}$ deduced from

Section II.5 without making any assumptions about the relationship between $\overline{L}$ and $\overline{\Gamma}$.

A method possessing some of the features of effect (a) is based on the assumption that the cylindrical trailing-vortex sheet coincides with the trailing edge of the configuration. Therefore values of $\sigma^{(w)}$ for the modified Trefftz-plane shapes may be determined and used in conjunction with equation (4.7) to obtain $\overline{C}_{Di}^{(w)}$. Unfortunately, the theory of Section II.7 does not yield $\overline{\Gamma}$ as a function of $\alpha^{(w)}$ and $\alpha_b^{(E)}$. Thus, in order to check the possible improvement obtained with this method in the case $\alpha^{(w)} = 5^o$, $\alpha_b^{(E)} = 0^o$, the value of $2\overline{\Gamma}/U_o c$ deduced from the experimental circulation distributions will be employed. Hence it is found that the new method yields an inviscid-drag coefficient of 0.0084 compared with the value 0.0072 deduced from experiment and that of the previous theory 0.0096. Evidently, the improvement in agreement is only slight.

Perhaps the most important fact to emerge from this analysis is that the inviscid drag of the wing can be large. In fact, in the case $\alpha^{(w)} = 8^o$, $\alpha_b^{(E)} = 0^o$, it is almost as large as the overall drag. But, as may be inferred from Figs. 69 and 80, the overall boundary-layer drag is almost the same size as the overall drag. This suggests, therefore, that in the case mentioned the end plates provide a large negative inviscid drag. The coefficient of this force component is $\overline{C}_D^{(E)} - \overline{C}_{DB}^{(E)}$, the latter coefficient being deduced from equation (4.5). However, before this equation can be used to find $\overline{C}_{DB}^{(E)}$, it is necessary to know $\overline{C}_S$. For this particular purpose, therefore, measurements were made of the overall side force on the port end plate and its image by using the balance and gap position C (Fig. 62). As with the other overall-force measurements, the limiting method was used and the results obtained for $\overline{C}_S$ are illustrated in Fig. 84 where they are plotted against $\alpha_b^{(E)}$ for

$\alpha^{(w)} = 2^\circ$, 5° and 8°. By using these results and equation (4.5) $\bar{C}_{DB}^{(E)}$ has been calculated, thus enabling results for $\bar{C}_D^{(E)} - \bar{C}_{DB}^{(E)}$ to be calculated. These are shown in Fig. 85 plotted against $\alpha_b^{(E)}$ for $\alpha^{(w)} = 2^\circ$, 5°, and 8°. Also included are theoretical curves calculated by using the same method as that used to obtain the theoretical curves of Fig. 83 except with $\sigma^{(w)}$ replaced by $\sigma^{(E)}$. Again the agreement between theory and experiment is not good presumably for similar reasons to those advanced for the wing inviscid drag. On the other hand, theory and experiment do agree in a large number of cases in indicating that when there is an inviscid drag acting on the wing the end plates give an inviscid thrust of almost the same magnitude. Similarly, when there is an inviscid drag acting on the end plates the wing yields an inviscid thrust of nearly the same size. The reason for this is that if there is a mean downwash induced at the wing by the chordwise and trailing vortices an 'outwash' will be caused at the end plates. Thus, as the circulation varies slowly round the configuration in the cases considered, there results an inviscid drag at the wing and an inviscid thrust at the end plates. This situation is reversed if $\alpha^{(w)}$ and $\alpha_b^{(E)}$ are such as to give a mean upwash at the wing.

It will be seen in Fig. 85 that in accord with observations based on an examination of the circulation distributions the theory overestimates the inviscid drag of the end plates in the case $\alpha^{(w)} = 2^\circ$, $\alpha_b^{(E)} = 9^\circ$.

Table 2 shows the various values of $\bar{C}_{DB}^{(w)}$ and $\bar{C}_{DB}^{(E)}$ calculated by employing equations (4.4) and (4.5). This table, which is included in order to show the relative importance of the constituents of the overall drag, also contains theoretical estimates of $\bar{C}_{Di}$. These are calculated by using the method employed in the determination of the theoretical curves of Fig. 83 except that $\sigma^{(w)}$

and $\bar{C}_{Di}^{(w)}$ are replaced by σ and $\bar{C}_{Di}$ in equation (4.6).

The coefficients $\bar{C}_{DB}^{(w)}$ and $\bar{C}_{DB}^{(E)}$ have been added to the theoretical $\bar{C}_{Di}$ to provide an estimate of $\bar{C}_D$ which is shown in the sixth column of the table. This may be compared with the value of $\bar{C}_D$ obtained from balance measurements which appears in the last column. Thus it will be seen that, in seven of the twelve cases shown, the two values of $\bar{C}_D$ differ by less than 7% of the measured value. In three other cases, for which the agreement between the two values is not as good, bracketed figures are included by the side of the measured $\bar{C}_D$. These represent values interpolated from carpet plots of the measured $\bar{C}_D$ against $\bar{C}_L$ for various t_p/c and $\alpha_b^{(E)}$. It will be seen that they are in better agreement with the estimated values.

The most obvious discrepancy between the measured and estimated $\bar{C}_D$ occurs for $\alpha^{(w)} = 2^\circ$, $\alpha_b^{(E)} = 9^\circ$. In this case, the estimated $\bar{C}_D$ is larger than the measured $\bar{C}_D$ by approximately 16% of the measured value. The reason for this is not known although it is suspected that it is due in some measure to the vortex distribution assumed in the theory being incorrect at the end plates.

For $0^\circ \lesssim \alpha_b^{(E)} \lesssim 6^\circ$ the estimated and measured $\bar{C}_D$ are relatively insensitive to changes in $\alpha_b^{(E)}$ if $\alpha^{(w)}$ is kept constant. Thus, as a result of $\bar{C}_L$ increasing with $\alpha_b^{(E)}$, the $\bar{C}_D/\bar{C}_L$ curve is depressed as $\alpha_b^{(E)}$ increases (see Fig. 69). The reason for this appears to be that, in this interval of $\alpha_b^{(E)}$, $\bar{C}_{DB} = \bar{C}_{DB}^{(w)} + \bar{C}_{DB}^{(E)}$ and $\bar{C}_{Di}$ vary slowly with $\alpha_b^{(E)}$. Furthermore, from $\alpha_b^{(E)} = 0^\circ$ to $\alpha_b^{(E)} = 3^\circ$, the changes in $\bar{C}_{DB}$ are opposite in sign to those of $\bar{C}_{Di}$.

Although $\bar{C}_{Di}$ is not an insignificant part of $\bar{C}_D$ in the range of $\alpha_b^{(E)}$ and $\alpha^{(w)}$ examined it is generally small compared with the overall-drag coefficient. As previously noted, however, the inviscid-drag coefficient of the wing can, in certain cases, be comparable with $\bar{C}_{DB}$. Thus in these cases it is important to ensure that the end plates can sustain the required thrust. As an

illustration, consider the case $\alpha^{(w)} = 5^o, \alpha_b^{(E)} = 0^o$. This yielded an overall lift to drag ratio of nearly 71. However, if the end plates were unable to sustain the inviscid thrust they gave during the test, this ratio would drop to 51 provided the overall lift coefficient remained the same.

CHAPTER IV

CONCLUDING REMARKS

A theoretical and experimental discussion concerned with the lift and induced drag of open and closed G.E.Ws. has been presented. In this final chapter, the salient conclusions of this study will be outlined and suggestions for possible future work will be mentioned.

1. Open configurations

A generalization of the combined-flow method of Munk (1921) has been employed to determine, to a linear approximation, the minimum induced drag of a planar G.E.W. The 'exact' solution thus obtained for σ was compared with de Haller's (1936) calculations which were shown to be in error.

In the case of a planar wing with end plates in ground effect, the Schwarz-Christoffel transformation was found not to be amenable to explicit integration. Therefore a perturbation technique, valid for small $2h/b$, was devised. The accuracy of this method was determined by comparing the result obtained for the minimum induced-drag factor of the planar G.E.W. with the 'exact'solution. It was found that the zeroth approximation for σ was in excellent agreement with the 'exact' value in the interval $0 \leq 2h/b \leq 1.6$. Indeed, for $2h/b = 0.48$, the error in $\sigma^{(o)}$ was shown to be $O(10^{-8})$ compared with σ. On this basis, therefore, the zeroth approximation was employed to determine the minimum induced drag of a wing with end plates in ground proximity.

Two interpretations of the linearized theory for minimum induced drag, theories A and B (see Section III.3), were compared with experiment on the basis of $\overline{C}_D$ against $\overline{C}_L$. It was found that for the planar configuration the experimental results were in better agreement

with A than B, the latter theory generally underestimating $\bar{C}_{Di}$. This was attributed, in part, to the presence of non-planar vortex sheets shed from the side edges of the wing. These vortex sheets effectively increase the mean height of the trailing-vortex sheet. Thus, as a result, $\bar{C}_{Di} \neq 0$ when $h_t = 0$.

The agreement between theory A and experiment was found to be not as good when end plates were fitted to the wing. Furthermore, it was evident that as l_p increases in comparison with h_p the experimental results approach the curve of theory B. The reasons put forward for this were, firstly, that the end plates tend to suppress the non-planar vortex sheets shed from the tips of the wing. Secondly, the end plates reduce the sidewash induced at the wing by the image chordwise and trailing vortices.

In both planar and non-planar cases the slopes $\left[\partial \bar{C}_{Di}/\partial \bar{C}_L^2\right]_{\bar{C}_L=0}$ predicted by both theories were found to be in good agreement with experiment. Thus it was inferred that for a given h_p/c the end plates not only reduce the constant in the expression $\bar{C}_{Di}(\bar{C}_L)/\bar{C}_L^2$ but also decrease the variable terms arising from the above-described non-linear effects.

The derivatives $\left[\partial \bar{C}_L/\partial \alpha^{(w)}\right]_{\alpha(w)=0}$ deduced from the experiments on the planar configuration were found to compare well with those of the linearized, inviscid theory of Saunders (1963). This theory does not include the effect of wing thickness and boundary-layer displacement on $\left[\partial \bar{C}_L/\partial \alpha^{(w)}\right]_{\alpha(w)=0}$. It was supposed, therefore, that these two effects cancel. Nevertheless, there is a need for a fundamental study of the effect of the boundary layer on the lifting characteristics of wings in ground proximity.

The indications of the experiments were that for a given $\alpha^{(w)}$ and h_p/c an increase in the end-plate length, l_p, produces an increase in $\bar{C}_L$. Furthermore, it was found that, for small $(h_p - l_p)/c$, $\partial \bar{C}_L/\partial \alpha^{(w)}$ increases with increasing $\alpha^{(w)}$.

2. Closed configurations

A theory has been presented for determining the overall lift and induced drag of a closed configuration consisting of a substantially planar wing with end plates. This theory, which was deduced from a study of the sectional-drag characteristics of wings, is based on the linearized theory and the assumption that the vortex distribution $\gamma(x,s)$ is of the form $\gamma(x)f(s)$.

As a check on validity of the theory it was applied to the case of an isolated planar wing of rectangular planform, zero chordwise camber and zero thickness. For this type of wing it was found to be similar to a theory given by Küchemann (1952) except in one important detail. It was shown that this discrepancy explains an inconsistent feature of Küchemann's method. As the present theory does not exhibit this inconsistency it was concluded that it is the more fundamental of the two theories.

In common with Küchemann's method, the present theory involves the solution of an equation similar to the 'lifting-line' equation. This was solved by employing particular solutions for the flow in the Trefftz plane and a variational principle which was specifically devised for the present problem.

The calculations performed for the above-mentioned closed configuration have indicated that the lift derivative $a^{(w)}$ increases slowly with AR and decreases with λ. On the other hand, it was found that $a^{(E)}$ decreases with AR and increases with λ. Furthermore, it was ascertained that, in the absence of chordwise camber and thickness, $\sigma = 0$ for $\alpha^{(E)} = \alpha^{(w)}$ whilst, for $\alpha^{(E)}/\alpha^{(w)} = 0$, σ increases with AR but decreases with λ. However, even for $\alpha^{(E)}/\alpha^{(w)} = 0$, σ is very small in the range of AR and λ of interest to G.E.W. designers and is much smaller than $\sigma^{(w)}$.

Calculations of $\bar{C}_L$ for closed configurations tested in the 8 ft. x 6 ft. wind tunnel were made by using the theory, suitably modified to include chordwise camber, thickness and non-linear effects. The results thereby obtained were found to be in substantially better agreement with experiment than the linearized version of the theory. It was evident, however, that both theories overestimate negatively the incidence of the wing for zero lift. It was suggested that this could be due to the approximations made regarding the thickness-induced normal velocity at the configuration. Future work should be aimed at improving this feature of the theory.

The prediction of the theory that $\bar{C}_L$ is linearly dependent on end-plate incidence was adequately confirmed by experiment. Also the results obtained from the 'non-linear' theory for $\partial\bar{C}_L/\partial\alpha_b^{(E)}$ were found to be in reasonable accord with experiment in the cases examined.

The linearized theory was found to be in reasonable agreement with experimentally-deduced circulation distributions in its predictions of combinations of wing and end plate incidences yielding sensibly zero overall induced drag.

Chordwise circulation distributions obtained from experiment indicate that the vortex distribution employed in the linearized theory is representative over the majority of the wing part of the configuration. However, in one case ($l_p/c = 0.167$, $\alpha^{(w)} = 2^\circ$, $\alpha_b^{(E)} = 9^\circ$) this type of distribution was found to be unsuitable in the region of the end plates.

An experimental drag analysis and the linearized theory were found to agree insofar as they both predict that when there is a large inviscid drag acting on the wing the end plates give an almost equal inviscid thrust and vice versa. On the other hand, the quantitative agreement between the analysis and the theory is not particularly good and suggestions have been made for the possible

reasons for this.

Of particular significance is the conclusion of the drag analysis that in certain cases it is important to ensure that the end plates can sustain the required inviscid thrust. Failure to do this could result in a significant increase in the overall drag.

3. Experimental technique

The image technique was employed to simulate the presence of a water surface on the flow round a G.E.W. This technique is not completely representative but the justification for its use was based on the argument that provided that it gave a steady plane of symmetry it could be used to check the accuracy of many features of the theories. It has been held by some authors, however, that the method fails to represent a steady plane of symmetry. Nevertheless, the indications of this investigation were that for the configurations examined the flow round the wing and image was symmetrical.

It remains a task for the future to examine the importance of such effects as the deformation of the water surface and the interaction between the dynamic condition at the water surface and the viscosity of the fluids. A particularly suitable device for achieving this is the whirling arm, currently being developed at The College of Aeronautics by Kumar (1967). It is also hoped to use this apparatus in the near future to examine the non-steady behaviour of ground-effect wings.

REFERENCES

Ando, S., Miyashita, J. and Terai, K. (1964). Summary of the model tests for simple ram wing KAG - 3. Proc. Hovercraft Symposium, Swansea University College.

Ando, S. (1966). An idealised ground effect wing. Aeronaut. Quart. 17, 53.

Alexander, A.J. (1961). The aerodynamic characteristics of the jet wing and its application to high speed aircraft. Thesis. London University.

Bagley, J.A. (1960). The pressure distribution on two-dimensional wings near the ground. R.A.E. Rep. Aero. 2625.

Brown, E.S. (1938). Wind tunnel interference on ground effect. Rep. Memor. aero. Res. Coun., Lond. 1865.

Byrd, P.F. and Friedman, M.D. (1954). Handbook of elliptic integrals for engineers and physicists. Springer-Verlag. Berlin.

Carter, A.W. (1961). Effect of ground proximity on the aerodynamic characteristics of aspect-ratio-1 aerofoils with and without end plates. N.A.S.A. Tech. Note D - 970.

Dwight, H.B. (1961). Tables of integrals and other mathematical data. Macmillan, New York.

Fink, M.P. and Lastinger, J.L. (1961). Aerodynamic characteristics of low-aspect-ratio wings in close proximity to the ground. N.A.S.A. Tech. Note D - 926.

Flax, A.H. (1950). On a variational principle in lifting-line theory. J. aero. Sci. 17, 596.

Gates, S.B. (1928). An analysis of a rectangular monoplane with hinged tips. Rep. Memor. aero. Res. Coun., Lond. 1175.

Glauert, H. (1926). The elements of aerofoil and airscrew theory. Cambridge University Press.

Goldstein, S. (Editor). (1938). Modern developments in fluid dynamics. Clarendon Press, Oxford.

Haller, P. de (1936). La portance et la traînée induite minimum d'une aile au voisinage du sol. Mitt. Inst. Aerodyn. Zurich, 5, 99.

Heaslet, M.A. and Lomax, H. (1955). Supersonic and transonic small perturbation theory. Section D in Vol. VI of High speed aerodynamics and jet propulsion, Oxford University Press.

Hoerner, S.F. (1951). Aerodynamic drag. Published by Hoerner.

Jones, B.M. (1936). Measurement of profile drag by the pitot traverse method. Rep. Memor. aero. Res. Coun.,Lond. 1688.

Jones, R.T. (1946). Properties of low-aspect-ratio pointed wings at speeds below and above the speed of sound. Rep. nat. adv. Comm. Aero., Wash. 835.

Jones, R.T. (1951). The minimum drag of thin wings in frictionless flow. J. aero. Sci. 18, 75.

Jones, R.T. and Cohen, D. (1957).
High speed wing theory. Section A in Vol. VII of High speed aerodynamics and jet propulsion, Oxford University Press.

Karman, Th. von and Burgers, J.M. (1935).
General aerodynamic theory-perfect fluids. Section E in Durand, W.F. (1935). Aerodynamic Theory 2. Springer-Verlag, Berlin.

Küchemann, D. (1952). A simple method for calculating the span and chordwise loading on straight and swept wings of any given aspect ratio at subsonic speeds. Rep. Memor. aero. Res. Coun., Lond. 2935.

Kumar, P. (1967). The College of Aeronautics whirling arm initial tests. Coll. Aero. Cranfield. Note Aero. 174.

Lawrence, H.R. (1951). The lift distribution on low aspect ratio wings at subsonic speeds. J. aero. Sci. 18, 683.

Multhopp, H. (1950). Methods for calculating the lift distribution of wings (subsonic lifting-surface theory). Rep. Memor. aero. Res. Coun., Lond. 2884.

Munk, M.M. (1921). The minimum induced drag of aerofoils. Rep. nat. adv. Comm. Aero., Wash. 121.

Pankhurst, R.C. and Holder, D.W. (1952).
Wind-tunnel technique. Pitman, London.

Robinson, A. and Laurmann, J.A. (1956).
Wing theory. Cambridge University Press.

Rosenhead, L. (Editor). (1963).
Laminar boundary layers. Clarendon Press, Oxford.

Saunders, G.H. (1963). Aerodynamic characteristics of wings in ground proximity. Thesis. Mass. Inst. Tech.

Sievers, A. de (1965). Étude en soufflerie de l'effet de sol. O.N.E.R.A. Tech. Note 87.

Strand, T. (1960). On V.R.C. channel G.E.M. concept. Unpublished paper presented at G.E.M. contractors meeting at Washington.

Strand, T., Royce, W.W. and Fujita, T. (1962).
The cruise performance of channel-flow ground effect machines. J. Aerospace Sci. 29, 702.

Thwaites, B. (Editor). (1960).
Incompressible aerodynamics. Clarendon Press, Oxford.

Weber, J. (1954). The effect of aspect ratio on the chordwise load distribution of flat and cambered rectangular wings. Rep. aero. Res. Coun., Lond. 17522.

Werlé, H. (1963). Simulation de l'effet de sol au tunnel hydrodynamic. O.N.E.R.A. La Recherche Aérospatiale 95.

Wieghardt, K. (1940). Chordwise load distribution of a simple rectangular wing. Tech. Memor. nat. adv. Comm. Aero., Wash. 963.

Wieselsberger, C. (1921). Über den Flugwiderstand in der Nähe des Boden. Zeitschrift für Flugtechnik u. Motorluftschiffahrt. 10, 145.

Woods, L.C. (1961). The theory of subsonic plane flow. Cambridge University Press.

Young, A.D. (1948). Note on a method of measuring profile drag by means of an integrating comb. Rep. Memor. aero. Res. Coun., Lond. 2257.

Ziller, F. (1940). Beitrag zur Theorie des Tragflügels von endlicher Spanweite. Ingen.-Arch. 11, 239.

APPENDIX I : Evaluation of the limit of the residual

An examination of equations (II.2.30) and (II.2.37) shows that the first multiple integral inside the limit sign of equation (II.2.37) may be written as

$$I_1 = \varepsilon \int_0^1 \frac{(1-\varepsilon\eta_1)d\eta_1}{(2\eta_1-\varepsilon\eta_1^2)^{\frac{1}{2}}} \int_0^1 \frac{d\eta}{(2\eta-\varepsilon\eta^2)^{\frac{1}{2}}} \frac{\partial}{\partial y_1} \int_{-b/2}^{+b/2} \frac{c(y)f(2y/b)}{(y_1-y)} \cdot$$

$$\cdot \frac{\left[\{c(y_1)(1-\varepsilon\eta_1) - c(y)(1-\varepsilon\eta)\}^2 + 4(y_1-y)^2\right]^{\frac{1}{2}} dy}{\{c(y_1)(1-\varepsilon\eta_1) - c(y)(1-\varepsilon\eta)\}}.$$

Therefore

$$I_1 \sim \frac{\varepsilon}{2} \int_0^1 \frac{d\eta_1}{\eta_1^{\frac{1}{2}}} \int_0^1 \frac{d\eta}{\eta^{\frac{1}{2}}} \frac{\partial}{\partial y_1} \int_{-b/2}^{+b/2} \frac{c(y)f(2y/b)}{(y_1-y)} \cdot$$

$$\cdot \frac{\{(c(y_1) - c(y))^2 + 4(y_1-y)^2\}^{\frac{1}{2}} dy}{\{c(y_1)(1-\varepsilon\eta_1) - c(y)(1-\varepsilon\eta)\}}, \quad \varepsilon \to 0.$$

It is apparent that as $\varepsilon \to 0$ an increasingly large contribution to I_1 comes from the y integrand in the near vicinity of $y = y_1$. This suggests the possibility of simplifying the integrand by expanding the term $c(y)$ in powers of $(y-y_1)$ to yield the result

$$I_1 \sim \varepsilon \int_0^1 \frac{d\eta_1}{\eta_1^{\frac{1}{2}}} \int_0^1 \frac{d\eta}{\eta^{\frac{1}{2}}} \frac{\partial}{\partial y_1} \int_{-b/2}^{+b/2} \frac{c(y_1)f(2y/b)|y_1-y|}{(y_1-y)} \cdot$$

$$\cdot \frac{\left[\{1 + \frac{1}{4}(dc(y_1)/dy_1)^2\}^{\frac{1}{2}} + O(y_1-y)\right] dy}{\{c(y_1)(1-\varepsilon\eta_1) - c(y)(1-\varepsilon\eta)\}}, \quad \varepsilon \to 0.$$

An examination of the term $O(y_1-y)$ in the above expression indicates that it contributes a term $O(\varepsilon)$ (at most) compared with I_1 except possibly for isolated values of y_1. Therefore this term is neglected, leaving the first term of the expansion to be integrated. This is best performed with the aid of the result

$$\frac{\partial F}{\partial y}(u,y,\varepsilon,\eta,\eta_1) = \frac{f(2y/b)}{\{c(y_1)(1-\varepsilon\eta_1) - c(y)(1-\varepsilon\eta)\}}, \qquad \text{(AI.1)}$$

where $u = y - y_1$.

By employing this information, the necessary y integration may be performed to yield the expression

$$I_1 \sim \varepsilon \int_0^1 \frac{d\eta_1}{\eta_1^{\frac{1}{2}}} \int_0^1 \frac{d\eta}{\eta^{\frac{1}{2}}} \frac{\partial}{\partial y_1}\left[c(y_1)\{1 + \frac{1}{4}(\frac{dc(y_1)}{dy_1})^2\}^{\frac{1}{2}}\{ - F(b/2-y_1, b/2, \varepsilon, \eta, \eta_1) + \right.$$

$$\left. + 2F(0, y_1, \varepsilon, \eta, \eta_1) - F(-b/2-y_1, b/2, \varepsilon, \eta, \eta_1)\}\right] . \qquad \text{(AI.2)}$$

An inspection of the form of $F(u,y,\varepsilon,\eta,\eta_1)$ indicates that the contribution to I_1 multiplied by the quantity

$\frac{\partial}{\partial y_1}\left[c(y_1)\{1 + \frac{1}{4}(\frac{dc(y_1)}{dy_1})^2\}^{\frac{1}{2}}\right]$ is at most $O(\varepsilon \ln \varepsilon)$ except possibly for isolated values of y_1. Also, the terms multiplied by $\partial F(b/2-y_1, b/2, \varepsilon, \eta, \eta_1)/\partial y_1$ and $\partial F(-b/2-y_1, b/2, \varepsilon, \eta, \eta_1)/\partial y_1$ contribute at most $O(\varepsilon)$ to I_1, again except perhaps for certain discrete values of y_1. Therefore, by noting from equation (AI.1) that

$$\frac{\partial F}{\partial y_1}(0, y_1, \varepsilon, \eta, \eta_1) = \frac{f(2y_1/b)}{\varepsilon\, c(y_1)(\eta-\eta_1)} ,$$

it is possible to deduce from equation (AI.2) the result

$$I_1 \sim 2f(2y_1/b)\{1 + \frac{1}{4}(\frac{dc(y_1)}{dy_1})^2\}^{\frac{1}{2}} \int_0^1 \frac{d\eta_1}{\eta_1^{\frac{1}{2}}} \int_0^1 \frac{d\eta}{\eta^{\frac{1}{2}}(\eta-\eta_1)} , \qquad \varepsilon \to 0.$$

A similar analysis applied to the second multiple-integral term inside the limit sign of equation (II.2.37),

$$I_2 = -\varepsilon \int_0^1 \frac{d\eta}{(2\eta-\varepsilon\eta^2)^{\frac{1}{2}}} \int_0^1 \frac{(1-\varepsilon\eta_1)d\eta_1}{(2\eta_1-\varepsilon\eta_1^2)^{\frac{1}{2}}} \frac{\partial}{\partial y_1} \int_{-b/2}^{+b/2} \frac{c(y)f(2y/b)}{(y_1-y)} \cdot$$

$$\cdot \frac{[\{c(y_1)(1-\varepsilon\eta_1) - c(y)(1-\varepsilon\eta)\}^2 + 4(y_1-y)^2]^{\frac{1}{2}}dy}{c(y_1)(1-\varepsilon\eta_1) - c(y)(1-\varepsilon\eta)} ,$$

yields the result

$$I_2 \sim -2\, f(2y_1/b)\{1 + \frac{1}{4}(\frac{dc(y_1)}{dy_1})^2\}^{\frac{1}{2}} \int_0^1 \frac{d\eta}{\eta^{\frac{1}{2}}} \int_0^1 \frac{d\eta_1}{\eta_1^{\frac{1}{2}}(\eta-\eta_1)}, \qquad \varepsilon \to 0.$$

Hence, by replacing I_1 and I_2 in equation (II.2.37) with the above asymptotic forms and taking the limit, is is found that

$$R_1(y_1) = \frac{a_o^{(e)} a_o^{(o)} U_o^2\, c(y_1) f^2(2y_1/b)}{4\pi}\{1 + \frac{1}{4}(\frac{dc(y_1)}{dy_1})^2\}^{\frac{1}{2}} \int_0^1 \frac{d\eta_1}{\eta_1^{\frac{1}{2}}} \int_0^1 \frac{d\eta}{\eta^{\frac{1}{2}}(\eta-\eta_1)}.$$

APPENDIX II : Evaluation of integrals for the variational equation

Consider, first, the quantities $P_m^{(w)}$ and $P_m^{(E)}$. By combining equations (II.5.5), (II.5.18) and (II.5.21) it is possible to obtain the results

$$\left.\begin{aligned} P_m^{(w)} &= 4m\left(\frac{2}{b}\right)^{2m-1}(2m-1)!\int_{-b/2}^{+b/2}\sum_{n=1}^{n=m}\frac{(-1)^n y^{2n-1} y^{2(m-n)}}{\{2(m-n)\}!(2n-1)!\,b}\,dy\,; \\ P_m^{(E)} &= 8m(2m-1)!\int_0^{\ell}\sum_{n=o}^{n=m-1}\frac{(-1)^n (2z/b)^{2n}}{\{2(m-n)-1\}!(2n)!\,b}\,dz\,. \end{aligned}\right\}\ (m > o)$$

Therefore, on the assumption that it is permissible to interchange the order of the integration and summation in these expressions, it is found that

$$\left.\begin{aligned} P_m^{(w)} &= 4m(2m-1)!\sum_{n=1}^{n=m}\frac{(-1)^n (2\ell/b)^{2n-1}}{\{2(m-n)\}!\,(2n-1)\,!\,\{2(m-n)+1\}}\,; \\ P_m^{(E)} &= 4m(2m-1)!\sum_{n=o}^{n=m-1}\frac{(-1)^n (2\ell/b)^{2n+1}}{\{2(m-n)-1\}\,!\,(2n)!\,(2n+1)}\,. \end{aligned}\right\}\ (m > o)^*$$

By a similar process, the quantities $Q_{mn}^{(w)}$ and $Q_{mn}^{(E)}$ are found to be given by

$$\left.\begin{aligned} Q_{mn}^{(w)} &= 16\,mn\,(2m-1)\,!\,(2n-1)\,!\sum_{i=1}^{i=m}\sum_{j=1}^{j=n} \\ &\qquad \frac{(-1)^{i+j}(2\ell/b)^{2(i+j-1)}}{\{2(m-i)\}!(2i-1)!\{2(n-j)\}!(2j-1)!\{2(m+n-i-j)+1\}}\,; \\ Q_{mn}^{(E)} &= 16\,mn\,(2m-1)\,!\,(2n-1)\,!\sum_{i=o}^{i=m-1}\sum_{j=o}^{j=n-1} \\ &\qquad \frac{(-1)^{i+j}(2\ell/b)^{2(i+j)+1}}{\{2(m-i)-1\}!(2i)!\{2(n-j)-1\}!(2j)!\{2(i+j)+1\}}\,. \end{aligned}\right\}\ (m,n > o)^*$$

*It is also evident that $P_o^{(w)} = P_o^{(E)} = Q_{on}^{(w)} = Q_{on}^{(E)} = 0$ for $n = 0,1,2\ldots$

By combining equations (II.5.14), (II.5.19) and (II.5.21) it is found that $R_m^{(w)}$ and $R_m^{(E)}$ may, for $m < 4$, be written as follows:

$$\left.\begin{aligned}
R_o^{(w)} &= \int_{-b/2}^{+b/2} dy/b \;;\quad R_o^{(E)} = 2\int_o^{l} dz/b;\\
R_1^{(w)} &= \int_{-b/2}^{+b/2} t^2\, dy/b;\quad R_1^{(E)} = 2\int_o^{l} t^2\, dz/b;\\
R_2^{(w)} &= \int_{-b/2}^{+b/2} \{t^4-2k'^2t^2/k^2\}dy/b;\quad R_2^{(E)} = 2\int_o^{l} \{t^4-2k'^2t^2/k^2\}dz/b;\\
R_3^{(w)} &= \int_{-b/2}^{+b/2} \{t^6-3k'^2t^4/k^2+t^2(3-7k^2+4k^4)/k^4\}dy/b;\\
R_3^{(E)} &= 2\int_o^{l} \{t^6-3k'^2t^4/k^2+t^2(3-7k^2+4k^4)/k^4\}dz/b.
\end{aligned}\right\} \quad \text{(AII.1)}$$

The first two integrals of equation (AII.1) are easily evaluated to give the results

$$R_o^{(w)} = 1 \;;\quad R_o^{(E)} = 2l/b.$$

The remaining integrals, on the other hand, are not simple. However, they may be evaluated by employing transformation (I.2.3) and the result, which may be deduced from equation (II.5.6) by using transformation (I.2.3) and equation (I.2.4),

$$d\Omega/d2Ks = C(1 - sn^2 2Ks). \qquad \text{(AII.2)}$$

Thus, by noting that on the wing part of the vortex trace $dy/d2Ks \equiv d\Omega/d2Ks$, one obtains

$$R_1^{(w)} = (C/b)\{A_2 - A_4\} \;;$$

$$R_2^{(w)} = (C/b)\{A_4 - A_6 - 2k'^2(A_2 - A_4)/k^2\} \;;$$

$$R_3^{(w)} = \frac{C}{b}\{A_6 - A_8 - \frac{3k'^2}{k^2}(A_4 - A_6) + \frac{(3 - 7k^2 + 4k^4)}{k^4}(A_2 - A_4)\} ,$$

where $$A_m = \int_{-K}^{+K} sn^m 2Ks \; d2Ks, \quad m = 0, 1, 2, 3, \ldots$$

This type of integral is considered by Byrd and Friedman (1954) whose results (p.p. 191 - 192) enable one to derive the expressions

$$A_o = 2K \; ; \quad A_2 = 2\{K - E(K)\}/k^2 \; ;$$

$$A_{2n+2} = \{2n(1+k^2)A_{2n} + (1-2n)A_{2n-2}\}/(2n+1)k^2 ,$$
$$n = 1, 2, 3, \ldots .$$

Thus, by employing this information in combination with equations (II.5.8) and (II.5.9), it is possible to evaluate $R_m^{(w)}$ for a given $2\ell/b$.

By observing that $dz/d2Ks \equiv Im(d\Omega/d2Ks)$ it may be concluded from equations (AII.1), (AII.2) and transformation (I.2.3) that

$$R_1^{(E)} = (C/b)\{\bar{A}_4 - \bar{A}_2\} \; ;$$

$$R_2^{(E)} = (C/b)\{\bar{A}_6 - \bar{A}_4 - 2k'^2(\bar{A}_4 - \bar{A}_2)\} \; ;$$

$$R_3^{(E)} = \frac{C}{b}\{\bar{A}_8 - \bar{A}_6 - \frac{3k'^2}{k^2}(\bar{A}_6 - \bar{A}_4) + \frac{(3 - 7k^2 + 4k^4)}{k^4}(\bar{A}_4 - \bar{A}_2)\} .$$

Here

$$\bar{A}_m = Im\{\int_K^{K+iK'} sn^m 2Ks \; d2Ks\} , \quad m = 0, 1, 2, 3, \ldots . .$$

Again it is possible to employ results given by Byrd and Friedman on pages 191 and 192 to obtain the expressions

$$\bar{A}_o = K' \; ; \quad \bar{A}_2 = E'(K)/k^2 \; ;$$

$$\bar{A}_{2n+2} = \{2n(1+k^2)\bar{A}_{2n} + (1-2n)\bar{A}_{2n-2}\}/(2n+1)k^2, \quad n = 1, 2, 3, \ldots . .$$

Therefore $R_m^{(E)}$ may be evaluated for a given $2\mathfrak{l}/b$ by using these expressionsin conjunction with equations (II.5.8) and (II.5.9).

The method used to determine $S_{mn}^{(w)}$ and $S_{mn}^{(E)}$ is essentially the same as that employed to determine $R_m^{(w)}$ and $R_m^{(E)}$. Therefore only the results will be quoted ($m,n < 4$). These are as follows:

$$S_{01}^{(w)} = R_1^{(w)}; \quad S_{01}^{(E)} = R_1^{(E)};$$

$$S_{02}^{(w)} = R_2^{(w)}; \quad S_{02}^{(E)} = R_2^{(E)};$$

$$S_{03}^{(w)} = R_3^{(w)}; \quad S_{03}^{(E)} = R_3^{(E)};$$

$$S_{11}^{(w)} = CT_4/b; \quad S_{11}^{(E)} = C\overline{T}_4/b;$$

$$S_{12}^{(w)} = (C/b)\{T_6 - 2k'^2 T_4\}; \quad S_{12}^{(E)} = (C/b)\{\overline{T}_6 - 2k'^2\overline{T}_4\};$$

$$S_{13}^{(w)} = (C/b)\{T_8 - 3k'^2 T_6/k^2 + (3-7k^2+4k^4)T_4/k^4\};$$

$$S_{13}^{(E)} = (C/b)\{\overline{T}_8 - 3k'^2\overline{T}_6/k^2 + (3-7k^2+4k^4)\overline{T}_4/k^4\};$$

$$S_{22}^{(w)} = (C/b)\{T_8 - 4k'^2 T_6/k^2 + 4k'^4 T_4/k^4\};$$

$$S_{22}^{(E)} = (C/b)\{\overline{T}_8 - 4k'^2\overline{T}_6/k^2 + 4k'^4\overline{T}_4/k^4\};$$

$$S_{23}^{(w)} = \frac{C}{b}\{T_{10} - \frac{5k'^2}{k^2}T_8 + \frac{(9-19k^2+10k^4)}{k^4}T_6 - \frac{2k'^2}{k^6}(3-7k^2+4k^4)T_4\};$$

$$S_{23}^{(E)} = \frac{C}{b}\{\overline{T}_{10} - \frac{5k'^2}{k^2}\overline{T}_8 + \frac{(9-19k^2+10k^4)}{k^4}\overline{T}_6 - \frac{2k'^2}{k^6}(3-7k^2+4k^4)\overline{T}_4\};$$

$$S_{33}^{(w)} = \frac{C}{b}\{T_{12} - \frac{6k'^2}{k^2}T_{10} + \frac{(15-32k^2+17k^4)}{k^4}T_8 - \frac{6k'^2}{k^6}(3-7k^2+4k^4)T_6 + \frac{(3-7k^2+4k^4)^2}{k^8}T_4\};$$

$$S_{33}^{(E)} = \frac{C}{b}\{\overline{T}_{12} - \frac{6k'^2}{k^2}\overline{T}_{10} + \frac{(15-32k^2+17k^4)}{k^4}\overline{T}_8 - \frac{6k'^2}{k^6}(3-7k^2+4k^4)\overline{T}_6 +$$

$$+ \frac{(3-7k^2+4k^4)^2}{k^8}\overline{T}_4\} \ .$$

Here

$$T_m = A_m - A_{m+2} \ ; \qquad \overline{T}_m = \overline{A}_{m+2} - \overline{A}_m \ .$$

Also, it should be noted that

$$S_{mn}^{(w)} = S_{nm}^{(w)} \ ; \qquad S_{mn}^{(E)} = S_{nm}^{(E)} \ .$$

APPENDIX III : The flow velocity field of a closed, rectangular vortex distribution

The vortex distribution $\gamma(x_1)$ placed on the cylindrical surface of Fig. 18 may, when combined with the image distribution, be considered to be a chordwise distribution of elementary rectangular vortices of strength $\gamma(x_1)dx_1$. An example of such a vortex is shown in the figure at the end of this appendix. This figure also illustrates the notation and coordinate system required for the following analysis.

According to Robinson and Laurmann, (1956) the vectorial velocity $d\underset{\sim}{V}$ induced at the point P(x,y,z) by a vortex element of strength $\gamma(x_1)dx_1$ is given by

$$d\underset{\sim}{V} = \gamma(x_1)dx_1 \; d\underset{\sim}{s} \wedge \underset{\sim}{r}/4\pi \; r^3 \; .$$

Here ds is the length of the element which has a vortex vector in the direction of the unit vector $d\underset{\sim}{s}/ds$. Also

$$\underset{\sim}{r} = \underset{\sim}{i}(x-x_1) + \underset{\sim}{j}(y-y_1) + \underset{\sim}{k}(z-z_1),$$

where $\underset{\sim}{i}$, $\underset{\sim}{j}$, $\underset{\sim}{k}$ are unit vectors in the direction of the x,y,z axes and x_1, y_1, z_1 are the coordinates of the element.

Thus, by integrating the contributions of all the elements of the rectangular vortex, one finds that only the vortex segments AB and CD contribute to the upwash at P which is given by

$$dw(x,y,z) = \frac{\gamma(x_1)dx_1(x_1-x)}{4\pi}\left[\int_{-b/2}^{+b/2} \frac{dy_1}{\{(x_1-x)^2 + (y_1-y)^2 + (1-z)^2\}^{3/2}} + \right.$$

$$\left. + \int_{-b/2}^{+b/2} \frac{dy_1}{\{(x_1-x)^2 + (y_1-y)^2 + (1+z)^2\}^{3/2}}\right] .$$

Therefore, by performing the integration indicated in this expression and integrating the contributions of all the elementary vortices of the cylindrical surface, $(-c/2 \leq x_1 \leq c/2)$ it is found that the z-wash at the wing plane of the cylindrical surface is given by

$$w_f(\xi,\eta) \equiv w(x,y,\ell) = \frac{P}{4\pi}\int_{-1}^{+1}\gamma(\xi_1)\left(\frac{1}{\xi_1-\xi}\left[\frac{AR\,(1-\eta)}{\{AR^2(1-\eta)^2+(\xi_1-\xi)^2\}^{\frac{1}{2}}}+\right.\right.$$

$$\left.+\frac{AR\,(1+\eta)}{\{AR^2(1+\eta)^2+(\xi_1-\xi)^2\}^{\frac{1}{2}}}\right]+\frac{\xi-\xi_1}{(\xi_1-\xi)^2+4\lambda^2}\left[\right.$$

$$\left.\left.\frac{AR\,(1-\eta)}{\{AR^2(1-\eta)^2+(\xi_1-\xi)^2+4\lambda^2\}^{\frac{1}{2}}}+\frac{AR\,(1+\eta)}{\{AR^2(1+\eta)^2+(\xi_1-\xi)^2+4\lambda^2\}^{\frac{1}{2}}}\right]\right)d\xi_1. \qquad \text{(AIII.1)}$$

Here

$$\xi = 2x/c, \qquad \eta = 2y/b, \qquad \lambda = 2\ell/c, \qquad AR = b/c$$

and P denotes that the integral is to be interpreted according to the Cauchy principal value.

By symmetry considerations it may be deduced from equation (AIII.1) that the y-wash at the starboard end plate of the cylindrical surface is written as

$$v_f(\xi,\zeta) = \frac{P}{4\pi}\int_{-1}^{+1}\gamma(\xi_1)\left(\frac{1}{\xi_1-\xi}\left[\frac{\lambda(1-\zeta)}{\{\lambda^2(1-\zeta)^2+(\xi_1-\xi)^2\}^{\frac{1}{2}}}+\frac{\lambda(1+\zeta)}{\{\lambda^2(1+\zeta)^2+(\xi_1-\xi)^2\}^{\frac{1}{2}}}\right]+\right.$$

$$+\frac{\xi-\xi_1}{(\xi_1-\xi)^2+4AR^2}\left[\frac{\lambda(1-\zeta)}{\{\lambda^2(1-\zeta)^2+(\xi_1-\xi)^2+4AR^2\}^{\frac{1}{2}}}+\right.$$

$$\left.\left.+\frac{\lambda(1+\zeta)}{\{\lambda^2(1+\zeta)^2+(\xi_1-\xi)^2+4AR^2\}^{\frac{1}{2}}}\right]\right)d\xi_1, \qquad \text{(AIII.2)}$$

where $\zeta = z/\ell$.

It is a routine matter to write equations (AIII.1) and (AIII.2) in the form shown in Section II.5.3, that is equations (II.5.33).

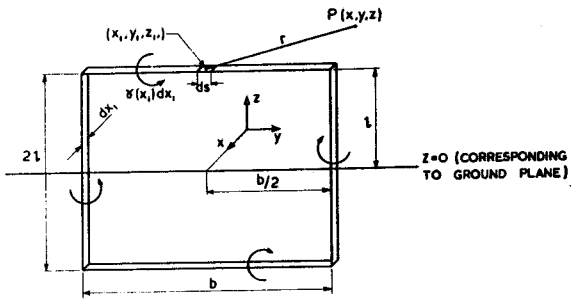

FIGURE FOR APPENDIX III. COORDINATE SYSTEM AND NOTATION USED IN THE DETERMINATION OF THE VELOCITY FIELD OF AN ELEMENTARY RECTANGULAR VORTEX.

AR	λ	β	
		EQU.^{n} (II. 3·6)	EQU^{n} (II.5·43)
1·000	0·101	4·698	4·680
1·000	0·191	2·871	2·905
1·000	0·253	2·437	2·474
2·000	0·119	3·952	3·900
2·000	0·201	2·666	2·683
2·000	0·313	2·062	2·081
3·000	0·179	2·850	2·852
3·000	0·302	2·059	2·074
3·000	0·573	1·540	1·549
4·000	0·283	2·339	2·350
4·000	0·402	1·759	1·768
4·000	0·626	1·468	1·474

TABLE 1. THE PARAMETER β OF A CLOSED WING / END-PLATE CONFIGURATION.

$\alpha_{(W)}^{\circ}$	$\alpha_{b}^{(E)\circ}$	$\bar{C}_{DB}^{(W)}$ EQ.(III.4·4)	$\bar{C}_{DB}^{(E)}$ EQ.(III.4·5)	THEORETICAL $\bar{C}_{Di}$	ESTIMATED $\bar{C}_{D}$	MEASURED $\bar{C}_{D}$
2	0	0·0093	0·0007	0·0003	0·0103	0·0110
5	0	0·0107	0·0008	0·0012	0·0127	0·0134
8	0	0·0136	0·0009	0·0022	0·0167	0·0151 (0·0164)
2	3	0·0097	0·0008	0·0000	0·0105	0·0109
5	3	0·0113	0·0008	0·0004	0·0125	0·0136
8	3	0·0143	0·0010	0·0006	0·0159	0·0151 (0·0160)
2	6	0·0102	0·0008	0·0006	0·0116	0·0113
5	6	0·0122	0·0009	0·0000	0·0131	0·0136
8	6	0·0152	0·0011	0·0003	0·0166	0·0149 (0·0160)
2	9	0·0105	0·0008	0·0021	0·0134	0·0115
5	9	0·0125	0·0009	0·0004	0·0138	0·0139
8	9	0·0163	0·0011	0·0000	0·0174	0·0164

TABLE 2. A COMPARISON BETWEEN THE ESTIMATED AND MEASURED OVERALL-DRAG COEFFICIENT OF THE CONFIGURATION; $l_p/c = h_p/c = 0·167$; $R_c = 1·26 \times 10^{6}$

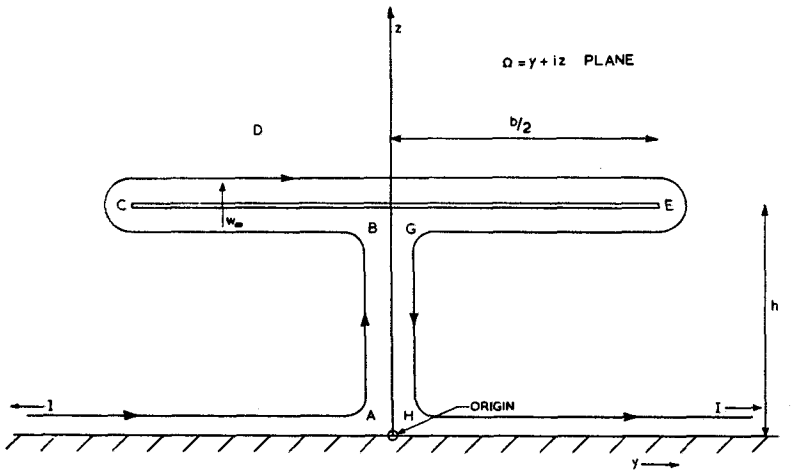

FIG.1. THE TREFFTZ PLANE OF A PLANAR GROUND-EFFECT WING.

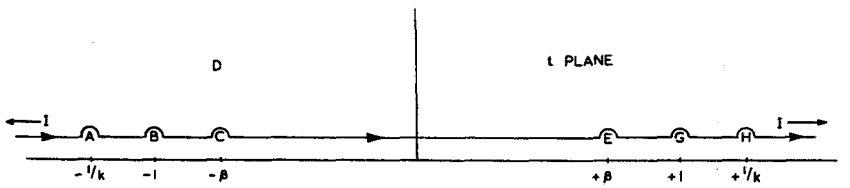

FIG 2. UPPER HALF-PLANE t FOR A PLANAR GROUND-EFFECT WING.

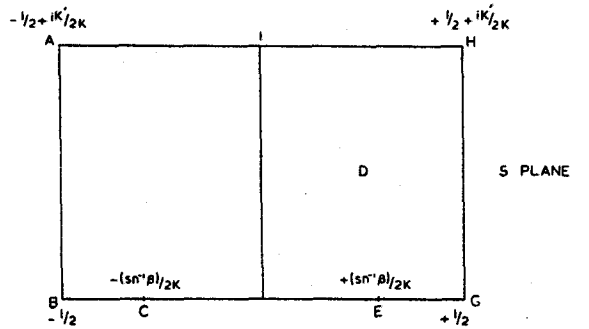

FIG.3. RECTANGULAR S PLANE FOR A PLANAR GROUND-EFFECT WING.

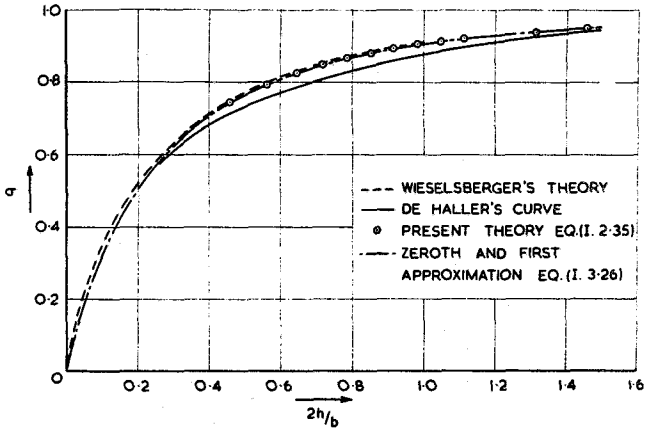

FIG. 4. THE INDUCED-DRAG FACTOR OF A PLANAR GROUND-EFFECT WING.

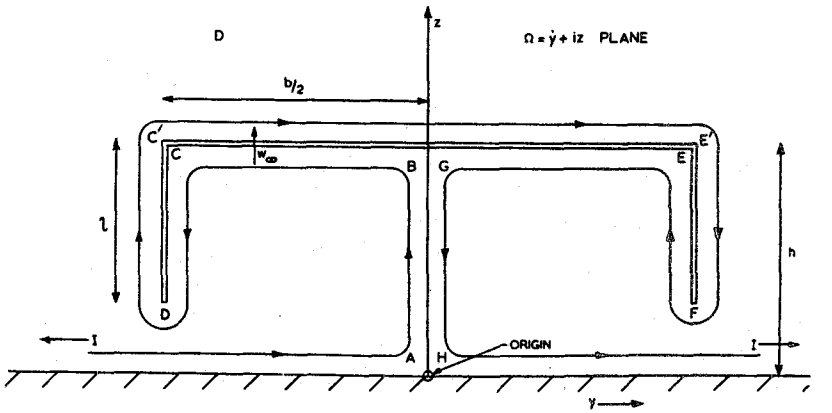

FIG. 5. THE TREFFTZ PLANE OF A PLANAR GROUND-EFFECT WING WITH LOWER VERTICAL END PLATES.

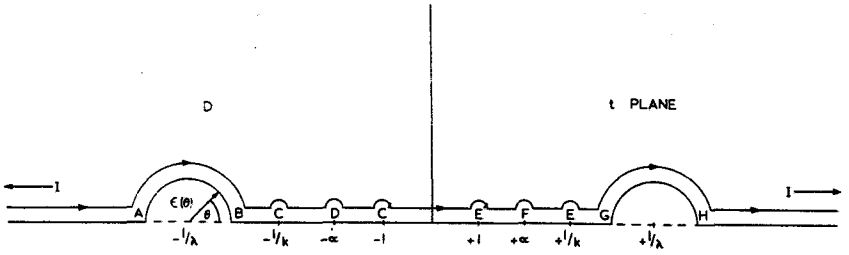

FIG. 6. PERTURBED UPPER HALF-PLANE t FOR A PLANAR GROUND-EFFECT WING WITH LOWER VERTICAL END PLATES.

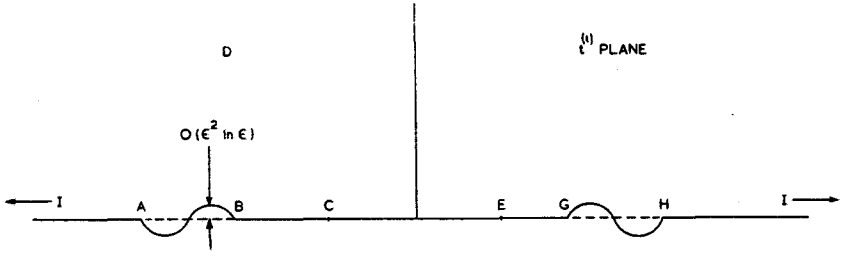

FIG. 7. THE FIRST APPROXIMATION TO AN EXACT UPPER HALF-PLANE FOR A PLANAR WING.

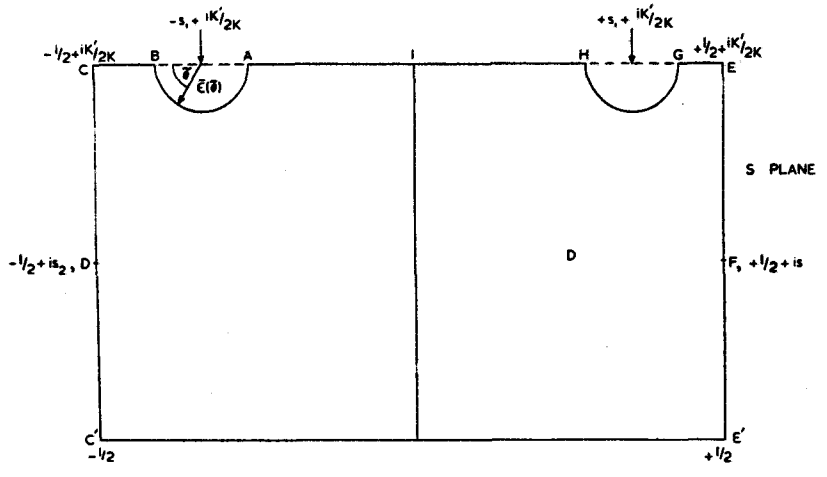

FIG. 8. PERTURBED RECTANGULAR S PLANE FOR A PLANAR GROUND-EFFECT WING WITH LOWER VERTICAL END PLATES.

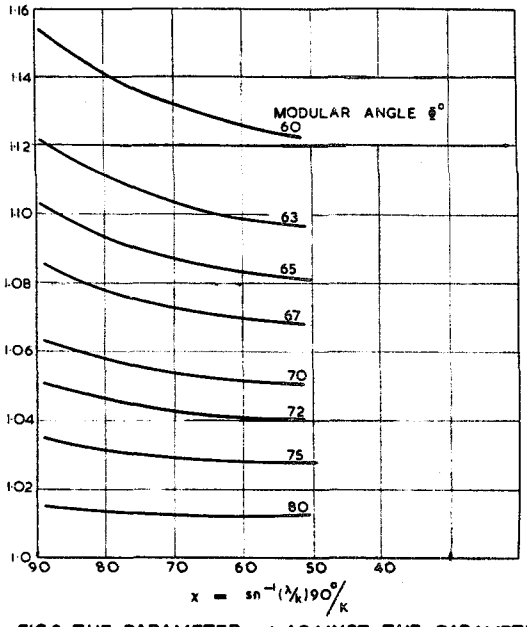

FIG 9. THE PARAMETER α AGAINST THE PARAMETER X FOR VARIOUS MODULAR ANGLES.

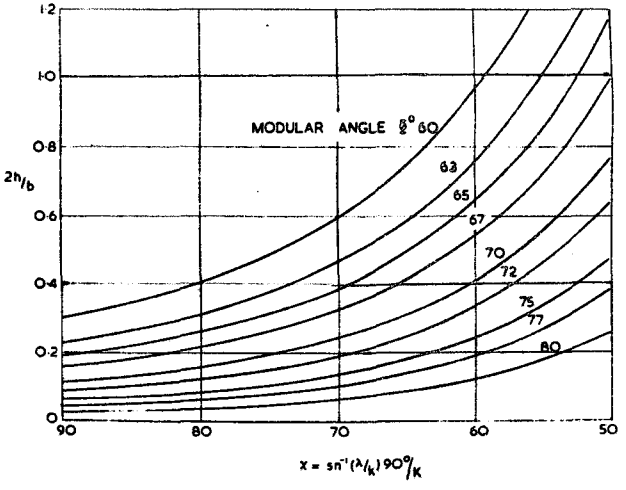

FIG.10. $2h/b$ AGAINST THE PARAMETER X FOR VARIOUS MODULAR ANGLES.

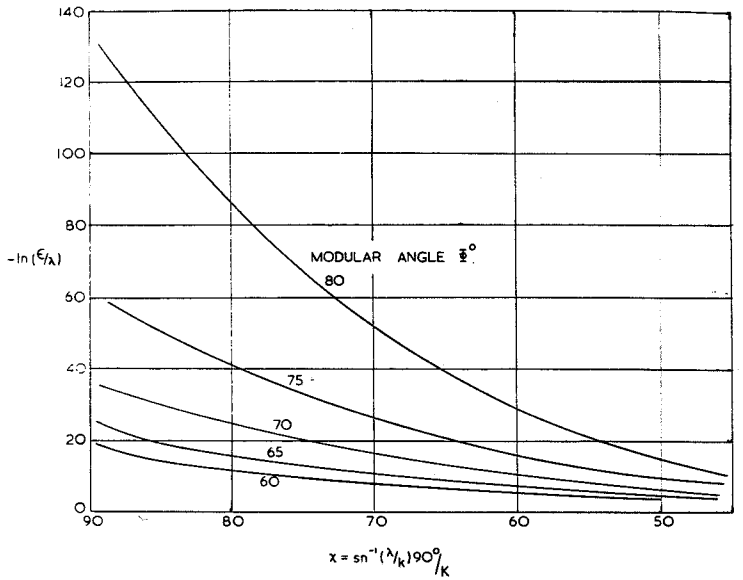

FIG.11. $\ln(\epsilon/\lambda)$ AGAINST THE PARAMETER X FOR VARIOUS MODULAR ANGLES.

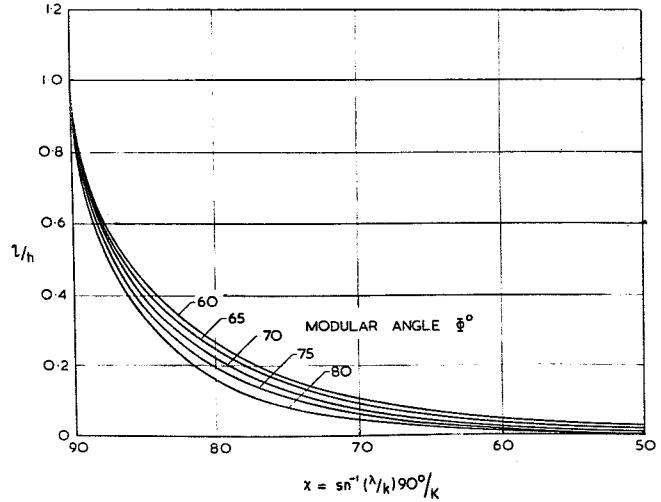

FIG.12. ℓ/h AGAINST THE PARAMETER X FOR VARIOUS MODULAR ANGLES.

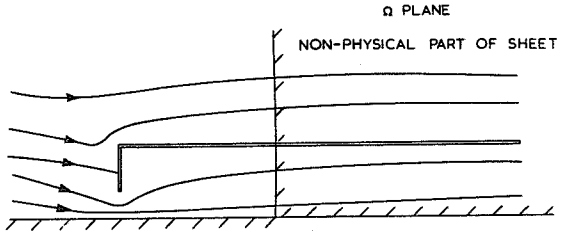

FIG. 13. THE APPROXIMATE FORM OF THE SOURCE-DISTRIBUTION FLOW FOR SMALL h/b.

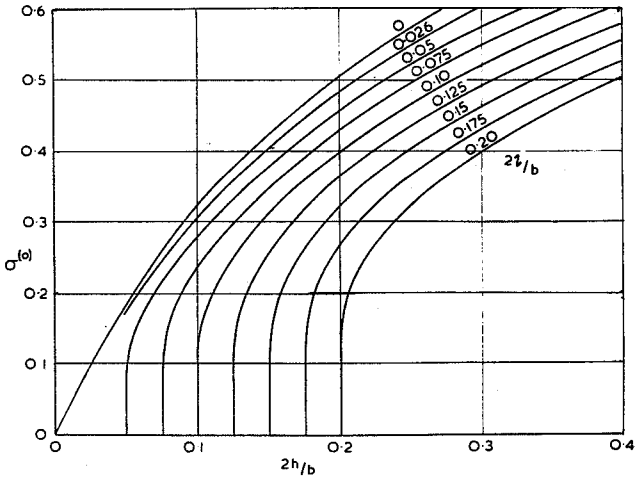

FIG. 14. THE MINIMUM INDUCED DRAG FACTOR OF A PLANAR WING WITH LOWER VERTICAL END PLATES AS A FUNCTION OF $2h/b$ FOR VARIOUS VALUES OF $2\ell/b$.

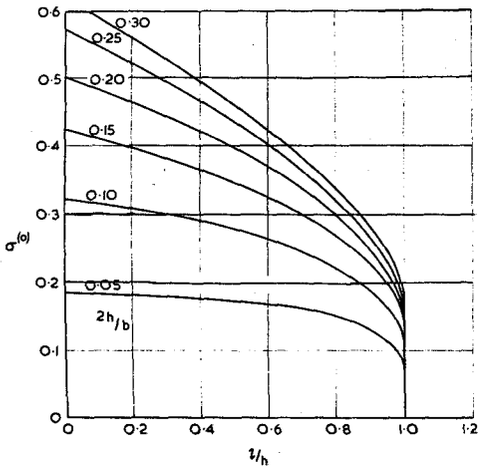

FIG.15. THE MINIMUM INDUCED DRAG FACTOR OF A PLANAR WING WITH LOWER VERTICAL END PLATES AS A FUNCTION OF l/h FOR VARIOUS $2h/b$.

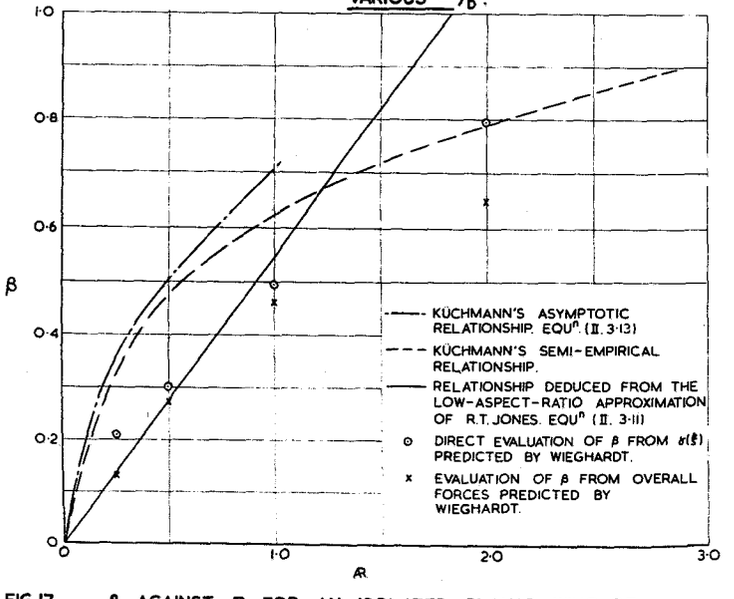

FIG.17. β AGAINST AR FOR AN ISOLATED PLANAR WING OF RECTANGULAR PLANFORM.

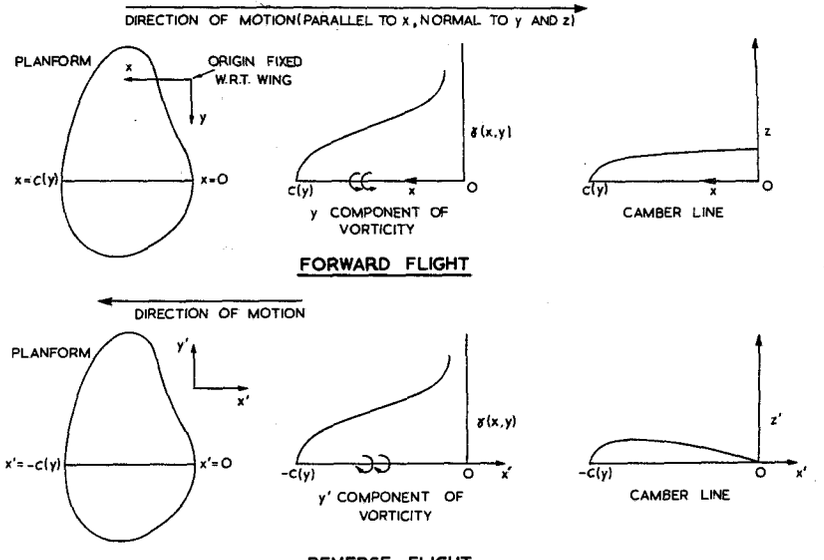

FIG. 16. NOTATION AND COORDINATE SYSTEMS OF AN ISOLATED PLANAR WING OF ARBITRARY PLANFORM.

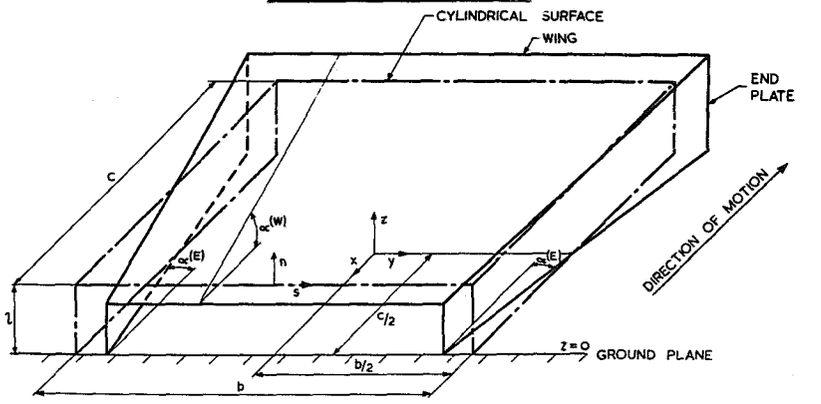

FIG. 18. NOTATION AND COORDINATE SYSTEM OF THE CHORDAL SURFACE OF A CLOSED PLANAR-WING / END-PLATE CONFIGURATION.

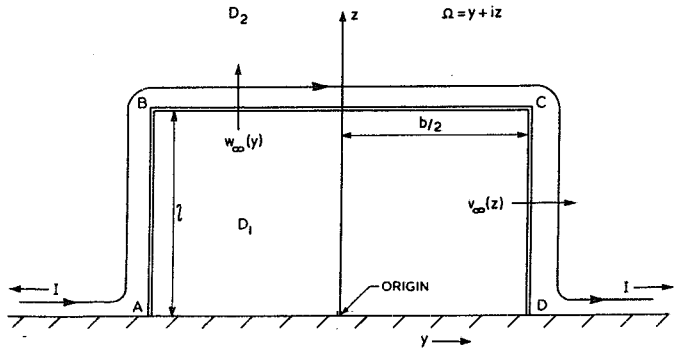

FIG.19. THE TREFFTZ PLANE OF A CLOSED PLANAR-WING AND END-PLATE CONFIGURATION.

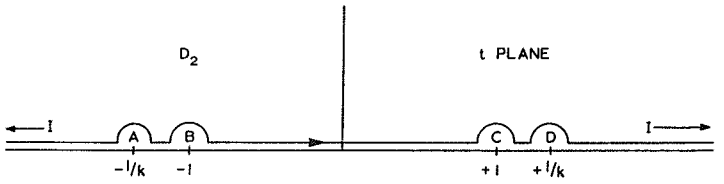

FIG. 20. THE DOMAIN D_2 OF THE TREFFTZ PLANE TRANSFORMED TO THE UPPER HALF-PLANE t.

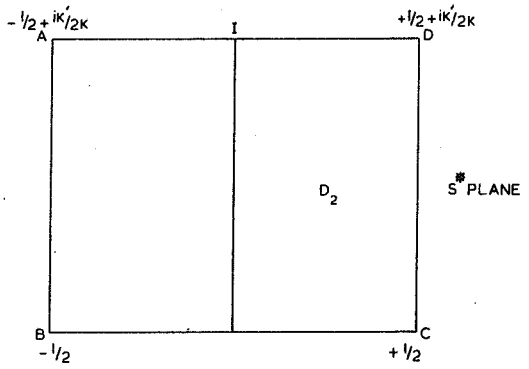

FIG.21. THE DOMAIN D_2 OF THE TREFFTZ PLANE TRANSFORMED TO THE S^*PLANE.

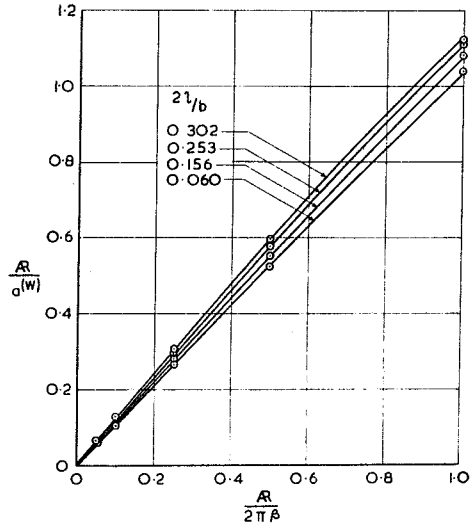

FIG. 22. THE LIFT DERIVATIVE $a^{(W)}$ OF A CLOSED WING/END-PLATE CONFIGURATION.

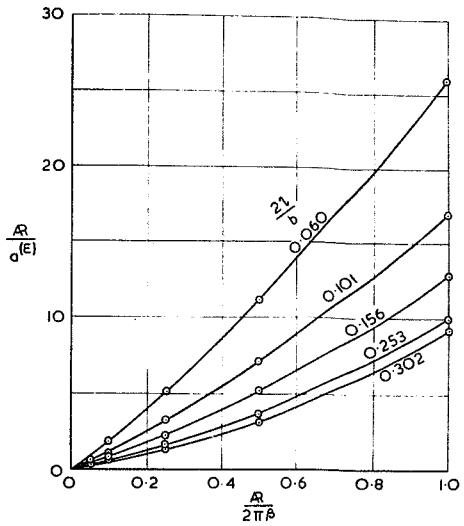

FIG. 23. THE LIFT DERIVATIVE $a^{(E)}$ OF A CLOSED WING/END-PLATE CONFIGURATION.

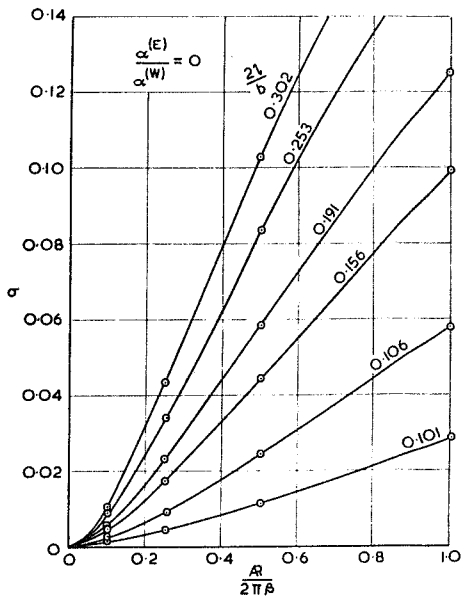

FIG. 24. INDUCED-DRAG FACTOR OF A CLOSED WING / END-PLATE CONFIGURATION.

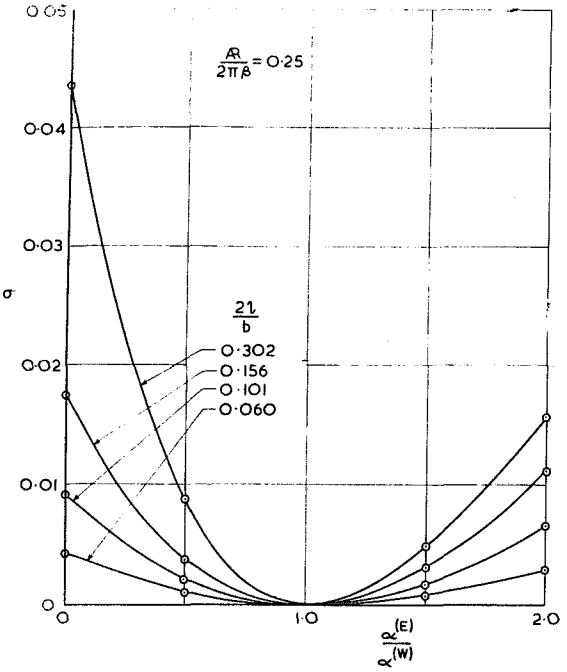

FIG. 25. INDUCED-DRAG FACTOR OF A CLOSED WING / END-PLATE CONFIGURATION.

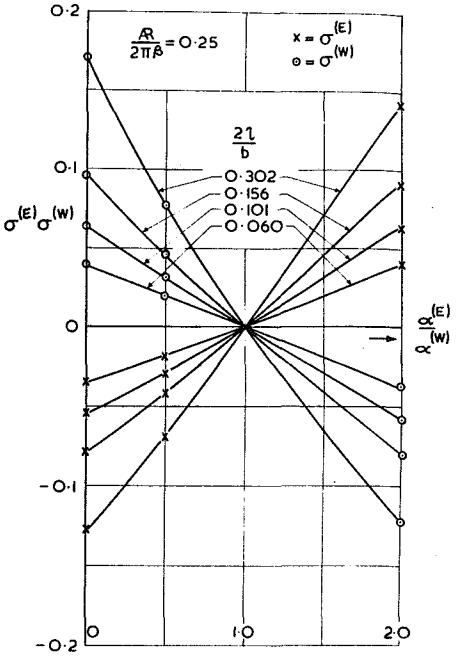

FIG. 26. INDUCED-DRAG FACTORS OF A CLOSED WING/END-PLATE CONFIGURATION.

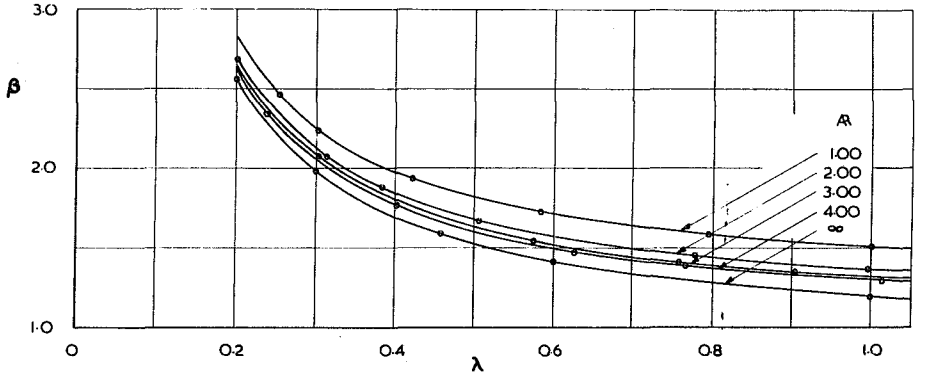

FIG 27. THE PARAMETER β OF A CLOSED WING / END-PLATE CONFIGURATION.

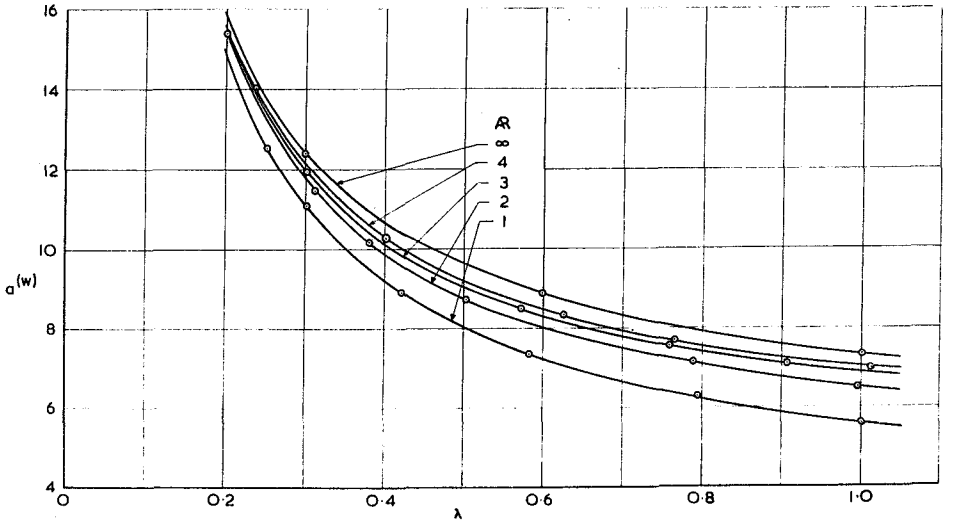

FIG. 28. THE LIFT DERIVATIVE $a^{(W)}$ OF A CLOSED WING / END-PLATE CONFIGURATION.

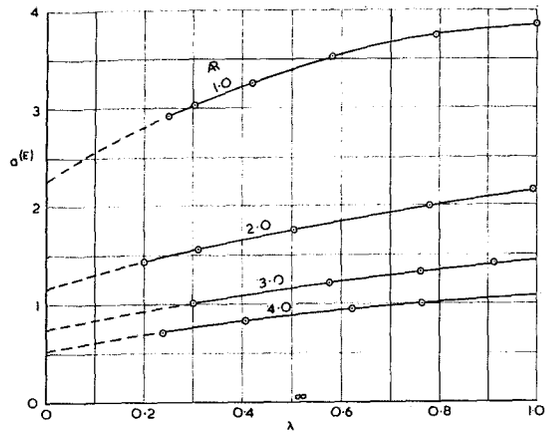

FIG. 29. THE LIFT DERIVATIVE $a^{(E)}$ OF A CLOSED WING / END-PLATE CONFIGURATION.

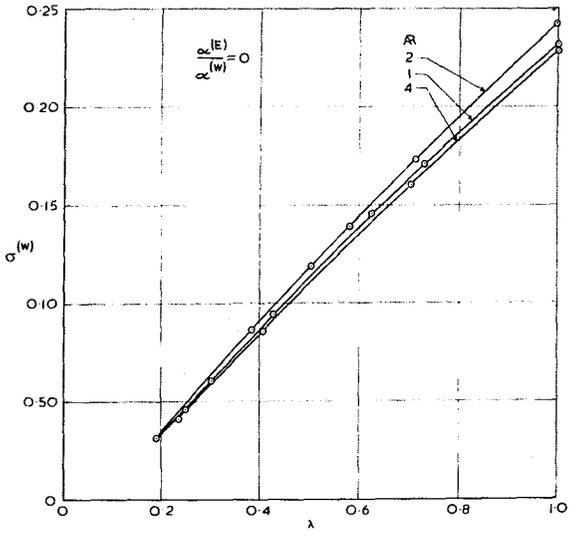

FIG. 31. INDUCED-DRAG FACTOR OF THE WING PLANE OF A CLOSED WING / END-PLATE CONFIGURATION.

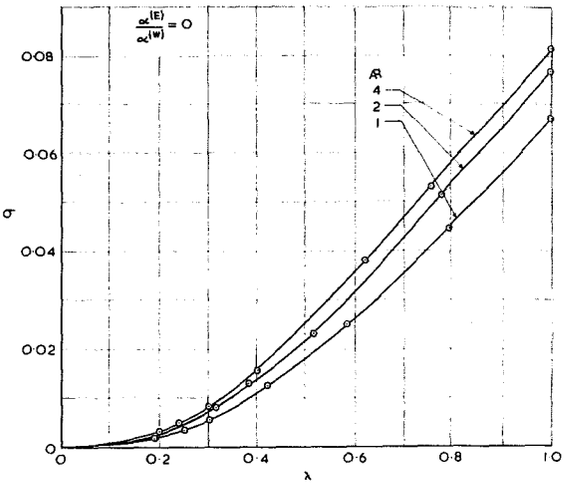

FIG. 30. THE INDUCED-DRAG FACTOR OF A CLOSED WING / END-PLATE CONFIGURATION.

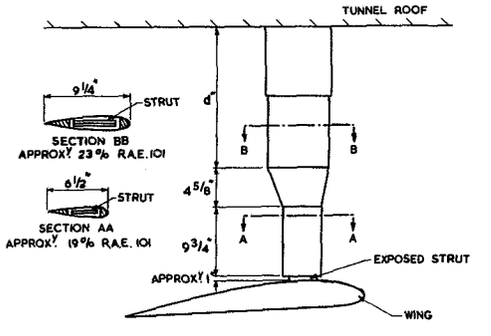

DIMENSION "d" DEPENDS ON THE HEIGHT OF THE WING ABOVE THE 'GROUND'

FIG. 32. SKETCH SHOWING GEOMETRY OF WING STRUT FAIRINGS.

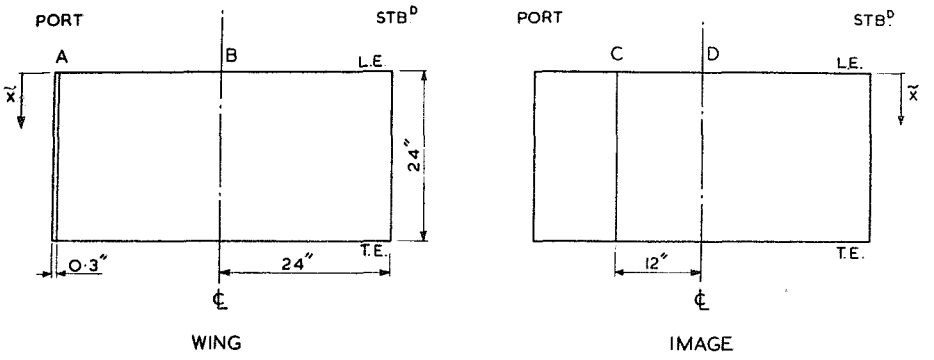

CHORDWISE POSITIONS ($\tilde{x}/c$) OF PRESSURE TAPPINGS.

SPANWISE STATION A,B,C.		D	
		'IMAGE UPPER'	'IMAGE LOWER'
0	0·280		
0·010	0·250	0·042	
0·021	0·292	0·167	0·167
0·031	0·333	0·333	0·333
0·042	0·418	0·500	
0·052	0·500	0·667	0·667
0·062	0·584	0·833	0·833
0·073	0·667		0·916
0·083	0·750		
0·125	0·833		
0·167	0·916		
	0·958		

FIG. 33. SPANWISE AND CHORDWISE LOCATIONS OF PRESSURE TAPPINGS.

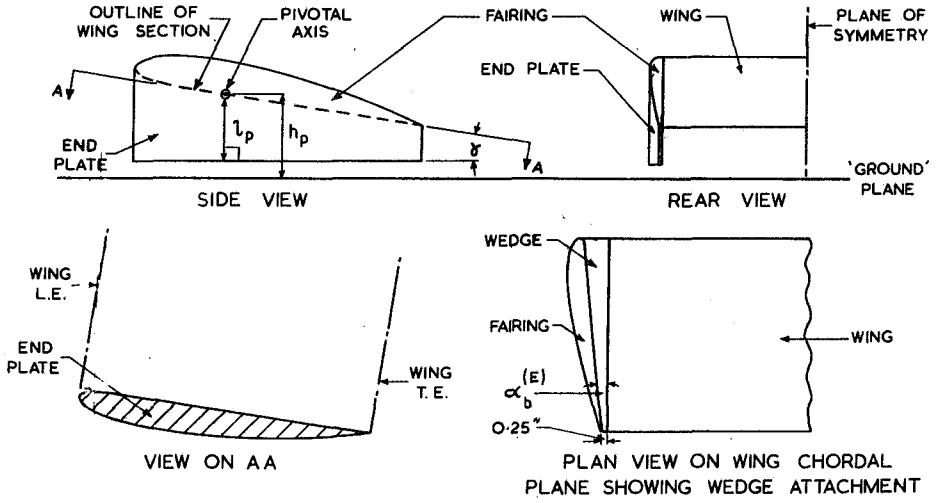

FIG. 34. GEOMETRY OF END PLATES AND METHOD OF ATTACHING THEM TO THE WING.

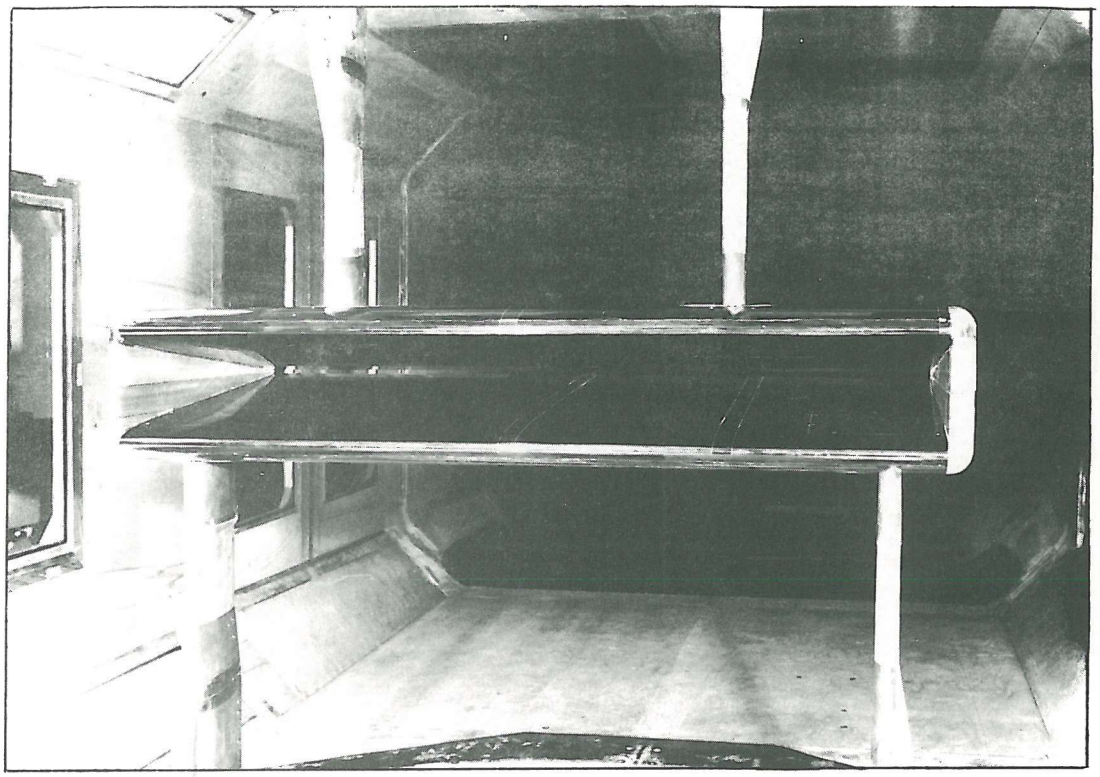

FIG. 35. A GENERAL VIEW OF THE WING AND IMAGE WITH END PLATES FITTED

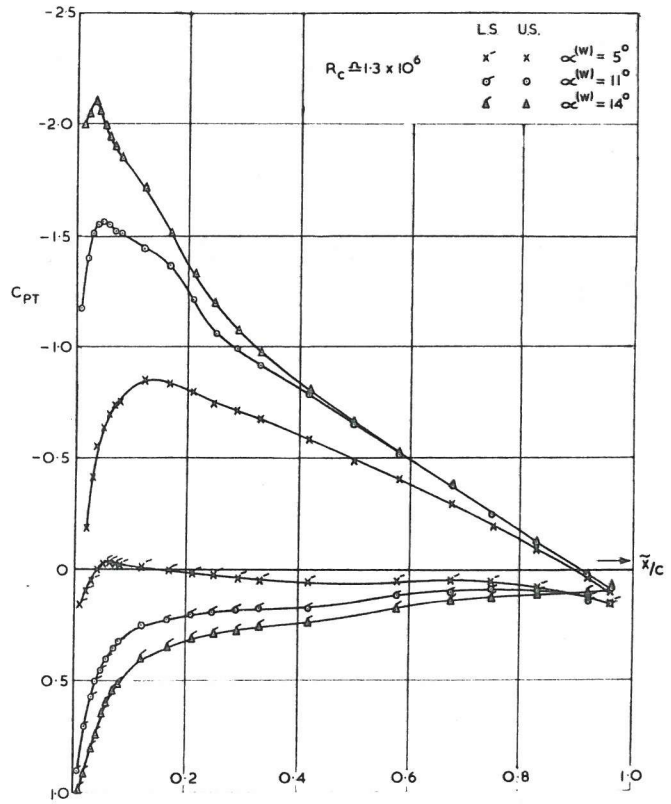

FIG. 36. PRESSURE DISTRIBUTIONS AT THE CENTRE SPAN OF THE ISOLATED WING : HALF-BODY TIP FAIRINGS FITTED.

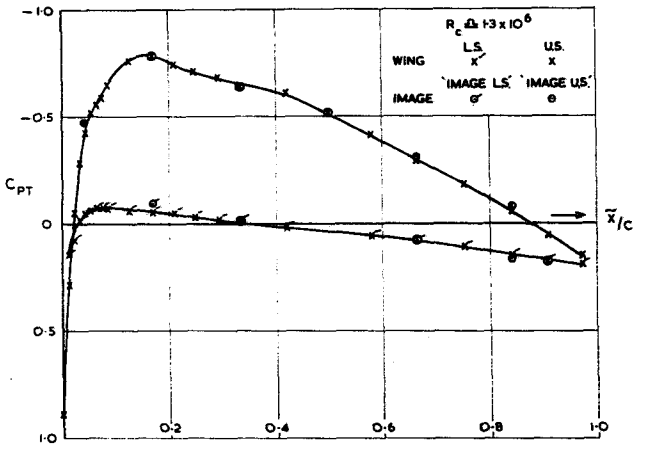

FIG. 37. COMPARISON BETWEEN THE PRESSURE DISTRIBUTIONS OF THE WING AND IMAGE AT CENTRE SPAN; $h_p/c = 0{\cdot}125$, $\alpha^{(w)} = 2°$; HALF-BODY TIP FAIRINGS.

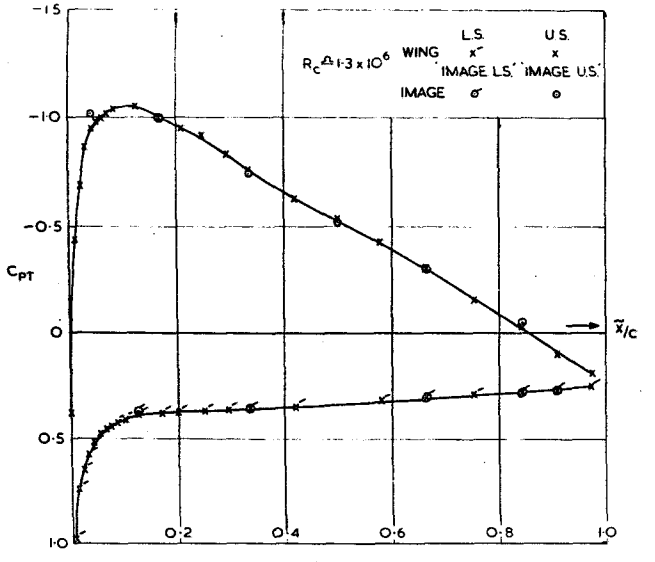

FIG. 38. COMPARISON BETWEEN THE PRESSURE DISTRIBUTIONS OF THE WING AND IMAGE AT CENTRE SPAN; $h_p/c = 0{\cdot}125$ $\alpha^{(w)} = 5°$; HALF-BODY TIP FAIRINGS.

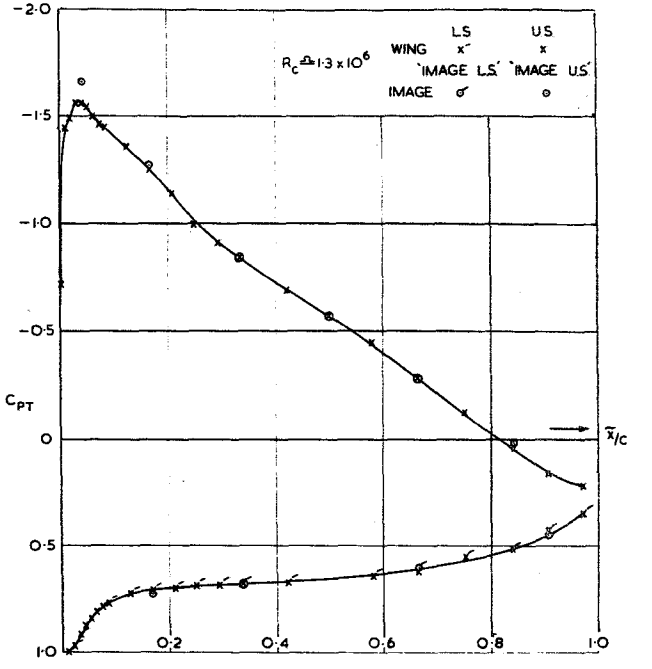

FIG. 39. COMPARISON BETWEEN THE PRESSURE DISTRIBUTIONS OF THE WING AND IMAGE AT CENTRE SPAN; $h_p/c = 0{\cdot}125$ $\alpha^{(w)} = 8°$; HALF-BODY TIP FAIRINGS.

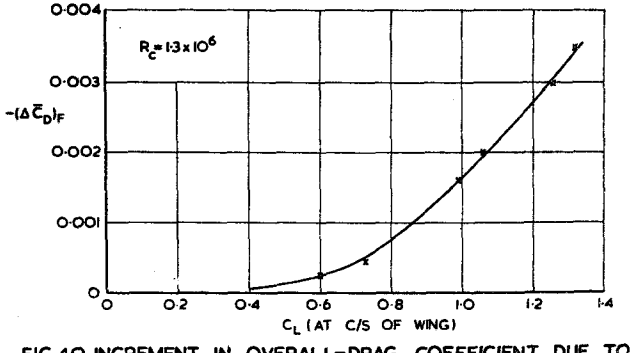

FIG. 40. INCREMENT IN OVERALL-DRAG COEFFICIENT DUE TO DUMMY FAIRING AGAINST CENTRE-SPAN C_L OF WING (WITHOUT DUMMY FAIRING); $h_p/c = 0{\cdot}167$; END PLATES FITTED IN THE MANNER DESCRIBED IN SECTION III.2.3.3.

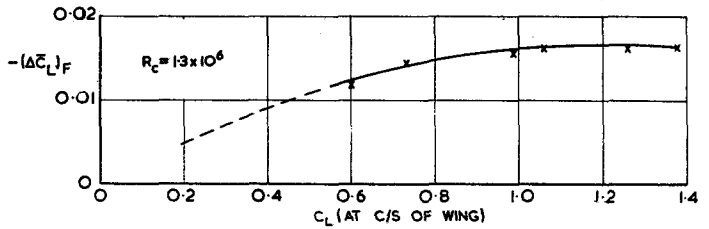

FIG. 41. INCREMENT IN OVERALL-LIFT COEFFICIENT DUE TO DUMMY FAIRING AGAINST CENTRE-SPAN C_L OF WING (WITHOUT DUMMY FAIRING); $h_p/c = 0{\cdot}167$; END PLATES FITTED IN THE MANNER DESCRIBED IN SECTION III.2.3.3.

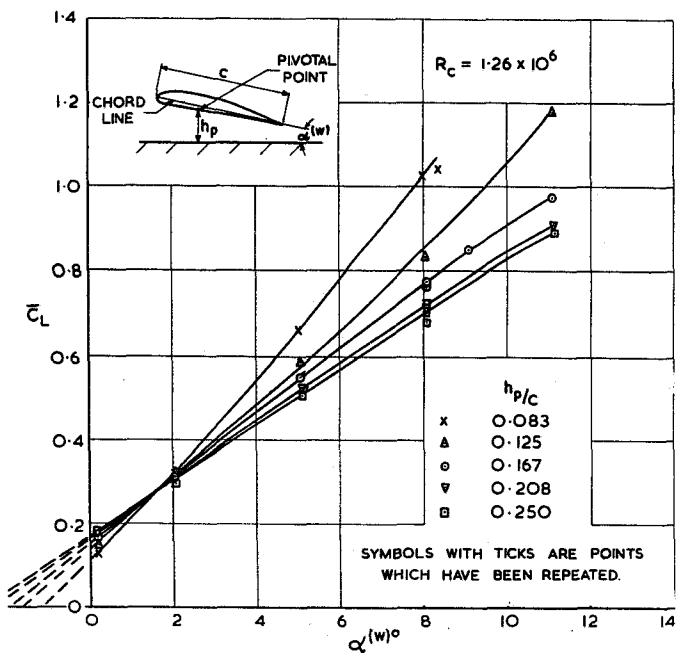

FIG. 43. OVERALL-LIFT COEFFICIENT AGAINST INCIDENCE FOR A RECTANGULAR WING WITH HALF-BODY FAIRINGS AT THE TIPS.

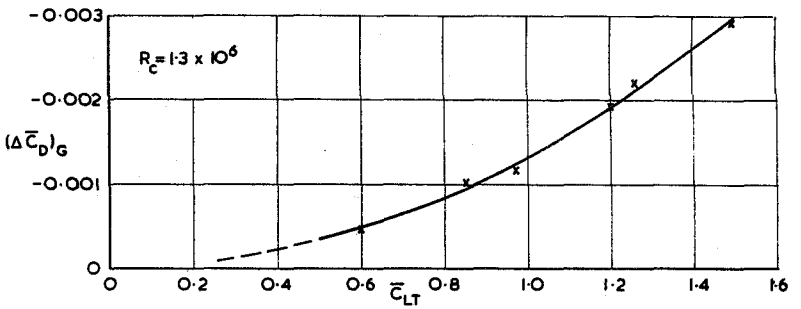

FIG. 42. CORRECTION TO $\bar{C}_D$ FOR 0·02 in. GAPS AT BASES OF STRUT FAIRINGS AGAINST OVERALL-LIFT COEFFICIENT (UNCORRECTED FOR TUNNEL INTERFERENCE); $h_p/c = 0{\cdot}167$; END PLATES FITTED IN THE MANNER DESCRIBED IN SECTION III. 2.3.3.

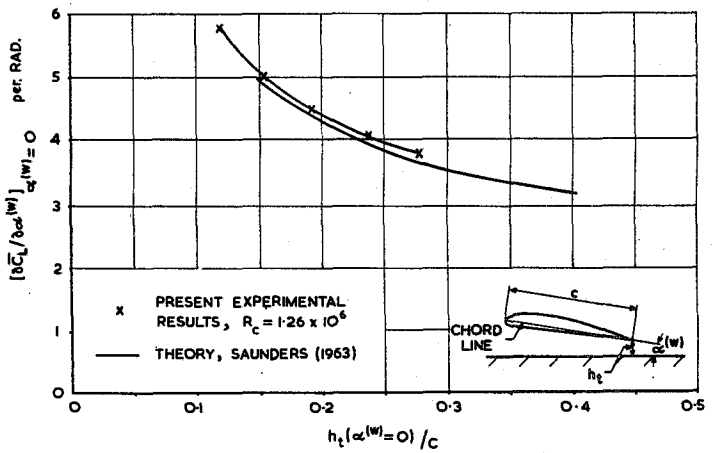

FIG. 44. LIFT-CURVE SLOPE OF A RECTANGULAR WING WITH HALF-BODY FAIRINGS AT THE TIPS: COMPARISON BETWEEN THEORY AND EXPERIMENT.

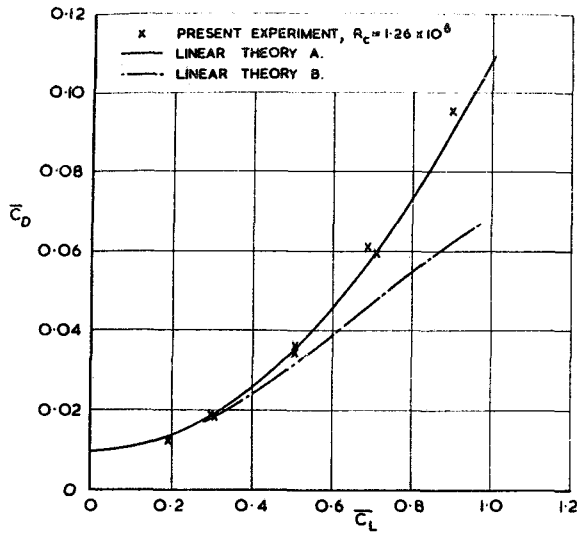

FIG. 45. OVERALL-DRAG COEFFICIENT AGAINST OVERALL-LIFT COEFFICIENT; WING FITTED WITH HALF-BODY FAIRINGS AT THE TIPS; $h_p/c = 0{\cdot}25$

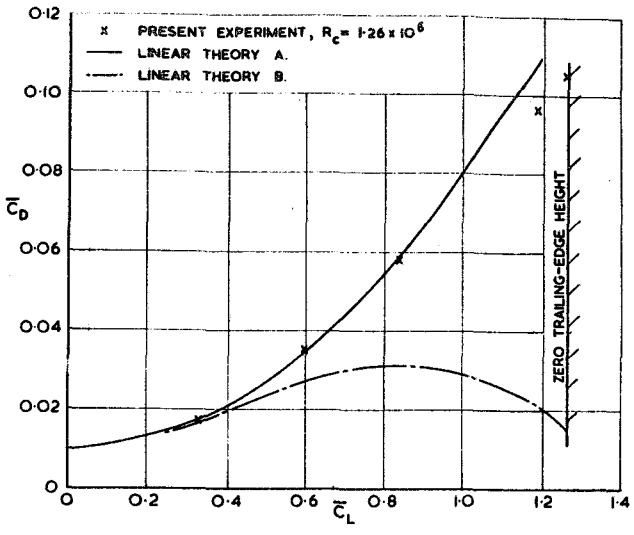

FIG. 47. OVERALL-DRAG COEFFICIENT AGAINST OVERALL-LIFT COEFFICENT; WING FITTED WITH HALF-BODY FAIRINGS AT THE TIPS; $h_p/c = 0{\cdot}125$

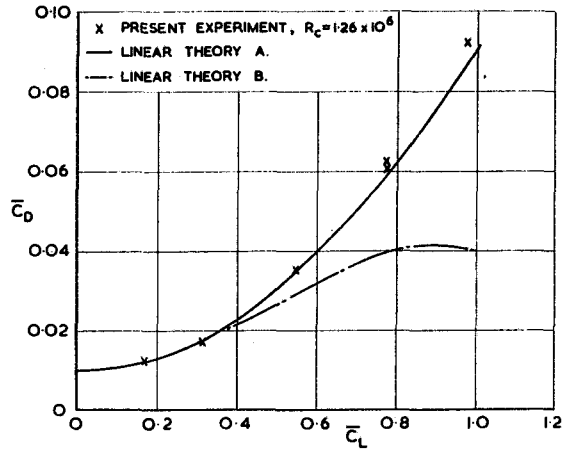

FIG. 46. OVERALL-DRAG COEFFICIENT AGAINST OVERALL-LIFT COEFFICIENT; WING FITTED WITH HALF-BODY FAIRINGS AT THE TIPS; $h_p/c = 0{\cdot}167$.

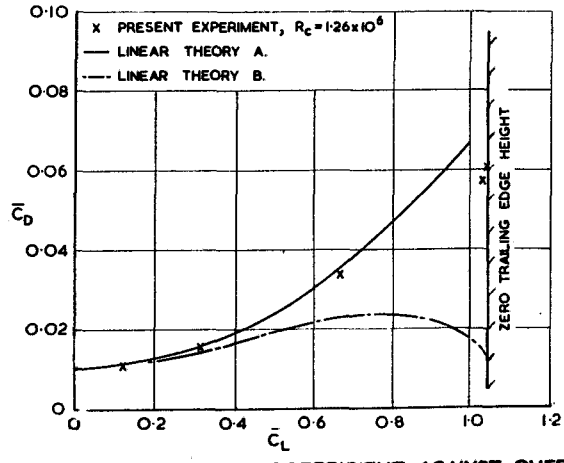

FIG. 48. OVERALL-DRAG COEFFICIENT AGAINST OVERALL-LIFT COEFFICIENT; WING FITTED WITH HALF-BODY FAIRINGS AT THE TIPS; $h_p/c = 0{\cdot}083$.

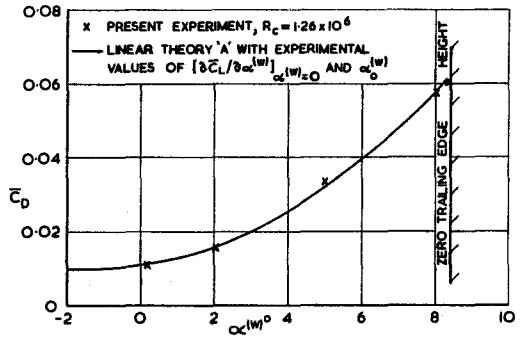

FIG. 49. OVERALL-DRAG COEFFICIENT AGAINST WING INCIDENCE; WING FITTED WITH HALF-BODY FAIRINGS AT THE TIPS; $h_p/c = 0{\cdot}083$

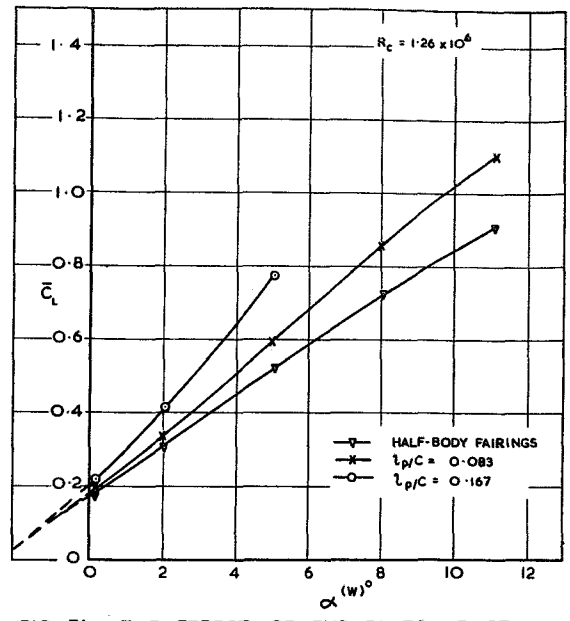

FIG. 51. THE EFFECT OF END-PLATE LENGTH ON THE CURVE OF OVERALL-LIFT COEFFICIENT AGAINST WIND INCIDENCE; $\gamma = 0$, $h_p/C = 0{\cdot}208$.

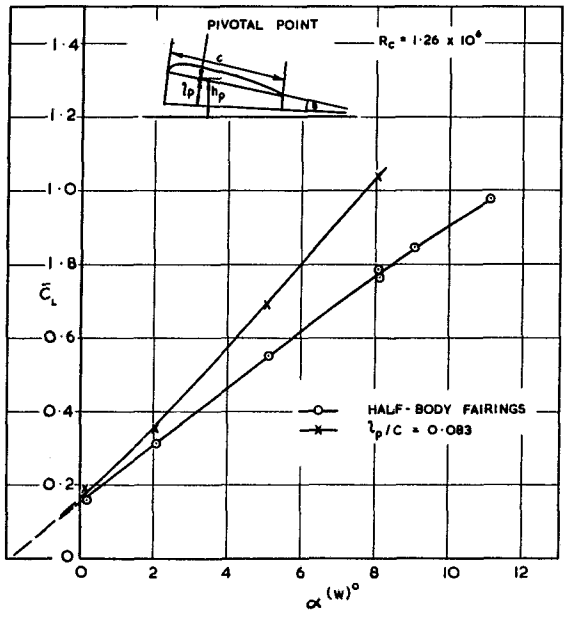

FIG. 50. THE EFFECT OF END-PLATE LENGTH ON THE CURVE OF OVERALL-LIFT COEFFICIENT AGAINST WING INCIDENCE; $\gamma = 0$, $h_p/C = 0{\cdot}167$.

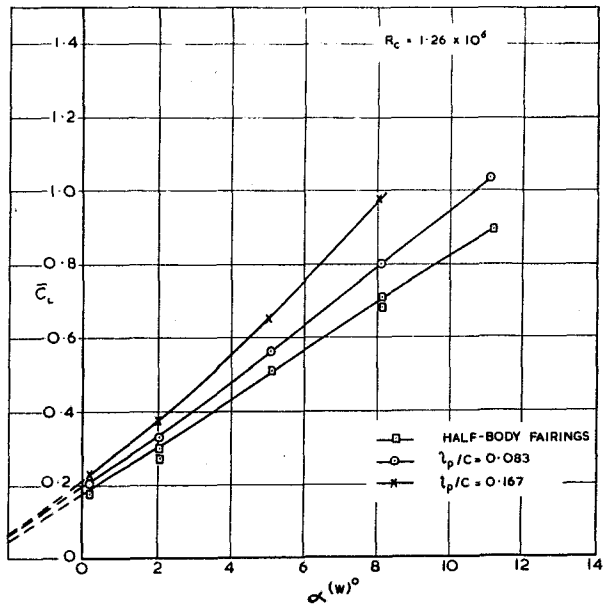

FIG. 52. THE EFFECT OF END-PLATE LENGTH ON THE CURVE OF OVERALL-LIFT COEFFICIENT AGAINST WING INCIDENCE; $\gamma = 0$, $h_p/C = 0{\cdot}250$

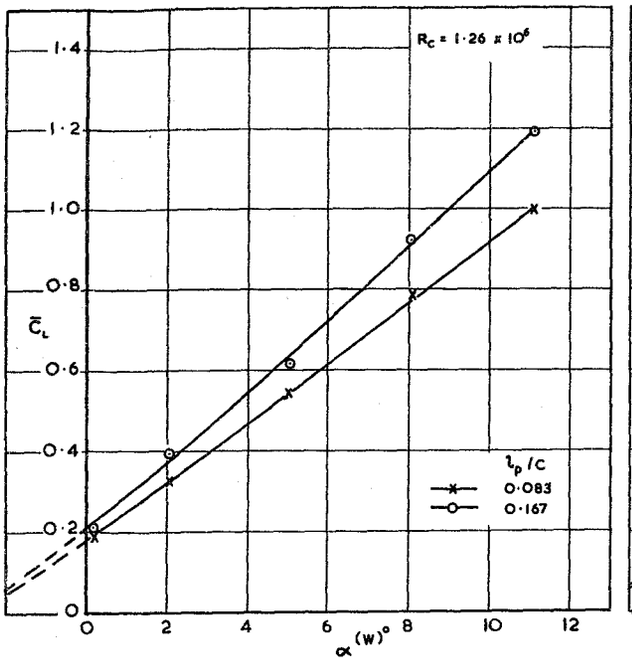

FIG. 53. THE EFFECT OF END-PLATE LENGTH ON THE CURVE OF OVERALL-LIFT COEFFICIENT AGAINST WING INCIDENCE; $\gamma = 3°$, $h_p/c = 0{\cdot}250$.

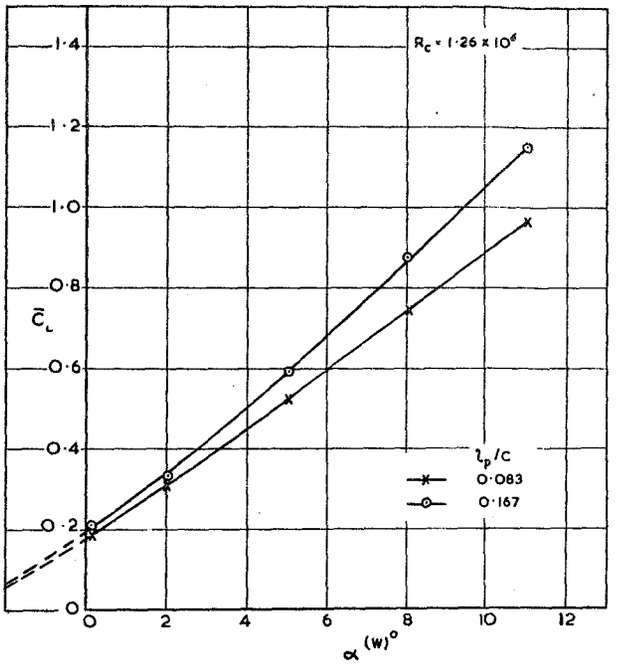

FIG. 54. THE EFFECT OF END-PLATE LENGTH ON THE CURVE OF OVERALL-LIFT COEFFICIENT AGAINST WING INCIDENCE; $\gamma = 6°$, $h_p/c = 0{\cdot}250$

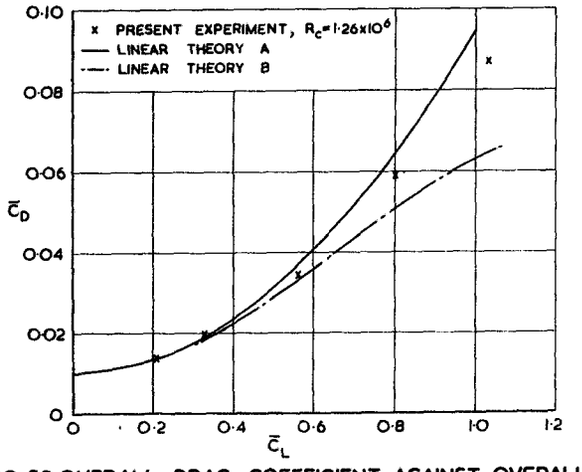

FIG. 55. OVERALL-DRAG COEFFICIENT AGAINST OVERALL-LIFT COEFFICIENT; WING FITTED WITH END PLATES; $\gamma = 0$, $l_p/c = 0{\cdot}083$, $h_p/c = 0{\cdot}250$

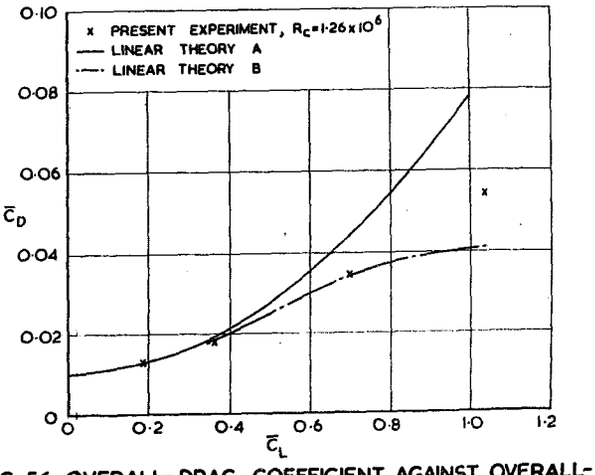

FIG. 56. OVERALL-DRAG COEFFICIENT AGAINST OVERALL-LIFT COEFFICIENT; WING FITTED WITH END PLATES; $\gamma = 0$, $l_p/c = 0{\cdot}083$, $h_p/c = 0{\cdot}167$

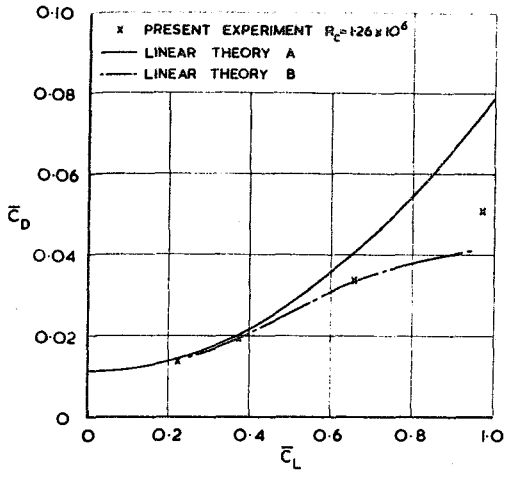

FIG. 57. OVERALL-DRAG COEFFICIENT AGAINST OVERALL-LIFT COEFFICIENT; WING FITTED WITH END PLATES; $l_p/c = 0{\cdot}167$ $\gamma = 0$, $h_p/c = 0{\cdot}250$

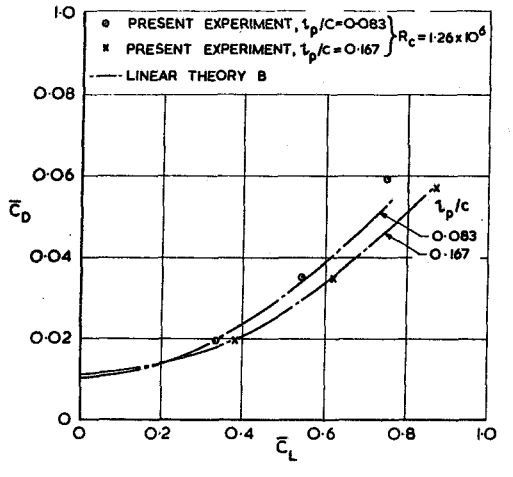

FIG. 58. OVERALL-DRAG COEFFICIENT AGAINST OVERALL-LIFT COEFFICIENT; END PLATE BASES PARALLEL TO THE 'GROUND'; $l_p/c = 0{\cdot}250$

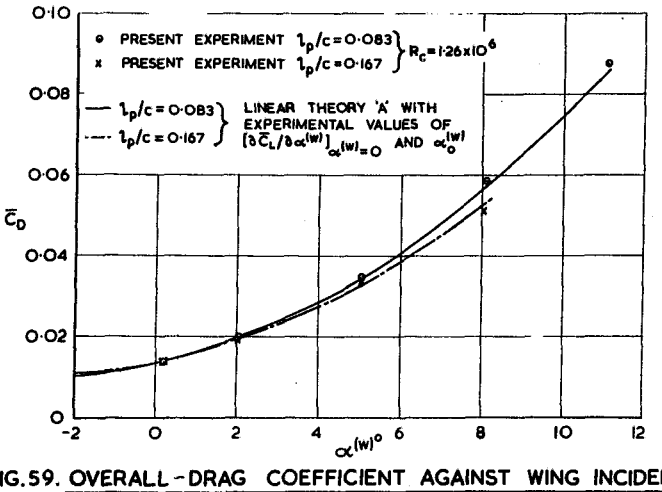

FIG. 59. OVERALL-DRAG COEFFICIENT AGAINST WING INCIDENCE; WING FITTED WITH END PLATES; $\gamma = 0$, $h_p/c = 0{\cdot}250$.

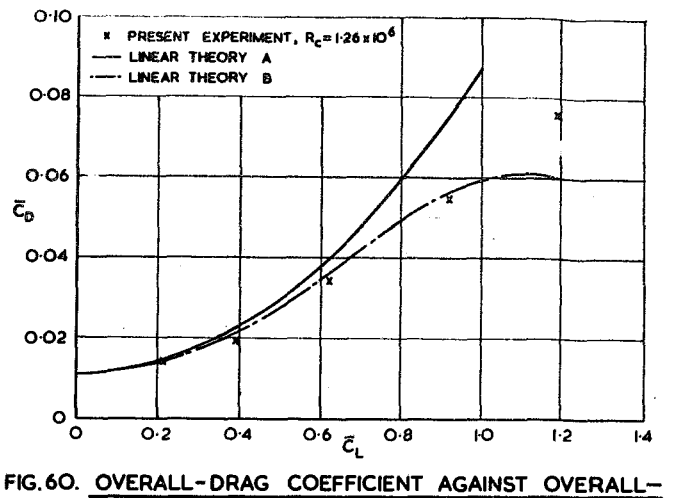

FIG. 60. OVERALL-DRAG COEFFICIENT AGAINST OVERALL-LIFT COEFFICIENT; WING FITTED WITH END PLATES $\gamma = 3°$, $l_p/c = 0{\cdot}167$, $h_p/c = 0{\cdot}250$

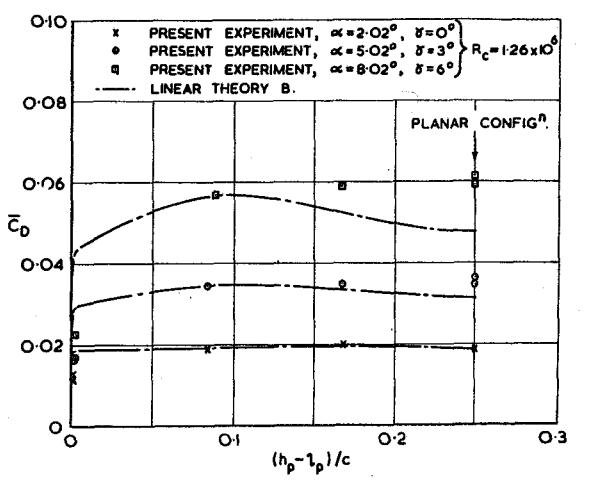

FIG. 61. INFLUENCE OF THE GAP AT THE BASE OF THE END PLATES ON THE OVERALL-DRAG COEFFICIENT; END-PLATE BASES PARALLEL TO THE GROUND; $h_p/c = 0{\cdot}250$

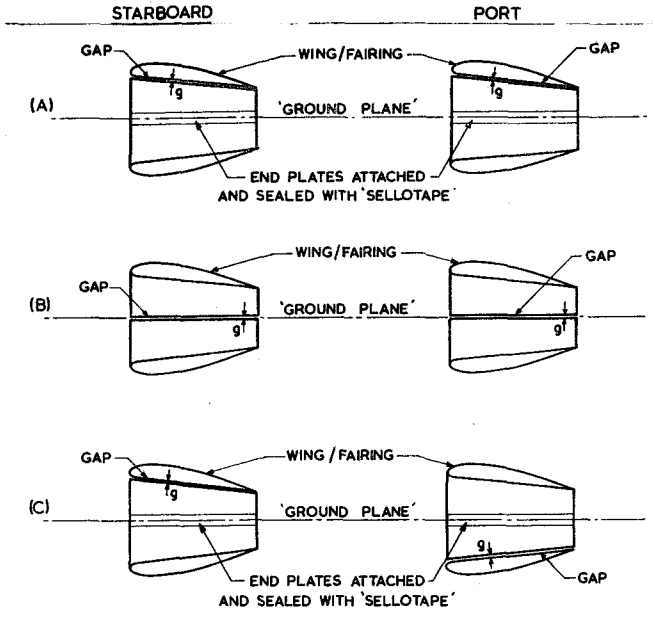

FIG.62. POSITIONS OF GAPS IN THE END PLATES FOR OVERALL-FORCE MEASUREMENTS

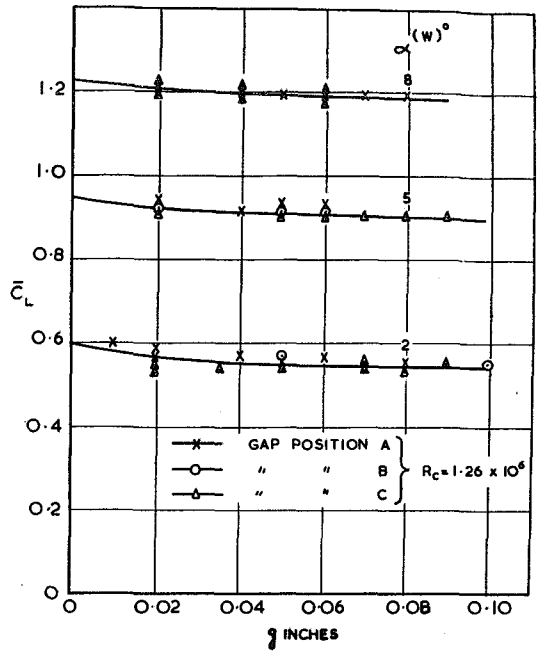

FIG. 63. THE INFLUENCE OF END-PLATE GAP ON THE OVERALL-LIFT COEFFICIENT; $h_p/c = 0.167$; $\alpha_b^{(E)} = 0°$

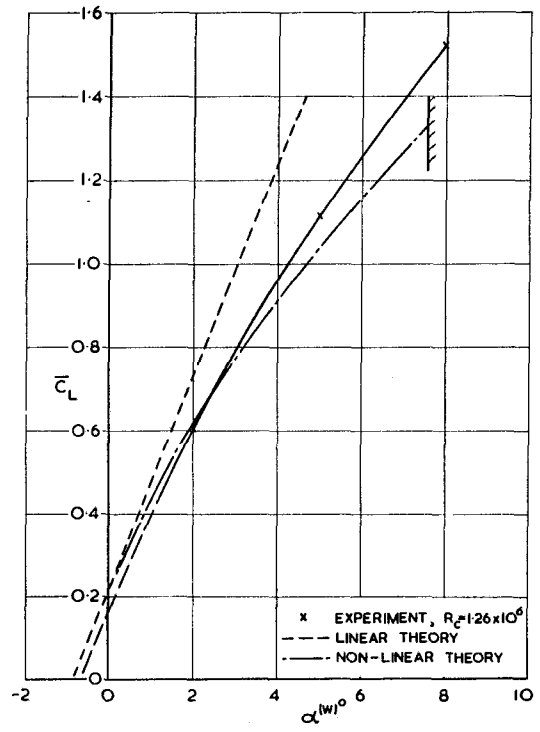

FIG.65. THE OVERALL LIFT OF CLOSED CONFIGURATIONS; l_p/c=0·083, $\alpha_b^{(E)}$=0

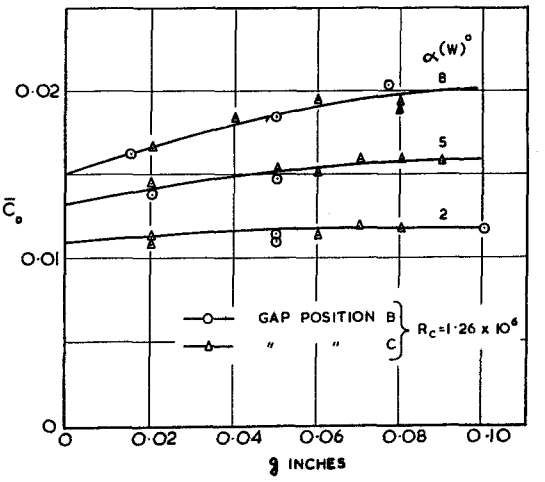

FIG. 64. THE INFLUENCE OF END-PLATE GAP ON THE OVERALL-DRAG COEFFICIENT; $h_p/c = 0.167$; $\alpha_b^{(E)} = 0°$

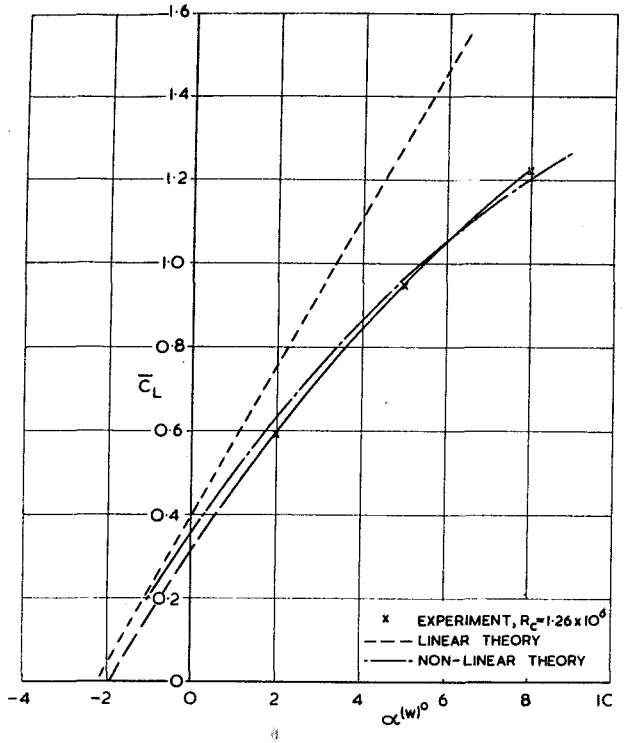

FIG. 66. THE OVERALL LIFT OF CLOSED CONFIGURATIONS; $l_p/c = 0{\cdot}167, \alpha_b^{(E)} = 0$

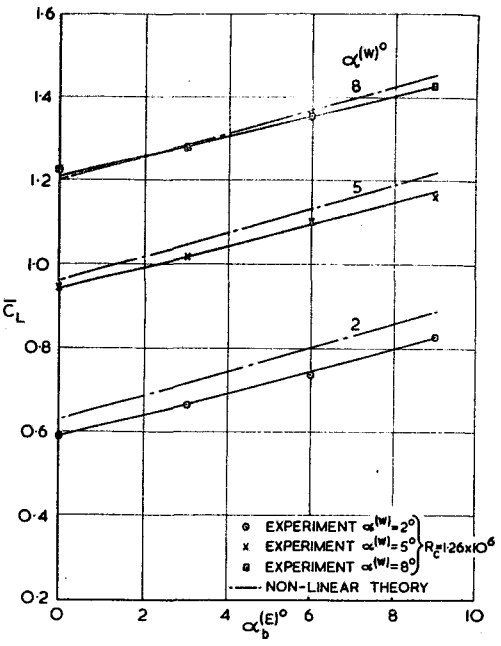

FIG.68. THE EFFECT OF END-PLATE INCIDENCE ON THE OVERALL LIFT OF A CLOSED CONFIGURATION; $l_p/c = 0{\cdot}167$

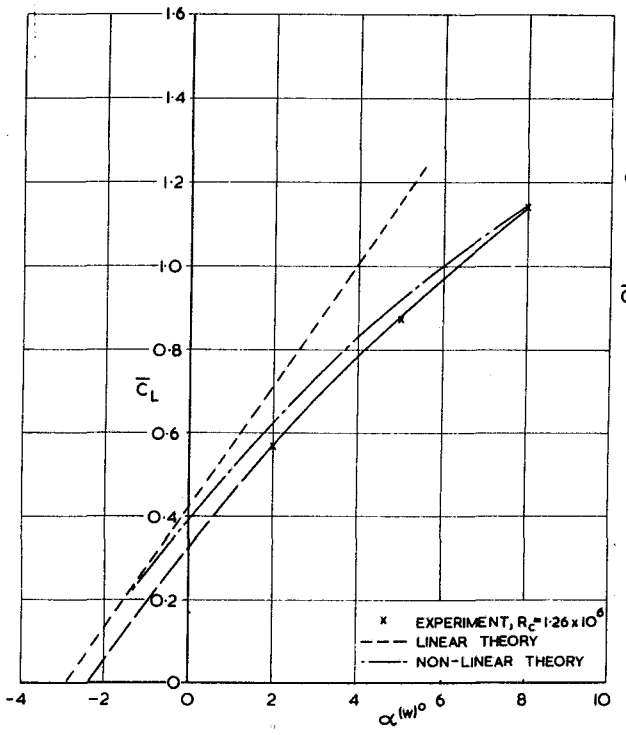

FIG. 67. THE OVERALL LIFT OF CLOSED CONFIGURATIONS; $l_p/c = 0{\cdot}250, \alpha_b^{(E)} = 0$

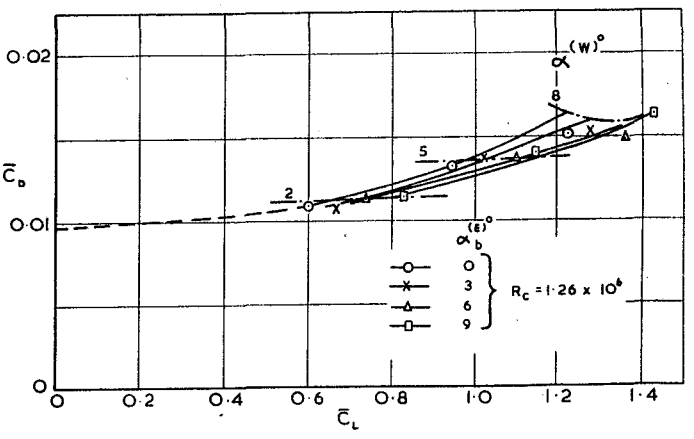

FIG. 69. THE OVERALL-DRAG COEFFICIENT AS A FUNCTION OF OVERALL-LIFT COEFFICIENT FOR VARIOUS END-PLATE INCIDENCES; $l_p/c = h_p/c = 0{\cdot}167$.

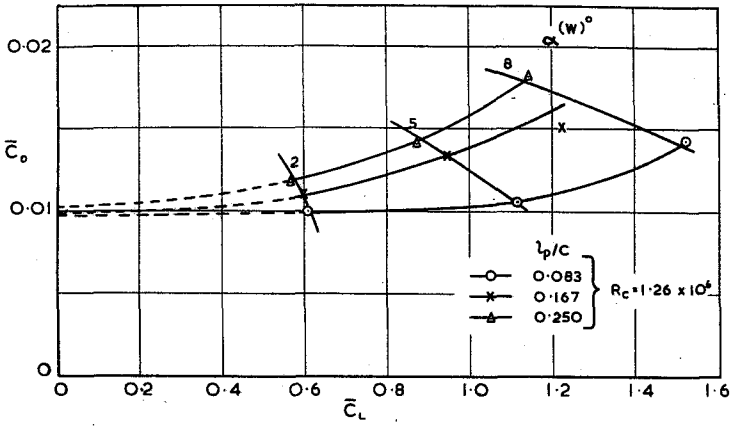

FIG. 70. THE OVERALL-DRAG COEFFICIENT AS A FUNCTION OF OVERALL-LIFT COEFFICIENT FOR VARIOUS END-PLATE LENGTHS; $\alpha_b^{(E)} = 0°$; $h_p/c = l_p/c$

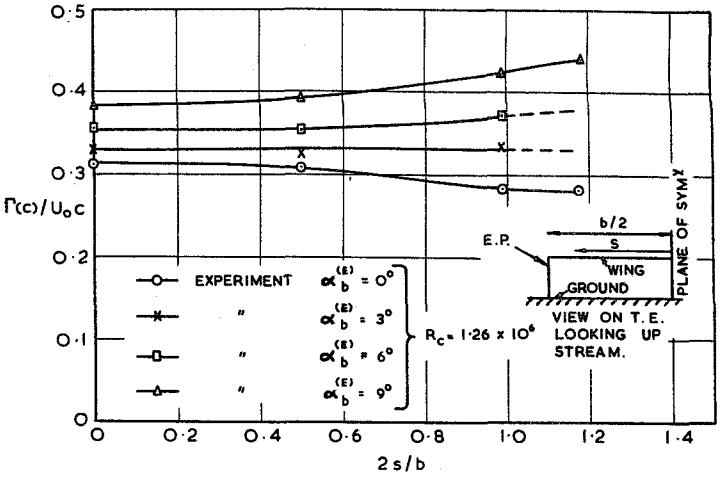

FIG. 71. NON-DIMENSIONAL CIRCULATION AT THE TRAILING EDGES OF CLOSED CONFIGURATIONS; $l_p/C = 0·167$, $\alpha^{(W)} = 2°$

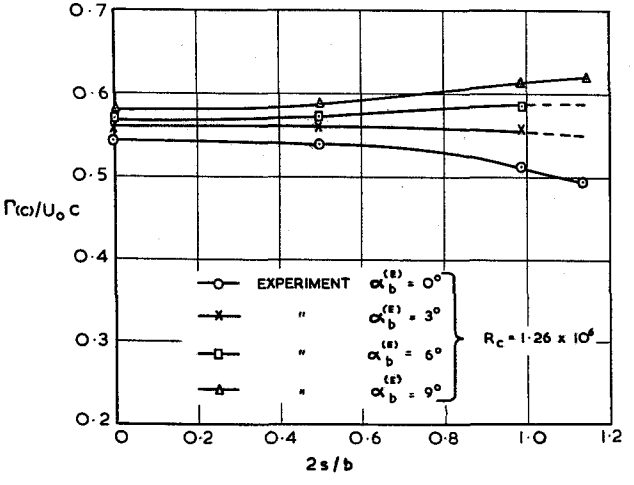

FIG. 72. NON-DIMENSIONAL CIRCULATION AT THE TRAILING EDGES OF CLOSED CONFIGURATIONS; $l_p/C = 0·167$, $\alpha^{(W)} = 5°$.

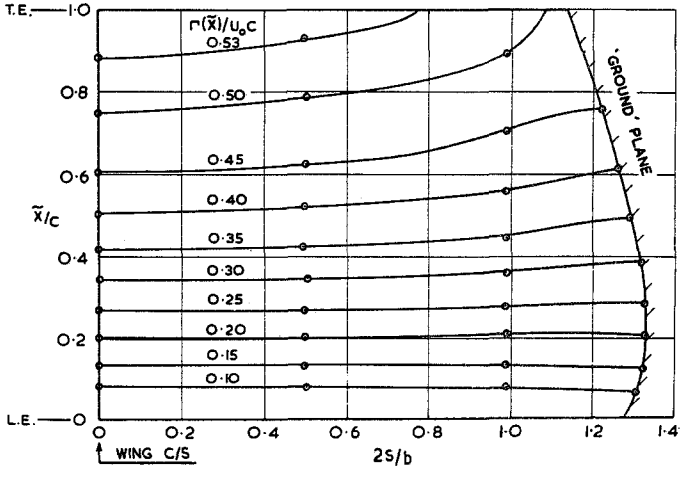

FIG. 73. EXPERIMENTALLY DETERMINED LINES OF CONSTANT CIRCULATION ; $l_p/c = h_p/c = 0·167$, $\alpha^{(W)} = 5°$, $\alpha_b^{(E)} = 0°$, $R_c = 1·26 \times 10^6$

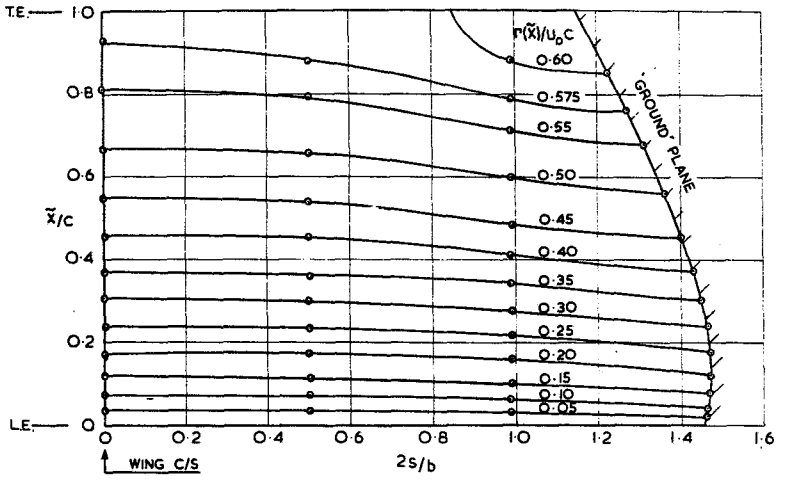

FIG. 74. EXPERIMENTALLY DETERMINED LINES OF CONSTANT CIRCULATION; $l_p/c = h_p/c = 0{\cdot}167$, $\alpha^{(W)} = 5°$, $\alpha_b^{(E)} = 9°$, $R_c = 1{\cdot}26 \times 10^6$

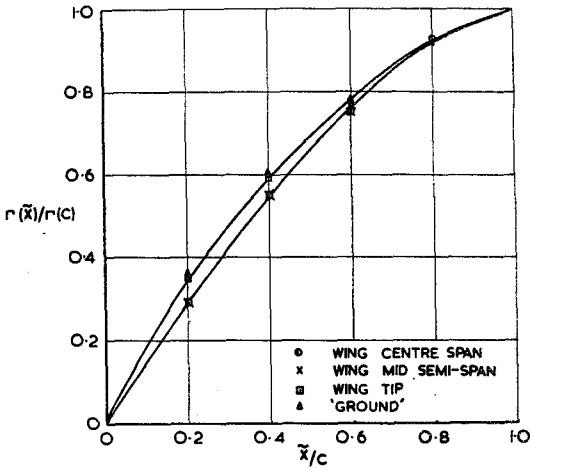

FIG. 75. COMPARISON BETWEEN THE CHORDWISE DISTRIBUTION OF CIRCULATION AT FOUR S-WISE STATIONS; $l_p/c = h_p/c = 0{\cdot}167$, $\alpha^{(W)} = 2°$, $\alpha_b^{(E)} = 0°$, $R_c = 1{\cdot}26 \times 10^6$

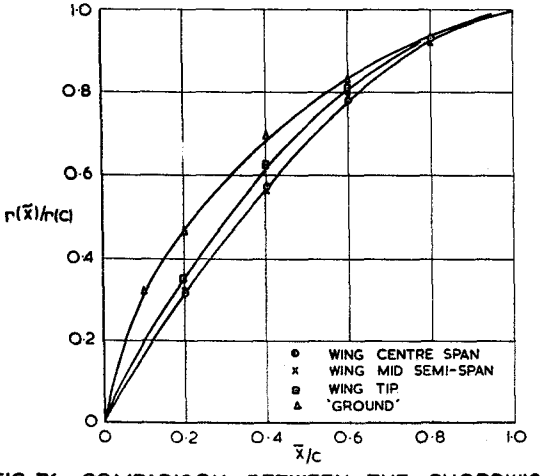

FIG. 76. COMPARISON BETWEEN THE CHORDWISE DISTRIBUTION OF CIRCULATION AT FOUR S-WISE STATIONS; $l_p/c = h_p/c = 0{\cdot}167$, $\alpha^{(W)} = 2°$, $\alpha_b^{(E)} = 9°$, $R_c = 1{\cdot}26 \times 10^6$

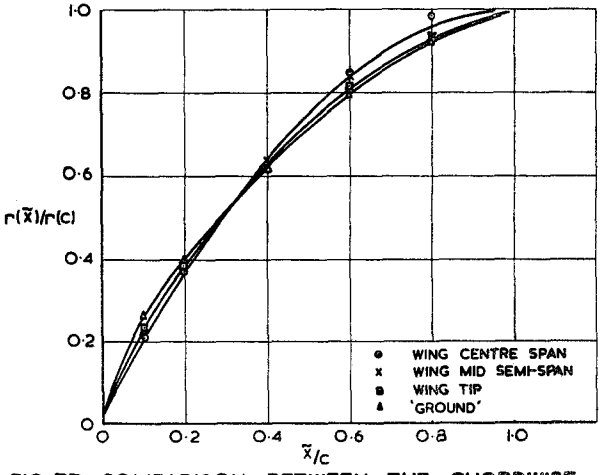

FIG. 77. COMPARISON BETWEEN THE CHORDWISE DISTRIBUTION OF CIRCULATION AT FOUR S-WISE STATIONS; $l_p/c = h_p/c = 0{\cdot}167$, $\alpha^{(W)} = 5°$, $\alpha_b^{(E)} = 0°$, $R_c = 1{\cdot}26 \times 10^6$

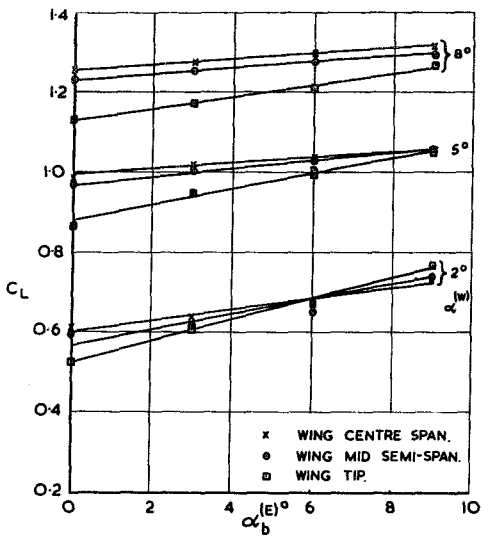

FIG. 78. SECTIONAL-LIFT COEFFICIENT AGAINST END-PLATE INCIDENCE; $l_p/c = h_p/c = 0{\cdot}167$, $R_c = 1{\cdot}26 \times 10^6$

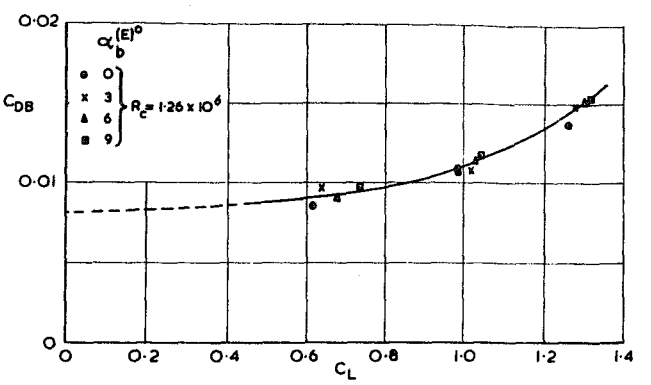

FIG. 80. THE BOUNDARY-LAYER DRAG AT THE CENTRE SPAN OF THE WING MEASURED BY THE WAKE-SURVEY TECHNIQUE; $l_p/c = h_p/c = 0{\cdot}167$

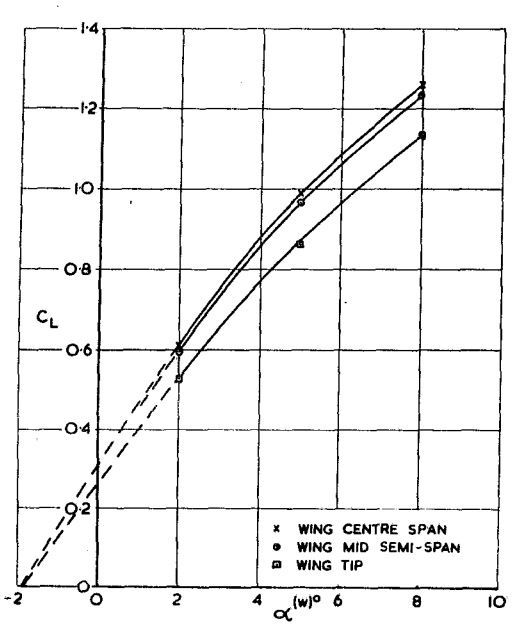

FIG. 79. SECTIONAL-LIFT COEFFICIENT AGAINST WING INCIDENCE; $l_p/c = h_p/c = 0{\cdot}167$, $\alpha_b^{(E)} = 0°$, $R_c = 1{\cdot}26 \times 10^6$

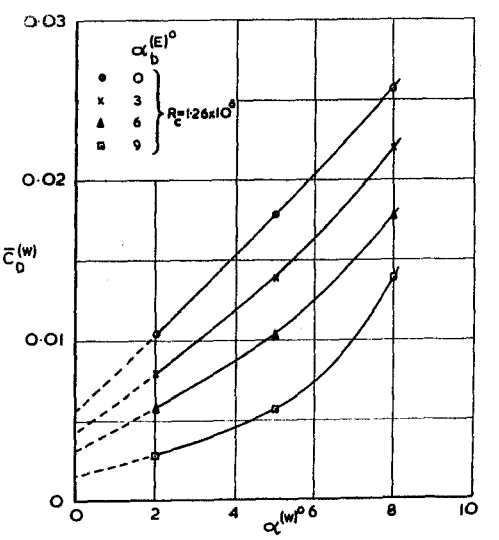

FIG. 81. THE OVERALL-DRAG COEFFICIENT OF WING AGAINST WING INCIDENCE; $l_p/c = h_p/c = 0{\cdot}167$

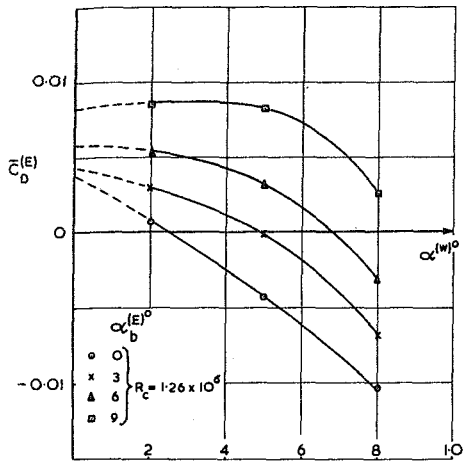

FIG. 82. THE OVERALL-DRAG COEFFICIENT OF ONE END PLATE PLUS IMAGE AGAINST WING INCIDENCE ; $l_p/c = h_p/c = 0{\cdot}167$.

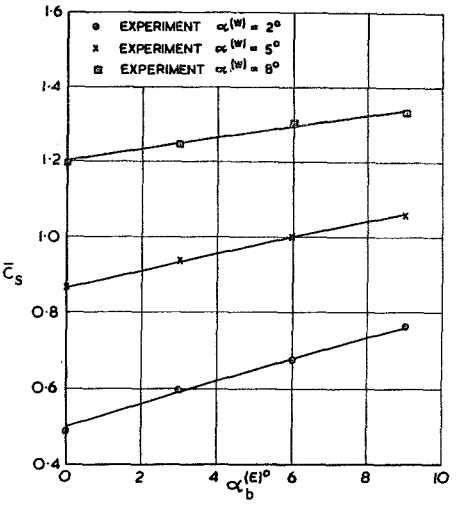

FIG. 84. OVERALL SIDE-FORCE COEFFICIENT OF ONE END PLATE PLUS ITS IMAGE BENEATH THE 'GROUND' AGAINST END-PLATE INCIDENCE ; $l_p/c = h_p/c = 0{\cdot}167$, $R_c = 1{\cdot}26 \times 10^6$

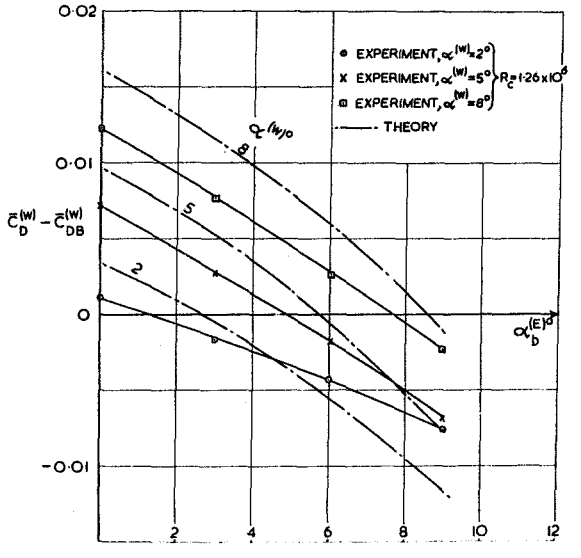

FIG. 83. THE OVERALL INVISCID-DRAG COEFFICIENT OF THE WING AGAINST END-PLATE INCIDENCE ; $l_p/c = h_p/c = 0{\cdot}167$

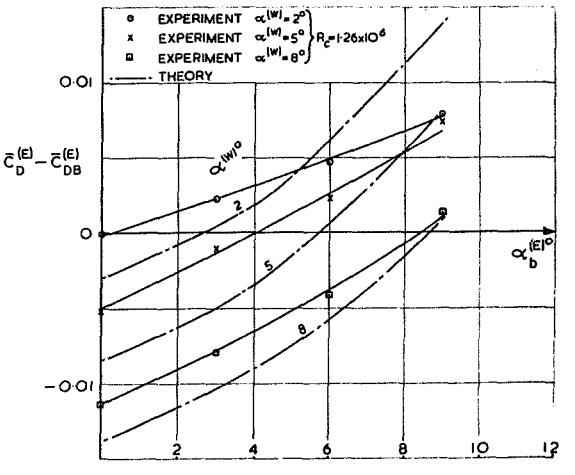

FIG. 85. THE OVERALL INVISCID-DRAG COEFFICIENT OF ONE END PLATE PLUS IMAGE AGAINST END-PLATE INCIDENCE ; $l_p/c = h_p/c = 0{\cdot}167$